

CENTRAL LIBRARY  
TEZPUR UNIVERSITY  
Accession No. 49654  
Date 14/9/11

REFERENCE BOOK  
NOT TO BE ISSUED  
TEZPUR UNIVERSITY LIBRARY

CENTRAL LIBRARY  
TEZPUR UNIVERSITY  
Accession No. T 150  
Date 27/02/13

# STUDIES ON SOLUTION OF EVOLUTION EQUATIONS FOR UNPOLARIZED AND POLARIZED HADRON STRUCTURE FUNCTIONS

A thesis submitted in partial fulfillment of the  
requirements for award of the degree of Doctor of  
Philosophy

**Ranjit Baishya**

Registration No: 003 of 2010



Department of Physics  
School of Science and Technology  
Tezpur University  
Napaam, Tezpur - 784028  
Assam, India

July, 2010

*I would like to dedicate this thesis*

*to*

*my beloved parents*

*Smt. Sabitri Baishya*

*and*

*Late Biren Baishya*

*"I never think of the future, it comes soon enough"*

*– Einstein*

# STUDIES ON SOLUTION OF EVOLUTION EQUATIONS FOR UNPOLARIZED AND POLARIZED HADRON STRUCTURE FUNCTIONS

## **Abstract**

Deep Inelastic Scattering (DIS) process is one of the basic processes for investigating the structure of hadrons. All information about the structure of hadrons participating in DIS comes from the hadronic structure functions. The structure function, depends on  $Q^2$ , contains both valence and sea quark distributions. It rises with  $Q^2$  at small  $x$ , where sea quarks dominate, and falls with  $Q^2$  at large  $x$ , where valence quarks dominate. These effects may be quantified using the evolution equations, which expresses the evolution of the quark and gluon distributions. The gluon distributions of the nucleon cannot be extracted directly from the measured structure functions in DIS experiments, but can be predicted by using the Quantum Chromodynamics (QCD) evolution equations.

The most important source of hadrons structure function values, amongst various experimental measurements through DIS, are certainly the HERA experiments {H1 and ZEUS}. Their latest sets of experimental data reached a level of precision very useful for theoretical tests and obtain the well known Bjorken scaling violation. The scaling violation implies that parton densities inside the proton become  $Q^2$  dependent and the resummation of the collinear divergences in the framework of perturbative QCD leads to  $Q^2$  evolution equations for these parton densities. These equations, called the Dokshitzer-Gribov-Lipatov-Altarelli-Parisi (DGLAP) equations, were found independently by Gribov-Lipatov in 1972, Altarelli-Parisi and Dokshitzer in 1977. Due to their very good agreement with experiment and its implications on scaling violation, the DGLAP equations are considered as one of the best

successes of QCD and, more precisely, perturbative QCD. Thus the solutions of DGLAP evolution equations are the powerful techniques to obtain the Parton Distribution Functions (PDF), hence the hadrons structure function and ultimately structure of proton or neutron.

There are various numerical methods to solve DGLAP evolution equations with a good degree of accuracy, but the interest in the analytical methods can not be ruled out. Though exact analytic solutions of the DGLAP equations are not possible in the entire range of  $x$  and  $Q^2$ , under certain conditions analytic solutions are possible which are quite successful as far as the HERA small  $x$  data are concerned. In recent years, such a scheme in the analytic study of the DGLAP equations has been pursued with quite good phenomenological success. One of the limitations of these solutions was the non uniqueness of the solution. However, by using the method of characteristics to solve DGLAP type partial differential equation of two variables ( $Q^2$  and  $x$ ) with one initial condition, we can get rid of the ad hoc assumption and obtain a unique solution. In this thesis, unpolarized DGLAP evolution equations are solved up to Next-Next-to-Leading Order (NNLO) and polarized DGLAP evolution equations are solved up to Next-to-Leading Order (NLO) analytically by using method of characteristic and compared our results with various experimental data and parameterizations.

**In Chapter 1**, we give a brief introduction to the basic building blocks of matter, standard model of elementary particles, quantum chromodynamics, deep inelastic scattering, small  $x$  physics, structure functions, quark parton model, evolution equations and about some important research centers and experiments.

**In Chapter 2**, we discussed about various methods to solve evolution equations and their comparative study was done. We briefly discussed about the advantages and disadvantages of method of characteristics. In the subsequent Chapters we have used method of characteristics to solve both unpolarized and polarized DGALP evolution equations to get deuteron, proton,

neutron and gluon structure functions at small- $x$ .

**In Chapter 3**, we present our solutions of unpolarized DGLAP evolution equations for singlet and non-singlet structure functions at small- $x$  in LO. The  $t$  and  $x$ -evolutions of deuteron and non-singlet (combination of proton and neutron) structure functions, thus obtained, have been compared with NMC deuteron data, E-665 data, CLAS Collaboration data and NNPDF Collaboration parameterization.

**In Chapter 4**, our solutions of unpolarized DGLAP evolution equations for singlet and non-singlet structure functions at small- $x$  in NLO are obtained. The  $t$  and  $x$ -evolutions of deuteron and non-singlet structure functions, thus obtained, have been compared with NMC deuteron data, E-665 data, CLAS Collaboration data and NNPDF Collaboration parameterization. Also these results are compared with our LO results from Chapter 3.

**In Chapter 5**, our solutions of unpolarized DGLAP evolution equations for singlet and non-singlet structure functions at small- $x$  in NNLO are obtained. The  $t$  and  $x$ -evolutions of deuteron and non-singlet structure functions thus obtained have been compared with NMC deuteron data, E-665 data, CLAS Collaboration data and NNPDF Collaboration parameterization. Also these results are compared with our LO and NLO results from Chapter 3 and Chapter 4 respectively.

**In Chapter 6**, our solutions of polarized DGLAP evolution equations for singlet and non-singlet structure functions at small- $x$  in LO are obtained. The  $t$  and  $x$ -evolutions of polarized deuteron and non-singlet structure functions, thus obtained, have been compared with E-143 at SLAC experimental data, SMC and COMPASS Collaboration data.

**In Chapter 7**, our solutions of polarized DGLAP evolution equations for singlet and non-singlet structure functions at small- $x$  in NLO are obtained. The  $t$  and  $x$ -evolutions of polarized deuteron and non-singlet structure functions,

thus obtained, have been compared with E-143 at SLAC experimental data, SMC and COMPASS Collaboration data. Our NLO results are also compared with LO results obtained from Chapter 6.

**In Chapter 8**, we present solution of unpolarized DGLAP evolution equations for gluon distribution functions at small- $x$  in LO and NLO. The  $t$  and  $x$ -evolutions of unpolarized gluon distribution functions thus obtained have been compared with GRV1998 and MRST2004 gluon parameterizations.

**In Chapter 9**, we present polarized DGLAP evolution equations for gluon distribution functions at small- $x$  in LO and NLO. The  $t$  and  $x$ -evolutions of polarized gluon distribution functions thus obtained have been compared with the graph obtained by B. Ziaja with the help of numerical method.


**In Chapter 10**, we include the overall conclusion drawn from our work.



## DECLARATION

I hereby declare that the thesis entitled "**Studies on Solution of Evolution Equations for Unpolarized and Polarized Hadron Structure Functions**" being submitted to Tezpur University, Tezpur, Assam in partial fulfillment of the requirements for the award of the degree of Doctor of Philosophy, has previously not formed the basis for the award of any degree, diploma, associateship, fellowship or any other similar title or recognition.

Date : 29-7-2010  
Place : Napaam, Tezpur

  
(Ranjit Baishya)  
Department of Physics  
Tezpur University  
Tezpur-784 028 (Assam)

## CERTIFICATE

**Dr. Jayanta Kumar Sarma**  
Professor  
Department of Physics  
Tezpur University  
Napaam, Tezpur- 784 028  
Assam, India

This is to certify that **Ranjit Baishya** has worked under my supervision and the thesis entitled "**Studies on Solution of Evolution Equations for Unpolarized and Polarized Hadron Structure Functions**" which is being submitted to Tezpur University in partial fulfillment of the requirements for the degree of Doctor of Philosophy, is a record of original bonafide research work carried out by him. He has fulfilled all the requirements under the Ph. D. rules and regulations of Tezpur University. Also, to the best of my knowledge, the results contained in the thesis have not been submitted in part or full to any other university or institute for award of any degree or diploma.

Date : 29.7.10  
Place : Napaam, Tezpur

  
(Dr. Jayanta Kumar Sarma)  
Supervisor

(Dr. J.K. Sarma)  
Research Supervisor  
Dept of Physics  
TEZPUR UNIVERSITY

## *Preface*

*This thesis deals with proton, neutron and deuteron structure functions determined from deep inelastic scattering experiments approximated for high  $Q^2$  and small- $x$  region. Structure functions have been calculated from solutions of well known DGLAP evolution equations which were deduced from perturbative quantum chromodynamics. Theoretical predictions of  $t$  and  $x$ -evolutions of structure functions at small- $x$  region have been compared with experimental data and parameterizations. In the first part of the thesis, the unpolarized singlet and non-singlet structure functions have been obtained up to next-to-next-to-leading order. Similarly, in the second part, the polarized singlet and non-singlet structure functions and in the third part the unpolarized and polarized gluon distribution function have been obtained up to next-to-leading order and obtained results have been compared with various leading experimental data as well as recent global parameterizations.*

*I cannot express in words to offer my gratitude to my research supervisor Professor Jayanta Kumar Sarma whose invaluable guidance with an expert hand brought me the proper path of knowledge in physics especially in High Energy Physics. Without his invaluable assistance in research and scientific discussion I could not develop this thesis. His encouragement and advice are manifest in this research work. At this moment I am deeply grateful to him for his valuable input.*

*I never forget to thank Tezpur University for providing me the research facility and would like to take the opportunity to thank all administrative staff for helping me throughout this research period. With immense pleasure, I*

*would like to express my profound sense of gratitude to all faculty members of Physics Department, Tezpur University for their inspiration and encouragement during this research work.*

*I would like to acknowledge the help I received from Bobby Baidew, Maini Mahi and Dr Biren Das who were constant sources of inspiration to me. I express my sincere thanks to Dr Anjan Bhatta, Dr Tapan Deka and all the faculty members of J. N. College, Boko for contributing their seasoned perspectives in this research work.*

*I would like to thank all my friends and colleagues of Tezpur University specially Sanjeev, Momee, Abu, Upamanyu, Ankur, Sourav, Mayuree, Sovan, Nayanmoni, Rathin, Ghanada and Narayan for their company, help and goodwill. My warm appreciation goes to Dada Gobinda Baishya, Baidew-Bhindew Abala Baishya, Lohit Das, Purnima Baishya, Ramesh Das, Mother-Father (In-law) Jamini Roy, Madan Roy, Bhaskar, Utpal, Shewali, Dalim, Ranjan, Pranab, Babu, Baba, Kuhi and a number of friends and well wishers who extended their helpful hands in a variety of ways and for their love, inspiration and close friendship, I offer my heartiest thanks to all of them.*

*Last but not least, I must acknowledge my family members for providing communal support and good humor, made this work possible. Particularly my beloved wife Anju is the unseen partner in my labour, without whose constant encouragement and inspiration, I could not have completed this work properly. In the long run, I offer my profound love to my little master Nrupal, whose melodious tunes and lovable expressions give me immense happiness and refreshment.*

*Date: 29-7-2010*

*Ranjit Baishya*

# STUDIES ON SOLUTION OF EVOLUTION EQUATIONS FOR UNPOLARIZED AND POLARIZED HADRON STRUCTURE FUNCTIONS

## Contents

### 1. Introduction

1.1 Basic Building Blocks of Matter	1
1.2 The Standard Model of Elementary Particles	5
1.3 Quantum Chromodynamics and Small- $x$ Physics	10
1.4 Deep Inelastic Scattering and Bjorken Scaling	12
1.5 Structure Functions	14
1.6 Quark Parton Model	16
1.7 Evolution Equations	19
1.8 Particle Accelerator Centres	27
1.9 Phenomenology	34

### 2. Solution of Evolution Equations

2.1 Brute force method	37
2.2 Laguerre polynomial method	38
2.3 Mellin transformation method	40
2.4 Matrix approach method	41
2.5 Taylor Expansion and particular solutions method	43
2.6 Regge theory method	45
2.7 Method of characteristics	48

## Part I: Unpolarized Hadron Structure Functions

### 3. Unpolarized DGLAP Evolution Equations in Leading Order

3.1 Theory	52
3.2 Results and Discussions	58
3.3 Conclusion	71

### 4. Unpolarized DGLAP Evolution Equations in Next-to-Leading Order

4.1 Theory	72
4.2 Results and Discussions	75
4.3 Conclusion	88

<b>5. Unpolarized DGLAP Evolution Equations in Next-Next-to-Leading Order</b>	
5.1 Theory	90
5.2 Results and Discussions	93
5.3 Conclusion	102
<b>Part II: Polarized Hadron Structure Functions</b>	
<b>6. Polarized DGLAP Evolution Equations in Leading Order</b>	
6.1 Theory	104
6.2 Results and Discussions	110
6.3 Conclusion	119
<b>7. Polarized DGLAP Evolution Equations in Next-to-Leading Order</b>	
7.1 Theory	120
7.2 Results and Discussions	124
7.3 Conclusion	130
<b>Part III: Gluon Distribution Functions</b>	
<b>8. Unpolarized Gluon Distribution Functions in Leading and Next-to-Leading Order</b>	
8.1 Theory	132
8.2 Results and Discussions	135
8.3 Conclusion	144
<b>9. Polarized Gluon Distribution Functions in Leading and Next-to-Leading Order</b>	
9.1 Theory	146
9.2 Results and Discussions	148
9.3 Conclusion	152
<b>10. Conclusions</b>	153
<b>Bibliography</b>	155
<b>Appendices</b>	164
<b>Publications</b>	172
<b>Addenda</b>	

## Introduction

### 1.1 Basic Building Blocks of Matter

The desire to identify the smallest constituents of matter is indeed very old thought. Since ancient time, people have been fascinated by some questions of the ultimate structure of matter e.g. are there fundamental, indivisible particles and if so, what are they? How do they behave? How do they group together to form the matter that we see? How do they interact with each other? According to Hindu mythology, there were five elements – fire, water, air, earth and sky. The great Philosopher Aristotle believed that there were just four elements – earth, air, fire and water, whose indefinitely large number of combinations were accounted for all things (Figure 1.1). In the fifth century B.C., a Greek named Empedocles took the ideas of several others before him and combined them to say that matter is made up of earth, wind, fire, water and that there are two forces – Love and Strife, that govern the way they grow and act. More scientifically, he was saying that matter is made of smaller substances that interact with each other through repulsion and attraction. Democritus, a contemporary of Empedocles, went a step further to say that all matter is made of fundamental particles that are indestructible. He called these particles as ‘Atoms’ - meaning indivisible [1]. Gradually the rules of what constitutes a satisfactory theory of sub-structure have changed throughout the ages, but one seemingly constant demand is that the different elementary objects at the substructure level should number at a few.

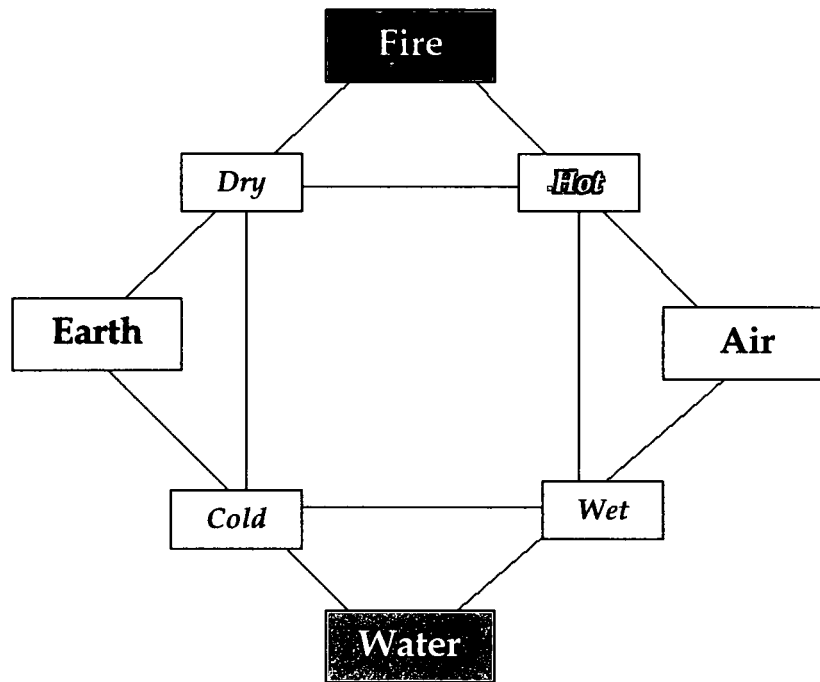


Figure 1.1: Aristotle's view of substructure

Elementary Particle Physics is perhaps the most fundamental of all the sciences. The very concept of elementariness conveyed in particle physics, means no internal structure or most fundamental building blocks of matter. With the passage of time, the concept of elementariness gradually changes. It is a relative concept subject to the progress in experimental techniques which can probe deeper and deeper in size or equivalently at higher and higher energy regime. The first scientific approach to substructure was John Dalton's atomic theory, proposed in the year 1809. The growth in the number of different atoms till today from Dalton's day, also suggested that the atoms were perhaps not as indivisible as Dalton had supposed. The Mandel's classification of atoms also pointed to some underlying simplicity of substructure. The final clue was the observation made by J J Thompson in 1897 those electrons were constituents of many different substances. In 1911, Rutherford's  $\alpha$  - particle experiment and in 1913 Neil Bohr's bold hypothesis of angular momentum quantization in an allowed orbit of revolving electron around the nucleus had explained the stable



atomic model. After discovery of neutron in 1932 by James Chadwick, the neutron - proton picture of the nucleus had clearly understood [2, 3, 4]. The scenario of basic building blocks of matter is changed as the numbers of elementary particles have been discovered day by day. The elementary particles that discovered up to 1960 are listed in Table 1.1.

Spin	Symbol	Generic name	Elementary?
0	$\pi^+, \pi^-, \pi^0, K^+, K^-, \dots$	Scalar mesons	No
1/2	$e, \mu, \nu_e, \nu_\mu$	Leptons	Yes
	$p, n, \Lambda, \Sigma, \dots$	Baryons	No
1	$\gamma$	Photon	Yes
	$\rho, \omega; \dots$	Vector Mesons	No
3/2	$\Delta^{++}, \Delta^+, \Delta^0, \Delta^-, \Xi^0, \Xi^-, \dots$	Baryon	No

**Table 1.1:** Elementary Particles in 1960

Our concept on the basic constituents of matter has changed during last century after two revolutionary experiments. The first was the Rutherford scattering experiment of 1911, bombarding  $\alpha$  - particle on the gold atoms. While most of them passed through straight, occasionally a few were deflected at very large angles. Rutherford scattering experiment showed the atom to consist of a hard compact nucleus, surrounded by a cloud of electrons. The nucleus was found later to be made up of protons and neutrons. The second experiment was the electron-proton scattering experiment of 1968 at the Stanford Linear Accelerator Centre. This was essentially a repeat of the Rutherford scattering type experiment, but at a much higher energy. It was again clear from the pattern of large angle scattering that the proton is itself made up of three compact objects called quarks. The proton was found later to be made up of two up quarks and one down quark, while the neutron consists of two down quarks and one up quark.

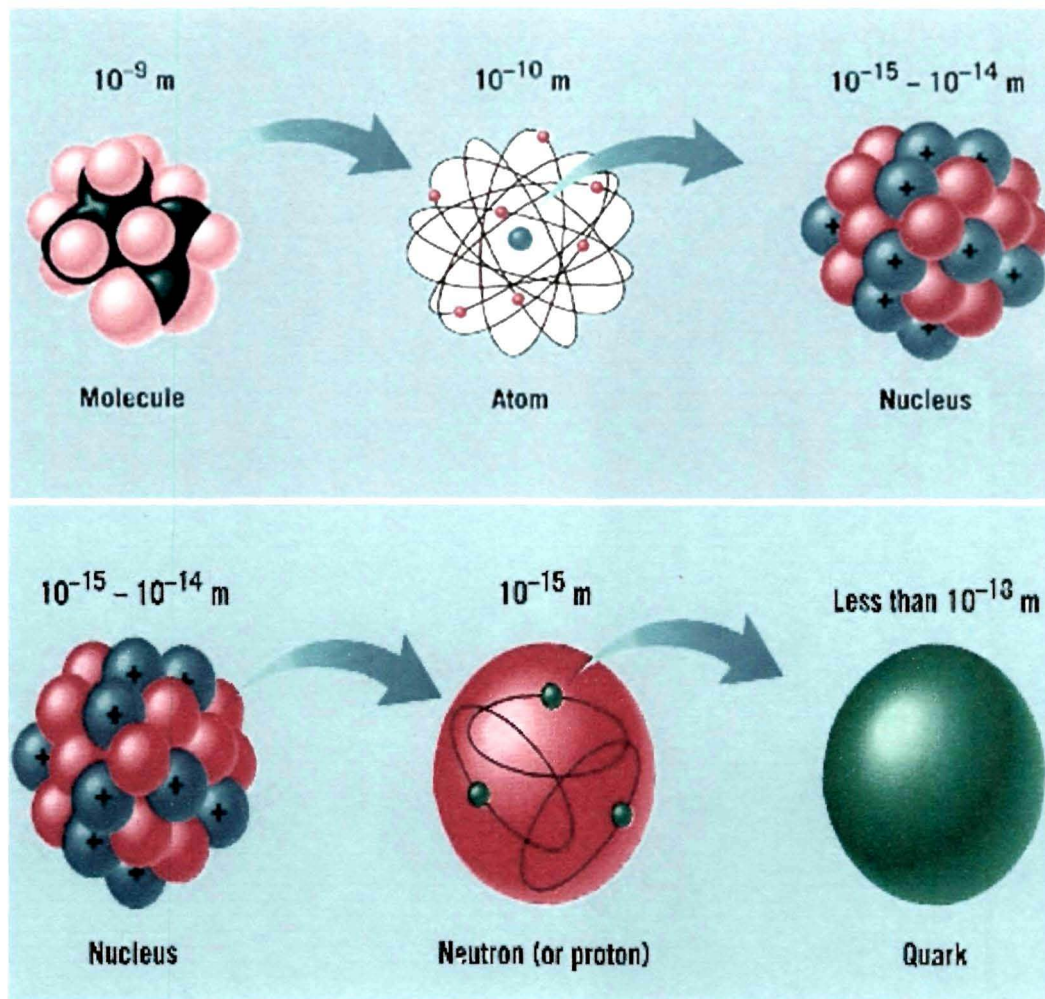


Figure 1.2: Dimensional representation of building blocks of matter

The main difference between the Rutherford and the electron-proton scattering experiments comes from the fact that, the dimension of the atom is typically  $1\text{\AA} = 10^{-10}$  m that of the proton is about  $1\text{fm} = 10^{-15}$  m (Figure 1.2). The Uncertainty Principle says that,  $\Delta E \cdot \Delta x \geq \hbar c \approx 0.2 \text{ GeV} \cdot \text{fm}$ , the smaller the distance we want to probe the higher must be the beam energy. Thus probing inside the proton ( $x \ll 1\text{fm}$ ) requires a beam energy  $E \gg 1 \text{ GeV}$ , which is the energy acquired by the electron on passing through a giga volts. It is this multi giga electron volt acceleration technique that accounts for the half a century gap between the two experiments.

We now, know that the nuclear particles i.e. proton, neutron and mesons, which are collectively called hadrons, are all made up of quarks - they are all quark atoms. The up and down quarks are the constituents of proton and neutron, together with the electron they constitute all the visible matter around us. The heavier quarks and charged leptons all decay into the lighter ones via interactions analogous to the muon decay. So they are not freely occurring in nature. But they can be produced in laboratory or cosmic ray experiments. The muon and the strange quark were discovered in cosmic ray experiments in the late forties, the latter in the form of K-meson. Next to come were the neutrinos. Although, practically massless and stable; the neutrinos are hard to detect because they interact only weakly with matter. The electron neutrino was discovered in atomic reactor experiment in 1956, for which Reines got the Nobel Prize in 1995. The muon neutrino was discovered in the Brookhaven proton synchrotron in 1962, for which Lederman and Steinberger got the Nobel Prize in 1988. The first cosmic ray observation of neutrino came in 1965, when the muon neutrino was detected in the Kolar Gold Field experiment. The rest of the particles have all been discovered during the last 40 years, at the experiments performed by the electron-positron and the antiproton-proton colliders. The quick successions of discoveries mainly at the  $e^-e^+$  colliders were charm quark (1974), Tau lepton (1975), bottom quark (1977) and the evidence for gluons, the carrier of the force between quarks, came out in 1978 from an electron - positron machine, called PETRA, at Hamburg in Germany which is able to observe collisions up to 30 GeV. This was followed by the discovery of W and Z bosons (1983) and finally the top quark (1995) at the proton antiproton colliders [5, 6, 7].

## 1.2 The Standard Model of Elementary Particles

As per our present understanding, the basic constituents of matter are a dozen of spin half particles (fermions) along with their antiparticles. These are

the three pairs of leptons like electron, muon, tau and their associated neutrinos and three pairs of quarks e.g. down - up, strange - charm and bottom - top. Apart from the electric charge the quarks also possess a new kind of charge called colour charge. This is relevant for their strong interaction, which binds them together inside the nuclear particles i.e. hadrons. There are two types of hadrons - meson and baryon. Quarks observed bound together in pair quark - antiquark, forming particles called mesons or in threes, forming particles called baryons. All quarks and leptons with their rest masses are listed in Table 1.2.

	1 <sup>st</sup> Generation	2 <sup>nd</sup> Generation	3 <sup>rd</sup> Generation	Electric Charge
Leptons	Electron (e) m = 0.511 MeV	Muon ( $\mu$ ) m=105.7MeV	Tau ( $\tau$ ) m=1.777 GeV	-1
	Electron Neutrino ( $\nu_e$ ) m < 2.2MeV	Muon-Neutrino ( $\nu_\mu$ ) m < 0.17 MeV	Tau- Neutrino ( $\nu_\tau$ ) m < 15.5 MeV	0
Quarks	Down (d) m = 4.8 MeV	Strange (s) m = 104 MeV	Bottom (b) m = 4.2 GeV	$-\frac{1}{3}$
	Up (u) m = 2.4 MeV	Charm (c) m = 1.27 GeV	Top (t) m = 171.2 GeV	$\frac{2}{3}$

**Table 1.2:** Lepton and Quark family with their rest masses

Two terms are used in referring to a quark's mass: 'current quark mass' refers to the mass of a quark by itself, while 'constituent quark mass' refers to the current quark mass plus the mass of the gluon particle field surrounding the quark [8]. These masses typically have very different values. Most of a hadron's mass comes from the gluons that bind the constituent quarks together, rather than from the quarks themselves. While gluons are inherently mass less, they

possess energy – more specifically, Quantum Chromodynamics Binding Energy (QCBE) – and it is this that contributes so greatly to the overall mass of the hadrons. For example, a proton has a mass of approximately 938 MeV, of which the rest mass of its three valence quarks only contributes about 10 MeV; much of the remainder can be attributed to the gluons' QCBE [9, 10].

According to Standard Model, there are four basic interactions among these particles - strong, electromagnetic, weak and gravitational. Apart from gravitation, which is too weak to have any practical effect on quarks interaction but having for massive bodies, the other three are all gauge interactions. They are all mediated by spin one particles called gauge bosons, whose interactions are completely specified by the corresponding gauge groups. Of these, our everyday world is controlled by gravity and electromagnetism (Figure 1.3). The strong force binds quarks together and holds hadrons. The weak force is responsible for the radioactive decay of unstable nuclei and for interactions of neutrinos and other leptons with matter. The intrinsic strengths of the forces can be compared relative to the strong force, here considered to have unit strength. In these terms, the electromagnetic force has an intrinsic strength of  $(1/137)$ . The weak force is a billion times weaker than the strong force. The weakest of them all is the gravitational force. This may seem strange, since it is strong enough to hold the massive Earth and planets in orbit around the Sun. Forces can be represented in the theory as arising from the exchange of specific particles called gauge bosons, the quanta of the force field. Just as photons are real i.e. quanta of light and can be radiated when charged particles are accelerated, the other gauge bosons can also be created and observed as real particles. All the bosons have zero or integer spins. The carriers of the strong force are called gluons, that hold quarks together in protons or neutrons and also helps form nuclei. The carriers of the weak force come in three forms, and are called weak bosons the  $W^+$ ,  $W^-$  and  $Z^0$ . The carriers of the gravitational field are called gravitons and are unique in having a spin of two.

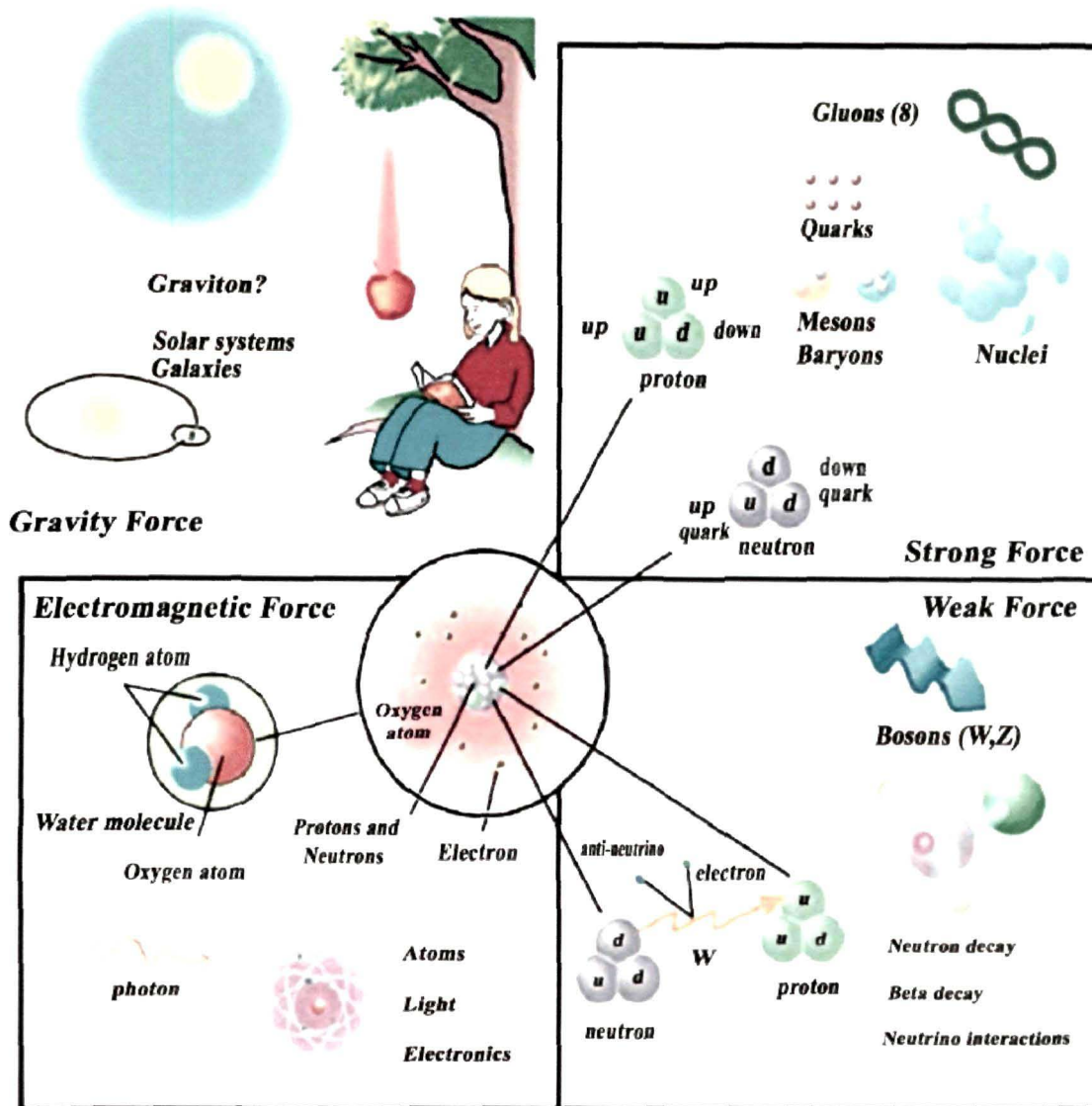


Figure 1.3: Schematic diagram of fundamental forces

The Standard Model was the great achievement of particle physics of the 1970's. It incorporated all that was known at that time and has since then successfully predicted the outcome of a large variety of experiments. Today, the Standard Model is a well established theory applicable over a wide range of conditions and according to total angular momentum ( $J$ ), the whole numbers of

elementary particles is classified into four groups and concept of elementary particles is listed in the Table 1.3. [11]

J	Symbol	Generic name	Observed
0	H	Higgs scalar	No
1/2	$e, \mu, \tau, \nu_e, \nu_\mu, \nu_\tau$	Leptons	Yes
	$u, d, c, s, t, b$	Quarks	Yes
1	$\gamma$	Photon	Yes
	$g$	Gluons(8)	Yes
	$W^+, W^-, Z^0$	Vector Mesons	Yes
2	G	Graviton	No

Table 1.3: Elementary particles in 2009

The Higgs boson is a massive scalar elementary particle predicted to exist by the Standard Model in particle physics. At present there are no known fundamental scalar particles in Nature. The Higgs boson is the only Standard Model particle that has not yet been observed. It is believed that Higgs boson couples strongly to the top quark so it may decay into top- antitop quark pairs. Experimental detection of the Higgs boson would help to explain the origin of mass in the universe. More specifically, the Higgs boson would explain the difference between the mass less photon, which mediates electromagnetism, and the massive W and Z bosons, which mediate the weak force. If the Higgs boson exists, it is an integral and pervasive component of the material world. The Large Hadron Collider (LHC) at CERN is expected to provide experimental evidence either confirming or refuting the Higgs boson's existence.

The Higgs mechanism, which gives mass to vector bosons, was theorized in 1964 by F. Englert and R. Brout [12]. In October of the same year, P. Higgs [13] worked from the ideas of P. Anderson also independently by G. Guralnik, C. R. Hagen, and T. Kibble [14], who worked out the results by the spring of 1963 [15]. The three papers written on this discovery by Guralnik, Hagen, Kibble, Higgs, Brout, and Englert were each recognized as milestone papers during Physical Review Letters 50th anniversary celebration [16]. Steven Weinberg and Abdus Salam were the first to apply the Higgs mechanism to the electroweak symmetry breaking. The electroweak theory predicts a neutral particle whose mass is not far from that of the W and Z bosons.

### 1.3 Quantum Chromodynamics and small-x Physics

The strong force is subject to the particles have properties called colour. The field theory that describes, this is called Quantum Chromodynamics (QCD) [17] and was first proposed in 1965 by Han, Nambu and Greenberg. This theory predicts the existence of the gluon, which is the mediator of the strong force between two matter particles. The common model of quark and gluon interactions is an SU(3) gauge theory, arbitrarily called 'colour' [18]. According to QCD, quarks carry any one of the colours - red (R), blue (B) or green (G). Anti-quarks carry anti-colours - anti-red (cyan  $\bar{R}$ ), anti-blue (yellow  $\bar{B}$ ) and anti-green (magenta  $\bar{G}$ ). The eight gauge fields associated with the eight SU (3) generators are called Gluons and we can label each gluon as follows:

$$g_{\alpha}^{\beta} = \begin{pmatrix} R\bar{R} & R\bar{G} & R\bar{B} \\ G\bar{R} & G\bar{G} & G\bar{B} \\ B\bar{R} & B\bar{G} & B\bar{B} \end{pmatrix}.$$

Here the upper index is the anti-colour index and denotes the column of the matrix and the lower index is the colour index denoting the row of the matrix.



Then consider the gluon  $g_R^G = \begin{pmatrix} 0 & 1 & 0 \\ 0 & 0 & 0 \\ 0 & 0 & 0 \end{pmatrix}$ ,

and quarks are  $q_R = \begin{pmatrix} 1 \\ 0 \\ 0 \end{pmatrix}$ ,  $q_G = \begin{pmatrix} 0 \\ 1 \\ 0 \end{pmatrix}$  and  $q_B = \begin{pmatrix} 0 \\ 0 \\ 1 \end{pmatrix}$ .

It is easy to see that this gluon will interact as  $g_R^G q_R = 0$ ,  $g_R^G q_G = q_R$ ,  $g_R^G q_B = 0$ . Or, in other words, the gluon with the anti-green index will only interact with a green quark. There will be no interaction with the other quarks. As the quarks are assigned to a triplet of an SU (3) colour group, SU (3) colour symmetry is expected to be exactly conserved. The gluons, which mediate the QCD force between colour charges, come in eight different colour combinations:  $R\bar{G}$ ,  $R\bar{B}$ ,  $G\bar{R}$ ,  $G\bar{B}$ ,  $B\bar{R}$ ,  $B\bar{G}$ ,  $\sqrt{1/2}(R\bar{R} - G\bar{G})$  and  $\sqrt{1/6}(R\bar{R} + G\bar{G} - 2B\bar{B})$  i.e. the gluons belong to an SU (3) colour octet. The remaining combination of the SU(3) colour singlet  $\sqrt{1/3}(R\bar{R} + G\bar{G} + B\bar{B})$  does not carry colour and can not mediate between colour charges [19-21]. The cancellations of the colour charges of quarks ensure that the nuclear particles composed of them are colour neutral. The gluons themselves carry colour charge and hence have self-interaction unlike the photons, which have no electric charge hence no self-interaction (Figure 1.4).

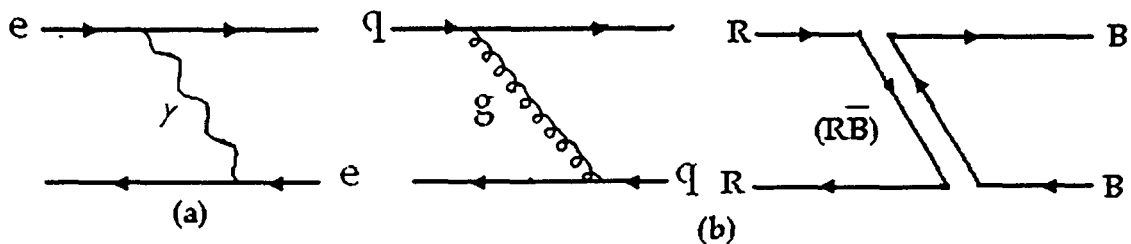


**Figure 1.4:** (a) Electromagnetic interaction by photon exchange, (b) Strong interaction by gluon exchange and flow of colour

Small- $x$  (the four momentum fraction carried by the struck quark) physics is comparably a new and exciting field of lepton-nucleon scattering. The behavior of the parton distributions of the hadrons in this small- $x$  region is of considerable importance both theoretically and phenomenologically. First, the predictions of the rates of various processes at the high energy hadrons colliders depend on the parton densities at small- $x$ . According to QCD, at small- $x$  and large- $Q^2$  (square of the exchanged four momentum or virtuality of photon), a nucleon consists predominantly of gluons and sea quarks. Their densities grow rapidly in the limit  $x \rightarrow 0$  leading to possible spatial overlap and to interactions between the partons i.e. at small- $x$ , the structure function is proportional to the sea quarks density. At large values of  $Q^2$ , i.e. at small scale distance, DIS probes the constituents of the hadron (i.e. quarks), not the hadron as a whole. Here, the quarks act as almost free particles and because the interactions are relatively weak at those scales, perturbative Quantum Chromodynamics (pQCD) techniques can be used for DIS. A typical lower- $Q^2$  limit, for which pQCD is applicable, is  $1 \text{ GeV}^2$ .

## 1.4 Deep Inelastic Scattering and Bjorken Scaling

The direct evidence for the existence of quarks inside the hadrons and the first information on the nature of quark-quark interactions are provided by Lepton-nucleon Deep Inelastic Scattering (DIS). The DIS is the process, in which constituents of the hadrons are probed, by means of lepton-hadron scattering. The interaction is 'Inelastic' when a lepton is knocked out of the proton and the proton is broken up. It is called 'Deep' when the proton is probed with a gauge boson with small wavelength, resolving small distance scale. Here the lepton enters the proton deeply, and knocked out one of the quarks, provided that the lepton had sufficient energy. To reach high enough energy, the leptons need to be accelerated in enormous particle colliders. The first deep inelastic scattering experiments were done in 1968 at the Stanford Linear Accelerator Centre (SLAC) in California where electrons of  $7 \text{ GeV}$  were collided with a hydrogen

target. The schematic picture of the neutral current DIS, where neutral bosons  $\gamma$  or  $Z^0$  are exchanged between the lepton and the quark is shown in Figure 1.5.

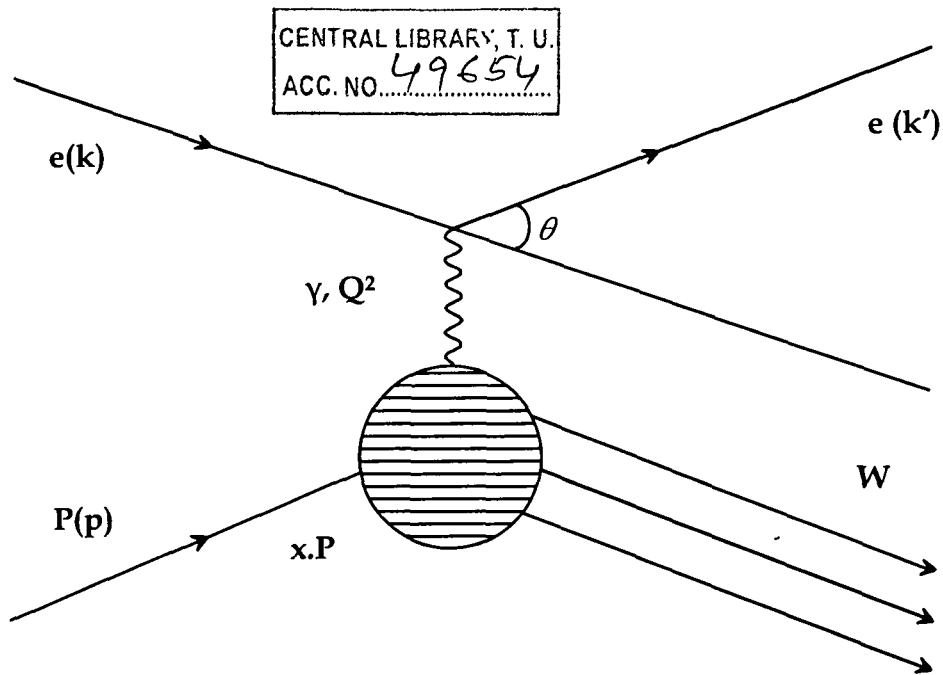


Figure 1.5: Four vector of incoming and outgoing particle in DIS and most commonly used variables in DIS kinematics

In the kinematics of the DIS, the most commonly used variables are:

- $Q^2 \equiv -q^2 = (k - k')^2$ : Square of the exchanged four momentum or virtuality of photon.
- $x \equiv \frac{-q^2}{2P \cdot q}$ : The Bjorken scaling variable defined as the four momentum fraction carried by the struck quark.
- $y \equiv \frac{P \cdot q}{P \cdot k}$ : Inelasticity defined as the fraction of the initial lepton energy transferred to the boson.
- $W^2 \equiv (P + q)^2$ : Square of the invariant mass of the hadronic final state.

These four kinematics variables are not independent, the interaction is characterised by only two independent variables  $x$  and  $Q^2$ . Neglecting the masses of the electron,  $Q^2$ ,  $x$  and  $y$  are related through:  $Q^2 = s \cdot x \cdot y$ , with  $s$  the centre of mass energy squared of the electron proton system, whereas the mass of the hadronic final state,  $W$ , is related to  $x$  and  $Q^2$  through:  $W^2 = Q^2 (1-x)/x + m_p^2$ , where  $m_p$  is the mass of the proton. In 1969, Bjorken proposed that in the limit  $Q^2 \rightarrow \infty$ ,  $W^2 \rightarrow \infty$ ,  $x$  is fixed. At fixed  $x$  (scaling variable), the scattering is independent of  $q^2$ . This suggests that the probing 'virtual photon' scatters against something point like called parton. The kinematics variables describe above, have a limited range of allowed values as  $0 < Q^2 < s$ ,  $0 < x < 1$ ,  $0 < y < 1$ ,  $m_p < W < \sqrt{s}$ . In DIS, three types of events are distinguished: (i) inclusive events, where only the scattered lepton is detected; (ii) semi-inclusive events, where apart from the lepton also a hadron is detected; and (iii) exclusive events, where all reaction products are identified.

## 1.5 Structure Functions

Hadron structure functions are very useful entities in the study of structure of hadrons as well as their interactions. It is a mathematical picture of hadron's structure at high energy region. The precise determination of the partonic structure of the proton is very important. The parton distributions are determined by the values of the structure functions. The determination of structure functions and their comparison with experimental results are important tests for QCD.

The unpolarized DIS [19] cross section can be expressed in three independent structure functions  $F_1$ ,  $F_2$  and  $F_3$ :

$$\frac{d^2\sigma}{dQ^2 dx} = \frac{2\pi\alpha^2}{xQ^2} [2xy^2 F_1(x) + 2(1-y)F_2(x) - (2y+y^2)x F_3(x)]. \quad (1.1)$$

Here  $\alpha = e^2/4\pi\hbar c \approx 1/137$ , is the fine structure constant. These three structure functions give information on the number and properties of quark and gluon

constituents in the proton. The structure function  $F_1$  is proportional to the transverse component of the cross section, whereas the difference of  $F_2$  and  $F_1$  gives the longitudinal part of the cross section. The longitudinal part of the cross section is suppressed, because of the spin  $\frac{1}{2}$  nature of the quark. Omitting the longitudinal part of the cross section results in the Callan - Gross Relation:

$$2xF_1(x) = F_2(x). \quad (1.2)$$

Here

$$F_2(x) \equiv vW_2(v, Q^2) = \sum_i e_i^2 x f_i(x), \quad (1.3)$$

$$F_1(x) \equiv MW_1(v, Q^2) = \frac{1}{2x} F_2(x). \quad (1.4)$$

Here  $W_1$  and  $W_2$  are dimensionless structure functions,  $M$  is the total mass of hadron and  $f_i(x)$  is the probability density of finding the  $i$ -th parton with fractional momentum  $x$  and charge  $e_i$ . The structure function  $F_3$ , often referred to as  $xF_3$  contains the parity violating part of the cross section. Since the electromagnetic coupling conserves parity, this term can be neglected at low- $Q^2$ , where photon exchange dominates the cross section.

Similar to the unpolarized structure functions  $F_1$  and  $F_2$ , the polarized structures functions  $g_1$  and  $g_2$  contain information on the helicity dependent contribution to the DIS cross section. To access these structure functions, a polarized target and a polarized beam are needed. Results are obtained by measuring the difference in cross section for a parallel or anti-parallel orientation of the spins of the struck nucleon and the lepton. A measure for the helicity dependent contributions to the cross section is obtained by evaluating the asymmetry. This is called a double spin asymmetry. Similarly, in case of a single spin asymmetry, either the target or the beam is polarized, while the other is unpolarized [22, 23, 24]. The inclusive scattering cross section gives access to longitudinally polarized structure function  $g_1$ , which is the sum of helicity distributions for different quark flavours  $\Delta q_f$  weighted by the electric charge  $e_f$  squared,  $g_1 = \frac{1}{2} \sum_f e_f^2 \Delta q_f$ .

By determining the double spin asymmetry in semi inclusive DIS for hadrons with a different quark composition, the helicity distributions of the individual quark flavors can be determined. Whereas transversely polarized structure functions  $g_2$  has contributions from quark-gluon correlations and other higher twist terms which cannot be described perturbatively. The contribution of the gluon spin  $\Delta G$  to the nucleon spin can be determined from events created in the photon-gluon fusion process, where the virtual photon interacts with a gluon from the nucleon by splitting into a quark-antiquark pair.

## 1.6 Quark Parton Model

In 1969, the point like constituents of the nucleon were termed partons by Feynman, well before quarks and gluons became established. At high- $Q^2$  the electron sees point like objects called partons and makes at elastic electron-parton scattering. Thus quark parton model is a static model, assuming free (non-interacting), and point like partons inside the proton. This assumption is confirmed by the notion of asymptotic freedom of non abelian theories: at small distance scales the strength of the force between quarks decreases rapidly. It has been shown that the quark distributions can be factored off and absorbed in universal parton distributions, a procedure known as factorisation. The cross section of elastic e-q scattering can be convoluted with the probability of finding a quark with momentum fraction between  $x$  and  $x + dx$  is  $q(x).dx$  in the proton, where  $q(x)$  is the parton densities. The proton is seen as a collection of partons and the e-p scattering cross section as an incoherent sum of the individual cross sections. Subsequently, these universal parton densities can be used in the calculation of cross section of other processes, involving protons.

The deep inelastic e-p differential cross section in the quark-parton model at low- $Q^2$  becomes:

$$\frac{d^2\sigma}{dQ^2 dx} = \frac{2\pi\pi^2}{xQ^2} [1 + (1-y)^2] F_2(x), \quad (1.5)$$

$$F_2(\mathbf{x}) = \sum_q e_q^2 [\mathbf{x}q(\mathbf{x}) + \mathbf{x}\bar{f}(\mathbf{x})], \quad (1.6)$$

where  $e_q$  is the charge of the quark.

After establishing Bjorken scaling, equations (1.3) and (1.4) become the tools for extracting further information. The sum in equation (1.3) runs over the charged partons in the proton:

$$\frac{1}{\mathbf{x}} F_2^{\text{ep}}(\mathbf{x}) = \left(\frac{2}{3}\right)^2 [\mathbf{u}^p(\mathbf{x}) + \bar{\mathbf{u}}^p(\mathbf{x})] + \left(\frac{1}{3}\right)^2 [\mathbf{d}^p(\mathbf{x}) + \bar{\mathbf{d}}^p(\mathbf{x})] + \left(\frac{1}{3}\right)^2 [\mathbf{s}^p(\mathbf{x}) + \bar{\mathbf{s}}^p(\mathbf{x})], \quad (1.7)$$

where  $\mathbf{u}^p(\mathbf{x})$  and  $\bar{\mathbf{u}}^p(\mathbf{x})$  are the probability distributions of  $u$  quarks and antiquarks within the proton. We have neglected the possibility of a sizable presence of charm and heavier quarks inside the proton. The inelastic structure functions for neutrons are experimentally accessible by scattering electrons from a deuterium target and can be expressed as:

$$\frac{1}{\mathbf{x}} F_2^{\text{en}}(\mathbf{x}) = \left(\frac{2}{3}\right)^2 [\mathbf{u}^n(\mathbf{x}) + \bar{\mathbf{u}}^n(\mathbf{x})] + \left(\frac{1}{3}\right)^2 [\mathbf{d}^n(\mathbf{x}) + \bar{\mathbf{d}}^n(\mathbf{x})] + \left(\frac{1}{3}\right)^2 [\mathbf{s}^n(\mathbf{x}) + \bar{\mathbf{s}}^n(\mathbf{x})]. \quad (1.8)$$

As the proton and neutron are members of an isospin doublet, their quark content is related. There are as many  $u$  quarks in a proton as  $d$  quarks in a neutron and so we can consider as:

$$\mathbf{u}^p(\mathbf{x}) = \mathbf{d}^n(\mathbf{x}) \equiv \mathbf{u}(\mathbf{x}); \quad \mathbf{d}^p(\mathbf{x}) = \mathbf{u}^n(\mathbf{x}) \equiv \mathbf{d}(\mathbf{x}); \quad \mathbf{s}^p(\mathbf{x}) = \mathbf{s}^n(\mathbf{x}) \equiv \mathbf{s}(\mathbf{x}) \quad (1.9)$$

The quantum numbers of the proton must be exactly those of the  $uud$  combination of 'valence' quarks i.e. the proton as three constituents or three valence quarks  $u_v, u_v, d_v$  accompanied by many quark-antiquark pairs  $u_s, \bar{u}_s, d_s, \bar{d}_s, s_s, \bar{s}_s$  and so on. These are known as 'sea' quarks. As a first approximation, we may assume that the three lightest flavor quarks ( $u, d, s$ ) occur in the 'sea' with roughly the same frequency and momentum distribution, and neglect the heavier flavour quark pairs  $c_s, \bar{c}_s$  and so on. This picture of the proton can be summarized as follows:  $\mathbf{u}_s(\mathbf{x}) = \bar{\mathbf{u}}_s(\mathbf{x}) = \mathbf{d}_s(\mathbf{x}) = \bar{\mathbf{d}}_s(\mathbf{x}) = \mathbf{s}_s(\mathbf{x}) = \bar{\mathbf{s}}_s(\mathbf{x}) = \mathbf{S}(\mathbf{x})$ ,

$$\mathbf{u}(\mathbf{x}) = \mathbf{u}_v(\mathbf{x}) + \mathbf{u}_s(\mathbf{x}); \quad \mathbf{d}(\mathbf{x}) = \mathbf{d}_v(\mathbf{x}) + \mathbf{d}_s(\mathbf{x}), \quad (1.10)$$

where  $\mathbf{S}(\mathbf{x})$  is the sea quark distribution common to all quark flavors.

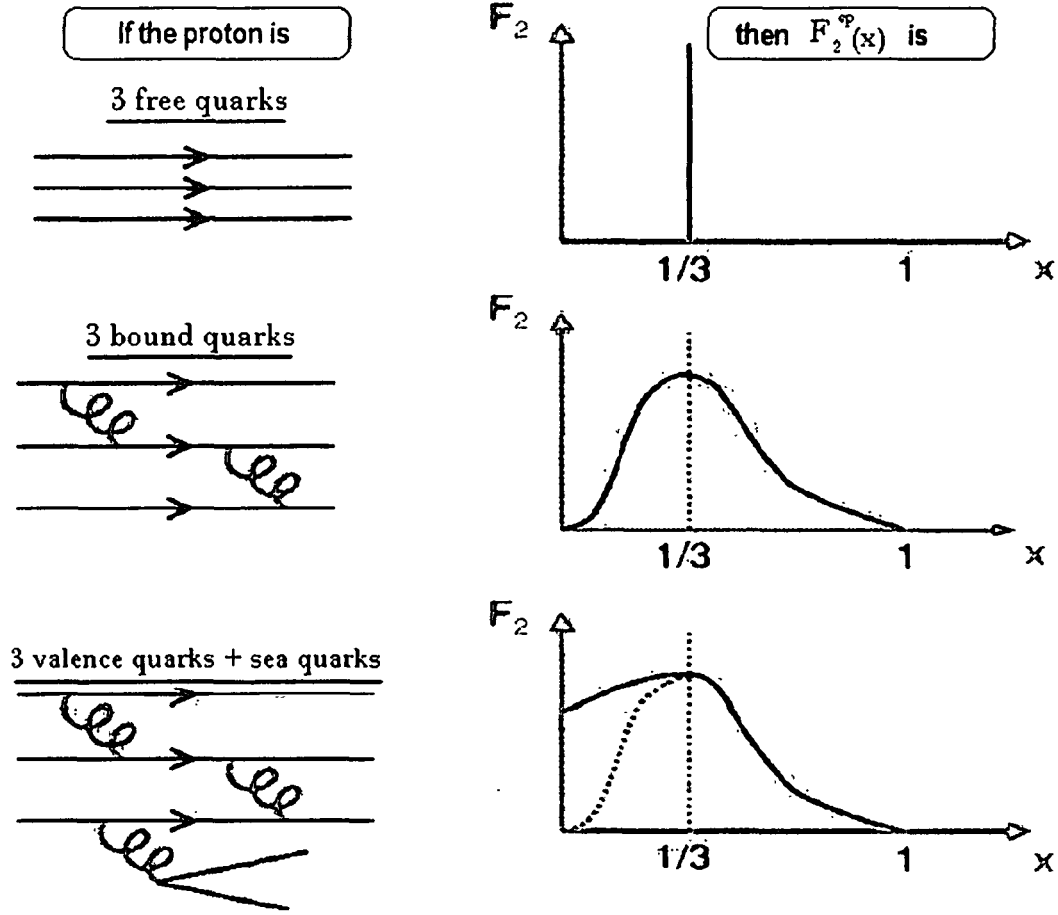


Figure 1.6: The structure function pictured corresponding to different compositions assumed for the proton

By summing over all contributing partons, we must recover the quantum numbers of the proton as: charge =1, baryon no. =1, strangeness no. = 0.

It follows that

$$\int_0^1 [u(x) - \bar{u}(x)] dx = 2; \int_0^1 [d(x) - \bar{d}(x)] dx = 1; \int_0^1 [s(x) - \bar{s}(x)] dx = 0 \quad (1.11)$$

These sum rules express the requirement that the net number of each kind of valence quark corresponds to the uud combination of constituents. The sum rules are true in any picture where the sea is taken to be made of quark-antiquark pairs, and so does not affect the quantum numbers of the proton, which are exclusively determined by the valence quarks, as expressed in equation (1.11).



Combining equation (1.10) with equations (1.7) and (1.8), we obtain:

$$\frac{1}{x}F_2^{\text{ep}}(x) = \left(\frac{1}{9}\right)[4u_v + d_v] + \left(\frac{4}{3}\right)S, \quad (1.12)$$

$$\frac{1}{x}F_2^{\text{en}}(x) = \left(\frac{1}{9}\right)[u_v + 4d_v] + \left(\frac{4}{3}\right)S, \quad (1.13)$$

where  $\frac{4}{3}$  is the sum of  $e_i^2$  over the six sea quark distributions. As gluons create the  $q\bar{q}$  pairs in the sea, so the number of sea quarks grows logarithmically as  $x \rightarrow 0$ . In Figure 1.6, the proton structure function has pictured corresponding to different compositions assumed for the proton.

## 1.7 Evolution Equations

The structure function, depends on  $Q^2$ , rises with  $Q^2$  at small values of  $x$ , and falls with  $Q^2$  at large values of  $x$ . The parton being probed may not be an 'original' constituent, but may arise from the strong interactions within the nucleon. The smaller the wavelength of the probe (i.e. the larger the scale  $Q^2$ ) the more of such quantum fluctuations can be observed and hence the amount of  $q\bar{q}$  pairs and gluons in the partonic 'sea' increases. Although, these sea partons carry only a small fraction of the nucleon momentum, their increasing number leads to a softening of the valence quark distributions as  $Q^2$  increases. Thus  $F_2$ , which contains both valence and sea quark distributions, will rise with  $Q^2$  at small- $x$ , where sea quarks dominate and fall with  $Q^2$  at large- $x$ , where valence quarks dominate. We may quantify these effects using the evolution equations, which expresses the evolution of the quark and gluon distributions. The gluon distributions of the nucleon cannot be extracted directly from the measured structure functions in DIS experiments. They mainly are predicted by using the QCD evolution equations.

At very small values of  $x$ , it is expected that the number density of parton within the hadrons becomes so large that they begin to recombine with each other. This phenomenon of parton recombination is also referred to as absorptive correction, nonlinear effects and screening, shadowing or unitarity

corrections, all leading to saturation. At small- $x$  or large- $Q^2$ , the transition of the regime described by the linear dynamics, where only the parton emissions are considered, is expected for a new regime where the physical processes of recombination of parton become important in the parton cascade. In that case, the evolution is given by a nonlinear evolution equation. Thus there are mainly two types of evolution equations – linear and non-linear evolution equations. They are the DGLAP equation (by Dokshitzer, Gribov, Lipatov, Alterelli and Parisi) [25-28], the BKFL equation (by Balitsky, Kuraev, Fadin and Lipatov) [29-31], the GLR equation (by Gribov, Levin and Ryskin) [32-34] and the CCFM equation (by Ciafaloni, Catani, Fiorani and Marchesini) [35-38]. In spite of them, some other equations are also proposed like the Modified DGLAP equation (by Zhu and Ruan) [39-43], the Modified BKFL or BK equation (by Balitsky and Kovchegov) [44, 45] and the JIMWLK equation (by Jalilian-Marian, Iancu, McLerran, Weigert, Leonidov and Kovner) [46-48] etc.

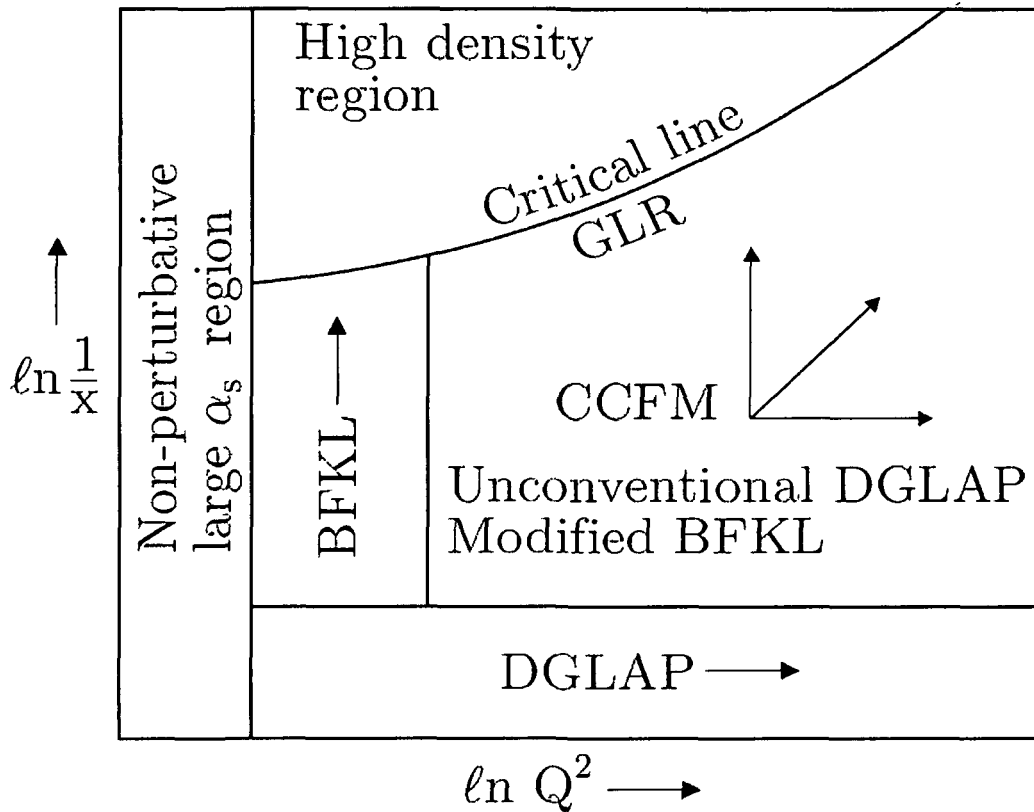


Figure 1.7: Schematic representation of the applicability of various evolution equations across the  $x$ - $Q^2$  plane

The  $Q^2$  dependence of structure functions can be calculated by using the DGLAP equations and they are successful in describing many experimental data. But, as it becomes possible to reach the small- $x$  region by high energy accelerators, it is necessary to investigate the details of small- $x$  physics. The parton in different nucleons could interact in the nucleus, and the interaction is called Parton Recombination (PR). This mechanism is used for explaining nuclear shadowing and can be explained by equations like the evolution equations proposed by Mueller and Qiu [39 -41]. Since, all stories about small- $x$  physics are written by using the QCD evolution equations, there are active field of research in modified DGLAP [42, 43] and modified BKFL [49] equations to study the small- $x$  region properly.

Modified DGLAP  $\equiv$  DGLAP + shadowing ( - ) + anti-shadowing ( + ),

Modified BKFL  $\equiv$  BKFL + shadowing ( - ) + anti-shadowing ( + ).

Here, the negative shadowing corrections are from the gluon recombination, and the suppression to the gluon splitting comes from its inverse process. The positive anti-shadowing corrections are the general conclusion of the momentum conservation. The anti-shadowing effect always co-exists with the shadowing effect in the QCD recombination processes.

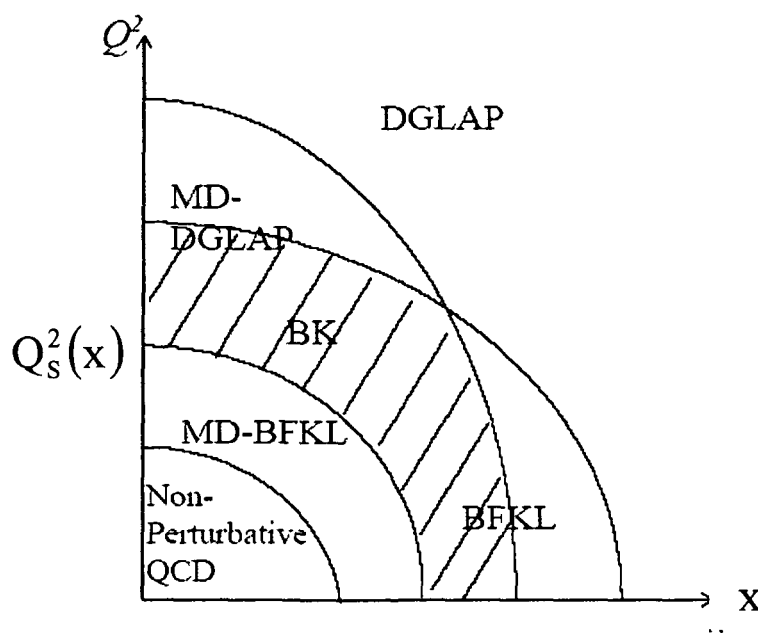


Figure 1.8: Schematic kinematics regions of modified evolution equations

### 1.7.1 DGLAP Evolution Equation

The DGLAP evolution equations for quark and gluon in Leading Order (LO) are respectively

$$\frac{\partial q_i(x, t)}{\partial t} = \frac{\alpha_s(t)}{2\pi} \int_x^1 \frac{dy}{y} \left[ \sum_i P_{qq}(x/y) q_i(y, t) + P_{qg}(x/y) g(y, t) \right], \quad (1.14)$$

$$\frac{\partial g(x, t)}{\partial t} = \frac{\alpha_s(t)}{2\pi} \int_x^1 \frac{dy}{y} \left[ \sum_i P_{gq}(x/y) q_i(y, t) + P_{gg}(x/y) g(y, t) \right]. \quad (1.15)$$

Here  $t = \ln(Q^2/\Lambda^2)$  and  $P_{qq}$ ,  $P_{qg}$ ,  $P_{gg}$ ,  $P_{gq}$  are denoting the ‘splitting functions’. The splitting functions  $P_{ij}(z)$  represent the probability of a parton  $j$  (quark or gluon) emitting a parton  $i$  with momentum fraction  $z$  of that of the parent parton, when the scale changes from  $Q^2$  to  $Q^2+d(\ln Q^2)$  [27]. In the equation (1.14), the first term mathematically expresses the fact that a quark with momentum fraction  $x$  [ $q(x, Q^2)$  on the left hand side] could have come from a parent quark with a larger momentum fraction  $y$  [ $q(y, Q^2)$  on the right-hand side] which has radiated a gluon. The probability is proportional to  $\alpha_s(t)P_{qq}(x/y)$ . The second term considers the possibility that a quark with momentum fraction  $x$  is the result of  $q\bar{q}$  pair creation by a parent gluon with momentum fraction  $y$  ( $>x$ ). The probability is proportional to  $\alpha_s(t) P_{qg}(x/y)$ . The integral in the equation is the sum over all possible momentum fractions  $y$  ( $>x$ ) of the parent [19]. For gluon we have given a symbolic representation of the gluon evolution equation (1.15) as in Figure 1.9.

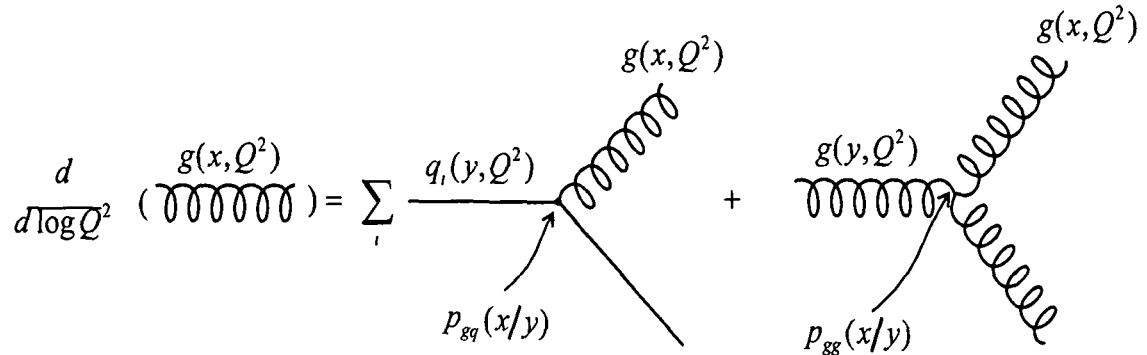


**Figure 1.9:** Symbolic representation of the gluon evolution equation in LO

The DGLAP evolution equation comes in the Leading Logarithmic  $Q^2$  (LLQ<sup>2</sup>) approximation by keeping only leading powers of  $\ln Q^2$  (i.e.  $\alpha_s^n \ln^n Q^2$ ) terms in the perturbative expansion. Figure 1.10 gives a schematic ladder diagram of quark and gluon exchange in LLQ<sup>2</sup> approximation of DIS. In ladder diagrams, the longitudinal momenta  $\sim x_i$  are ordered along the chain ( $x_i \geq x_{i+1}$ ) and the transverse momenta are strongly ordered, that is,  $k_{\perp,i}^2 \ll k_{\perp,i+1}^2$ . It is this strong ordering of transverse momenta towards  $Q^2$  which gives the maximal power of  $\ln(Q^2)$ , since the integration over transverse momentum in each cell is logarithmic.

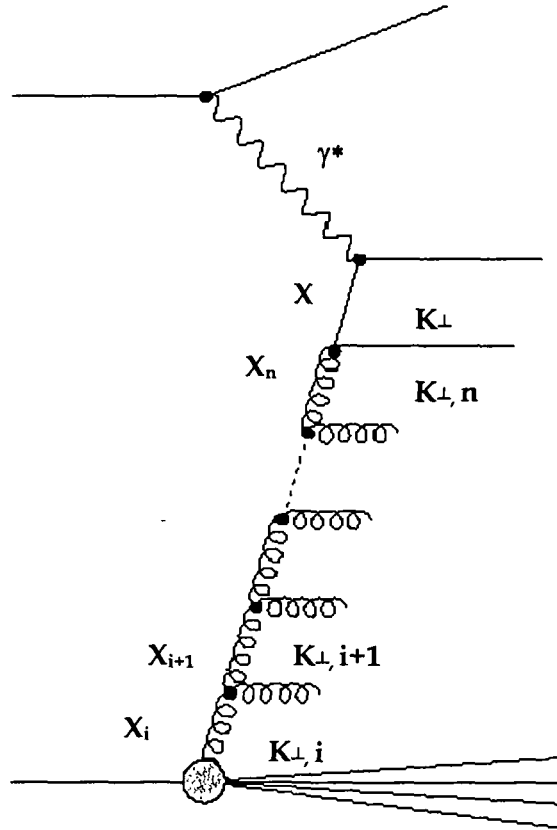


Figure 1.10: Ladder diagram for the DIS in LLQ<sup>2</sup>

The splitting functions contribute to the evolution of the parton distributions at order  $\alpha_s$ ,  $\alpha_s^2$  etc.

$$P_{qq}(z) = P_{qq}^0(z) + \frac{\alpha_s(t)}{2\pi} P_{qq}^1(z) + \left(\frac{\alpha_s(t)}{2\pi}\right)^2 P_{qq}^2(z) + \dots, \quad (1.16)$$

$$P_{qq}^0(z) = \frac{4}{3} \frac{1+z^2}{1-z}. \text{ Similarly } P_{qg}^0(z) = \frac{1}{2} [z^2 + (1-z)^2], \quad P_{gq}^0(z) = \frac{4}{3} \frac{1+(1-z)^2}{z} \text{ and}$$

$$P_{gg}^0(z) = 6 \left[ \frac{z}{1-z} + \frac{1-z}{z} + z(1-z) \right]. \quad (1.17)$$

With the advent of data from the various colliders, we are into a new phase of testing the applicability of pQCD. We are interesting in testing its predictions at very small- $x$  where we may be moving out of the region where the conventional approximations (LO, NLO and NNLO) as include in the DGLAP equations are applicable. Considering equations (1.17) for the LO splitting functions as

$$z = \frac{x}{y} \rightarrow 0, P_{qq} \rightarrow \frac{4}{3}, P_{qg} \rightarrow \frac{1}{2}, P_{gq} \rightarrow \frac{4}{3} \frac{1}{z}, P_{gg} \rightarrow 6 \frac{1}{z}, \quad (1.18)$$

we see that the gluon splitting functions are singular as  $z \rightarrow 0$  (this result remains true for higher orders). Thus the gluon distribution will rise as  $x \rightarrow 0$ , and its contribution to the evolution of the quark distribution will become dominant, so that the quark singlet distributions and hence, the structure function  $F_2$ , will also rise as  $x \rightarrow 0$ .

### 1.7.2 BKFL Evolution Equation

At asymptotically large energies, it is believed that the theoretically correct description is given by the BKFL [29-31] evolution. Here, each emitted gluon is assumed to take a large fraction of the energy of the propagating gluon,  $(1-z)$  for  $z \rightarrow 0$ , and large logarithms of  $1/z$  are summed up to all orders. Keeping only leading powers of LL ( $1/x$ ) terms in the perturbative expansion, the BKFL evolution equation comes in the Leading Logarithmic  $1/x$  [LL( $1/x$ )] approximation. The BKFL evolution equation is

$$f(x, k^2) = f^0(x, k^2) + \frac{3\alpha_s(k^2)}{\pi} k^2 \int_x^1 \frac{dx'}{x'} \int_{k_0^1}^{\infty} \frac{dk'^2}{k'^2} \left\{ \frac{f(x', k'^2) - f(x', k^2)}{|k'^2 - k^2|} + \frac{f(x', k^2)}{\sqrt{4k'^4 + k^4}} \right\} \quad (1.19)$$

The function  $f(x, k^2)$  is the non-integrated gluon distribution, that is  $f(x, k^2) = \partial_x G(x, k^2) / \partial \ln k^2$ ,  $f^0(x, k^2)$  is a suitably defined inhomogeneous term;  $k^2, k'^2$  are the transverse momenta squared of the gluon in the final and initial states respectively, and  $k_0^2$  is the lower limit cut-off.

### 1.7.3 GLR Evolution Equation

In the approximation where only leading power of  $\ln Q^2$  and  $\ln(1/x)$  are kept, that is the double logarithmic approximation (DLA), compact forms of GLR equations are shown in the recent literature [32-34]. Further approximation is that the coupling of  $n \geq 2$  ladder to the hadron is proportional to the  $n$ -th power of a single ladder. As a result, the probability of finding two gluons (at low momentum  $Q_0^2$ ) with momentum fraction  $x_1$  and  $x_2$  is proportional to  $g(x_1, Q_0^2) \cdot g(x_2, Q_0^2)$ . It leads to a non-linear integro-differential equation for structure function, which gives the GLR equation as

$$\frac{\partial \Phi(x, Q^2)}{\partial \ln(1/x)} = \int \hat{k}(q^2, q'^2) \Phi(x, q'^2) \cdot \frac{4N_f \alpha_s(q'^2)}{4\pi} - \frac{1}{4\pi\pi^2} \left( \frac{\alpha_s(q'^2)}{4\pi} \right)^2 V \cdot \Phi^2(x, Q^2), \quad (1.20)$$

where  $\Phi = \partial F(x, Q^2) / \partial Q^2$ ,  $R$  denotes the transverse radius of the hadron and  $V$  stands for the triple ladder vertex. Here parton recombinations are considered.

### 1.7.4 CCFM Evolution Equation

The CCFM [35-38] evolution equation resumes also large logarithms of  $1/(1-z)$  in addition to the  $1/z$  ones. Here,  $z$  denotes the energy fraction of the emitted gluon. Furthermore, it introduces angular ordering of emissions to correctly treat gluon coherence effects. In the limit of asymptotic energies, it is almost equivalent to BKFL, but also similar to the DGLAP evolution for large- $x$  and high- $Q^2$ . An advantage of the CCFM evolution, compared to the BKFL evolution, is that it is fairly well suited for implementation into an event

generator program, which makes quantitative comparison with data feasible also for non-inclusive observables. The CCFM evolution equation with respect to the scale  $\bar{q}_i^2$  can be written in a differential form

$$\bar{q}_i \frac{d}{d\bar{q}^2} \frac{x A(x, k_{\perp}^2, \bar{q}^2)}{\Delta_s(\bar{q}^2, Q_0^2)} = \int dz \frac{d\phi}{2\pi} \frac{\tilde{P}(z, (\bar{q}/z)^2, k_{\perp}^2)}{\Delta_s(\bar{q}^2, Q_0^2)} x' A(x', k_{\perp}^2, (\bar{q}/z)^2), \quad (1.21)$$

where  $A(x, k_{\perp}^2, \bar{q}^2)$  is the unintegrated gluon density which depends on longitudinal momentum fraction  $x$ , transverse momentum  $k_{\perp}^2$  and the evolution variable  $\mu^2$  (factorization scale)  $= \bar{q}^2$ . The splitting variables are  $z=x/x'$  and  $\vec{k}'_{\perp} = (1-z)/z\vec{q} + \vec{k}_{\perp}$ , where the vector  $\vec{q}$  is at an azimuthal angle  $\phi$ . Here  $\Delta_s$  is the Sudakov form factor and is given as

$$\Delta_s(\bar{q}^2, Q_0^2) = \exp \left( - \int_{Q_0^2}^{\bar{q}^2} \frac{dq^2}{q^2} \int_0^{(Q_0/q)} dz \frac{\bar{\alpha}_s(q^2(1-z)^2)}{1-z} \right), \quad (1.22)$$

where  $\bar{\alpha}_s = 3\alpha_s/\pi$ . And the splitting function  $\tilde{P}$  for branching  $i$  is given by

$$\tilde{P}_g(z_i, q_i^2, k_{\perp i}^2) = \frac{\alpha_s(q_i^2(1-z_i)^2)}{1-z_i} + \frac{\bar{\alpha}_s(k_{\perp i}^2)}{z_i} \Delta_{ns}(z_i, q_i^2, k_{\perp i}^2), \quad \text{here } \Delta_{ns} \text{ is the}$$

non-Sudakov form factor defined as

$$\ln \Delta_{ns}(z_i, q_i^2, k_{\perp i}^2) = -\bar{\alpha}_s \int_{z_i}^1 \frac{dz'}{z'} \int \frac{dq^2}{q^2} \Theta(k_{\perp i} - q) \Theta(q - z'q_i) \quad (1.23)$$

Mueller and Qiu investigated gluon-gluon recombination effect on the evolution. The DGLAP and PR evolution equations are given by

$$\frac{\partial q_i(x, t)}{\partial t} = \int \frac{dy}{x y} \left[ \sum_j P_{q_i q_j}(x/y) q_j(y, t) + P_{qg}(x/y) g(y, t) \right] + \left[ \text{recombination terms proportional to } \frac{\alpha_s A^{1/3}}{Q^2} \right], \quad (1.24)$$



$$\frac{\partial g(x,t)}{\partial t} = \int_x^1 \frac{dy}{y} \left[ \sum_j P_{gq_j}(x/y) q_j(y,t) + P_{gg}(x/y) g(y,t) \right] + \left[ \text{recombination terms proportional to } \frac{\alpha_s A^{1/3}}{Q^2} \right], \quad (1.25)$$

where the variable  $t$  is defined by  $t = -\left(\frac{2}{\beta_0}\right) \ln \left[ \frac{\alpha_s(Q^2)}{\alpha_s(Q_0^2)} \right]$ . In the PR evolution case, there are additional higher-twist terms which are proportional to  $1/Q^2$ . These terms are also proportional to  $A^{1/3}$  because recombination effect is proportional to the magnitude of parton overlap in the longitudinal direction.

## 1.8 Particle Accelerator Centres

Particle accelerator, from which we get various data, provides a beam of energetic particles travel in vacuum chamber to study the structure of matter. It employs electric fields to impart energy to accelerate the particles and magnetic fields to steer and focus the beam. Particle accelerator makes collisions either against a fixed target, or between two beams of particles. The name beam given to a stream of energetic particles moving at speeds very close to that of light. Indeed, the choice of name is by analogy to a beam of light. There are two types of accelerators: Linear accelerator, beam travels from one end to the other and Circular accelerator, beam repeatedly circulates around ring. Some particle accelerator centres are briefly explained below.

### 1.8.1 SLAC (Stanford Linear Accelerator Centre)

SLAC was established in 1962 at Stanford University in Menlo Park, California, USA. Its mission is to design, construct and operate electron accelerators and related experimental facilities for use in high-energy physics and synchrotron radiation research. It houses the longest linear accelerator (linac), a machine of 3.2 km long that accelerates electrons up to energies of

10 GeV. In 1966 a new machine, designed to reach 20 GeV was completed. In 1968 experiments at SLAC found the first direct evidence for further structure (i.e., quarks) inside protons and neutrons. In 1972, an electron-positron collider called SPEAR (Stanford Positron-Electron Asymmetric Rings) producing collisions at energies of 2.5 GeV per beam was constructed. In 1974 SPEAR was upgraded to reach 4.0 GeV per beam. A new type of quark, known as charm, and a new, heavy leptons relative of the electron, called the tau were discovered using SPEAR. SPEAR was followed by a larger, higher-energy colliding-beam machine, the PEP (Positron-Electron Project), which began operation in 1980 and took electron-positron collisions to a total energy of 36 GeV. The SLAC Linear Collider (SLC) was completed in 1987. SLC uses the original linac, upgraded to reach 50 GeV, to accelerate electrons and positrons before sending them in opposite directions around a 600-metre loop, where they collide at a total energy of 100 GeV. This is sufficient to produce the Z particle, the neutral carrier of the weak nuclear force that acts on fundamental particles.

### 1.8.2 DESY (Deutsches Elektronen-Synchrotron)

DESY, one of the largest centres for particle-physics research located in Hamburg, Germany was founded in 1959. The construction of an electron synchrotron to generate an energy level of 7.4 billion electron-volts was completed in 1964. Ten years later the Double Ring Storage Facility (DORIS) was completed which is capable of colliding beams of electrons and positrons at 3.5 GeV per beam. In 1978 its power was upgraded to 5 GeV per beam. DORIS is no longer used as a collider, but its electron beam provides synchrotron radiation (mainly at X-ray and ultraviolet wavelengths) for experiments on a variety of materials. A larger collider capable of reaching 19 GeV per beam, the Positron-Electron Tandem Ring Accelerator (PETRA), began operational in 1978. Experiments with PETRA in the following year gave the first direct evidence of the existence of gluons. The Hadron-Electron Ring Accelerator

(HERA) capable of colliding electrons and protons was completed in 1992. HERA consists of two rings in a single tunnel with a circumference of 6.3 km, one ring accelerates electrons to 30 GeV and the other protons to 820 GeV. It is being used to continue the study of quarks.

### 1.8.3 FNAL (Fermi National Accelerator Laboratory)

FNAL, also called FERMILAB, centre for particle-physics research is located at Batavia, Illinois in USA named after the Italian-American physicist Enrico Fermi, who headed the team that first achieved a controlled nuclear reaction. The major components of Fermilab are two large particle accelerators called proton synchrotrons, configured in the form of a ring with a circumference of 6.3 km. The first, which went into operation in 1972, is capable of accelerating particles to 400 billion electron volts. The second, called the Tevatron, is installed below the first and incorporates more powerful superconducting magnets; it can accelerate particles to 1 trillion electron volts. The older instrument, operating at lower energy levels, now is used as an injector for the Tevatron. The high-energy beams of particles (notably muons and neutrinos) produced at the laboratory, have been used to study the structure of protons in terms of their most fundamental components, the quarks. In 1972 a team of scientists at Fermilab isolated the bottom quark and its associated antiquark. In 1977 a team led by Leon Lederman discovered the upsilon meson, which revealed the existence of the bottom quark and its accompanying antiquark. The existence of the top quark predicted by the standard model was established at Fermilab in March, 1994.

### 1.8.4 KEK (Koh-Ene-Ken)

KEK is a National Laboratory for High Energy Physics located at Tsukuba, Ibaraki Prefecture, Japan. Both proton accelerators and

electron/positron accelerators, including storage rings and colliders, are in operation in KEK to support various activities, ranging from particle physics to structure biology. A high-intensity proton accelerator was also constructed in this laboratory in collaboration with Japan Atomic Energy Research Institute. KEK is associated with two research institutes, Institute of Particle and Nuclear Studies (IPNS) and Institute of Materials Structure Science (IMSS) and two laboratories, Accelerator Laboratory and Applied Research Laboratory. IPNS carries out research programs in particle physics and nuclear physics. IMSS offers three types of probes for research programs in material science. Its two major accelerators are the 12 GeV Proton Synchrotron and the KEKB electron-positron collider where the Belle experiment is currently running. The Belle collaboration at the KEKB factory was highlighted by its observation of the CP violation of B-mesons. The Applied Research Laboratory, which has four research centres (Radiation Science Centre, Computing Research Centre, Cryogenics Science Centre and Mechanical Engineering Centre), providing basic technical support for all KEK activities with their high-level technologies. KEK is also associated in the J-PARC proton accelerator under construction in Tokaimura.

### 1.8.5 VECC (Variable Energy Cyclotron Centre)

VECC is a research and development unit located in Kolkata, India. The variable energy cyclotron (VEC) set up is used for research in Accelerator Science and Technology, Nuclear Science (Theoretical and Experimental), Material Science, Computer Science and Technology and in other relevant areas. The Variable Energy Cyclotron (VEC) is the main accelerator, operational at the Centre since 1980. The Centre is also constructing Radioactive Ion Beam (RIB) accelerator - highly complex and sophisticated - for most modern nuclear physics and nuclear astrophysics experiments. High level scientific activity goes on at the Centre for International collaborations in the areas of high energy

physics experiments at large accelerators in other parts of the world. The Centre has also developed frontline computational facilities to carry out research and development in the above mentioned areas. Exploration and recovery of helium gas from hot spring emanations and earthquake prediction utilizing related observations is another important area in which the Centre is actively engaged.

### 1.8.6 BNL (Brookhaven National Laboratory)

Brookhaven National Laboratory is located at Upton, New York. The setup of Relativistic Heavy Ion Collider (RHIC) is a heavy-ion collider used to collide ions at relativistic speeds. At present, RHIC is the most powerful heavy-ion collider in the world. The RHIC double storage ring is itself hexagonally shaped and its circumference is 3834 m with curved edges in which stored particles are deflected by 1,740 superconducting niobium titanium magnets. The six interaction points are at the middle of the six relatively straight sections, where the two rings cross, allowing the particles to collide. The interaction points are enumerated by clock positions, with the injection point at 6 o'clock. There are four detectors at RHIC – STAR (6 o'clock), PHENIX (8 o'clock), PHOBOS (10 o'clock), and BRAHMS (2 o'clock). PHOBOS has the largest pseudorapidity coverage of all detectors, and tailored for bulk particle multiplicity measurement and it has completed its operation after 2005. BRAHMS is designed for momentum spectroscopy, in order to study low-x and saturation physics and it has completed its operation after 2006. STAR is aimed at the detection of hadrons with its system of time projection chambers covering a large solid angle and in a conventionally generated solenoidal magnetic field, while PHENIX is further specialized in detecting rare and electromagnetic particles, using a partial coverage detector system in a superconductively generated axial magnetic field. There is an additional experiment PP2PP, investigating spin dependence in  $P^+ - P^-$  scattering.

Another collider eRHIC, also known as spin-dependent electron-hadron collider was designed based on the RHIC hadron rings and 10 to 20 GeV energy recovery electron linac. The designs of eRHIC, based on a high current superconducting energy-recovery linac (ERL) with energy of electrons up to 20 GeV, have a number of specific requirements on the ERL optics. Two of the most attractive features of this scheme are full spin transparency of the ERL at all operational energies and the capability to support up to four interaction points. The main goal of the eRHIC is to explore the physics at small- $x$ , and the physics of colour-glass condensate in electron-hadron collisions.

### 1.8.7 CERN (Conseil Europeen pour la Recherche Nucleaire)

CERN is the European Organization for Nuclear Research which is the international scientific organization for collaborative research in sub-nuclear physics (high-energy, or particle physics). Head office of CERN is in Geneva, Switzerland. The activation of a 600-mega volt synchrocyclotron in 1957 enabled CERN physicists to observe the decay of a pion, into an electron and a neutrino. The event was instrumental in the development of the theory of weak interaction. The laboratory grew steadily, activating the particle accelerator known as the Proton Synchrotron (1959), which used 'strong focusing' of particle beams; the Intersecting Storage Rings (ISR; 1971), enabling head-on collisions between protons; and the Super Proton Synchrotron (SPS; 1976), with a 7-kilometre circumference. With the addition of an Antiproton Accumulator Ring, the SPS was converted into a proton-antiproton collider in 1981 and provided experimenters with the discovery of the W and Z particles in 1983 by Carlo Rubbia and Simon van der Meer. In November 2000 the Large Electron-Positron Collider (LEP), a particle accelerator installed at CERN is an underground tunnel 27 km in circumference, closed down after 11 years service. LEP was used to counter-rotate accelerated electrons and positrons in a narrow evacuated tube at velocities close to that of light, making a complete

circuit about 11,000 times per second. Their paths crossed at four points around the ring. DELPHI, one of the four LEP detectors, was a horizontal cylinder about 10 m in diameter, 10 m long and weighing about 3,000 tones. It was made of concentric sub-detectors, each designed for a specialized recording task.

For the past few decades, physicists have been able to describe with increasing detail the fundamental particles that make up the Universe and the interactions between them. This understanding is encapsulated in the Standard Model of particle physics, but it contains gaps and cannot tell us the whole story. To fill in the missing knowledge requires experimental data, and the next big step to achieve this is with LHC (Large Hadrons Collider), the world's largest and most powerful particle accelerator, is the latest addition to CERN's accelerator complex. The LHC was built to help scientists to answer key unsolved questions in particle physics. The unprecedented energy it achieves may even reveal some unexpected results that no one has ever thought off.

The LHC, a circular accelerator, having circumference of 26 Km, depth underground ranges from 50 meters to 175 meters. In LHC two beams of particles travel at close to the speed of light with very high energies before colliding with one another. The beams travel in opposite directions in separate beam pipes - two tubes kept at ultrahigh vacuum. They are guided around the accelerator ring by a strong magnetic field, achieved using superconducting electromagnets. These are built from coils of special electric cable that operates in a superconducting state, efficiently conducting electricity without resistance or loss of energy. This requires chilling the magnets to about  $-271^{\circ}\text{C}$ , a temperature colder than outer space. For this reason, much of the accelerator is connected to a distribution system of liquid helium, which cools the magnets, as well as to other supply services. Physicists will use the LHC to recreate the conditions just after the Big Bang, by colliding the two beams head-on at very high energy. Proton-proton collisions are foreseen at energy of 7 TeV per beam. The beams in LHC are designed to collide within the detectors 40 million times per second. Teams of physicists from around the world will analyze the particles created in the collisions using special detectors in a number of

experiments dedicated to the LHC. Six detectors are being constructed at the CERN. They are located underground, in large caverns excavated at the LHC's intersection points. Two of them, ATLAS and CMS are large particle detectors. ALICE is a large detector designed to search for a quark-gluon plasma in the very messy debris of heavy ion collisions. The other three (LHCb, TOTEM, and LHCf) are smaller and more specialized. A seventh experiment, FP420 (Forward Physics at 420 m), has been proposed which would add detectors to four available spaces located 420 m on either side of the ATLAS and CMS detectors.

But the question is about the safety of the Large Hadron Collider. The LHC can achieve an energy that no other particle accelerators have reached before, but Nature routinely produces higher energies in cosmic-ray collisions. Concerns about the safety of whatever may be created in such high-energy particle collisions have been addressed for many years. In the light of new experimental data and theoretical understanding, the LHC Safety Assessment Group (LSAG) has updated a review of the analysis made in 2003 by the LHC Safety Study Group, a group of independent scientists. The LSAG re-affirms and extends the conclusions of the 2003 report that LHC collisions present no danger and that there are no reasons for concern. Whatever the LHC will do, Nature has already done many times over during the lifetime of the Earth and other astronomical bodies. The LSAG report has been reviewed and endorsed by CERN's Scientific Policy Committee, a group of external scientists that advises CERN's governing body, its Council.

## 1.9 Phenomenology

Physics is a subject that can only thrive when there is strong interplay between theory and experiment. New theoretical ideas lead to predictions that can be tested experimentally, and new experimental findings challenge theorists to produce better ideas. Phenomenology is research on this boundary between theory and experiment. It is concerned with identifying interesting



physical observables, making theoretical predictions for them and then confronting experimental data gathered at the major international laboratories. The main aim of phenomenology is to find evidence for new physics and to develop new theories that describe the Universe at a more fundamental level than our current theories can. Close collaboration with experimental colleagues is a vital aspect of phenomenologist work.

The last thirty years have seen the spectacular success of the Standard Model gauge quantum field theory of electromagnetic, weak and strong interactions. The high-energy accelerator programme at various experimental group have confirmed the validity of the Standard Model, however, there are still important elements of the Standard Model which lack either experimental observation or a well-established theoretical basis. The main missing element is the Higgs boson, whose existence is ultimately related to the understanding of the origin of the mass of all other particles. Existing precision electroweak observables show excellent consistency with the Standard Model and constrain the mass of the Higgs boson significantly. Even if the Higgs boson is found, the Standard Model is far from complete and the electroweak symmetry breaking mechanism, which is a fundamental element in the theoretical construction of the Standard Model, is not yet well understood. It seems certain that more fundamental theories remain to be discovered. □

## Solution of Evolution Equations

As soon as QCD was introduced [50-52], theoretical physicists faced the problem of computing physical quantities in strong interaction processes. The most important source of  $F_2$  values, amongst various experimental measurements through DIS, are certainly the HERA experiments (H1 [53] and ZEUS [54]). Their latest sets of experimental data reached a level of precision very useful for theoretical tests. In this type of collision, when we compute the proton structure function in the QED framework, by a single photon exchange, we obtain the well known Bjorken scaling [55]: the structure functions are independent of the virtuality  $Q^2$  of the exchanged photon. If we compute QCD corrections in the large  $Q^2$  limit, we meet collinear divergences, appearing through  $\log(Q^2)$  corrections [25, 27, 28]. This is known as scaling violation. The scaling violation implies that parton densities inside the proton become  $Q^2$  dependent and the resummation of the collinear divergences in the framework of perturbative QCD leads to  $Q^2$  evolution equations for these parton densities. These equations, called the DGLAP equations, were found independently by Gribov-Lipatov in 1972, Altarelli-Parisi and Dokshitzer in 1977. Due to their very good agreement with experiment [56] and its implications on scaling violation, the DGLAP equations are considered as one of the best successes of QCD and, more precisely, perturbative QCD. Thus the solutions of DGLAP evolution equations are the powerful techniques to obtain the Parton Distribution Functions (PDF), hence the hadrons structure function and ultimately structure of proton or neutron.

As more and more sophisticated computing systems are developed, people are interested in numerical methods to solve various complex equations.

Some available programs deal with the DGLAP evolution are PEGASUS [57], QCDNUM [58], CANDIA [59], HOPPET [60] etc. Though various numerical methods are present to solve DGLAP evolution equations with a good degree of accuracy, but the interest in the analytical methods can not be ruled out. Some popular numerical as well as analytical methods to solve DGLAP evolution equations are – Brute force method [61], Laguerre polynomial method [62, 63], Mellin transformation method [64 - 66], Matrix approach method [67, 68], Taylor expansion and particular solution method [69 - 75], Regge theory method [76] , method of characteristics [75, 77, 78, 79] etc.

## 2.1 Brute force method

The simplest way amongst numerical methods is possibly to use the brute-force method. It may seem to be too simple, but it is especially suitable for solving more complicated equations with higher-twist terms [39]. These equations could not be easily handled by the orthogonal polynomial methods such as the Laguerre polynomial and by the Mellin transformation method. Furthermore, a computer code [61] is so simple that the possibility of a program mistake is small, which means the code could be used for checking other numerical methods. In the brute force method, the two variables  $t$  and  $x$  are divided into small steps, and then the differentiation and integration are defined by

$$\frac{\partial f(x, t)}{\partial t} \Rightarrow \frac{f(x_j, t_{j+1}) - f(x_j, t_j)}{\Delta t_j}, \quad \int dx f(x, t) \Rightarrow \sum_{k=1}^{N_x} \Delta x_k f(x_k, t_j),$$

where  $\Delta t_j$  and  $\Delta x_k$  are the steps at the positions  $j$  and  $k$ , and they are given by  $\Delta t_j = t_{j+1} - t_j$  and  $\Delta x_k = x_k - x_{k-1}$ . The numbers  $t$  and  $x$  steps are denoted  $N_t$  and  $N_x$ , respectively. Applying these equations to DGLAP, we write the non-singlet evolution from  $t_j$  to  $t_{j+1}$  as

$$q_{NS}(x_j, t_{j+1}) = q_{NS}(x_j, t_j) + \Delta t_j \sum_{k=1}^{N_x} \frac{\Delta x_k}{x_k} P_{qq} \left( \frac{x_j}{x_k} \right) q_{NS}(x_k, t_j). \quad (2.1)$$

If the distribution  $q_{NS}$  is supplied at  $t_1 = 0$ , the next one  $q_{NS}(x, t_2)$  can be calculated by the above equation. Repeating this step  $N_t - 1$  times, we obtain the final distribution at  $t_{N_t}$ . However, it is obvious that the step numbers  $N_t$  and  $N_x$  should be large enough to obtain an accurate evolution result.

The advantage of brute-force method is that the computer code is very simple. More complicated evolution equations with higher twists could be handled easily. The evolution could be accurate in the small and large  $x$  regions. But the main disadvantage is the computation time. In order to obtain an accurate evolution, large numbers of steps are needed. If one uses the code for many evolution calculations, it takes a significant amount of time.

## 2.2 Laguerre polynomial method

The evolution equations could be solved by expanding the distribution and splitting functions in terms of orthogonal polynomials. A popular method of this type is to use the Laguerre polynomials [62, 63]. They are defined in the region from 0 to 1, thus the variable  $x$  should be transformed to  $x'$  by relation  $x' = -\ln x$ . The non-singlet evolution is discussed in the following. The evolution function  $E_{NS}(x, t)$ , which describes the distribution evolution from  $t = 0$  to  $t$ , is defined by

$$f_{NS}(s, t) = \int_x^1 \frac{dy}{y} E_{NS}\left(\frac{x}{y}, t\right) f_{NS}(y, t = 0). \quad (2.2)$$

Then, it satisfies

$$\frac{\partial}{\partial t} E_{NS}(x, t) = \int_x^1 \frac{dy}{y} P_{NS}\left(\frac{x}{y}, t\right) E_{NS}(y, t). \quad (2.3)$$

Here  $E_{NS}$  and  $P_{NS}$  are evolution functions and polynomials. They are introduced into get the equation (2.3), same integro-differential equation form as the original DGLAP equation. There is an advantage that the evolution function should be the delta function at  $t = 0$ :  $E_{NS}(x, t = 0) = \delta(1 - x)$  because of its

definition in equation (2.2). It makes the following analysis simpler. The functions are expanded in terms of the polynomials:

$$P_{NS}(e^{-x}) = \sum_n P_{NS}^n L_n(x') \text{ and } E_{NS}(e^{-x}, t) = \sum_n E_{NS}^n(t) L_n(x'),$$

where  $P_{NS}^n$  and  $E_{NS}^n(t)$  are the expansion coefficients. The coefficient  $F^n$  for a

function  $F(x)$  is given by  $F^n = \int_0^1 dx E_n(x') F(x)$ , and it could be calculated

analytically for a simple function. If the two functions on the right hand side of equation (2.3) are expanded, it becomes an integration of two Laguerre polynomials. Using the formula

$$\int_0^{x'} dy' L_n(x' - y') L_m(y') = L_{n+m}(x') - L_{n+m+1}(x'),$$

for this integration, we obtain

$$\frac{d}{dt} E_{NS}^m(t) = \sum_{m=0}^n (P_{NS}^{n-m} - P_{NS}^{n-m-1}) E_m(t).$$

Because the evolution function is a delta function at  $t=0$ , all the expansion coefficients are one. Therefore, this equation is easily solved to give a summation form:

$$E_{NS}^m(t) = e^{P_{NS}^0 t} \sum_{k=0}^m \frac{t^k}{k!} B_m^k, \quad B_m^{k+1} = \sum_{i=k}^{m-1} (P_{NS}^{m-i} - P_{NS}^{m-i-1}) B_i^k.$$

This recursion relation is calculated with the relations  $B_i^0 = 1$ ,

$$B_i^1 = \sum_{j=1}^i (P_{NS}^j - P_{NS}^{j-1}) \text{ and } B_0^k = B_1^k = \dots = B_{k-1}^k = 0.$$

After all, the evolution is calculated by the simple summation:

$$f_{NS}(x, t) = \sum_{n=0}^{N_{\text{inf}}} \sum_{m=1}^n [E_{n-m}(t) - E_{n-m-1}(t)] L_n(-\ln x) f_{NS}^m(t=0). \quad (2.4)$$

Thus the integro-differential equation becomes a simple summation of Laguerre expansion coefficients, so that this method is considered to be a very efficient numerical method for the solution.

In computer, Laguerre polynomial method is very fast. As long as one does not mind the very small and large- $x$  region, it is a good method for repeated evolution calculations. But depending on the initial functional form, the results do not converge at small- $x$  unless a large number of polynomials are used. It is also difficult to obtain accurate evolution at large- $x$ .

### 2.3 Mellin transformation method

The Mellin transformation method [64] is one of the popular evolution methods. It is used because the Mellin transformation of the DGLAP equation becomes a simple multiplication of two moments, namely the moments of the splitting function and the distribution function. The moments of the splitting functions are well known, and a simple functional form is usually assumed for the distribution at certain small -  $Q^2$  so as to calculate its moments easily. Then, it is straightforward to obtain the analytical solution in the moment space. Furthermore, the computation time is fairly short. These are the reasons why this method has been used as a popular method. The Mellin transformation and Mellin inversion are defined [65, 66] by

$$\hat{f}(s, t) = \int_0^1 dx x^{s-1} f(x, t) \quad \text{and} \quad f(x, t) = \frac{1}{2i\pi} \int_{c-i\infty}^{c+i\infty} ds x^{-s} \hat{f}(s, t).$$

Here the upper limit of the  $x$  integration is taken one because the distribution  $f(x)$  vanishes in the region  $x \geq 1$ . The Mellin inversion is a complex integral with an arbitrary real constant  $c$ , which should be taken so that the integral

$\int_0^1 dx f(x) x^{c-1}$  is absolutely convergent. If this transformation is used, the

integro-differential equations become very simple. For example the non-singlet evolution equation becomes

$$\frac{\partial}{\partial t} \hat{f}_{NS}(s, t) = \hat{P}_{NS}(s) \hat{f}_{NS}(s, t). \quad (2.5)$$

Its solution is simply given by

$$\hat{f}_{NS}(s, t) = e^{\hat{P}_{NS}(s)t} \hat{f}_{NS}(s, t = 0).$$

Because the moments  $\hat{P}_{NS}(s)$  are well known quantities and the moments of the initial function  $\hat{f}_{NS}(s, t = 0)$  could be evaluated, it is straight forward to calculate the evolution in the moment space. However, the numerical integration is needed for the Mellin inversion for transforming the moments into a corresponding  $x$  distribution

Mellin transformation method is a faster method than the Brute force computation. For repeated evolution calculations with certain accuracy, this method is appropriate. But one should be careful about the Mellin inversion process at very large- $x$ .

## 2.4 Matrix approach method

The shortcomings common to almost all above numerical methods are the computer time required and decreasing accuracy for  $x \rightarrow 0$ . But application of matrix approach for numerical solution is highly satisfactory both in terms of precision and computing time [67, 68].

The non-singlet DGLAP equation is in the form of

$$\frac{d f(x, Q^2)}{d \ln Q^2} = \frac{\alpha_s(Q^2)}{2\pi} \int_x^1 \frac{dy}{y} P\left(\frac{x}{y}\right) f(y, Q^2), \quad (2.6)$$

where  $f(x, Q^2)$  represents some non-singlet parton density and  $P$  the corresponding splitting function. The convolution form does allow exact  $\ln Q^2$  integration if transformed to Mellin moment space. However, this requires knowledge of the function over the entire  $x$  region. Thus as data analysis is our main aim, it is desirable to remain in  $x$  space [68]. Now let,

$$t = \ln \frac{\alpha_s(Q_0^2)}{\alpha_s(Q^2)}, \quad u = \ln \frac{1}{x}, \quad v = \ln \frac{1}{y}.$$

Thus equation (2.6) gives

$$\frac{d f(u, t)}{d t} = \int_0^u dv P(u - v) f(v, t). \quad (2.7)$$

To examine the numerical approach, consider performing the integral on the right hand side of equation (2.7) via a naive trapezoidal rule over subintervals of size  $h$ ,

$$\frac{d f_m(t)}{d t} = \sum_{k=1}^m P_{mk} f_k(t), \quad (2.8)$$

where the following rather obvious definitions have been made:

$$u_k = kh, f_k(t) = f(u_k, t), P_{mk} = hP(u_m - u_k).$$

The typical vanishing of  $f(x)$  at  $x=1$  has been exploited and a factor one half in the last term of the series has been omitted. By noting that the sum in equation (2.8) runs only up to  $m$ , we see that the matrix  $P_{mk}$  is lower triangular. Finally, writing the equation in matrix form [68], we obtain

$$\dot{f}(t) = Pf(t), \quad (2.9)$$

where the over dot indicates a derivative with respect to  $t$ .

We should now need only diagonalized  $P$ , via a matrix  $D$ , left multiplication by  $D^{-1}$  would then result in

$$D^{-1} \dot{f}(t) = D^{-1} P D D^{-1} f(t) \Rightarrow \tilde{\dot{f}}(t) = P_D \tilde{f}(t). \quad (2.10)$$

The exact solution could thus be written down directly:

$$\tilde{f}_m(t) = e^{\gamma_m t} \tilde{f}_m(0), \quad (2.11)$$

where the  $\gamma_m$  would be just the eigen values of the matrix  $P$ . Transformation back to the original basis would then

$$f_m(t) = \sum e^{\gamma_m t} d_{mk} \tilde{f}_k(0). \quad (2.12)$$

This would be an exact solution in  $t$  of the differential equation, only the  $x$  variable have been discretized and treated numerically. It turns out that the eigen values are very close to one another and so diagonalization is very nearly singular.



## 2.5 Taylor expansion and particular solutions method

Considering the splitting functions [28, 80, 81], the DGLAP evolution equations for non-singlet and singlet structure functions in standard [81-85] form in LO at small- $x$  are

$$\begin{aligned} \frac{\partial F_2^{\text{NS}}}{\partial t} - \frac{A_f}{t} \left[ \{3 + 4 \ln(1-x)\} F_2^{\text{NS}}(x, t) \right] \\ + 2 \frac{A_f}{t} \int_x^1 \frac{dw}{1-w} \left[ (1+w^2) F_2^{\text{NS}}\left(\frac{x}{w}, t\right) - 2 F_2^{\text{NS}}(x, t) \right] = 0, \end{aligned} \quad (2.13)$$

and

$$\begin{aligned} \frac{\partial F_2^{\text{S}}}{\partial t} - \frac{A_f}{t} \left[ \{3 + 4 \ln(1-x)\} F_2^{\text{S}}(x, t) \right] \\ + 2 \frac{A_f}{t} \int_x^1 \frac{dw}{1-w} \left[ (1+w^2) F_2^{\text{S}}\left(\frac{x}{w}, t\right) - 2 F_2^{\text{S}}(x, t) \right] \\ + 2 N_f \frac{A_f}{t} \int_x^1 \left\{ w^2 + (1-w)^2 \right\} G\left(\frac{x}{w}, t\right) dw = 0. \end{aligned} \quad (2.14)$$

Here  $F_2^{\text{NS}}\left(\frac{x}{w}, t\right)$ ,  $F_2^{\text{S}}\left(\frac{x}{w}, t\right)$  and  $G\left(\frac{x}{w}, t\right)$  can be expand by using Taylor series expansion.

Let us introduce the variable  $u = 1-\omega$  and note that

$$\frac{x}{\omega} = \frac{x}{1-u} = x \left( 1 + \frac{1}{1-u} - 1 \right) = \left( x + \frac{xu}{1-u} \right). \text{ Now}$$

$$\begin{aligned} F_2^{\text{NS}}\left(\frac{x}{\omega}, t\right) &= F_2^{\text{NS}}\left(x + \frac{xu}{1-u}, t\right) \\ &= F_2^{\text{NS}}(x, t) + \frac{xu}{1-u} \frac{\partial F_2^{\text{NS}}(x, t)}{\partial x} + \frac{1}{2} \left( \frac{xu}{1-u} \right)^2 \frac{\partial^2 F_2^{\text{NS}}(x, t)}{\partial^2 x} + \dots \end{aligned} \quad (2.15)$$

Since  $x$  is small in our region of discussion, the terms containing  $x^2$  and higher powers of  $x$ , can be neglected and we can rewrite

$$F_2^{NS}\left(\frac{x}{\omega}, t\right) \approx F_2^{NS}(x, t) + \frac{xu}{1-u} \frac{\partial F_2^{NS}(x, t)}{\partial x}. \quad (2.16a)$$

Similarly

$$F_2^S\left(\frac{x}{\omega}, t\right) \approx F_2^S(x, t) + \frac{xu}{1-u} \frac{\partial F_2^S(x, t)}{\partial x}, \quad (2.16b)$$

$$G\left(\frac{x}{\omega}, t\right) \approx G(x, t) + \frac{xu}{1-u} \frac{\partial G(x, t)}{\partial x}. \quad (2.16c)$$

Using equation (2.16a) in equation (2.13) and performing u-integrations we get

$$-t \frac{\partial F_2^{NS}(x, t)}{\partial t} + L_1(x) \frac{\partial F_2^{NS}(x, t)}{\partial x} + M_1(x) F_2^{NS}(x, t) = 0 \quad (2.17)$$

where  $L_1(x)$  and  $M_1(x)$  are two functions. The general solution [73] of equation (2.17) is  $F(U, V) = 0$ , where  $F(U, V)$  is an arbitrary function and  $U(x, t, F_2^S) = K_1$  and  $V(x, t, F_2^S) = K_2$  are two independent solutions of the equations -

$$\frac{dx}{L_1(x, t)} = \frac{dt}{-t} = \frac{dF_2^{NS}(x, t)}{-M_1(x, t)F_2^{NS}(x, t)}. \quad (2.18)$$

Solving equation (2.18) we obtain

$$U\left(x, t, F_2^{NS}\right) = t \cdot \exp\left[\int \frac{1}{L_1(x)} dx\right] \text{ and } V\left(x, t, F_2^{NS}\right) = F_2^{NS}(x, t) \exp\left[\int \frac{M_1(x)}{L_1(x)} dx\right].$$

If  $U$  and  $V$  are two independent solutions of equation (2.18) and if  $\alpha$  and  $\beta$  are arbitrary constants, then  $V = \alpha U + \beta$  may be taken as a complete solution of equation (2.17). We take this form as this is the simplest form of a complete solution which contains both the arbitrary constants  $\alpha$  and  $\beta$ . Now the complete solution -

$$F_2^{NS}(x, t) \exp\left[\int \frac{L_1(x)}{M_1(x)} dx\right] = \alpha t \exp\left[\frac{1}{A_f} \int \frac{1}{M(x)} dx\right] + \beta, \quad (2.19)$$

is a two-parameter family of surfaces, which does not have an envelope, since the arbitrary constants enter linearly [73]. Differentiating equation (2.19) with

respect to  $\beta$  we get  $0 = 1$ , which is absurd. Hence there is no singular solution. The one parameter family determined by taking  $\beta = a^2$  has equation

$$F_2^{NS}(x, t) \exp \left[ \int \frac{L_1(x)}{M_1(x)} dx \right] = \alpha t \exp \left[ \frac{1}{A_f} \int \frac{1}{M_1(x)} dx \right] + \alpha^2. \quad (2.20)$$

Differentiating equation (2.20) with respect to  $a$ , we get

$$\alpha = -\frac{1}{2} t \exp \left[ \frac{1}{A_f} \int \frac{1}{M_1(x)} dx \right].$$

Putting the value of  $a$  in equation (2.20), we obtain the envelope

$$F_2^{NS}(x, t) = -\frac{1}{4} t^2 \exp \left[ \int \left( \frac{2}{A_f M_1(x)} - \frac{L_1(x)}{M_1(x)} \right) dx \right], \quad (2.21)$$

which is merely a particular solution of the general solution. Unlike the case of ordinary differential equations, the envelope is not a new locus. It is to be noted that when  $\beta$  is an arbitrary function of  $\alpha$ , then the elimination of  $\alpha$  in equation (2.20) is not possible. Thus the general solution can not be obtained from the complete solution [74]. Actually, the general solution of a linear partial differential equation of order one is the totality of envelopes of all one parameter families (2.21) obtained from a complete solution.

## 2.6 Regge theory method

The two body scattering of hadrons is strongly dominated by small momentum transfer or by small scattering angles. According to Regge theory [76], this scattering amplitude is successfully described by the exchange of a particle with appropriate quantum numbers and these are known as Regge Poles. Regge Pole exchange is a generalization of a single particle exchange. There are two types of Regge Poles: (a) Reggeon and (b) Pomeron. A very simple expression for the behaviour of scattering amplitude  $A(s, t)$  is predicted by Regge is given by

$A(s, t) \approx S^{\alpha(t)}$ ; for large-S.

The number quantities to consider are the structure functions which are proportional to the total virtual photon-nucleon cross section and which are expected to have Regge behaviour corresponding to pomeron or reggeon exchange. So the hadronic cross sections as well as structure functions will be dominated by two contributions: (a) a Pomeron, reproducing the rise of  $F_2$  at small-  $x$  and (b) a Reggeon associated with meson trajectories.

For the pomeron contribution to  $F_2$ , we will give three different simple possibilities [86, 87]:

(a) It may show a power behaviour like:

$$F_2(x, Q^2) = a(Q^2) x^{-\varepsilon}, \quad (2.22)$$

where  $a(Q^2)$  is a function of  $Q^2$  and the exponent  $\varepsilon$  is called intercept. This term, with  $\varepsilon \approx 0.09$  is called the soft pomeron, but is unable to describe the steeper rise of  $\gamma^*p$  amplitudes. The solution is to add another contribution, called the hard pomeron, which leads to

$$F_2(x, Q^2) = a_s(Q^2) x^{-\varepsilon_s} + a_h(Q^2) x^{-\varepsilon_h}. \quad (2.23)$$

where  $a_s(Q^2)$  and  $a_h(Q^2)$  are functions of  $Q^2$  and the exponents  $\varepsilon_s$  and  $\varepsilon_h$  are the intercepts for the soft and hard parts contributions to the structure function respectively. The hard pomeron has  $\varepsilon_h \approx 0.4$ . In the complex angular momentum plane, i.e. complex -  $j$  plane, this corresponds to two simple poles at  $j=1+\varepsilon_h \approx 1.4$  and  $j=1+\varepsilon_s \approx 1.1$ :

$$F_2(j, Q^2) = \frac{a_s(Q^2)}{j-1-\varepsilon_s} + \frac{a_h(Q^2)}{j-1-\varepsilon_h}.$$

This is the Donnachie-Landshoff two-pomerons model [63, 64, 86, 87].

(b) Pomeron may show a logarithmic behaviour like:

$$F_2(\nu, Q^2) = A(Q^2) \log(2\nu) + B(Q^2), \quad (2.24)$$

where  $A(Q^2)$  and  $B(Q^2)$  are functions of  $Q^2$ . Here DIS variable  $v$  is used instead of  $x$ . In the complex -  $j$  plane, this expression becomes

$$F_2(j, Q^2) = \frac{A(Q^2)}{(j-1)^2} + \frac{B(Q^2)}{j-1}.$$

And this behaviour is often called the double pole pomeron.

(c) Pomeron may show a squared-logarithmic behaviour like:

$$F_2(v, Q^2) = A(Q^2)\log^2(2v) + B(Q^2)\log(2v) + C(Q^2) \quad (2.25)$$

where  $C(Q^2)$  is also a function of  $Q^2$ . Here also DIS variable  $v$  is used instead of  $x$ . In the complex- $j$  plane, this expression becomes

$$F_2(j, Q^2) = \frac{2A(Q^2)}{(j-1)^3} + \frac{B(Q^2)}{(j-1)^2} + \frac{C(Q^2)}{j-1}.$$

This behaviour is often called the triple pole pomeron.

Now, in order to apply Regge theory to DGLAP evolution equations, let us take the functions of  $Q^2$  to be the same as  $T(Q^2)$ . i.e.  $A_h(Q^2) = A_s(Q^2) = T(Q^2)$ .

The contributions of the Regge poles solely determine the high energy behaviour of all QCD amplitudes in the multi-Regge kinematics given by namely Fadin, Fiore, Kozlov and Reznichenko [88]. So we can assume a simple form for Regge behaviour of unpolarized structure function to solve DGLAP evolution equation, as [89 - 95]

$$F_2(x, t) = T(t)x^{-\lambda}, \quad (2.26)$$

where  $T(t)$  is a function of  $t$  and  $\lambda$  is the Regge intercept for unpolarized structure function. This form of Regge behaviour is well supported by the work in this field carried out by namely Badelek [96], Soffer and Teryaev [97] and also Desgrolard, Lengyel and Martynov [98]. According to Regge theory, the high energy i. e. small- $x$  behaviour of both gluons and sea quarks are controlled by the same singularity factor in the complex angular momentum plane [76].

## 2.7 Method of characteristics

The method of characteristics [75, 77, 78, 79], is a method which can be used to solve the initial value problem (IVP) for general first order Partial Differential Equations (PDE). Consider the first order linear PDE in two variables along with the initial condition  $u(x, 0) = f(x)$  as

$$a(x, t)u_x + b(x, t)u_t + c(x, t)u = 0 \quad (2.27)$$

The goal of the method of characteristics, when applied to this equation, is to change coordinates from  $(x, t)$  to a new coordinate system  $(S, \tau)$  in which the PDE becomes an ordinary differential equation (ODE) along certain curves in the  $x$ - $t$  plane, called the characteristic curves or just the characteristics. Such curves are  $[x(S), t(S); 0 < S < \infty]$ , along which the solution of the PDE reduces to an ODE. The new variable  $S$  will vary, and the new variable  $\tau$  will be constant along the characteristics. The variable  $\tau$  will change along the initial curve in the  $x$ - $t$  plane (along the line  $t = 0$ ).

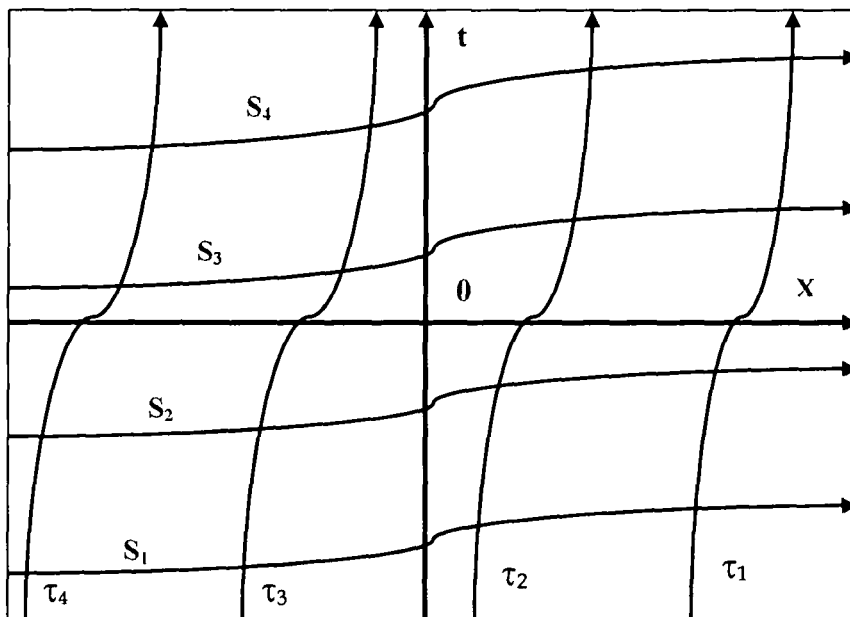


Figure 2.1: Characteristic curves

In figure 2.1, the co-ordinates  $(S, \tau)$  are considered as the value of  $S$  changing along a vertical curvy line where  $\tau$  is constant and  $\tau$  changes along a horizontal curvy line where  $S$  is constant. For  $t$ -evolution, we consider as  $S$  changes along the characteristic curve  $[x(S), t(S); 0 < S < \infty]$  and  $\tau$  changes along the initial  $(t = t_0)$  curve. On the other hand, for  $x$ -evolution,  $\tau$  changes along the characteristic curve  $[x(\tau), t(\tau); 0 < \tau < \infty]$  and  $S$  changes along the initial curve  $(x = \tau)$ . To get characteristic curves, let us choose the characteristic equations as

$$\frac{dx}{dS} = a(x, t), \quad a(x, t)u_x + b(x, t)u_t = \frac{dx}{dS}u_x + \frac{dt}{dS}u_t = \frac{du}{dS} \quad (2.28a)$$

$$\frac{dt}{dS} = b(x, t). \quad (2.28b)$$

Thus

$$a(x, t)u_x + b(x, t)u_t = \frac{dx}{dS}u_x + \frac{dt}{dS}u_t = \frac{du}{dS}.$$

Along the characteristic curve we get one ODE as

$$\frac{du}{dS} + c(x, t)u = 0. \quad (2.29)$$

This can be easily solved and after solving it and transforming  $(S, \tau)$  again to  $(x, t)$  we get unique solution.

The general strategies for applying the method of characteristics to a PDE are :

Step 1: We have to solve the two characteristic equations (2.28a) and (2.28b) and find the constants of integration setting  $x(0) = \tau$  and  $t(0)=0$ . Now the transformation from  $(x, t)$  to  $(S, \tau)$ ; i.e  $x = x(S, \tau)$  and  $t = t(S, \tau)$ .

Step 2: We have to solve the ODE (2.29) with initial condition  $u(0) = f(\tau)$ , where  $\tau$  are the initial points on the characteristic curves along the  $t = 0$  axis in the  $x$ - $t$  plane. We now have a solution of  $u(S, \tau)$ .

Step 3: We have to solve for  $S$  and  $\tau$  in terms of  $x$  and  $t$ , and substitute these values in  $u(S, \tau)$  to get the solution to the original PDE as  $u(x, t)$ .

The advantages of the Method of characteristics are that, (a) Method of characteristics is based on the exact theory of characteristics, (b) Method of characteristics follows closely the physics of the problem, and (c) Method of characteristics defines and uses the natural co-ordinate system independently of the particular choice of the computational grid employed. It was argued by Kentzer [99] that Method of characteristics affords exact means of incorporating algebraic boundary conditions into a finite-difference solution of partial differential equations. He suggested to differentiate the boundary conditions in the plane tangent to the boundary and to solve the resulting system of partial differential equations simultaneously.

Though exact analytic solutions of the DGLAP equations are not possible in the entire range of  $x$  and  $Q^2$ , under certain conditions analytic solutions are possible [100 - 104] which are quite successful as far as the HERA small- $x$  data are concerned. In recent years, such a scheme in the analytic study of the DGLAP equations has been pursued with quite good phenomenological success. One of the limitations of these solutions was an ad hoc assumption of the factorizability of  $x$  and  $Q^2$  dependence of the gluon momentum distribution [105] and the non uniqueness of the solution [37]. However, by using the method of characteristics [77] to solve partial differential equation of two variables with one initial condition, we can get rid of the ad hoc assumption and obtain a unique [78, 79] solution.  $\square$



*Part - I*

Unpolarized Hadron Structure  
Functions

*"God used beautiful mathematics in creating the world"*

– Dirac

The high-energy lepton-nucleon scattering has served as a sensitive probe for the substructure of the proton and neutron. Experiments with high energy electrons, muons and neutrinos have been used to characterize the parton substructure of the nucleon and to establish the current theory of the strong interaction – quantum chromodynamics. Observations of the experiments are scaling violation for the unpolarized nucleon structure functions, the measurement of the strong coupling constant  $\alpha_s(Q^2)$ , the confirmation of numerous QCD sum rules and the extraction of the parton distributions inside the nucleon. The parton distribution functions (PDFs) depend on two kinematical variables  $x$  and  $Q^2$ . Their  $Q^2$  dependence is called scaling violation, which is calculated by the DGLAP evolution equations [25-28] in the perturbative QCD region. The  $Q^2$  evolution equations are frequently used in describing high-energy hadron reactions. Because the PDFs vary significantly in the current accelerator-reaction range,  $Q^2=1 \text{ GeV}^2$  to  $10^5 \text{ GeV}^2$ , the  $Q^2$  dependence should be calculated accurately. Furthermore, it is known that high-energy cosmic rays have energies much more than the TeV scale. Analytical forms of current PDFs are supplied typically in the GeV region, so that they have to be evolved to the scale which could be more than TeV in order to use them for investigating the cosmic rays [106, 107, 108].

Various numerical as well as analytical methods to solve DGLAP evolution equations are discussed in Chapter 2. The solutions of the unpolarized DGLAP equation for the quantum chromodynamics evolution of parton distribution functions have been discussed considerably over the past years [100-104, 109-112]. But exact analytical method with unique solution is not known. Here we will solve unpolarized DGLAP evolution equations up to next-next-to-leading order (NNLO) analytically by using method of characteristics and get unique solutions. Our results are compared with various experimental data.

## Unpolarized DGLAP Evolution Equations in Leading Order

It is well known that all information about the structure of hadrons participating in DIS comes from the hadronic structure functions. According to QCD, at small values of  $x$  and at large values of  $Q^2$  hadrons consist predominately of gluons and sea quarks. In that region, the DGLAP evolution equations give  $t$  [ $= \ln(Q^2/\Lambda^2)$ ,  $\Lambda$  is the QCD cut off parameter] and  $x$  evolutions of structure functions. Hence the solutions of DGLAP evolution equations give quark and gluon structure functions that produce ultimately proton, neutron and deuteron structure functions. In this chapter, the singlet and non-singlet structure functions have been obtained by solving DGLAP evolution equations in leading order (LO) at the small- $x$  limit. Here we have used a Taylor series expansion and then the method of characteristics to solve the evolution equations. We have also calculated  $t$  and  $x$  evolutions of deuteron as well as non-singlet (combination of proton and neutron) structure functions and the results are compared with the New Muon Collaboration (NMC) [113], E665 [114], CLAS [115, 116] and NNPDF collaboration [117, 118, 119] data.

### 3.1 Theory

The DGLAP evolution equations [25 - 28] in matrix form

$$\frac{\partial}{\partial \ln Q^2} \begin{pmatrix} F_2^S \\ G \end{pmatrix} = \begin{pmatrix} P_{qq} & P_{qg} \\ P_{gq} & P_{gg} \end{pmatrix} \otimes \begin{pmatrix} F_2^S \\ G \end{pmatrix}, \quad (3.1)$$

where  $F_2^S$  and  $G$  are singlet and gluon structure functions respectively and  $P_{qq}, P_{qg}, P_{gq}, P_{gg}$  are splitting functions. For evolution of singlet structure function, the quark-quark splitting function  $P_{qq}$  and gluon-quark splitting function  $P_{qg}$  have to be calculated and for non-singlet structure function, we have to calculate only quark-quark splitting function  $P_{qq}$ , which can be expressed as [112].

$$P_{qq}(x, Q^2) = \frac{\alpha_s(Q^2)}{2\pi} P_{qq}^{(0)}(x) + \left( \frac{\alpha_s(Q^2)}{2\pi} \right)^2 P_{qq}^{(1)}(x) + \left( \frac{\alpha_s(Q^2)}{2\pi} \right)^3 P_{qq}^{(2)}(x) + \dots$$

where  $P_{qq}^{(0)}(x)$ ,  $P_{qq}^{(1)}(x)$  and  $P_{qq}^{(2)}(x)$  are LO, NLO and NNLO splitting functions respectively. Again  $\otimes$  represents the standard Mellin Convolution with the notation

$$a(x) \otimes b(x) \equiv \int_0^1 \frac{dy}{y} a(y) b\left(\frac{x}{y}\right). \quad (3.2)$$

Similarly, other splitting functions can be expressed.

The strong coupling constant,  $\alpha_s(Q^2)$  is related with the  $\beta$ -function [112] as

$$\beta(\alpha_s) = \frac{\partial \alpha_s(Q^2)}{\partial \log Q^2} = -\frac{\beta_0}{4\pi} \alpha_s^2 - \frac{\beta_1}{16\pi^2} \alpha_s^3 - \frac{\beta_2}{64\pi^3} \alpha_s^4 + \dots,$$

with

$$\frac{\alpha(Q^2)}{2\pi} = \frac{2}{\beta_0 t} \left[ 1 - \frac{\beta_1 \log t}{\beta_0^2 t} + \frac{1}{\beta_0^3 t} \left\{ \frac{\beta_1^2}{\beta_0} (\log^2 t - \log t - 1) + \beta_2 \right\} + O\left(\frac{1}{t^3}\right) \right],$$

$$\beta_0 = \frac{11}{3} N_c - \frac{4}{3} T_f,$$

$$\beta_1 = \frac{34}{3} N_c^2 - \frac{10}{3} N_c N_f - 2 C_F N_f,$$

$$\beta_2 = \frac{2857}{54} N_c^3 + 2 C_F^2 T_f - \frac{205}{9} C_F N_c T_f - \frac{1415}{27} N_c^2 T_f + \frac{44}{9} C_F T_f^2 + \frac{158}{27} N_c T_f^2,$$

where  $N_c$  is the number of colour,  $N_f$  is the number of active flavour and  $T_f, C_F$  are constants associated with the colour  $SU(3)$  group. We have set  $N_c = 3$ ,

$$C_F = \frac{N_c^2 - 1}{2N_c} = \frac{4}{3} \text{ and } T_f = \frac{1}{2} N_f. \text{ Here } \beta_0, \beta_1 \text{ and } \beta_2 \text{ are the one loop, two loop and}$$

three loop corrections to the QCD  $\beta$ -function. We can neglect  $\beta_1$  and  $\beta_2$  in LO.

Considering splitting functions [28, 80, 81], the DGLAP evolution equations for singlet and non-singlet structure functions in LO in standard form are

$$\frac{\partial F_2^S}{\partial t} - \frac{\alpha_s(t)}{2\pi} \frac{2}{3} \left[ \{3 + 4 \ln(1-x)\} F_2^S(x, t) + I_1^S(x, t) + I_2^S(x, t) \right] = 0, \quad (3.3)$$

$$\frac{\partial F_2^{NS}}{\partial t} - \frac{\alpha_s(t)}{2\pi} \frac{2}{3} \left[ \{3 + 4 \ln(1-x)\} F_2^{NS}(x, t) + I_1^{NS}(x, t) \right] = 0, \quad (3.4)$$

here functions  $I_1^S, I_2^S, I_1^{NS}$  are defined in Appendix A.

Here  $\frac{\alpha_s(t)}{2\pi} = \frac{3A_f}{2t}$  with  $A_f = \frac{4}{33 - 2N_f}$ . Let us introduce the variable  $u = 1 - \omega$

and note that

$$\frac{x}{\omega} = \frac{x}{1-u} = \left( x + \frac{xu}{1-u} \right) \quad (3.5)$$

Since  $x < \omega < 1$ , so  $0 < u < 1 - x$  and hence the series (3.5) is convergent for  $|u| < 1$ .

So, we can use Taylor's series expansion in  $F_2^S\left(\frac{x}{\omega}, t\right)$ ,  $F_2^{NS}\left(\frac{x}{\omega}, t\right)$  and  $G\left(\frac{x}{\omega}, t\right)$  as

$$\begin{aligned} F_2^S\left(\frac{x}{\omega}, t\right) &= F_2^S\left(x + \frac{xu}{1-u}, t\right) \\ &= F_2^S(x, t) + \frac{xu}{1-u} \frac{\partial F_2^S(x, t)}{\partial x} + \frac{1}{2} \left(\frac{xu}{1-u}\right)^2 \frac{\partial^2 F_2^S(x, t)}{\partial^2 x} + \dots, \end{aligned}$$

$$G\left(\frac{x}{\omega}, t\right) = G(x, t) + \frac{xu}{1-u} \frac{\partial G(x, t)}{\partial x} + \frac{1}{2} \left(\frac{xu}{1-u}\right)^2 \frac{\partial^2 G(x, t)}{\partial^2 x} + \dots,$$

$$F_2^{NS}\left(\frac{x}{\omega}, t\right) = F_2^{NS}(x, t) + \frac{xu}{1-u} \frac{\partial F_2^{NS}(x, t)}{\partial x} + \frac{1}{2} \left(\frac{xu}{1-u}\right)^2 \frac{\partial^2 F_2^{NS}(x, t)}{\partial^2 x} + \dots.$$

Since  $x$  is small in our region of discussion, the terms containing  $x^2$  and higher powers of  $x$  can be neglected and we can rewrite

$$F_2^S\left(\frac{x}{\omega}, t\right) \approx F_2^S(x, t) + \frac{xu}{1-u} \frac{\partial F_2^S(x, t)}{\partial x}, \quad (3.6a)$$

$$G\left(\frac{x}{\omega}, t\right) \approx G(x, t) + \frac{xu}{1-u} \frac{\partial G(x, t)}{\partial x}, \quad (3.6b)$$

$$F_2^{NS}\left(\frac{x}{\omega}, t\right) \approx F_2^{NS}(x, t) + \frac{xu}{1-u} \frac{\partial F_2^{NS}(x, t)}{\partial x}. \quad (3.6c)$$

Here if we introduce the higher order terms in Taylor's expansion, then also there is no modification of the solution. Because when we solve the second order partial differential equation by Monges Method [75], which will be produced by introducing the second order terms in Taylor expansion, then ultimately it becomes the first order as before due to the form of the DGLAP equation. Similarly by introducing more terms in Taylor expansion, we hope for these cases also the terms can be neglected due to still smaller values of  $x$  [82 - 85].

Using equations (3.6a) and (3.6b) and performing  $u$ -integrations we get

$$I_1^S(x,t) = \{-3+2x+x^2\}F_2^S(x,t) + \{x-x^3-2x\ln(x)\} \frac{\partial F_2^S(x,t)}{\partial x}, \quad (3.7a)$$

$$I_2^S(x,t) = 2N_f \left[ \left( \frac{2}{3} - x + x^2 - \frac{2}{3}x^3 \right) G(x,t) + \left( -\frac{5}{2}x + 3x^2 - 2x^3 + \frac{2}{3}x^4 - x \ln(x) \right) \frac{\partial G(x,t)}{\partial x} \right]. \quad (3.7b)$$

Putting equations (3.7a) and (3.7b) in equation (3.3) we get

$$\frac{\partial F_2^S(x,t)}{\partial t} - \frac{\alpha_s}{2\pi} \left[ A_1(x)F_2^S(x,t) + A_2(x) \frac{\partial F_2^S(x,t)}{\partial x} + A_3(x)G(x,t) + A_4(x) \frac{\partial G(x,t)}{\partial x} \right] \quad (3.8)$$

where  $A_1(x) = 2x + x^2 + 4\ln(1-x)$ ,  $A_2(x) = x - x^3 - 2x\ln(x)$ ,

$$A_3(x) = 2N_f \left( \frac{2}{3} - x + x^2 - \frac{2}{3}x^3 \right) \quad \text{and} \quad A_4(x) = 2N_f \left( -\frac{5}{2}x + 3x^2 - 2x^3 + \frac{2}{3}x^4 - x \ln(x) \right).$$

In order to solve equation (3.8), we need to relate the singlet structure function  $F_2^S(x,t)$  with the gluon structure function  $G(x,t)$ . For small- $x$  and high- $Q^2$ , the gluon is expected to be more dominant than the sea quark. But for lower- $Q^2$ , there is no such clear cut distinction between the two [79, 82]. Hence for simplicity, let us assume

$$G(x,t) = k(x)F_2^S(x,t), \quad (3.9)$$

where  $k(x)$  is a suitable function of  $x$  or may be a constant. Here we may assume  $k(x) = k, ax^b, ce^{-dx}$  where  $k, a, b, c$  and  $d$  are suitable parameters which can be determined by phenomenological analysis. But the possibility of the breakdown of relation also can not be ruled out [79, 82, 85]. Now equation (3.8) gives

$$-t \frac{\partial F_2^s(x, t)}{\partial t} + L_1(x) \frac{\partial F_2^s(x, t)}{\partial x} + M_1(x) F_2^s(x, t) = 0, \quad (3.10)$$

where

$$L_1(x) = A_f [(A_2 + kA_4)], \quad (3.11a)$$

$$M_1(x) = A_f \left[ \left( A_1 + kA_3 + \frac{\partial k}{\partial x} A_4 \right) \right]. \quad (3.11b)$$

To introduce Method of characteristics, let us consider two new variables  $S$  and  $\tau$  instead of  $x$  and  $t$ , such that

$$\frac{dt}{dS} = -t, \quad (3.12a)$$

$$\frac{dx}{dS} = L(x), \quad (3.12b)$$

which are known as characteristic equations [77]. Again according to the rule of PDE we have

$$\frac{dt}{dS} \frac{\partial F_2^s(x, t)}{\partial t} + \frac{dx}{dS} \frac{\partial F_2^s(x, t)}{\partial x} = \frac{dF_2^s(x, t)}{dS}.$$

Thus putting equations (3.12a) and (3.12b) in equation (3.10), we get

$$\frac{dF_2^s(S, \tau)}{dS} + M_1(S, \tau) F_2^s(S, \tau) = 0 \quad (3.13)$$

Then equation (3.13) gives  $\frac{dF_2^s(S, \tau)}{F_2^s(S, \tau)} = -M_1(S, \tau) dS$ , which can be solved as

$$F_2^s(S, \tau) = F_2^s(0, \tau) \exp \left[ - \int_0^S M_1(S, \tau) dS \right]. \quad (3.14)$$

For  $t$ -evolution, structure function varies with  $t$  remaining  $x$  constant [79]. Thus

the equation (3.14) becomes  $F_2^s(S, \tau) = F_2^s(\tau) \left( \frac{t}{t_0} \right)^{M_1(S, \tau)}$  with the initial condition:

when  $S = 0$  then  $t = t_0$  and  $F_2^s(S, \tau) = F_2^s(0, \tau)$ . Now we have to replace the coordinate system  $(S, \tau)$  to  $(x, t)$  with the input function  $F_2^s(0, \tau) = F_2^s(x, t_0)$  and will get the  $t$ -evolution of singlet structure function in LO as

$$F_2^s(x, t) = F_2^s(x, t_0) \left( \frac{t}{t_0} \right)^{M_1(x)}. \quad (3.15)$$

Similarly for x-evolution, structure function varies with x remaining t constant.

Thus the equation (3.14) becomes  $F_2^S(S, \tau) = F_2^S(S) \exp \int -\frac{M_1(S, \tau)}{L_1(S, \tau)} dx$  with the initial condition: when  $\tau = 0$  then  $x = x_0$  and  $F_2^S(S, \tau) = F_2^S(S, 0)$ . Now we have to replace the co-ordinate system  $(S, \tau)$  to  $(x, t)$  with the input function  $F_2^S(S, 0) = F_2^S(x_0, t)$  and will get the x-evolution of singlet structure function in LO as

$$F_2^S(x, t) = F_2^S(x_0, t) \exp \int_{x_0}^x -\frac{M_1(x)}{L_1(x)} dx . \quad (3.16)$$

Proceeding in the same way, we get t and x evolutions of non-singlet structure function from equation (3.4) as

$$F_2^{NS}(x, t) = F_2^{NS}(x, t_0) \left(\frac{t}{t_0}\right)^{A_1} A_1(x) \quad (3.17a)$$

and

$$F_2^{NS}(x, t) = F_2^{NS}(x_0, t) \exp \int_{x_0}^x -\frac{A_1(x)}{A_2(x)} dx . \quad (3.17b)$$

The deuteron, proton and neutron structure functions measured in DIS can be written in terms of singlet and non-singlet quark distribution functions [80] as

$$F_2^d(x, t) = \frac{5}{9} F_2^S(x, t), \quad (3.18a)$$

$$F_2^p(x, t) = \frac{5}{18} F_2^S(x, t) + \frac{3}{18} F_2^{NS}(x, t), \quad (3.18b)$$

$$F_2^n(x, t) = \frac{5}{18} F_2^S(x, t) - \frac{3}{18} F_2^{NS}(x, t). \quad (3.18c)$$

Thus

$$F_2^{NS}(x, t) = 3[2F_2^p(x, t) - F_2^d(x, t)], \quad (3.18d)$$

$$F_2^{NS}(x, t) = 3[F_2^p(x, t) - F_2^n(x, t)]. \quad (3.18e)$$

The t and x-evolution of deuteron structure functions in LO can be obtained by putting equations (3.15) and (3.16) respectively in the equation (3.18a) as



$$F_2^d(x, t) = F_2^d(x, t_0) \left( \frac{t}{t_0} \right)^{M_1(x)} \quad (3.19a)$$

$$F_2^d(x, t) = F_2^d(x_0, t) \exp \int_{x_0}^x - \frac{M_1(x)}{L_1(x)} dx \quad (3.19b)$$

where

$$F_2^d(x, t_0) = \frac{5}{2} F_2^S(x, t_0), \quad (3.20a)$$

$$F_2^d(x_0, t) = \frac{5}{2} F_2^S(x_0, t). \quad (3.20b)$$

Equations (3.19a) and (3.19b) are used in our phenomenological work for deuteron structure function and equations (3.17a) and (3.17b) are used for non-singlet structure function which is the combination of proton and neutron related by the relations (3.18d) or (3.18e).

## 3.2 Results and Discussions

Here we compare our results of  $t$  and  $x$ -evolution of deuteron structure function  $F_2^d(x, t)$  as well as non-singlet structure function  $F_2^{NS}(x, t)$  measured by the NMC in muon-deuteron DIS [113], Fermilab E665 data in muon-deuteron DIS [114], CLAS Collaboration from the CEBAF Large Acceptance Spectrometer (CLAS) at the Thomas Jefferson National Accelerator Facility [115, 116] as well as NNPDF Collaboration [117, 118, 119] based on Artificial Neural Networks by considering their parameterization from NMC and BCDMS [120] data. We consider the QCD cut-off parameter  $\Lambda_{\overline{MS}} = 0.323$  GeV for  $\alpha_s(M_Z^2) = 0.119 \pm 0.002$  [57]. In all plots, solid curves are our best fit results. Experimental data and parameterization are given with vertical upper and lower error bars for total uncertainties of statistical and systematic errors. Structure functions at lowest- $Q^2$  for  $t$ -evolutions and at largest- $x$  for  $x$ -evolutions are taken as input functions.

The NMC data consist of four data sets for the proton and the deuteron structure functions corresponding to beam energies of 90 GeV<sup>2</sup>, 120 GeV<sup>2</sup>, 200

GeV<sup>2</sup> and 280 GeV<sup>2</sup>. They cover the kinematics range  $0.002 \leq x \leq 0.60$  and  $0.5 \text{ GeV}^2 \leq Q^2 \leq 75 \text{ GeV}^2$ . Again E665 data were taken at Fermilab in inelastic muon scattering with average beam energy of 470 GeV<sup>2</sup>. Similarly in CLAS Collaboration data, measurement of the deuteron structure function from the inclusive cross sections measured in interactions of electrons with a liquid deuterium target. The data cover  $Q^2$  values from 0.4 to 6 GeV<sup>2</sup>. The data are taken from the CLAS internal note from Osipenka et al. The authors combine these data with other world data to study the  $Q^2$  evolution of its moments and higher twist effects [115]. On the other hand, the BCDMS data consist of four data sets for the proton structure function, corresponding to beam energies of 100 GeV<sup>2</sup>, 120 GeV<sup>2</sup>, 200 GeV<sup>2</sup> and 280 GeV<sup>2</sup> and three data sets for the deuteron structure function corresponding to beam energies of 120 GeV<sup>2</sup>, 200 GeV<sup>2</sup> and 280 GeV<sup>2</sup>. They cover the kinematic range of  $0.06 \leq x \leq 0.80$  and  $7 \text{ GeV}^2 \leq Q^2 \leq 280 \text{ GeV}^2$ . For our phenomenological work, we consider the ranges as  $0.0045 \leq x \leq 0.180$  and  $0.75 \text{ GeV}^2 \leq Q^2 \leq 48.0 \text{ GeV}^2$  for NMC data,  $0.01 \leq x \leq 0.069$  and  $1.496 \text{ GeV}^2 \leq Q^2 \leq 13.391 \text{ GeV}^2$  for E665 data,  $0.1225 \leq x \leq 0.9055$  and  $5.075 \text{ GeV}^2 \leq Q^2 \leq 5.925 \text{ GeV}^2$  for CLAS collaboration, and also  $0.001 \leq x \leq 0.80$  and  $1 \text{ GeV}^2 \leq Q^2 \leq 100 \text{ GeV}^2$  for NNPDF collaboration respectively.

As NNPDF Collaboration are based on Artificial Neural Networks, considered their parameterization for deuteron and non-singlet structure functions from NMC and BCDMS data, thus for our phenomenological analysis we have considered the data sets of structure functions in the range of what the NMC and BCDMS provided at small- $x$ . Artificial neural networks provide unbiased robust universal approximation to incomplete or noisy data. In particular, artificial neural networks are now a well established technique in high energy physics, where they are used for event reconstruction in particle detectors. The NNPDF approach [117, 118, 119] can be divided into four main steps – (a) the generation of a large sample of Monte Carlo replicas of the original experimental data, in a way that central values, errors and correlations are reproduced with enough accuracy, (b) the training of a set of PDFs parameterized by neural networks on each of the above Monte Carlo replicas of

the data. PDFs are parameterized at the initial evolution scale  $Q_0^2$  and then evolved to the experimental data scale  $Q^2$  by means of the DGLAP equations, (c) the neural net training is stopped dynamically before entering into the over learning regime, that is, so that the PDFs learn the physical laws which underlie experimental data without fitting simultaneously statistical noise and finally, (d) once the training of the Monte Carlo replicas has been completed, a set of statistical estimators can be applied to the set of PDFs, in order to assess the statistical consistency of their results. Here the systematic errors are – (a) calibration of the incoming muon energy, (b) calibration of the outgoing muon energy, (c) spectrometer resolution, (d) absolute normalization uncertainty and (e) relative normalization uncertainties.

In figures 3.1, we have plotted computed values of  $F_2^d(x, t)$  against  $Q^2$  values for  $x = 0.0045$  and  $x = 0.008$  considering  $k(x) = k$ , a constant and compared with NMC data. It is found that agreements of our results with data are best for  $1.03 \leq k \leq 1.6$  in the entire range of our discussion.

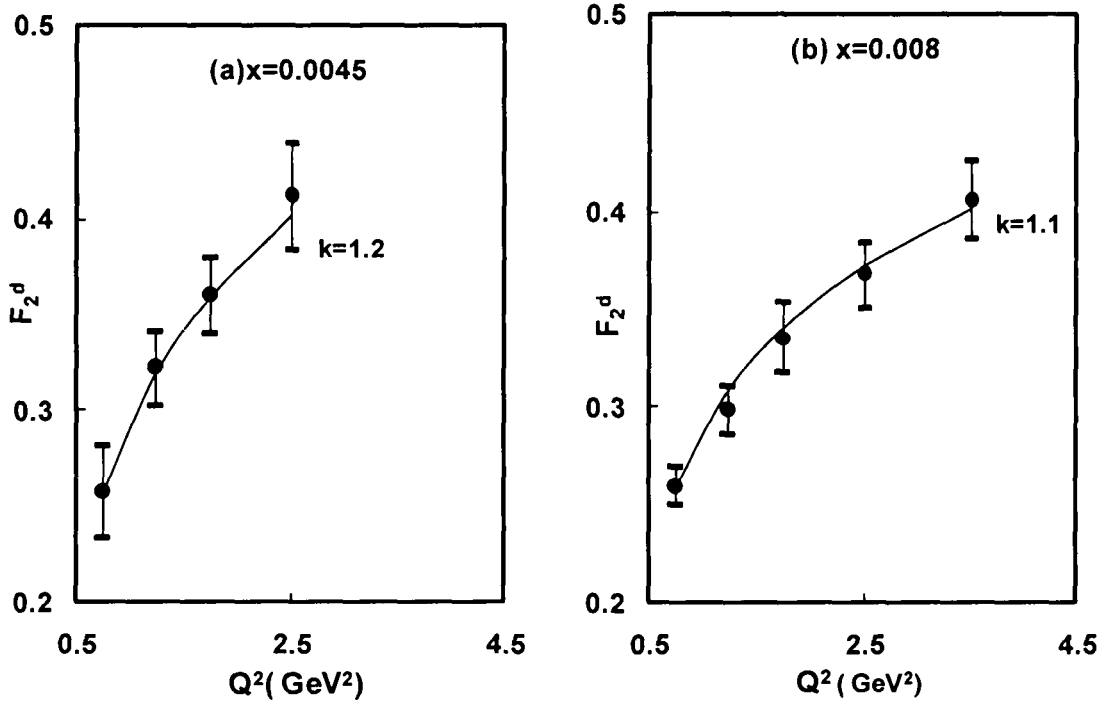


Figure 3.1: Comparison of  $t$ -evolution of deuteron structure function in LO with NMC data considering  $k(x) = k$ , a constant

In figures 3.2, we have plotted computed values of  $F_2^d(x,t)$  against  $Q^2$  values for a fixed  $x$  with  $k(x) = ax^b$ , a power function of  $x$  and compared with NMC data. Here we have plotted the graphs for  $x = 0.008$  and  $x = 0.0125$  respectively. It is found that agreements of our results with data are excellent for  $5 \leq a \leq 10$  and  $0.5 \leq b \leq 1.0$  in the range of our consideration.

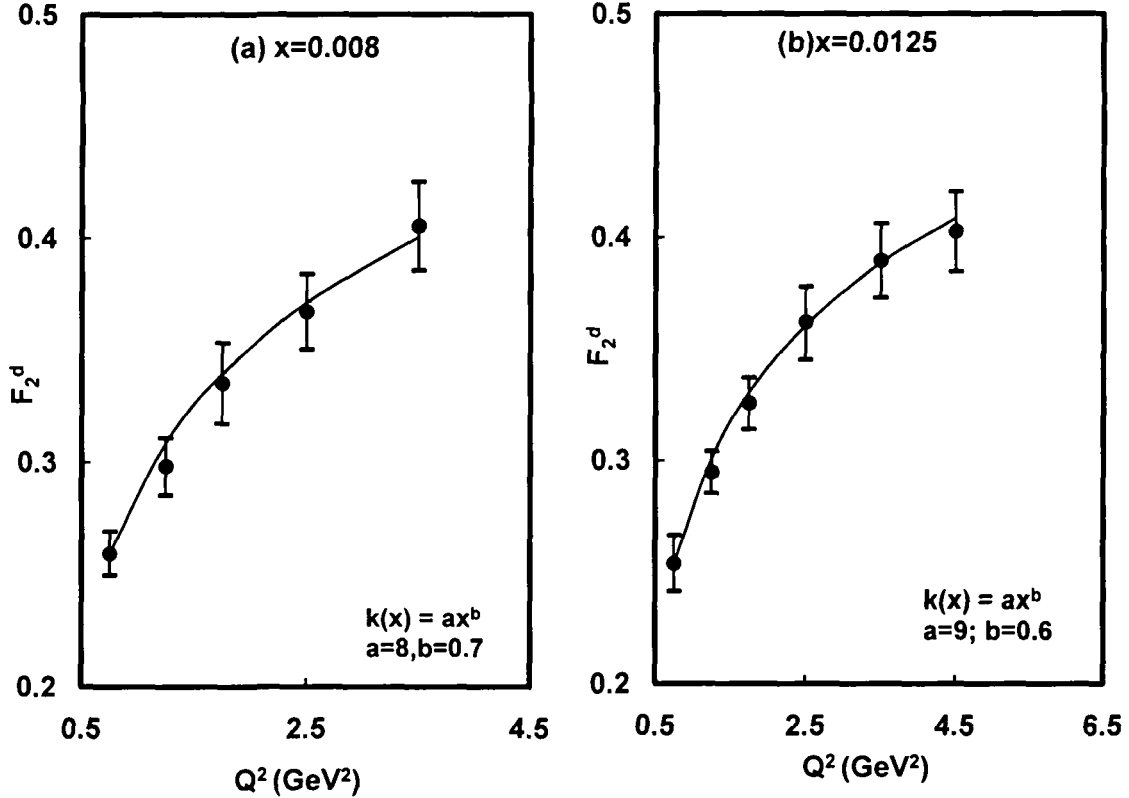


Figure 3.2: Comparison of t-evolution of deuteron structure function in LO with NMC data considering  $k(x) = ax^b$ , a power function of  $x$

In figures 3.3, we have plotted computed values of  $F_2^d(x,t)$  against  $Q^2$  for a fixed  $x$  considering  $k(x) = ce^{-dx}$  and compared with NMC data. It is found that agreements of our results with experimental data are excellent for  $3 \leq c \leq 7$  and  $10 \leq d \leq 20$  in the range of our consideration. In figures 3.4, we have tested the sensitivity of parameter  $k$  for t-evolution within our observation and found the best agreement with the range  $1.03 \leq k \leq 1.6$  for the NMC data. Here as we go for smaller  $x$ , the best fitting curve will get for higher value of  $k$ . Thus we say that gluon structure functions dominate at small- $x$ .

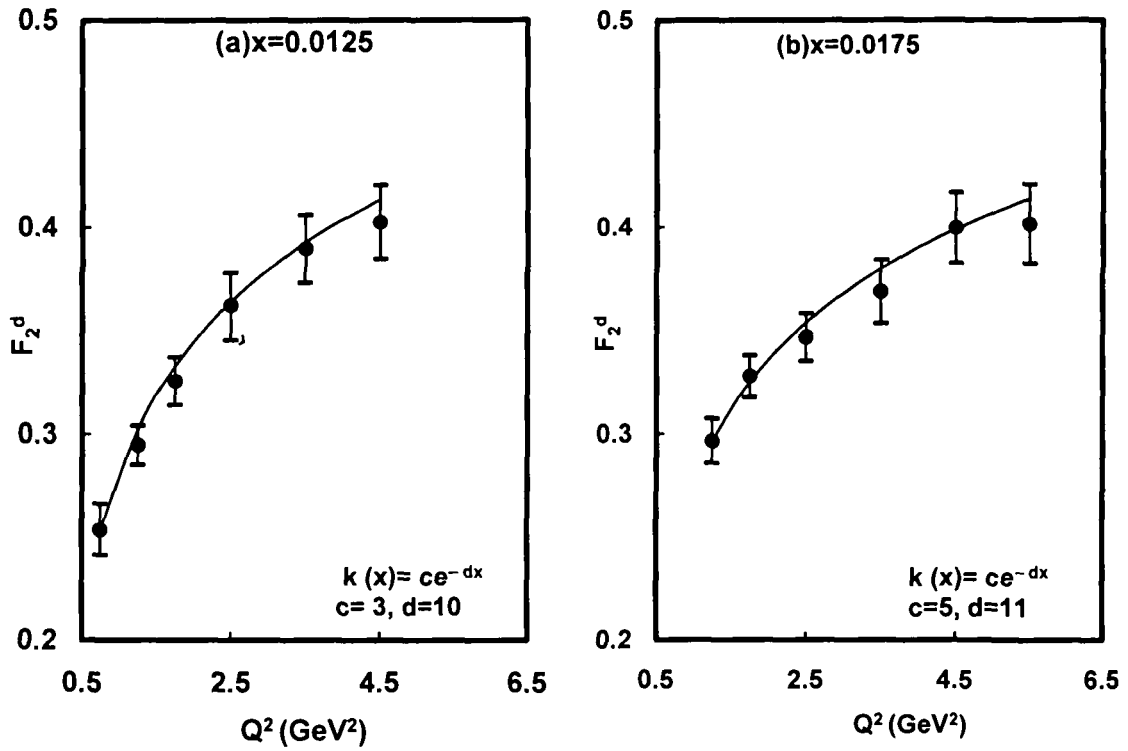


Figure 3.3: Comparing t-evolution of deuteron structure function in LO with NMC data considering  $k(x) = ce^{-dx}$ , an exponential function of  $x$

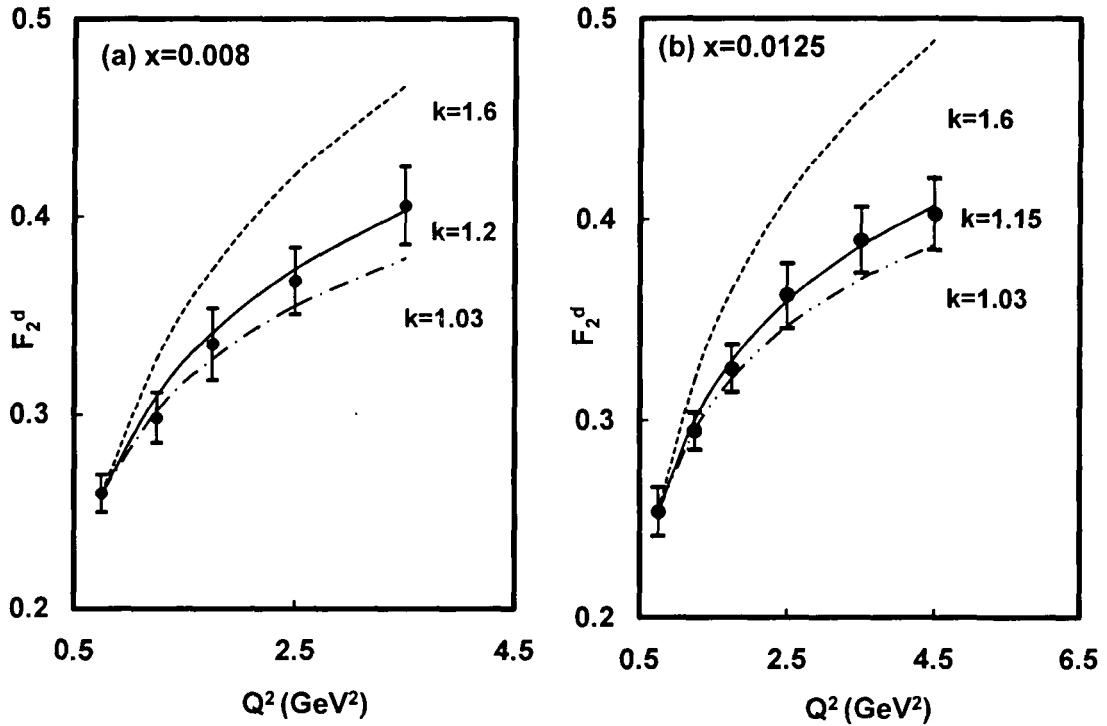


Figure 3.4: Sensitivity of parameter  $k$  in t-evolutions

In figures 3.5 for  $x$ -evolution, we have plotted computed values of  $F_2^d(x,t)$  against the  $x$  values for a fixed  $Q^2$  with considering  $k(x) = k$ , as a constant and compared with NMC data. Here we have plotted the graphs for  $Q^2 = 11.5$  and  $27 \text{ GeV}^2$  for the range of  $0.025 \leq x \leq 0.14$ . The best-fit curves get for the range of  $1.0 \leq k \leq 1.3$  and as  $Q^2$  increases the  $k$  value also increases.

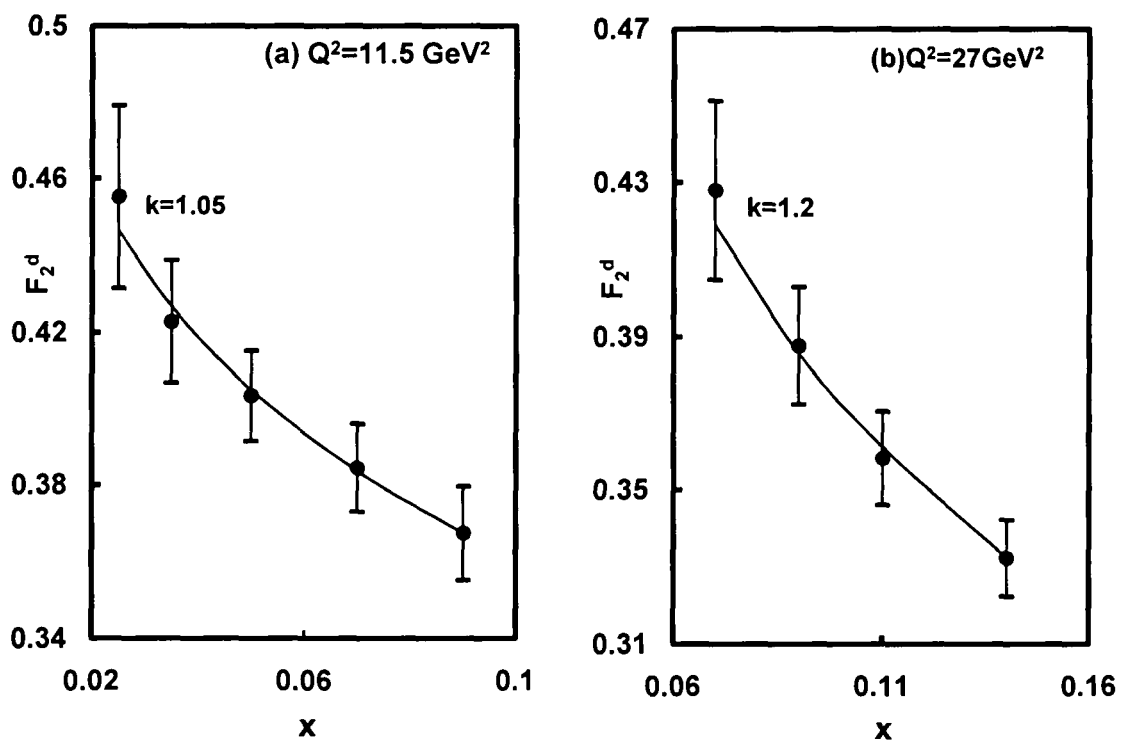


Figure 3.5: Comparing  $x$ -evolution of deuteron structure function in LO with NMC data considering  $k(x) = k$ , a constant

In figure 3.6 for  $x$ -evolution, we have plotted computed values of  $F_2^d(x,t)$  against the  $x$  values for a fixed  $Q^2$  with  $k(x) = ax^b$ , a power function of  $x$ . Our results are compared with NMC data. The best-fit curves are for the range of  $5 \leq a \leq 10$  and  $b=1.0$  in our region of discussion.

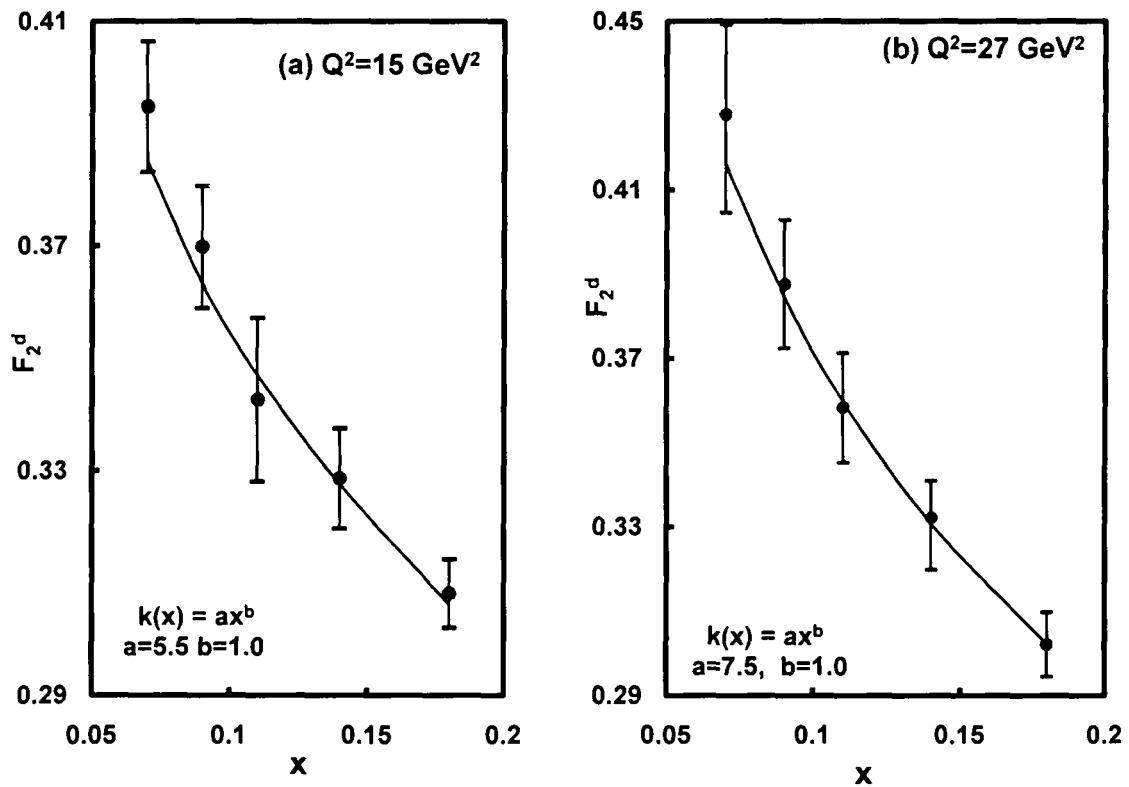


Figure 3.6: Comparing  $x$ -evolution of deuteron structure function in LO with NMC data considering  $k(x) = ax^b$ , a power function of  $x$

In figure 3.7 for  $x$ -evolution, we have plotted computed values of  $F_2^d(x, t)$  against the  $x$  values for a fixed  $Q^2$  with  $k(x) = ce^{-dx}$ , exponential function of  $x$ . Our results are compared with NMC data and the best-fit curves are for  $3 \leq c \leq 8$  and  $10 \leq d \leq 20$  within our range of discussion.

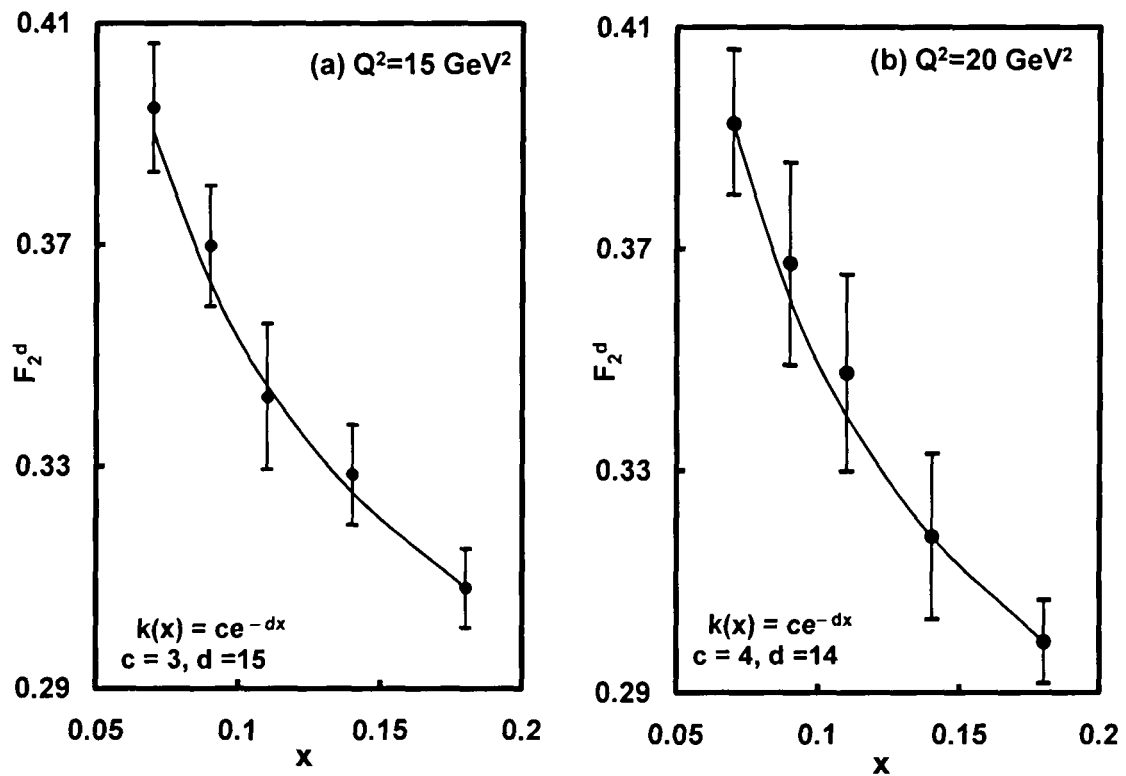


Figure 3.7: Comparing  $x$ -evolution of deuteron structure function in LO with NMC data considering  $k(x) = ce^{-dx}$ , an exponential function of  $x$



In figure 3.8, we have plotted computed values of  $F_2^d(x, t)$  against the  $x$  values for a fixed  $Q^2$  with  $k(x)=k$ , a constant and our results are compared with CLAS collaboration data. Though our theory on the DGLAP evolution equation are satisfied at high- $Q^2$  and small- $x$ , but CLAS data are available at comparably smaller- $Q^2$  and higher- $x$ . Thus our results are not properly satisfied with entire range of CLAS collaboration data. The best-fit curves are for  $0.6 \leq k \leq 1.0$  with high- $Q^2$  and small- $x$  ranges that available in CLAS collaboration. Since the results for  $k(x) = ax^b$  and  $k(x) = ce^{-dx}$  have no significant variation with the results for  $k(x) = k$ , so the earlier results are not included here.

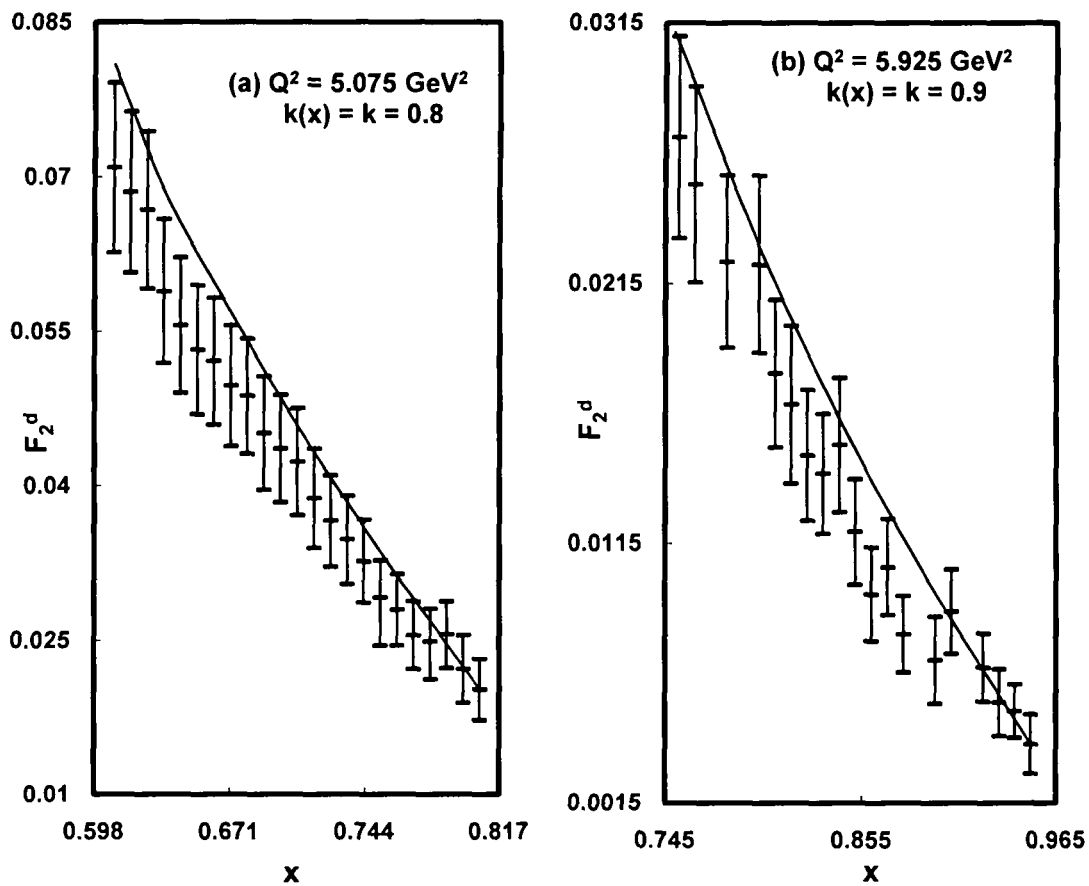


Figure 3.8: Comparing  $x$ -evolution of deuteron structure functions in LO with CLAS Collaboration data considering  $k(x) = k$ , a constant

In figures 3.9, we have plotted computed values of  $F_2^d(x, t)$  against the  $Q^2$  values for a fixed  $x$  and our results are compared with NNPDF collaboration data where the range of data used to train the 1000 nets which produced the results in ranges  $0.003 \leq x \leq 0.8$ ;  $0.5 \text{ GeV}^2 \leq Q^2 \leq 280 \text{ GeV}^2$  for the deuteron and non-singlet structure functions. Here we have considered  $k(x) = k$ , a constant and best-fit curves are for  $k = 1.1$ . The results for  $k(x) = ax^b$  and  $k(x) = ce^{-dx}$  have no significant variation, so these are not included here.

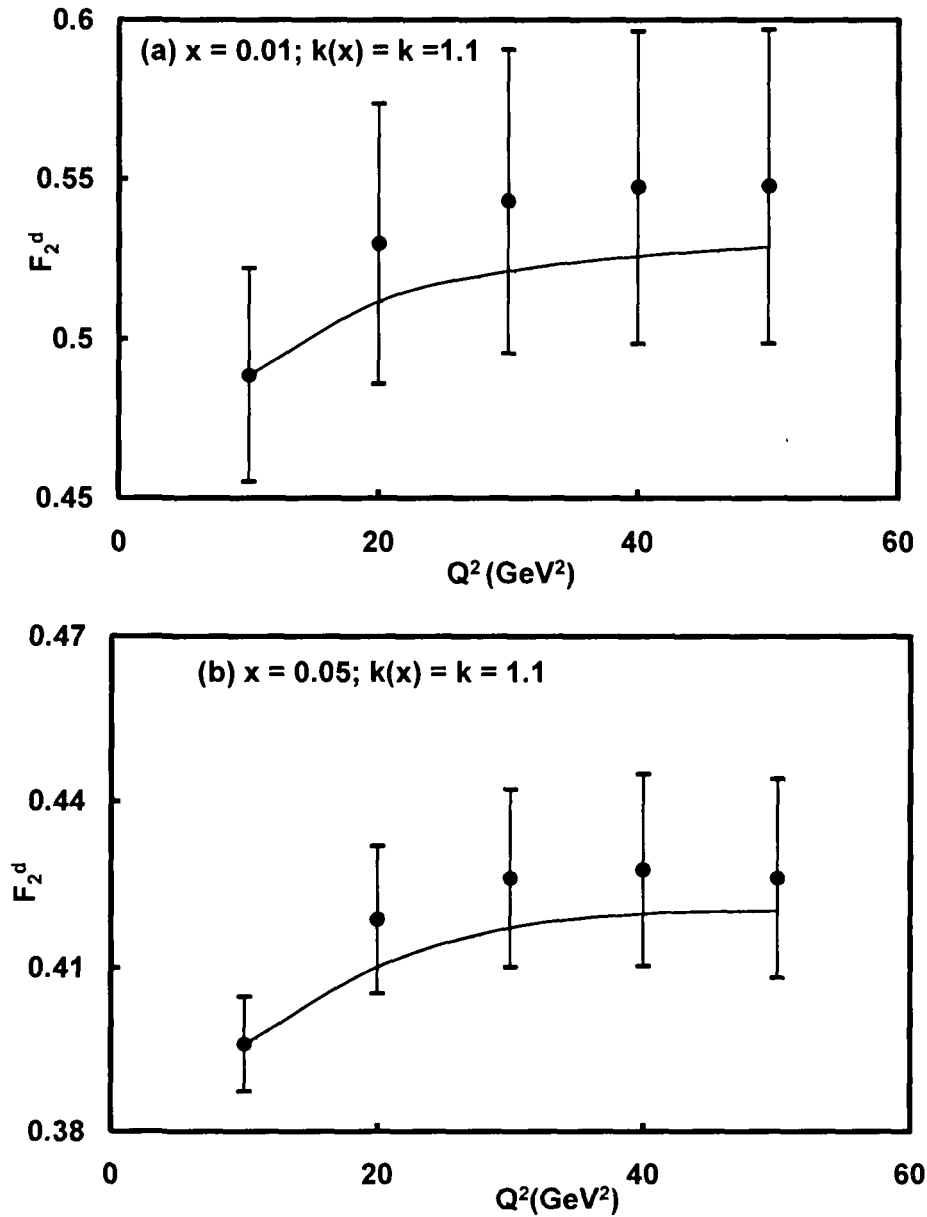


Figure 3.9: Comparing t-evolution of deuteron structure function in LO with NNPDF collaboration data considering  $k(x) = k$ , a constant

In figures 3.10, for  $x$ -evolution, we have plotted computed values of  $F_2^d(x, t)$  against the  $x$  values for a fixed  $Q^2$  with  $k(x)$  as a constant and our results are compared with NNPDF collaboration data. The best-fit curves are for  $k(x) = k = 1.2$ . The results for  $k(x) = ax^b$  and  $k(x) = ce^{-dx}$  have no significant variation, so these are not included here.

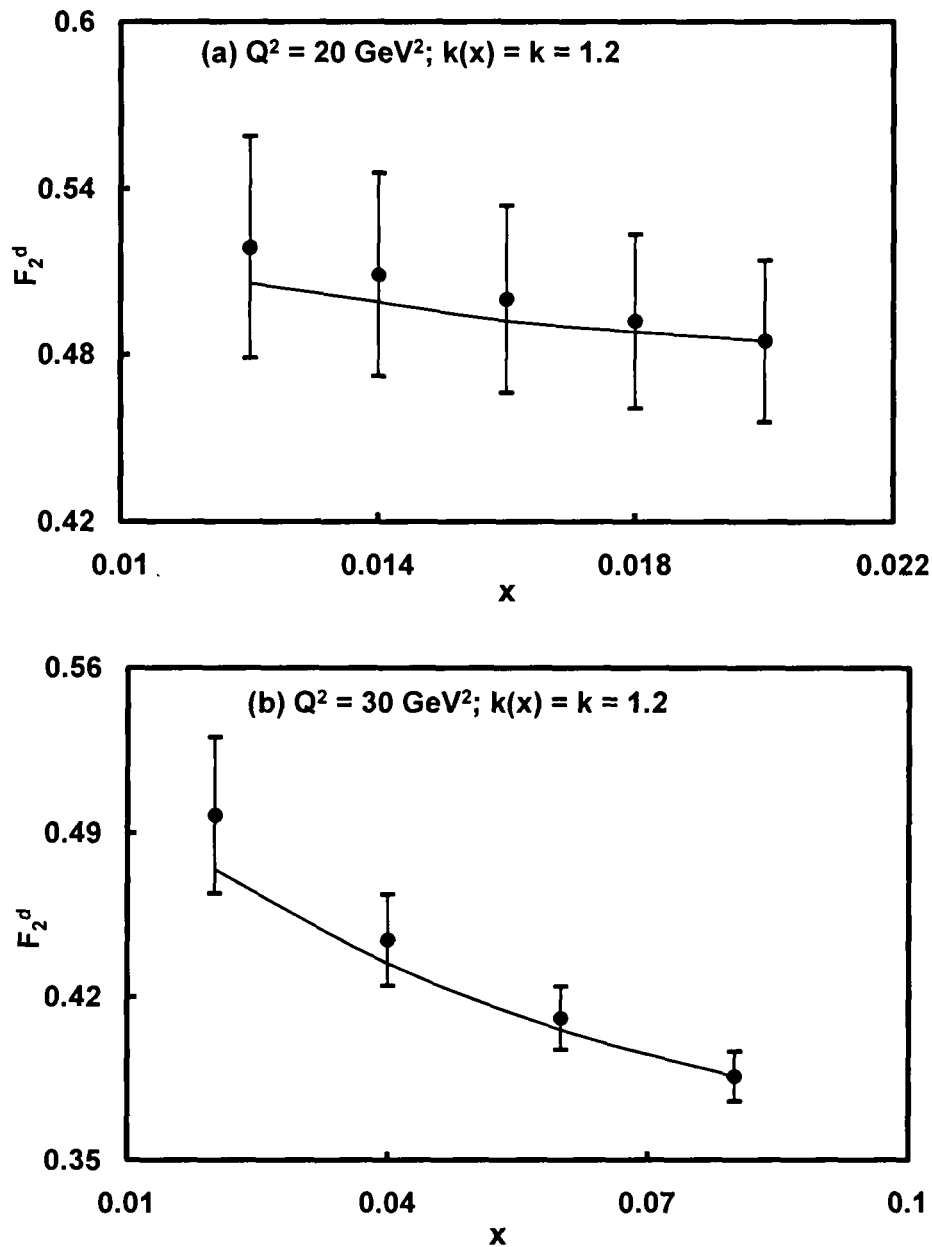
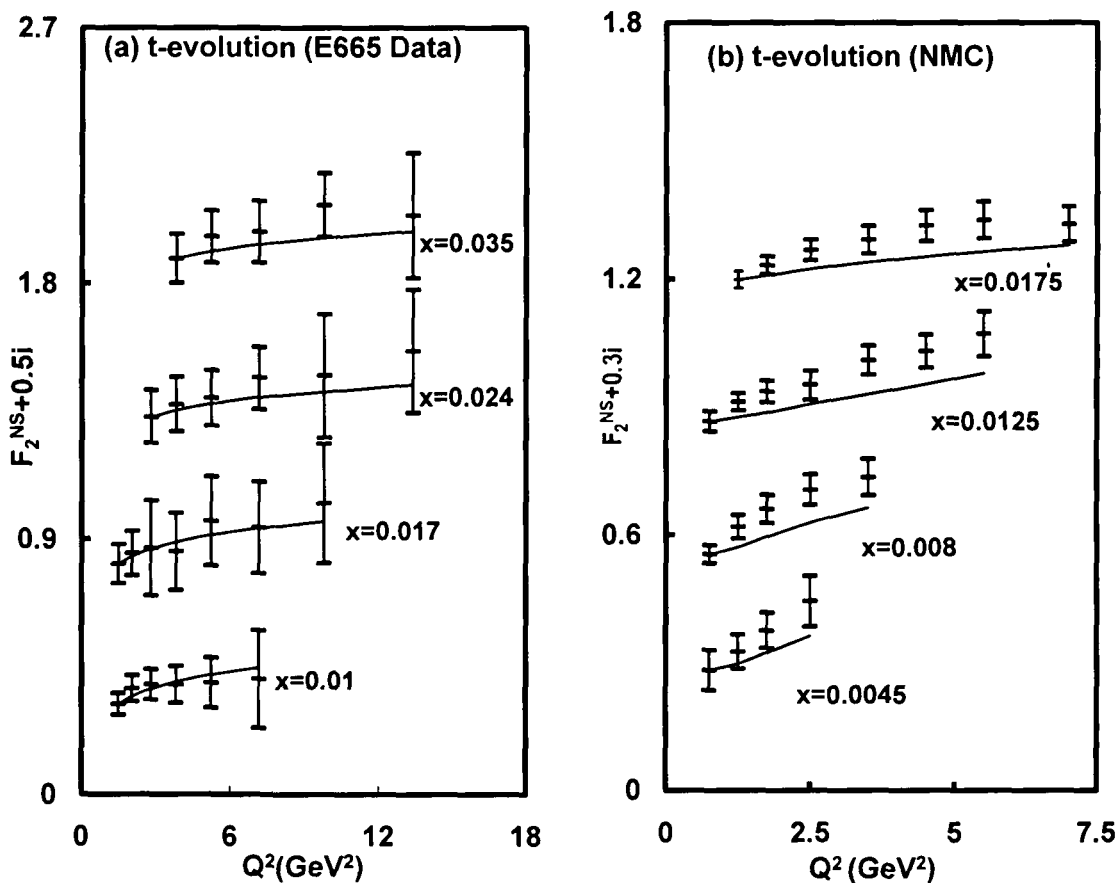


Figure 3.10: Comparing  $x$ -evolution of deuteron structure function in LO with NNPDF collaboration data considering  $k(x) = k$ , a constant

In figures 3.11, we have plotted computed values of  $F_2^{NS}(x,t)$  against  $Q^2$  values for fix values of  $x$  at 0.01, 0.017, 0.024, 0.035 for E665 data and at 0.0045, 0.008, 0.0125, 0.0175 for NMC data. The computed values are plotted against the corresponding values of  $Q^2$  for the range from 1.496 GeV<sup>2</sup> to 13.396 GeV<sup>2</sup> for E665 data and from 0.75 GeV<sup>2</sup> to 7.0 GeV<sup>2</sup> for NMC data.



**Figure 3.11:** t- evolution of non-singlet structure functions in LO compared with E665 and NMC data. Value of each data point is increased by adding 0.5*i* and 0.3*i*, where  $i = 0, 1, 2, 3, \dots$

In figure 3.12, the computed values of  $F_2^{NS}(x, t)$  against  $x$  are plotted for fix  $Q^2$  at 5.236 GeV<sup>2</sup>, 7.161 GeV<sup>2</sup>, 9.795 GeV<sup>2</sup>, 13.391 GeV<sup>2</sup> for E665 data and at 9.0 GeV<sup>2</sup>, 11.5 GeV<sup>2</sup>, 15.0 GeV<sup>2</sup>, 20.0 GeV<sup>2</sup> for NMC data. The data at highest values of  $x$  are taken as input values.

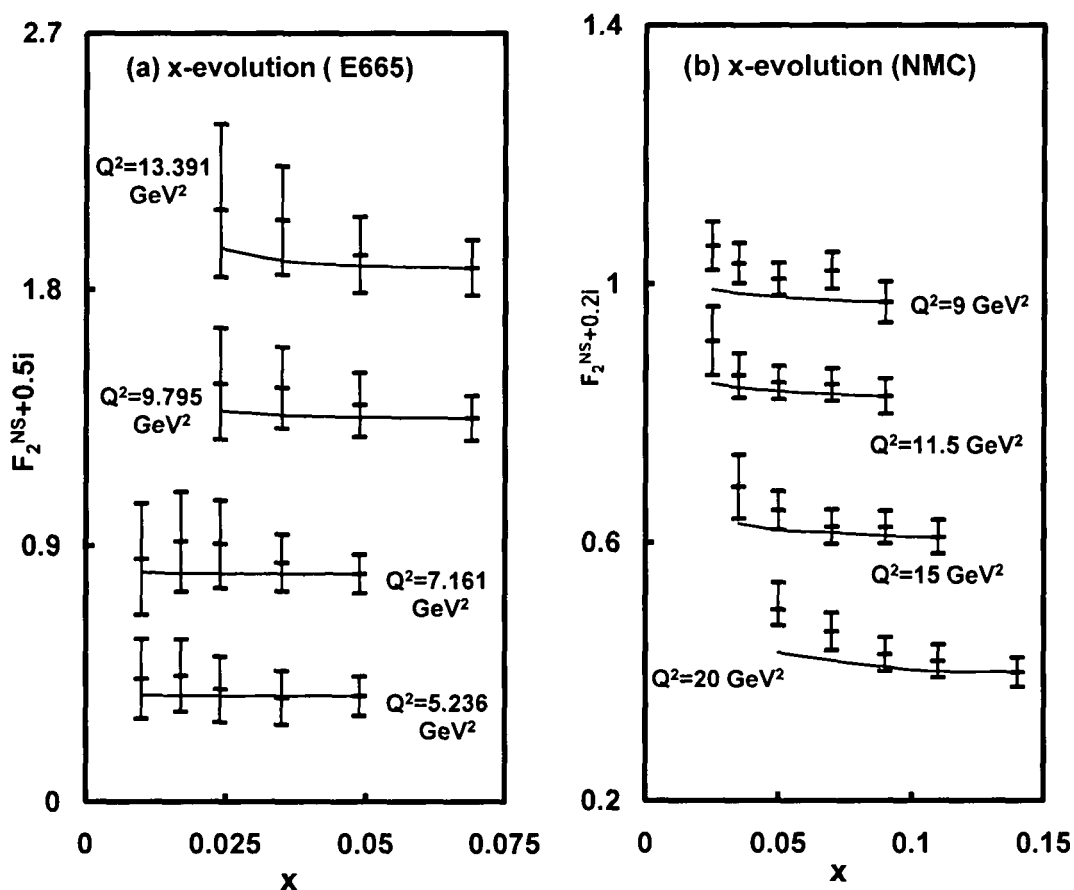


Figure 3.12: x-evolution of non-singlet structure functions in LO compared with E665 and NMC data. Value of each data point is increased by adding 0.5*i* and 0.2*i*, where  $i = 0, 1, 2, 3, \dots$

### 3.3 Conclusion

In this chapter, we have solved the unpolarized DGLAP evolution equations for singlet and non-singlet structure functions in LO by using method of characteristics. Also we have derived the  $t$  and  $x$ -evolutions of deuteron as well as non-singlet structure functions and our results are compared with NMC, E665, CLAS collaboration data and NNPDF parameterization results. It is seen that structure functions increase as  $Q^2$  increases from lower to higher values and decrease with  $x$  from higher to lower values. Our results are in good agreement with these data sets especially at small- $x$  and high- $Q^2$  region. Though results in some graphs do not agree very well with data sets, but our expectation is that it will be better in higher orders viz. NLO and NNLO which will discuss in chapter 4 and chapter 5 respectively.  $\square$

## Unpolarized DGLAP Evolution Equations in Next-to-Leading Order

The DGLAP evolution equations have been solved in NLO at the small- $x$  limit. Here we have used a Taylor series expansion and then the method of characteristics to solve the evolution equations. We have also calculated  $t$  and  $x$ -evolutions of deuteron structure function as well as non-singlet structure function and the results are compared with the New Muon collaboration (NMC) data [113], E665 data [114], CLAS collaboration data [115, 116] and NNPDF parameterization [117, 118, 119].

### 4.1 Theory

Considering the splitting functions in NLO [121, 122, 123], the DGLAP evolution equations for singlet and non-singlet structure functions in NLO in standard form are

$$\frac{\partial F_2^S}{\partial t} - \frac{\alpha_s(t)}{2\pi} \left[ \frac{2}{3} \{3 + 4 \ln(1-x)\} F_2^S(x, t) + I_1^S(x, t) + I_2^S(x, t) \right] - \left( \frac{\alpha_s(t)}{2\pi} \right)^2 I_3^S = 0, \quad (4.1)$$

$$\frac{\partial F_2^{NS}}{\partial t} - \frac{\alpha_s(t)}{2\pi} \left[ \frac{2}{3} \{3 + 4 \ln(1-x)\} F_2^{NS}(x, t) + I_1^{NS}(x, t) \right] - \left( \frac{\alpha_s(t)}{2\pi} \right)^2 I_2^{NS} = 0. \quad (4.2)$$

Here  $I_1^S, I_2^S, I_3^S, I_1^{NS}, I_2^{NS}$  are some functions defined in Appendices A and B.

The strong coupling constant for NLO can be written as  $\alpha_s(t) = \frac{4\pi}{\beta_0 t} \left[ 1 - \frac{\beta_1 \ln t}{\beta_0^2 t} \right]$ ,

where  $\beta_0 = \frac{11}{3} N_c - \frac{4}{3} T_f$ ,  $\beta_1 = \frac{34}{3} N_c^2 - \frac{10}{3} N_c N_f - 2 C_F N_f$  and  $t = \ln \left( \frac{Q^2}{\Lambda^2} \right)$ .

Let us introduce the variable  $u=1-\omega$  and as discussed in Chapter 3, we can use Taylor's expansion series in  $F_2^S\left(\frac{x}{\omega}, t\right)$  and  $G\left(\frac{x}{\omega}, t\right)$ . Since  $x$  is small in our region of discussion, the terms containing  $x^2$  and higher powers of  $x$  can be neglected, i.e.

$$F_2^S\left(\frac{x}{\omega}, t\right) = F_2^S(x, t) + \frac{xu}{1-u} \frac{\partial F_2^S(x, t)}{\partial x},$$

$$G\left(\frac{x}{\omega}, t\right) = G(x, t) + \frac{xu}{1-u} \frac{\partial G(x, t)}{\partial x}.$$

Using these equations and performing  $u$ -integrations, equation (4.1) becomes the form

$$\begin{aligned} & \frac{\partial F_2^S(x, t)}{\partial t} - \frac{\alpha_s}{2\pi} \left[ A_1(x) F_2^S(x, t) + A_2(x) \frac{\partial F_2^S(x, t)}{\partial x} + A_3(x) G(x, t) + A_4(x) \frac{\partial G(x, t)}{\partial x} \right] \\ & - \left( \frac{\alpha_s}{2\pi} \right)^2 \left[ B_1(x) F_2^S(x, t) + B_2(x) \frac{\partial F_2^S(x, t)}{\partial x} + B_3(x) G(x, t) + B_4(x) \frac{\partial G(x, t)}{\partial x} \right], \quad (4.3) \end{aligned}$$

where functions  $A_1(x)$ ,  $A_2(x)$ ,  $A_3(x)$  and  $A_4(x)$  are discussed in chapter 3 and others are

$$B_1(x) = x \int_0^1 f(\omega) d\omega - \int_0^x f(\omega) d\omega + \frac{4}{3} N_f \int_x^1 F_{qq}(\omega) d\omega,$$

$$B_2(x) = x \int_x^1 \left[ f(\omega) + \frac{4}{3} N_f F_{qg}^S(\omega) \right] \frac{1-\omega}{\omega} d\omega,$$

$$B_3(x) = \int_x^1 F_{qg}^S(\omega) d\omega \quad \text{and} \quad B_4(x) = x \int_x^1 \frac{1-\omega}{\omega} F_{qg}^S(\omega) d\omega.$$

Now let us assume  $G(x, t) = k(x) F_2^S(x, t)$ , where  $k(x)$  is a suitable function of  $x$  or may be a constant. We may assume  $k(x) = k, ax^b, ce^{-dx}$  where  $k, a, b, c, d$  are suitable parameters which can be determined by phenomenological analysis. Thus equation (4.5) takes the form

$$-t \frac{\partial F_2^S(x, t)}{\partial t} + L_2(x) \frac{\partial F_2^S(x, t)}{\partial x} + M_2(x) F_2^S(x, t) = 0, \quad (4.4)$$

$$\text{where } \frac{\alpha_s(t)}{2\pi} = \frac{3A_f}{2t},$$



$$L_2(x) = A_f [(A_2 + k(x)A_4) + T_0(B_2 + k(x)C_4)], \quad (4.5a)$$

$$M_2(x) = A_f \left[ \left( A_1 + k(x)A_3 + \frac{\partial k(x)}{\partial x} A_4 \right) + T_0 \left( B_1 + k(x)B_3 + \frac{\partial k(x)}{\partial x} B_4 \right) \right]. \quad (4.5b)$$

Here we consider an extra assumption  $T^2 = T.T_0$  with  $T = \frac{\alpha_s(t)}{2\pi}$ , where  $T_0$  is a numerical parameter, which can be determined by phenomenological analysis [79, 124, 125].

To introduce the method of characteristics, let us consider two new variables  $S$  and  $\tau$  instead of  $x$  and  $t$ , such that  $\frac{dt}{dS} = -t$  and  $\frac{dx}{dS} = L_2(x)$ , which are known as characteristics equations. Putting these in equation (4.4) we get

$$\frac{dF_2^S(S, \tau)}{dS} + M_2(S, \tau)F_2^S(S, \tau) = 0. \quad (4.6)$$

This can be solved as

$$F_2^S(S, \tau) = F_2^S(0, \tau) \exp \left[ - \int_0^S M_2(S, \tau) dS \right]. \quad (4.7)$$

For  $t$ -evolution, structure function varies with  $t$  remaining  $x$  constant. Thus the equation (4.7) becomes  $F_2^S(S, \tau) = F_2^S(\tau) \left( \frac{t}{t_0} \right)^{M_2(S, \tau)}$ ;  $F_2^S(S, \tau) = F_2^S(\tau)$  for  $S=0, t=t_0$ .

Now we have to replace the co-ordinate system  $(S, \tau)$  to  $(x, t)$  with the input function  $F_2^S(\tau) = F_2^S(x, t_0)$  and will get the  $t$ -evolution of singlet structure function in the NLO as

$$F_2^S(x, t) = F_2^S(x, t_0) \left( \frac{t}{t_0} \right)^{A_f [P_1 + T_0 P_2]}. \quad (4.8a)$$

Similarly the  $x$ - evolution of singlet structure function in NLO will be

$$F_2^S(x, t) = F_2^S(x_0, t) \exp \int_{x_0}^x - \frac{[P_1 + T_0 P_2]}{[Q_1 + T_0 Q_2]} dx. \quad (4.8b)$$

where

$$P_1 = \left\{ A_1 + k(x)A_3 + \frac{\partial k(x)}{\partial x} A_4 \right\}, \quad P_2 = \left\{ B_1 + k(x)B_3 + \frac{\partial k(x)}{\partial x} B_4 \right\},$$

$$Q_1 = \{A_2 + k(x)A_4\}, \quad Q_2 = \{B_2 + k(x)B_4\}.$$

Proceeding in the same way, we get  $t$  and  $x$ -evolutions of non-singlet structure function in NLO from equation (4.2) as

$$F_2^{\text{NS}}(x, t) = F_2^{\text{NS}}(x, t_0) \left( \frac{t}{t_0} \right)^{A_f [A_1(x) + T_0 B_1(x)]}, \quad (4.9a)$$

$$F_2^{\text{NS}}(x, t) = F_2^{\text{NS}}(x_0, t) \exp \left[ - \int_{x_0}^x \frac{A_1(x) + T_0 B_1(x)}{A_2(x) + T_0 B_2(x)} dx \right], \quad (4.9b)$$

The deuteron and proton structure functions measured in DIS can be written in terms of singlet and non-singlet quark distribution functions, which are shown in the chapter 3. Thus the  $t$  and  $x$ -evolution of deuteron structure functions in NLO can be obtained as

$$F_2^{\text{d}}(x, t) = F_2^{\text{d}}(x, t_0) \left( \frac{t}{t_0} \right)^{A_f [P_1 + T_0 P_2]}, \quad (4.10a)$$

$$F_2^{\text{d}}(x, t) = F_2^{\text{d}}(x_0, t) \exp \int_{x_0}^x - \frac{[P_1 + T_0 P_2 + T_1 P_3]}{[Q_1 + T_0 Q_2 + T_1 Q_3]} dx. \quad (4.10b)$$

Here the input functions are  $F_2^{\text{d}}(x, t_0) = \frac{5}{2} F_2^{\text{S}}(x, t_0)$ ,  $F_2^{\text{d}}(x_0, t) = \frac{5}{2} F_2^{\text{S}}(x_0, t)$  and

$$F_2^{\text{NS}}(x, t) = 3[2F_2^{\text{p}}(x, t) - F_2^{\text{d}}(x, t)].$$

Thus for phenomenological analysis, we use equations (4.10a) and (4.1b) to study deuteron structure functions and equations (4.9a) and (4.9b) to study non-singlet (combination of proton and neutron) structure functions in NLO.

## 4.2 Results and Discussions

In this chapter, we compare our result of  $t$  and  $x$ -evolution of deuteron structure function  $F_2^{\text{d}}$  measured by the NMC in muon deuteron DIS with incident momentum 90, 120, 200, 280 GeV<sup>2</sup>, E665 data taken at Fermilab in inelastic muon scattering with an average beam energy of 470 GeV<sup>2</sup>, CLAS collaboration data at the Thomas Jefferson National Accelerator Facility [115, 116] as well as NNPDF parameterization [117, 118, 119] based on Artificial

Neural Networks. It is observed that our results are very sensitive to arbitrary parameters  $k$ ,  $a$ ,  $b$ ,  $c$  and  $d$  in  $t$ -evolution. Figures 4.2, 4.3 and 4.4 are for  $t$ -evolution of deuteron structure function as  $k(x) = k$  a constant, a power function  $ax^b$  and an exponential function  $ce^{-dx}$  of  $x$  respectively. We have plotted computed values of  $F_2^d(x, t)$  against  $Q^2$  values for a fixed  $x$  in LO and NLO for the various values of  $k(x)$ . Here the solid lines represent the best fitting curves for the parameters in NLO and the dotted lines represent those for LO evolutions. Figures 4.5, 4.6 and 4.7 are for  $x$ -evolution of deuteron structure function as  $k(x)$  a constant  $k$ , a power function  $ax^b$  and an exponential function  $ce^{-dx}$  of  $x$ . Here we have plotted computing values of  $F_2^d$  against the  $x$  values for a fixed  $Q^2$ . Here also the solid lines represent the best-fit curves for the parameters in NLO and the dotted lines represent in LO evolutions. In figure 4.8, the  $t$  and  $x$ -evolutions for non-singlet structure functions are compared with experimental data. For  $t$ -evolutions, the structure functions at lowest- $Q^2$  represent the input values and for  $x$ -evolution, the structure functions at highest- $x$  represent the input values.

In figure 4.1, we put  $T^2(t)$  and  $T_0T(t)$  against  $Q^2$  and we can see that for  $T_0 = 0.048$ , the values of  $T^2$  and  $T.T_0$  are nearly same in our region of discussion. Thus the consideration of parameter  $T_0$  does not give any abrupt change in our results.

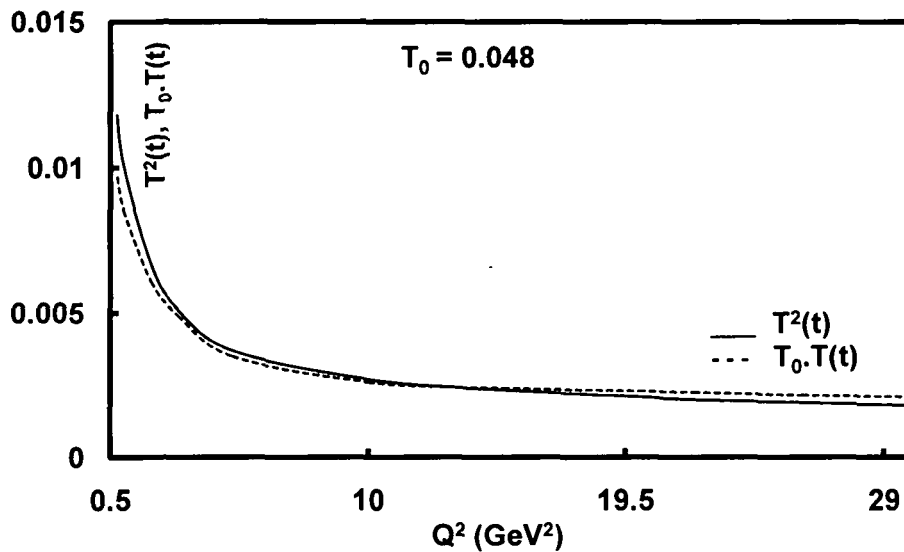


Figure 4.1 : Comparison of  $T^2$  and  $T_0.T$  values

In figures 4.2,  $t$ -evolutions of  $F_2^d$  has been obtained for fix values of  $x$  considering  $k(x) = k$ , a constant and our results are compared with NMC experimental data. Though the best fit curves found within  $1.0 \leq k \leq 2.0$  for our range of discussion, here excellent results are obtained for  $k= 1.4$  and  $1.1$  at  $x = 0.0045$  and  $0.0125$  respectively.

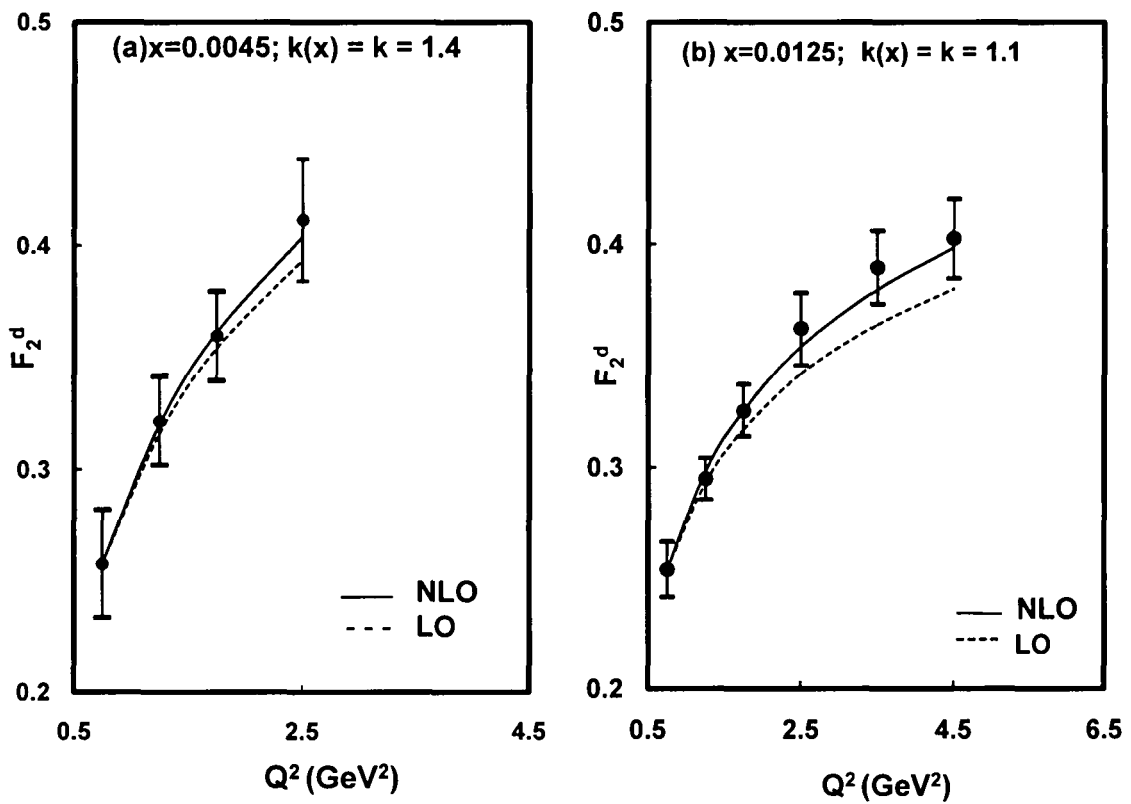


Figure 4.2:  $t$ -evolution of deuteron structure functions in NLO with  $k(x) = k$ , a constant, compared with NMC data

In figures 4.3,  $t$ -evolutions of  $F_2^d$  has been obtained for fixed values of  $x$  at  $x = 0.0045$  and  $0.0175$  considering  $k(x) = ax^b$ , a power function of  $x$  and our results are compared with NMC experimental data. Though the best fit curves are found within  $5.0 \leq a \leq 10.0$  and  $0.5 \leq b \leq 0.8$  for our range of discussion, here excellent results are obtained for  $a = 6.0$ ,  $b = 0.7$  and  $a = 8.0$ ,  $b = 0.7$  at  $x = 0.0045$  and  $0.0175$  respectively.

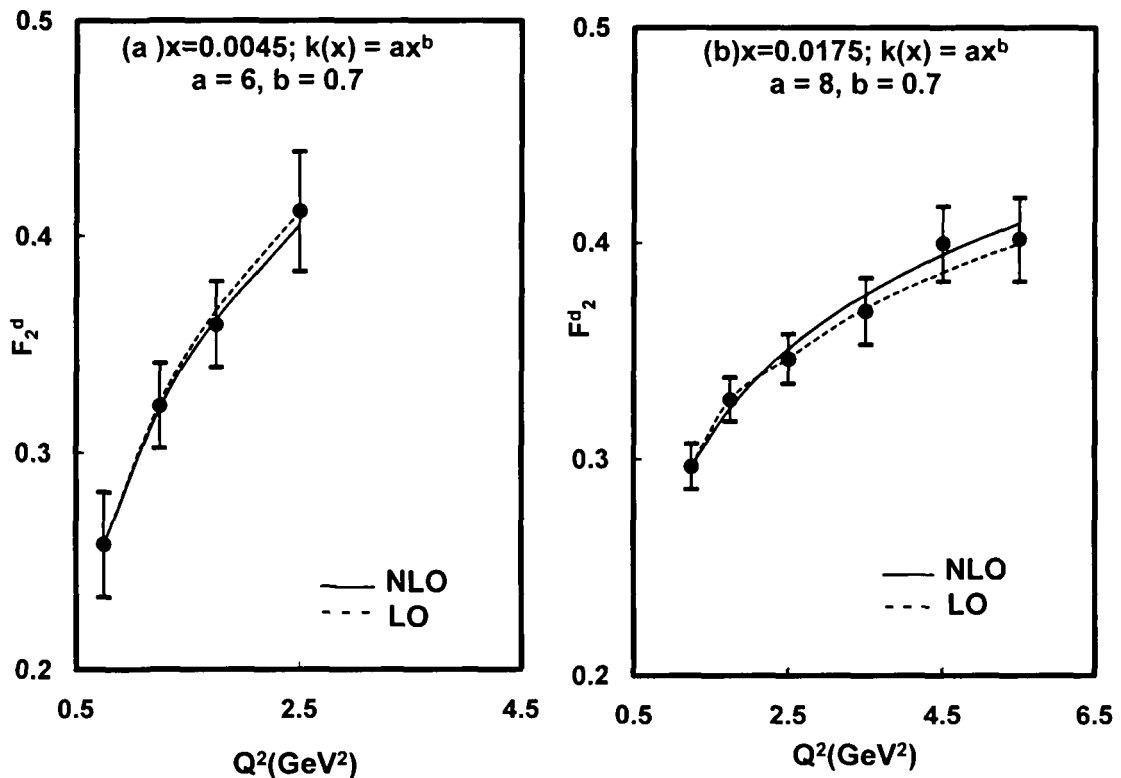


Figure 4.3:  $t$ -evolution of deuteron structure functions in NLO with  $k(x) = ax^b$ , a power function of  $x$ , compared with NMC data

In figures 4.4,  $t$ -evolutions of  $F_2^d$  has been obtained for fixed values of  $x$  at  $x = 0.0045$  and  $0.008$  considering  $k(x) = ce^{-dx}$ , an exponential function of  $x$  and our results are compared with NMC experimental data. Though the best fit curves are found within  $2.0 \leq c \leq 8.0$  and  $10.0 \leq d \leq 25.0$  for our range of discussion, here excellent results are obtained for  $c=4.0$ ,  $d=20.0$  and  $c=3.0$ ,  $d=15.0$  at  $x = 0.0045$  and  $0.008$  respectively.

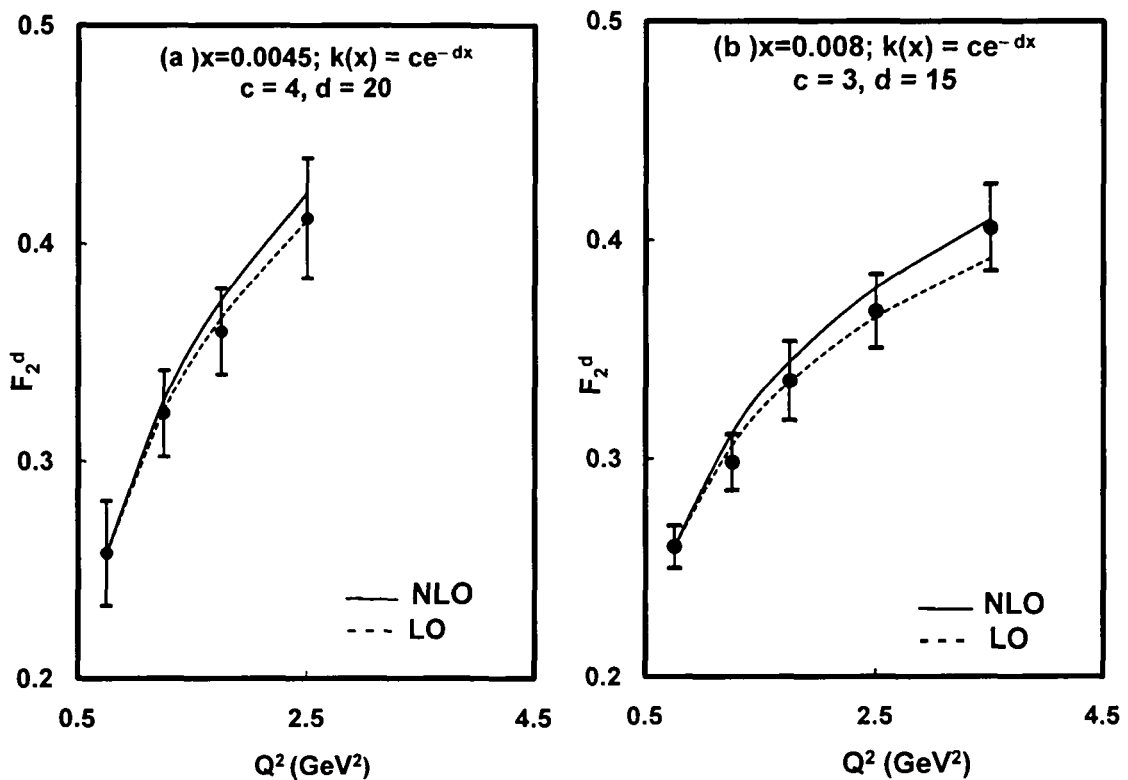


Figure 4.4:  $t$ -evolution of deuteron structure functions in NLO with  $k(x) = ce^{-dx}$ , an exponential function of  $x$ , compared with NMC data

In figures 4.5,  $x$ -evolutions of  $F_2^d$  has been obtained for fixed values of  $Q^2$  considering  $k(x) = k$ , a constant. Though the best fit curves are found within  $0.5 \leq k \leq 3.0$  for our range of discussion, here excellent results are obtained for  $k=1.1$  and  $k=1.3$  at  $Q^2 = 11.5 \text{ GeV}^2$  and  $27.0 \text{ GeV}^2$  respectively.

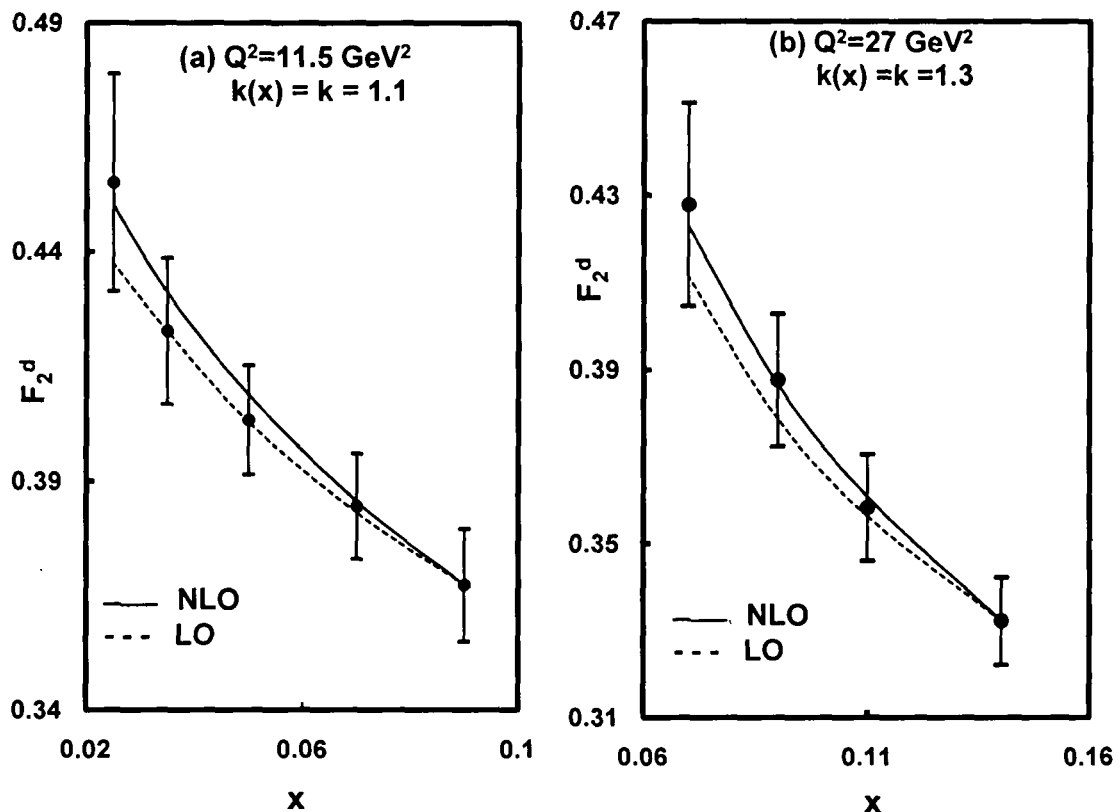


Figure 4.5:  $x$ -evolution of deuteron structure functions in NLO with  $k(x) = k$ , a constant, compared with NMC data

In figures 4.6,  $x$ -evolutions of  $F_2^d$  has been obtained for fixed values of  $Q^2$  considering  $k(x) = ax^b$ , a power function of  $x$ . Though the best fit curves are found within  $1.1 \leq a \leq 2.8$  and  $0.9 \leq b \leq 1.4$  for our range of discussion, here excellent results are obtained for  $a = 5.5, b = 1.0$  and  $a = 7.5, b = 1.0$  at  $Q^2 = 20.0$   $\text{GeV}^2$  and  $27.0$   $\text{GeV}^2$  respectively.

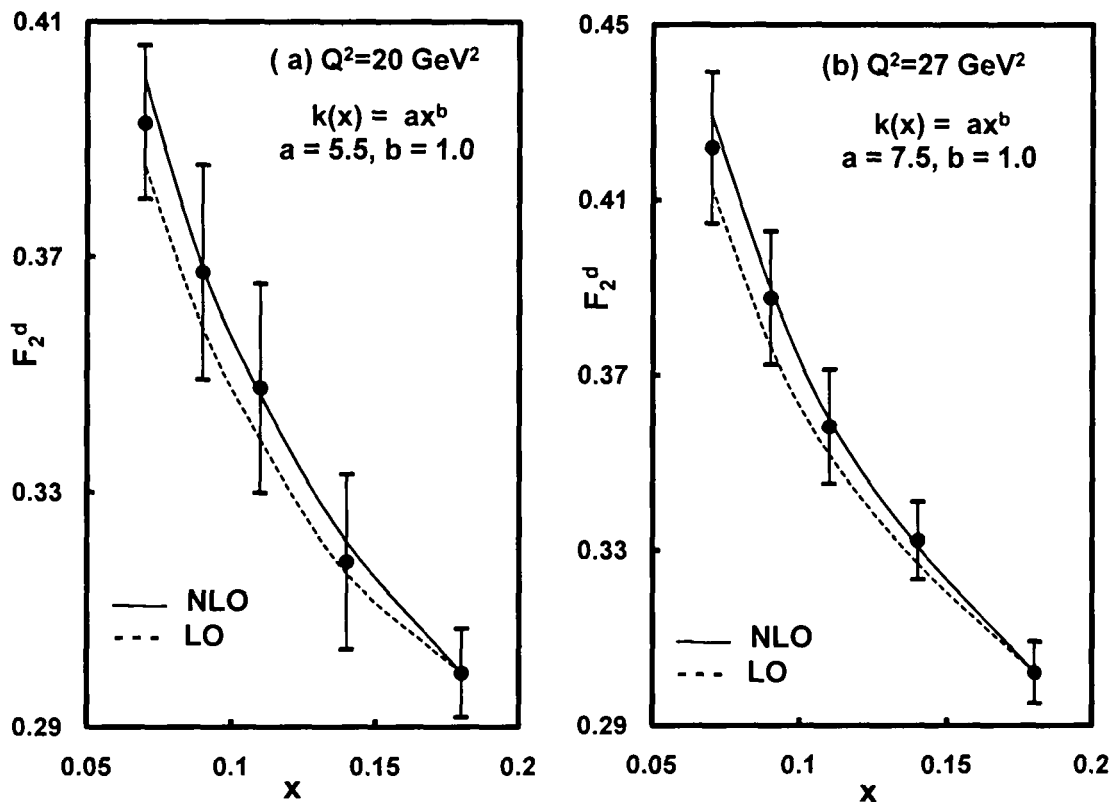
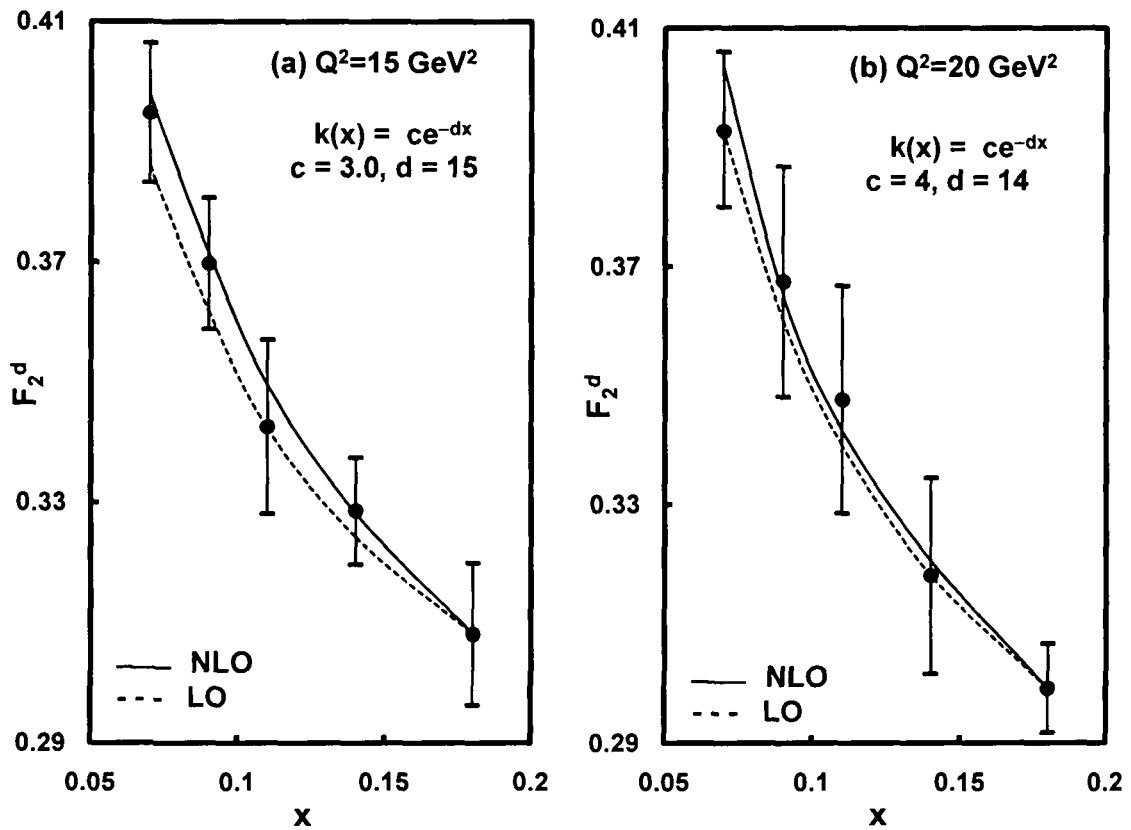


Figure 4.6:  $x$ -evolution of deuteron structure functions in NLO with  $k(x) = ax^b$ , a power function of  $x$ , compared with NMC data



In figures 4.7,  $x$ -evolutions of  $F_2^d$  has been obtained for fixed values of  $Q^2$  considering  $k(x) = ce^{-dx}$  as an exponential function of  $x$ . Though the best fit curves are found within  $3.0 \leq c \leq 8.0$  and  $10 \leq d \leq 20$  for our range of discussion, here excellent results are obtained for  $c=3.0$ ,  $d=15$  and  $c=4.0$ ,  $d=14$  at  $Q^2 = 15.0 \text{ GeV}^2$  and  $20.0 \text{ GeV}^2$ .



**Figure 4.7:**  $x$ -evolution of deuteron structure functions in NLO with  $k(x) = ce^{-dx}$ , an exponential function of  $x$ , compared with NMC data

In figure 4.8, we have plotted computing values of  $F_2^d(x,t)$  in NLO against the  $x$  values for a fixed  $Q^2$  with  $k(x) = k$ , a constant and results are compared with CLAS collaboration data and our LO results. Our solution of the DGLAP evolution equations are satisfied at high- $Q^2$  and small- $x$  but CLAS data are available at comparably smaller  $Q^2$  and higher- $x$ . Thus our results are not satisfied with entire range of CLAS collaboration data. The best-fit curves are obtained for  $0.6 \leq k \leq 1.0$  with high- $Q^2$  and small- $x$  ranges available in CLAS collaboration.

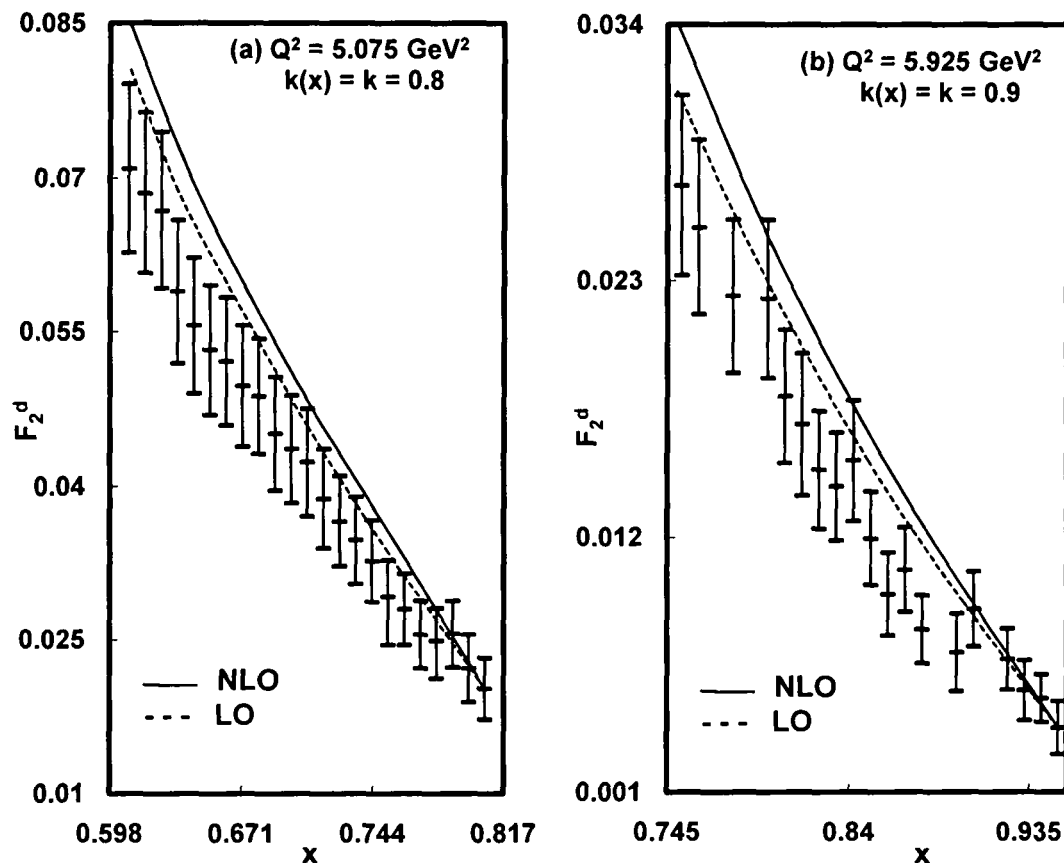


**Figure 4.8:**  $x$ -evolution of deuteron structure functions in NLO for  $k(x) = k$ , a constant, compared with CLAS collaboration data

In figures 4.9, we have plotted computed values of  $F_2^d(x,t)$  against the  $Q^2$  values for a fixed  $x$  and our results are compared with NNPDF collaboration parameterization where the range of data used to train the 1000 nets which produced the results in  $x = 0.003 - 0.8$ ;  $Q^2 = 0.5 - 280 \text{ GeV}^2$  for the deuteron and non-singlet structure functions. Here we have considered  $k(x) = k$ , a constant and best-fit curves are for  $k = 1.1$  at  $x = 0.05$  and  $0.01$ . The results for  $k(x) = ax^b$  and  $k(x) = ce^{-dx}$  have no significant variation, so these are not included here.

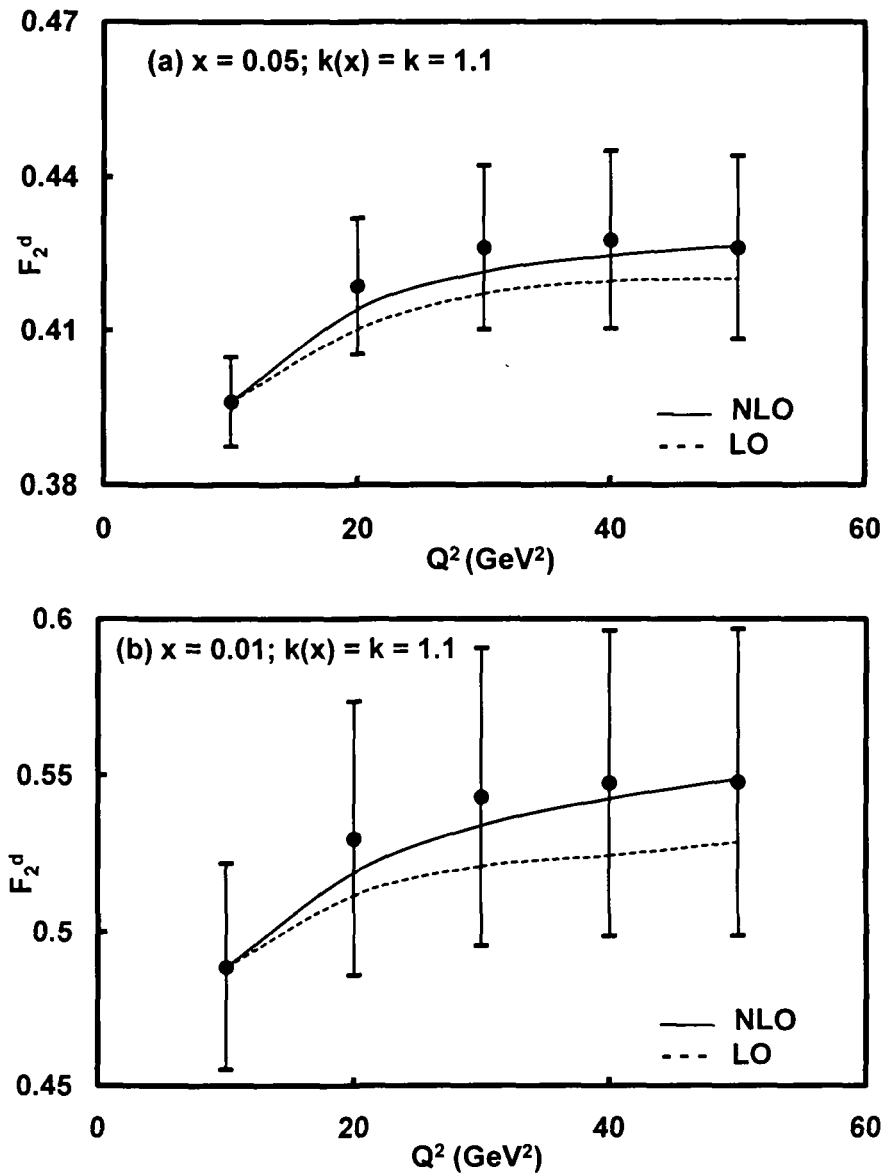


Figure 4.9:  $t$ -evolution of deuteron structure functions in NLO considering  $k(x) = k$ , a constant, compared with NNPDF parameterization

In figures 4.10, for  $x$ -evolution, we have plotted computed values of  $F_2^d(x, t)$  against the  $x$  values for a fixed  $Q^2$  with  $k(x) = k$ , a constant. The best-fit curves are for  $k(x) = k = 1.2$  at  $Q^2 = 20 \text{ GeV}^2$  and  $30 \text{ GeV}^2$ . The results for  $k(x) = ax^b$  and  $k(x) = ce^{-dx}$  have no significant variation, so these are not included here.

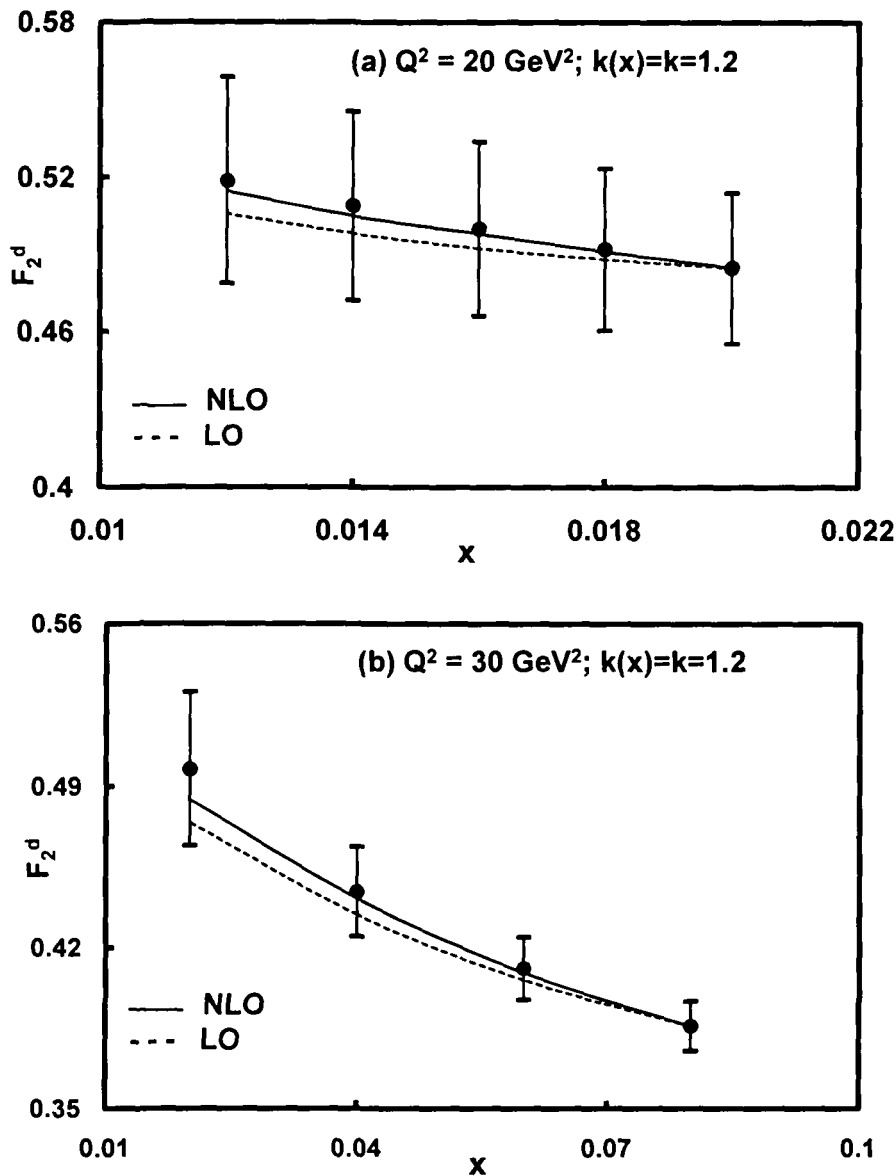


Figure 4.10:  $x$ -evolution of deuteron structure functions in NLO considering  $k(x) = k$ , a constant, compared with NNPDF parameterization

In figures 4.11, we have plotted computed values of  $F_2^{NS}(x, t)$  against the corresponding values  $Q^2$  for fixed values of  $x$ . Here the first plots are compared with E665 data for the values of  $Q^2$  from 1.496 GeV<sup>2</sup> to 13.396 GeV<sup>2</sup> at  $x = 0.01, 0.017, 0.024$  and  $0.035$ . Similarly second plots are compared with NMC data for the values of  $Q^2$  from 0.75 GeV<sup>2</sup> to 7.0 GeV<sup>2</sup> at  $x = 0.0045, 0.008, 0.0125$  and  $0.0175$ . Value of each data point is increased by adding  $0.5i$  and  $0.3i$  for E665 and NMC data, where  $i = 0, 1, 2, 3$  etc. Here we can mention that the non-singlet structure function does not include  $k(x)$ , hence our results are parameter free.

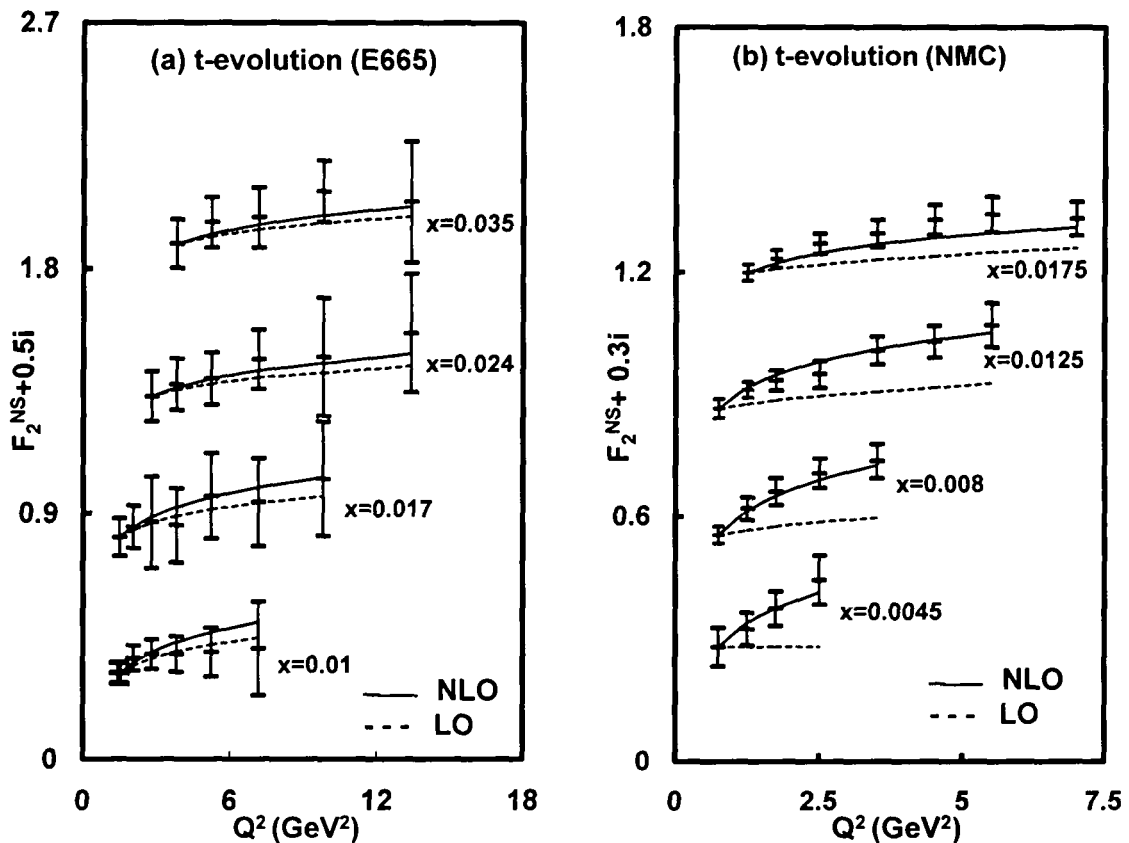
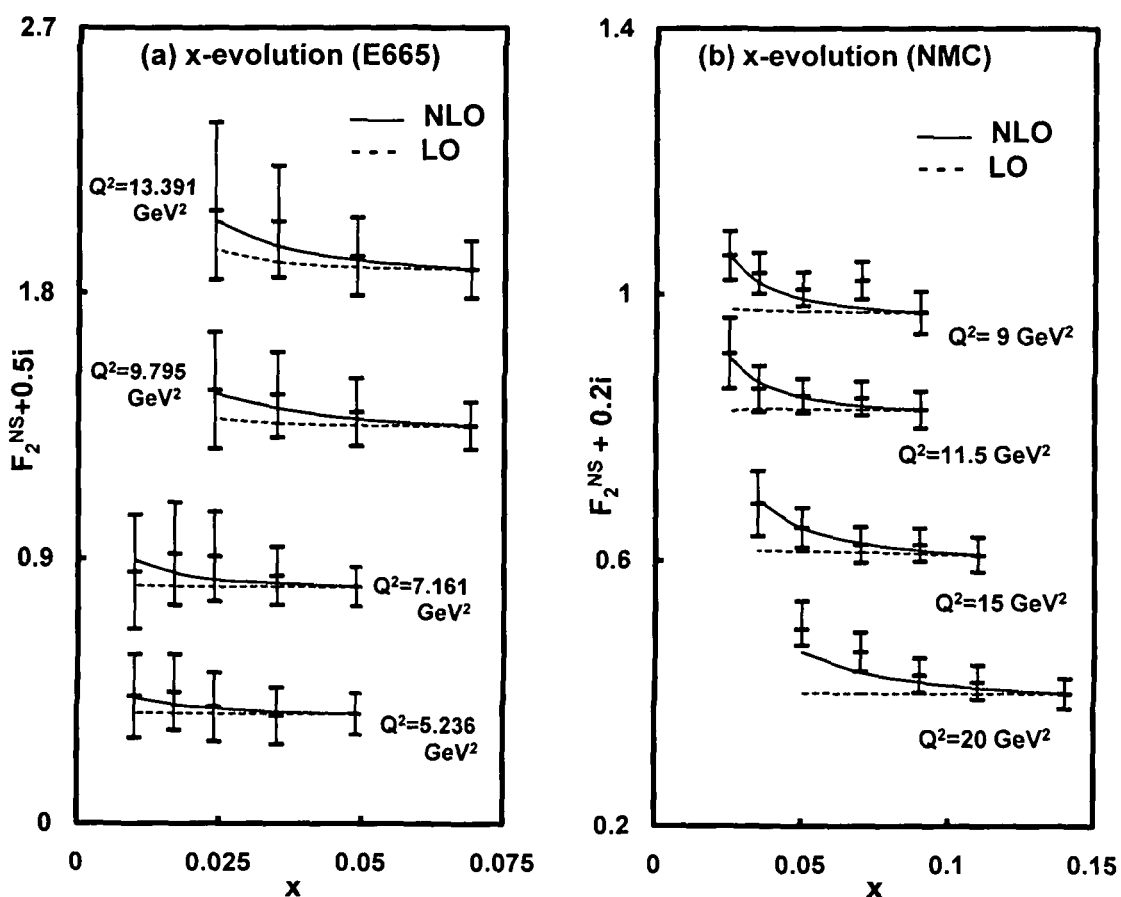


Figure 4.11: t-evolution of non-singlet structure functions in NLO compared with E665 and NMC data

In figures 4.12, the computed values of  $F_2^{NS}(x,t)$  against the corresponding values of  $x$  are plotted for fixed  $Q^2$ . Here the first plots are compared with E665 data for the values of  $x$  from 0.01 to 0.069 at  $Q^2 = 5.236$  GeV<sup>2</sup>, 7.161 GeV<sup>2</sup>, 9.795 GeV<sup>2</sup> and 13.396 GeV<sup>2</sup>. Similarly second plots are compared with NMC data for the values of  $x$  from 0.025 to 0.14 at  $Q^2 = 9.0$  GeV<sup>2</sup>, 11.5 GeV<sup>2</sup>, 15.0 GeV<sup>2</sup> and 20.0 GeV<sup>2</sup>. Value of each data point is increased by adding  $0.5i$  and  $0.2i$  for E665 and NMC data, where  $i = 0, 1, 2, 3$  etc. Here we can mention that the non-singlet structure function does not include  $k(x)$ , hence our results are parameter free.



**Figure 4.12:** x-evolution of non-singlet structure functions in NLO compared with E665 and NMC data

### 4.3 Conclusion

Here we solve the unpolarized DGLAP evolution equations in NLO for singlet and non-singlet structure functions by using method of characteristics. Also we calculate the deuteron structure function and non-singlet structure function in terms of proton and deuteron structure functions and our results are compared with NMC data, E665 data, CLAS collaboration data and NNPDF parameterization results. Our results are in good agreement with these data sets especially at small- $x$  and high- $Q^2$  region. It is seen that structure functions increase as  $Q^2$  increases from lower to higher values and decrease with  $x$  from higher to lower values also our results for NLO are better than that for LO. Though in some cases results do not agree with data sets very well, but our expectation is better in NNLO which will be discussed in chapter 5.  $\square$

## Unpolarized DGLAP Evolution Equations in Next-Next-to-Leading Order

The one and two-loop splitting functions have been known for a long time and we studied DGLAP evolution equations in LO and NLO in the chapter 3 and chapter 4 respectively. The computation of the three-loop contributions to the anomalous dimensions is needed to complete the NNLO calculations for DIS. The NNLO corrections should be included in order to arrive at quantitatively reliable predictions for hard processes at present and future high energy colliders. Recently the three loop splitting functions are introduced with a good phenomenological success [123 - 133]. Here we solve the DGLAP evolution equation in NNLO analytically by using method of characteristics and get unique solution with good agreement with experimental data. Hence it is significant as an important phenomenological work for studying structure functions. We have calculated  $t$  and  $x$ -evolutions of deuteron structure function as well as non-singlet structure function and the results are compared with the New Muon Collaboration (NMC) [113], E665 [114], CLAS collaboration [115, 116] data and NNPDF collaboration parameterization [117, 118, 119].



## 5.1 Theory

Considering the splitting functions  $P_{qq}^{(0)}(x)$  and  $P_{qq}^{(1)}(x)$ , the DGLAP equation have been solved in LO and NLO as discussed in Chapter 3 and Chapter 4 respectively. By adding  $P_{qq}^{(2)}(x)$  with previous terms we will get the NNLO evolution equations. The three loop quark-quark splitting function  $P_{qq}^{(2)}(x)$  can be expressed as

$$P_{qq}^{(2)} = P_{NS}^{(2)} + P_{PS}^{(2)} \quad (5.1)$$

The non-singlet contribution  $P_{NS}^{(2)}$  [131] dominates  $P_{qq}^{(2)}$  at large- $x$ , where the 'pure singlet' term  $P_{PS}^{(2)}$  [132] is very small. At small- $x$ , on the other hand, the latter contribution takes over as  $xP_{PS}^{(2)}$  does not vanish for  $x \rightarrow 0$ , unlike  $xP_{NS}^{(2)}$ . The splitting functions are obtained from the N-space results of the Mellin space by an inverse Mellin transformation [125-135].

After simplification, the singlet and non-singlet DGLAP evolution equations in NNLO take the form as

$$\begin{aligned} \frac{\partial F_2^S}{\partial t} - \frac{\alpha_s(t)}{2\pi} \left[ \frac{2}{3} \{3 + 4\ln(1-x)\} F_2^S(x, t) + I_1^S(x, t) + I_2^S(x, t) \right] \\ - \left( \frac{\alpha_s(t)}{2\pi} \right)^2 I_3^S(x, t) - \left( \frac{\alpha_s(t)}{2\pi} \right)^3 I_4^S(x, t) = 0 \end{aligned} \quad (5.2)$$

$$\begin{aligned} \frac{\partial F_2^{NS}}{\partial t} - \frac{\alpha_s(t)}{2\pi} \left[ \frac{2}{3} \{3 + 4\ln(1-x)\} F_2^{NS}(x, t) + I_1^{NS}(x, t) \right] \\ - \left( \frac{\alpha_s(t)}{2\pi} \right)^2 I_2^{NS}(x, t) - \left( \frac{\alpha_s(t)}{2\pi} \right)^3 I_3^{NS}(x, t) = 0. \end{aligned} \quad (5.3)$$

Functions  $I_1^S, I_2^S, I_3^S, I_4^S, I_1^{NS}, I_2^{NS}, I_3^{NS}$  are defined in Appendices A, B and C. Here  $x$ -space splitting functions are behaved well at small- $x$  [133].

Now introducing the variable  $u = 1 - \omega$ , as in Chapter 3, we have

$$F_2^S\left(\frac{x}{\omega}, t\right) = F_2^S(x, t) + \frac{xu}{1-u} \frac{\partial F_2^S(x, t)}{\partial x}, \quad (5.4)$$

$$G\left(\frac{x}{\omega}, t\right) = G(x, t) + \frac{xu}{1-u} \frac{\partial G(x, t)}{\partial x}. \quad (5.5)$$

Using these and performing u-integrations, equation (5.2) takes the form

$$\begin{aligned} & \frac{\partial F_2^S(x, t)}{\partial t} - \frac{\alpha_s}{2\pi} \left[ A_1(x)F_2^S(x, t) + A_2(x) \frac{\partial F_2^S(x, t)}{\partial x} + A_3(x)G(x, t) + A_4(x) \frac{\partial G(x, t)}{\partial x} \right] \\ & - \left( \frac{\alpha_s}{2\pi} \right)^2 \left[ B_1(x)F_2^S(x, t) + B_2(x) \frac{\partial F_2^S(x, t)}{\partial x} + B_3(x)G(x, t) + B_4(x) \frac{\partial G(x, t)}{\partial x} \right] \\ & - \left( \frac{\alpha_s}{2\pi} \right)^3 \left[ C_1(x)F_2^S(x, t) + C_2(x) \frac{\partial F_2^S(x, t)}{\partial x} + C_3(x)G(x, t) + C_4(x) \frac{\partial G(x, t)}{\partial x} \right] = 0. \quad (5.6) \end{aligned}$$

The functions  $A_1(x)$ ,  $A_2(x)$ ,  $A_3(x)$ ,  $A_4(x)$  are defined in Chapter 3 and  $B_1(x)$ ,  $B_2(x)$ ,  $B_3(x)$ ,  $B_4(x)$  are defined in Chapter 4. Now  $C_1(x)$ ,  $C_2(x)$ ,  $C_3(x)$  and  $C_4(x)$  are defined in the Appendix C due to their large sizes.

In order to solve equation (5.6), let us assume  $G(x, t) = k(x)F_2^S(x, t)$ , where  $k(x)$  is a suitable function of  $x$  or may be a constant. Thus equation (5.6) takes the form

$$-t \frac{\partial F_2^S(x, t)}{\partial t} + L(x) \frac{\partial F_2^S(x, t)}{\partial x} + M(x)F_2^S(x, t) = 0, \quad (5.7)$$

where

$$L(x) = A_f \left[ (A_2 + k(x)A_4) + T_0(B_2 + k(x)C_4) + T_1(C_2 + k(x)C_4) \right],$$

$$\begin{aligned} M(x) = A_f \left[ \left( A_1 + k(x)A_3 + \frac{\partial k(x)}{\partial x} A_4 \right) + T_0 \left( B_1 + k(x)B_3 + \frac{\partial k(x)}{\partial x} B_4 \right) \right] \\ + A_f T_1 \left( C_1 + k(x)C_3 + \frac{\partial k(x)}{\partial x} C_4 \right). \end{aligned}$$

Here we can consider two numerical parameters  $T_0$  and  $T_1$ , such that

$$T^2(t) = T_0 \cdot T(t) \text{ and } T^3(t) = T_0 \cdot T(t)T(t) = T_1 \cdot T(t), \text{ where } T(t) = \frac{\alpha_s(t)}{2\pi} \text{ [125].}$$

To introduce the method of characteristics, let us consider two characteristic equations  $\frac{dt}{dS} = -t$  and  $\frac{dx}{dS} = L(x)$ . Putting these in equation (5.7),

we get  $\frac{dF_2^S(S, \tau)}{dS} + M(S, \tau)F_2^S(S, \tau) = 0$ , which can be solved as

$$F_2^S(S, \tau) = F_2^S(0, \tau) \exp \left[ - \int_0^S M(S, \tau) dS \right]. \quad (5.8)$$

For initial condition  $S = 0 \Rightarrow t = t_0$  and  $F_2^S(S, \tau) = F_2^S(0, \tau)$ . Now we have to change the co-ordinate system from  $(S, \tau)$  to  $(x, t)$  with the input function  $F_2^S(0, \tau) = F_2^S(x, t_0)$  and will get the t-evolution of singlet structure function at NNLO as

$$F_2^S(x, t) = F_2^S(x, t_0) \left( \frac{t}{t_0} \right)^{A_f [P_1 + T_0 P_2 + T_1 P_3]}. \quad (5.9)$$

Similarly the x-evolution of singlet structure function at NNLO will be

$$F_2^S(x, t) = F_2^S(x_0, t) \exp \int_{x_0}^x - \frac{[P_1 + T_0 P_2 + T_1 P_3]}{[Q_1 + T_0 Q_2 + T_1 Q_3]} dx, \quad (5.10)$$

$$P_1 = \left( A_1 + k(x)A_3 + \frac{\partial k(x)}{\partial x} A_4 \right), \quad P_2 = \left( B_1 + k(x)B_3 + \frac{\partial k(x)}{\partial x} B_4 \right),$$

$$P_3 = \left( C_1 + k(x)C_3 + \frac{\partial k(x)}{\partial x} C_4 \right), \quad Q_1 = (A_2 + k(x)A_4),$$

$$Q_2 = (B_2 + k(x)C_4), \quad Q_3 = (C_2 + k(x)C_4)$$

Thus the t and x-evolutions of deuteron structure functions at NNLO can be obtained as

$$F_2^d(x, t) = F_2^d(x, t_0) \left( \frac{t}{t_0} \right)^{A_f [P_1 + T_0 P_2 + T_1 P_3]} \quad (5.11)$$

and

$$F_2^d(x, t) = F_2^d(x_0, t) \exp \int_{x_0}^x - \frac{[P_1 + T_0 P_2 + T_1 P_3]}{[Q_1 + T_0 Q_2 + T_1 Q_3]} dx, \quad (5.12)$$

where  $F_2^d(x, t_0) = \frac{5}{2} F_2^S(x, t_0)$  and  $F_2^d(x_0, t) = \frac{5}{2} F_2^S(x_0, t)$  are input functions.

Proceeding in the same way we will get the t and x-evolution of non-singlet structure function from equation (5.3) as

$$F_2^{NS}(x, t) = F_2^{NS}(x, t_0) \left( \frac{t}{t_0} \right)^{A_f [A_1 + T_0 B_1 + T_1 C_1]} \quad (5.13)$$

$$F_2^{\text{NS}}(x, t) = F_2^{\text{NS}}(x_0, t) \exp \int_{x_0}^x - \frac{[A_1 + T_0 B_1 + T_1 C_1]}{[A_2 + T_0 B_2 + T_1 C_2]} dx \quad (5.14)$$

with

$$F_2^{\text{NS}}(x, t_0) = 3[2F_2^{\text{p}}(x, t_0) - F_2^{\text{d}}(x, t_0)], \quad (5.15)$$

$$F_2^{\text{NS}}(x_0, t) = 3[2F_2^{\text{p}}(x_0, t) - F_2^{\text{d}}(x_0, t)]. \quad (5.16)$$

Thus for phenomenological analysis we use equations (5.11) and (5.12) to study unpolarized deuteron structure functions and equations (5.13) and (5.14) to study non-singlet (combination of proton and neutron) structure functions in NNLO.

## 5.2 Results and Discussions

Our results of equation (5.11) for t-evolution and equation (5.12) for x-evolution of deuteron structure function  $F_2^{\text{d}}(x, t)$  are compared with NMC data (in muon- deuteron DIS with incident momentum 90, 120, 200, 280  $\text{GeV}^2$ ), CLAC collaboration data and NNPDF collaboration parameterization. We have also compared our results of equations (5.13) and (5.14) for t and x-evolutions of non-singlet structure function  $F_2^{\text{NS}}(x, t)$  with NMC and E665 experiment data. We consider the range  $0.4 \leq Q^2 \leq 6.0 \text{ GeV}^2$  for CLAS collaboration data,  $5.0 \leq Q^2 \leq 50.0 \text{ GeV}^2$  for NNPDF collaboration parameterization,  $0.01 \leq x \leq 0.0489$  and  $1.496 \leq Q^2 \leq 13.391 \text{ GeV}^2$  for E665 data, also  $0.0045 \leq x \leq 0.14$  and  $0.75 \leq Q^2 \leq 27 \text{ GeV}^2$  for NMC data. It is observed from figure 5.1 that, within these range, for the lowest error we have to consider  $T_0 = 0.048$  and  $T_1 = 0.003$ . Figures 5.2 represent the t-evolution of deuteron structure function and figures 5.3 represent the x-evolution of deuteron structure functions which are compared with NMC data. Figures 5.4 represents the t- and x-evolution of deuteron structure functions which are compared with CLAS collaboration data. Similarly, figures 5.5 represent the t-evolution of deuteron structure functions and figures 5.6 represent the x-evolution of deuteron structure functions which are compared with NNPDF collaboration parameterization. On the other hand,

figures 5.7 represent the t-evolution and figures 5.8 represent x-evolution of non-singlet structure functions which are compared with E665 and NMC data. It is observed that the results for  $k(x)=ax^b$  and  $k(x) = ce^{-dx}$  have no significant variation with results for  $k(x)=k$ , so we consider only latter case and former two are not included here. The best-fit curves are obtained for  $0.5 \leq k \leq 2.0$ . Here errors are statistical and systematic uncertainty. Lowest-t and highest-x points are taken as inputs for t and x-evolution respectively.

In figure 5.1, we put  $T^2(t)$  and  $T_0.T(t)$  as well as  $T^3(t)$  and  $T_1.T(t)$  against  $Q^2$  and we can see that for  $T_0 = 0.048$  and  $T_1 = 0.003$ , the values of  $T^2$  and  $T.T_0$  as well as  $T^3$  and  $T.T_1$  are nearly same within the range of  $0 \leq Q^2 \leq 100 \text{ GeV}^2$ . Thus the consideration of parameters  $T_0$  and  $T_1$  does not give any abrupt change in our results. Value of each data point is increased by adding 0.015 for  $T^3(t)$  and  $T_1.T(t)$ .

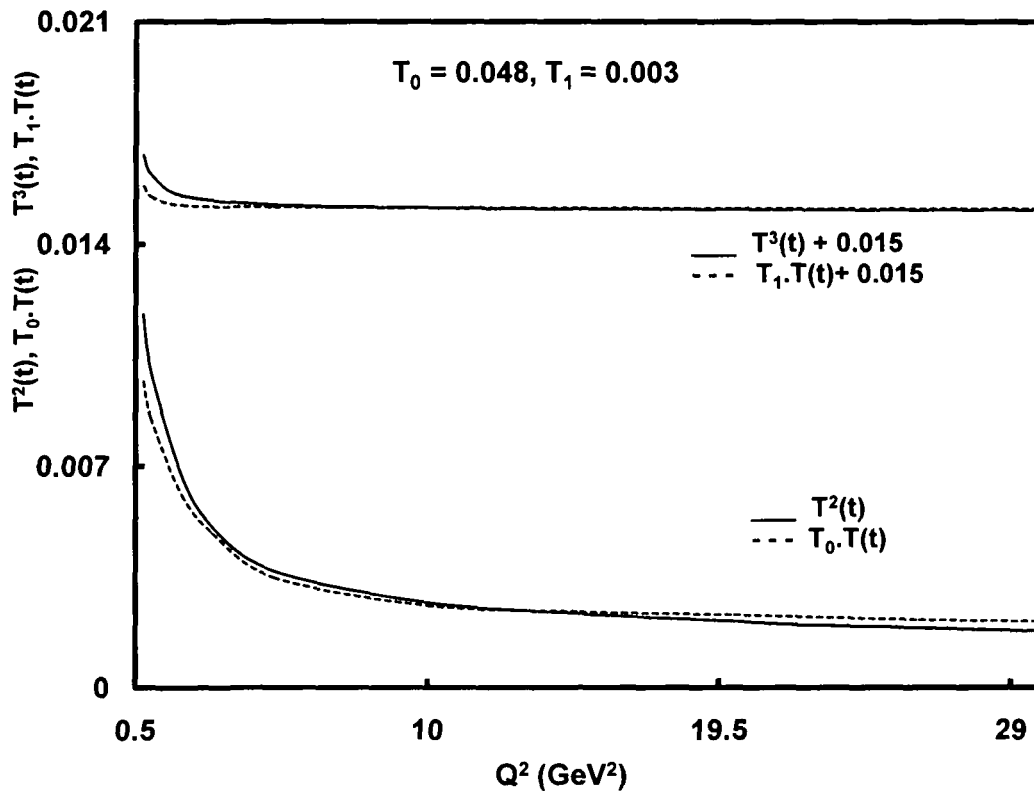


Figure 5.1: Comparison of  $T^2$  and  $T_0.T$  as well as  $T^3(t)$  and  $T_1.T(t)$  values

In figures 5.2,  $t$ -evolutions of  $F_2^d(x,t)$  have been plotted against  $Q^2$  keeping  $x$  constant with the values of 0.0045, 0.008, 0.0125 and 0.0175 respectively. Our NNLO results are compared with NMC data and our NLO and LO results.

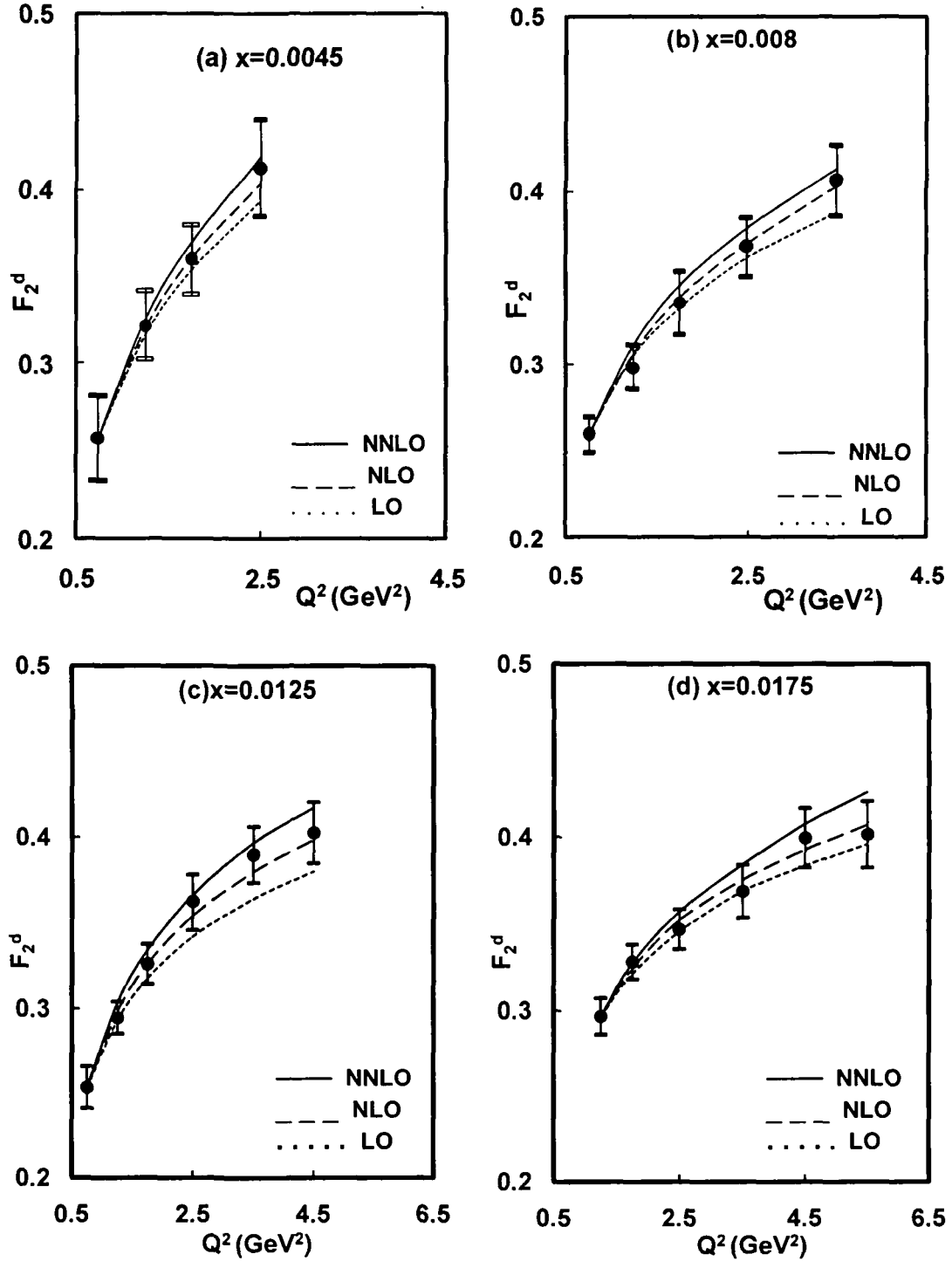


Figure 5.2:  $t$ -evolution of deuteron structure functions in NNLO compared with NMC data

In figures 5.3,  $x$ -evolutions of  $F_2^d(x, t)$  have been plotted against  $x$  keeping  $Q^2$  constant with the values of  $Q^2 = 11.5 \text{ GeV}^2$ ,  $15.0 \text{ GeV}^2$ ,  $20.0 \text{ GeV}^2$  and  $27.0 \text{ GeV}^2$  respectively and our NNLO results are compared with NMC data. Also we compared our NNLO results with our NLO and LO results. Here we consider  $k(x) = k$ , a constant and best fitting found for the values  $1.0 \leq k \leq 1.6$ .

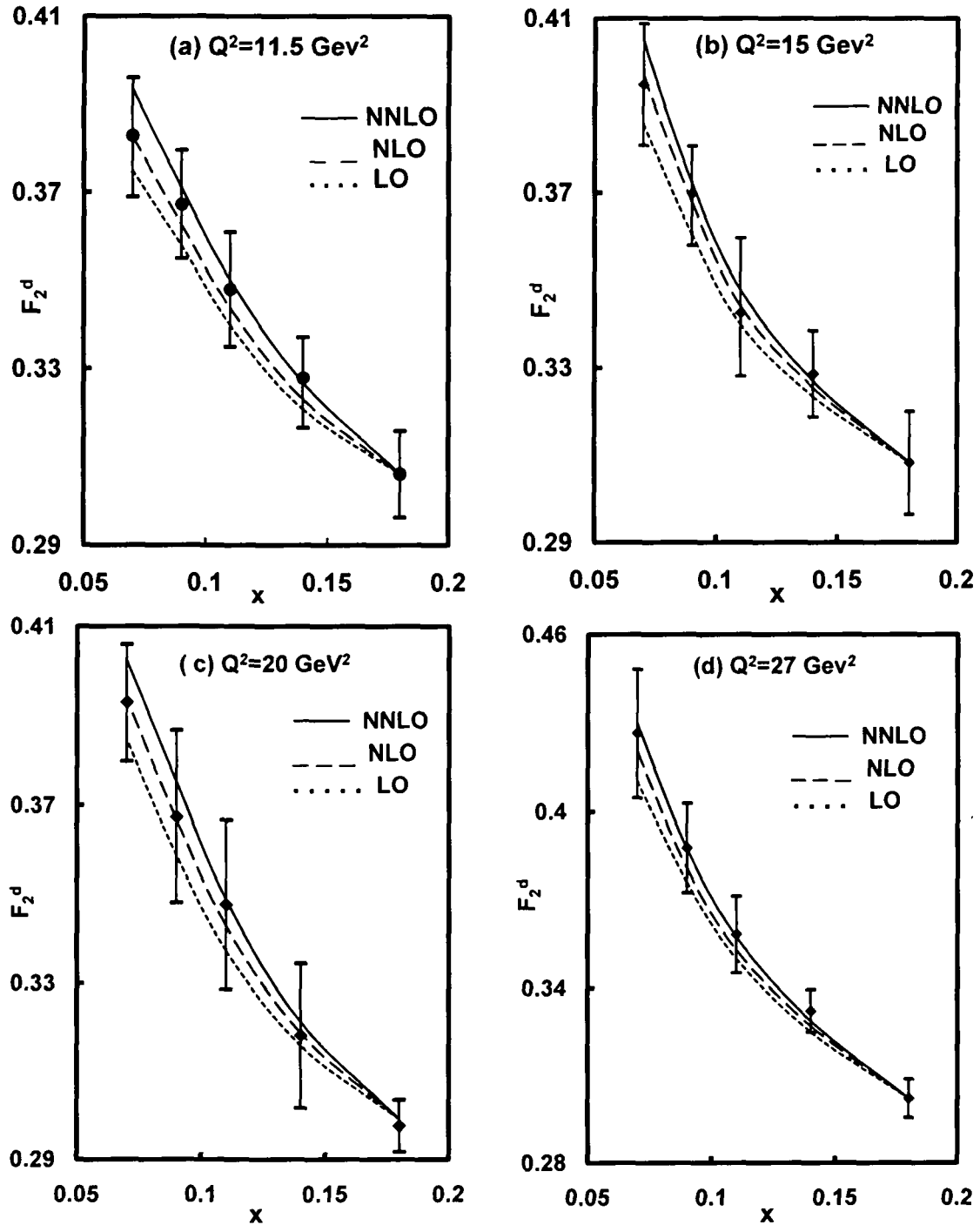


Figure 5.3:  $x$ -evolution of deuteron structure functions in NNLO compared with NMC data

In figures 5.4, we have plotted computed values of  $F_2^d(x,t)$  for NNLO, against the  $x$  values for a fixed- $Q^2$  with  $k(x) = k$ , a constant and our results are compared with CLAS collaboration data. Also we compared NNLO results with our NLO and LO results. Though our solution of the DGLAP evolution equations are better at high- $Q^2$  and small- $x$ , but CLAS data are available at comparably smaller- $Q^2$  and higher- $x$ . Thus our NNLO results are not properly satisfied with CLAS collaboration data. The nearly fit curves are obtained for  $0.6 \leq k \leq 1.0$  with high- $Q^2$  and small- $x$  ranges that available in CLAS collaboration.

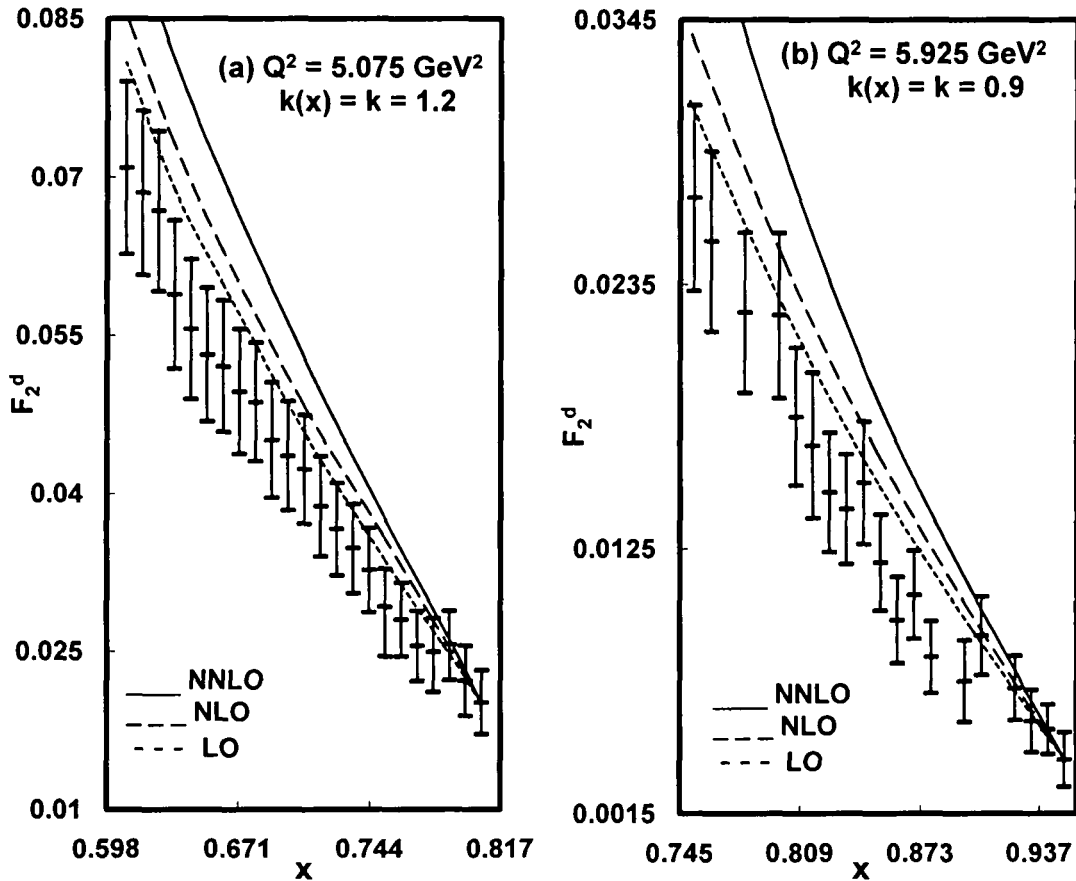


Figure 5.4:  $x$ -evolution of deuteron structure functions compared with CLAS collaboration data



In figures 5.5, we have plotted our computed NNLO values of  $F_2^d(x, t)$  against the  $Q^2$  values for a fixed- $x$  and our results are compared with NNPDF collaboration parameterization. Also we compared our NNLO results with our NLO and LO results. Here we have considered  $k(x) = k$ , a constant and best-fit curves are obtained for  $k = 1.1$  at  $x = 0.05$  and  $0.01$ .

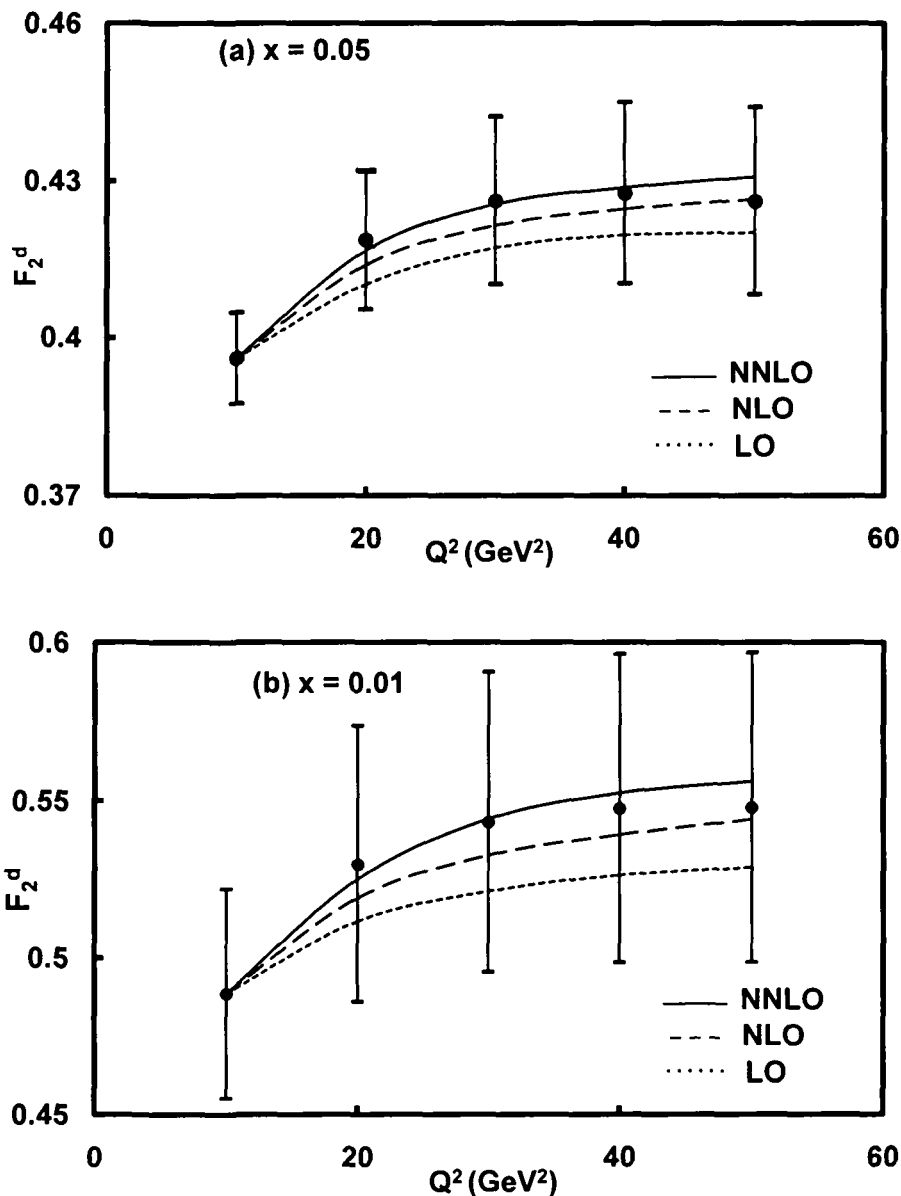


Figure 5.5:  $t$ -evolution of deuteron structure functions in NNLO considering  $k(x) = k$ , a constant, compared with NNPDF collaboration parameterization

In figures 5.6, we have plotted our computed NNLO results of  $F_2^d(x, t)$  against the  $Q^2$  values for a fixed- $x$  and compared with NNPDF collaboration parameterization. Also we compared our NNLO results with our NLO and LO results. Here we have considered  $k(x) = k$ , a constant and best-fit curves are obtained for  $k = 1.1$  at  $x = 0.05$  and  $0.01$ .

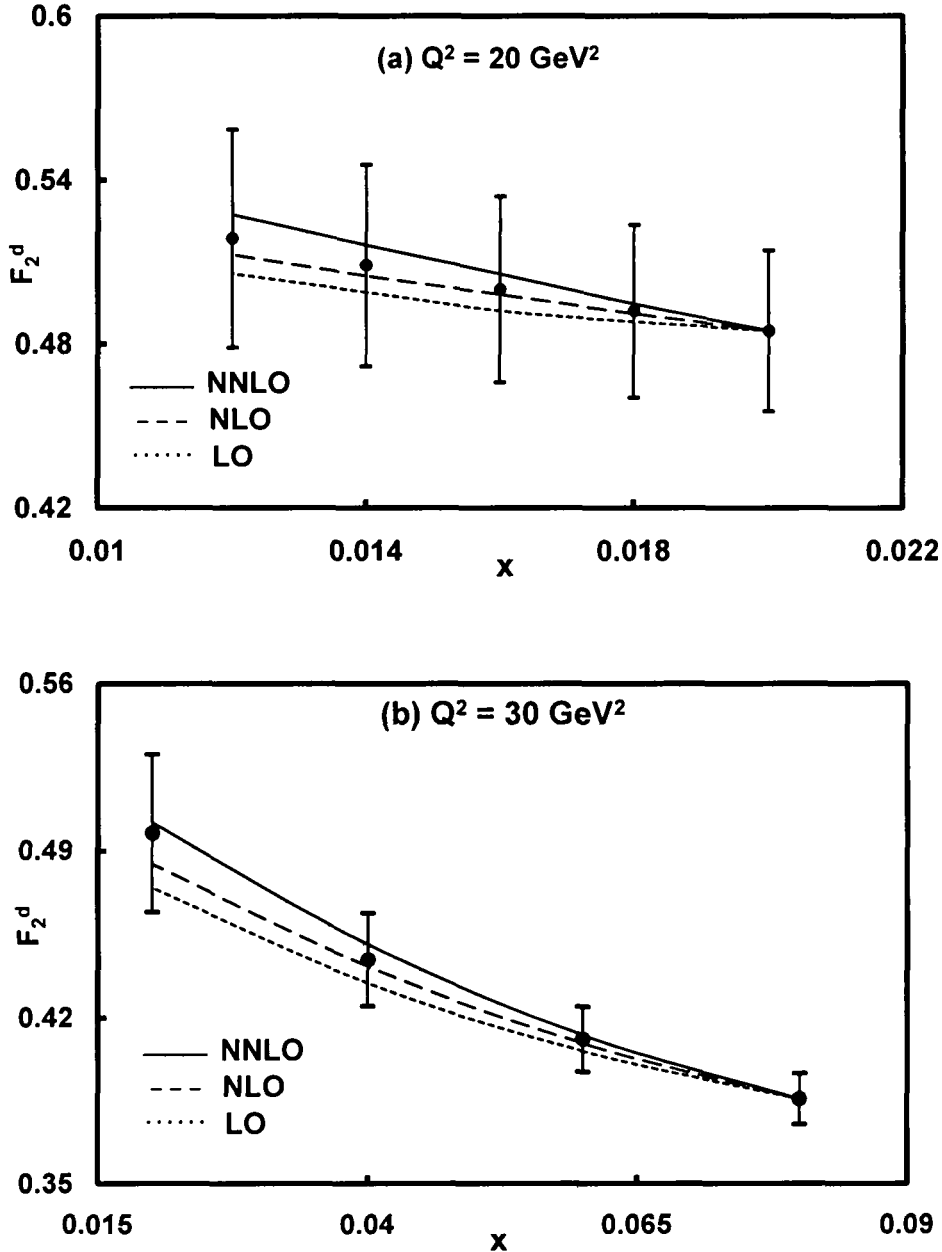


Figure 5.6:  $x$ -evolution of deuteron structure functions in NNLO considering  $k(x) = k$ , a constant, compared with NNPDF collaboration parameterization

In figures 5.7,  $t$ -evolutions have been plotted as  $F_2^{NS}(x,t)$  against  $Q^2$  keeping  $x$  constant with the values of 0.01, 0.017, 0.024 and 0.035 for E665 data and 0.0045, 0.008, 0.0125 and 0.0175 for NMC data. Here also we compared our NNLO results with our NLO and LO results. For clarity, data are scaled up by  $+0.5i$  ( $i=0, 1, 2, 3, \dots$ ) for E665 data and by  $+0.3i$  for NMC data, starting from bottom of all graphs in each figure.

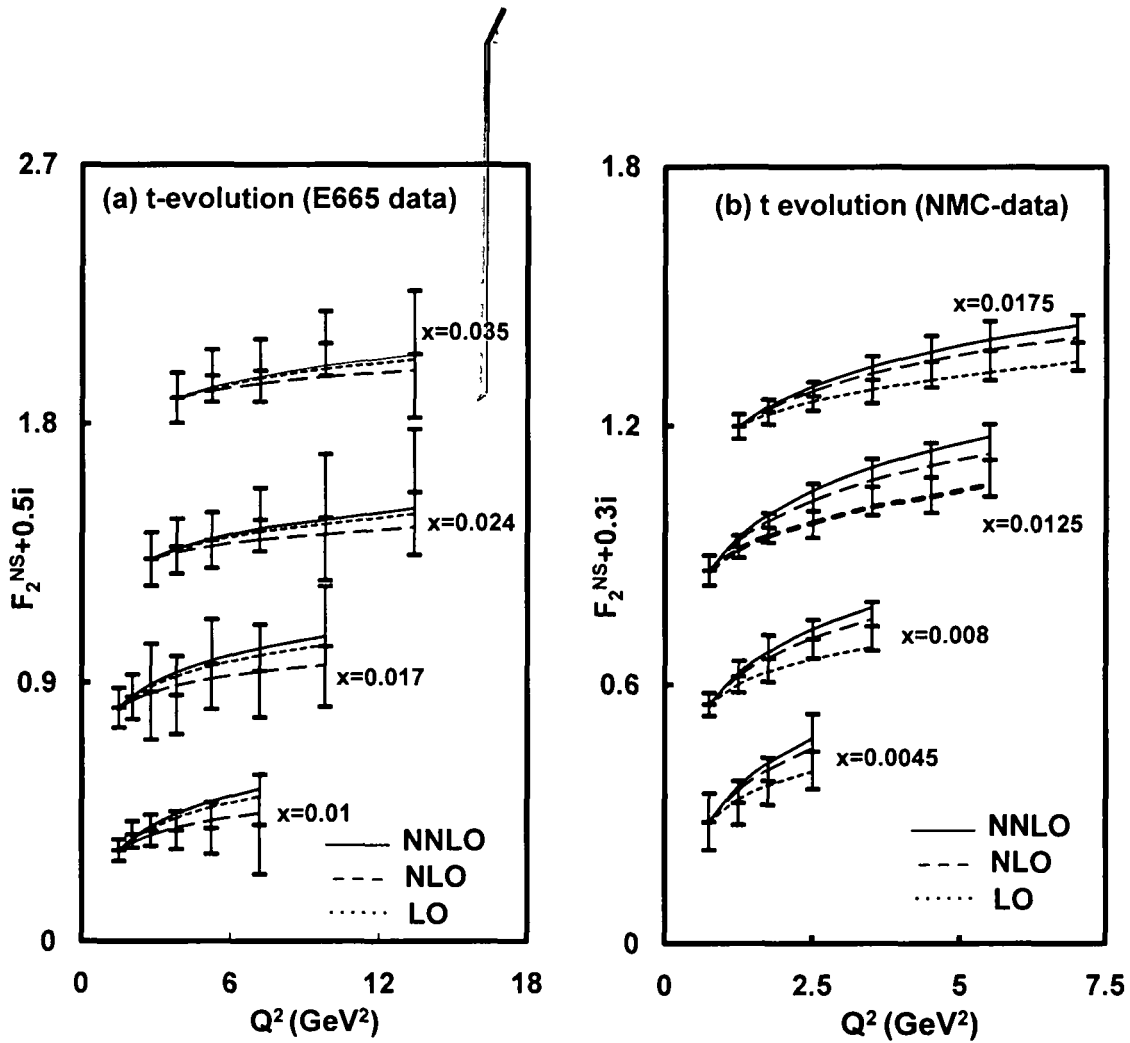


Figure 5.7:  $t$ -evolution of non-singlet structure functions in NNLO compared with E665 and NMC data

In figures 5.8, x-evolutions have been plotted as  $F_2^{\text{NS}}(x,t)$  against  $x$  keeping  $Q^2$  constant with the values of  $Q^2 = 5.236 \text{ GeV}^2, 7.176 \text{ GeV}^2, 9.795 \text{ GeV}^2, 13.391 \text{ GeV}^2$  for E665 data and  $9.0 \text{ GeV}^2, 11.5 \text{ GeV}^2, 15.0 \text{ GeV}^2, 20.0 \text{ GeV}^2$  for NMC data. Here also we compared our NNLO results with our NLO and LO results. For clarity, data are scaled up by  $+0.5i$  ( $i=0, 1, 2, 3, \dots$ ) for E665 data and by  $+0.2i$  for NMC data, starting from bottom of all graphs in each figure.

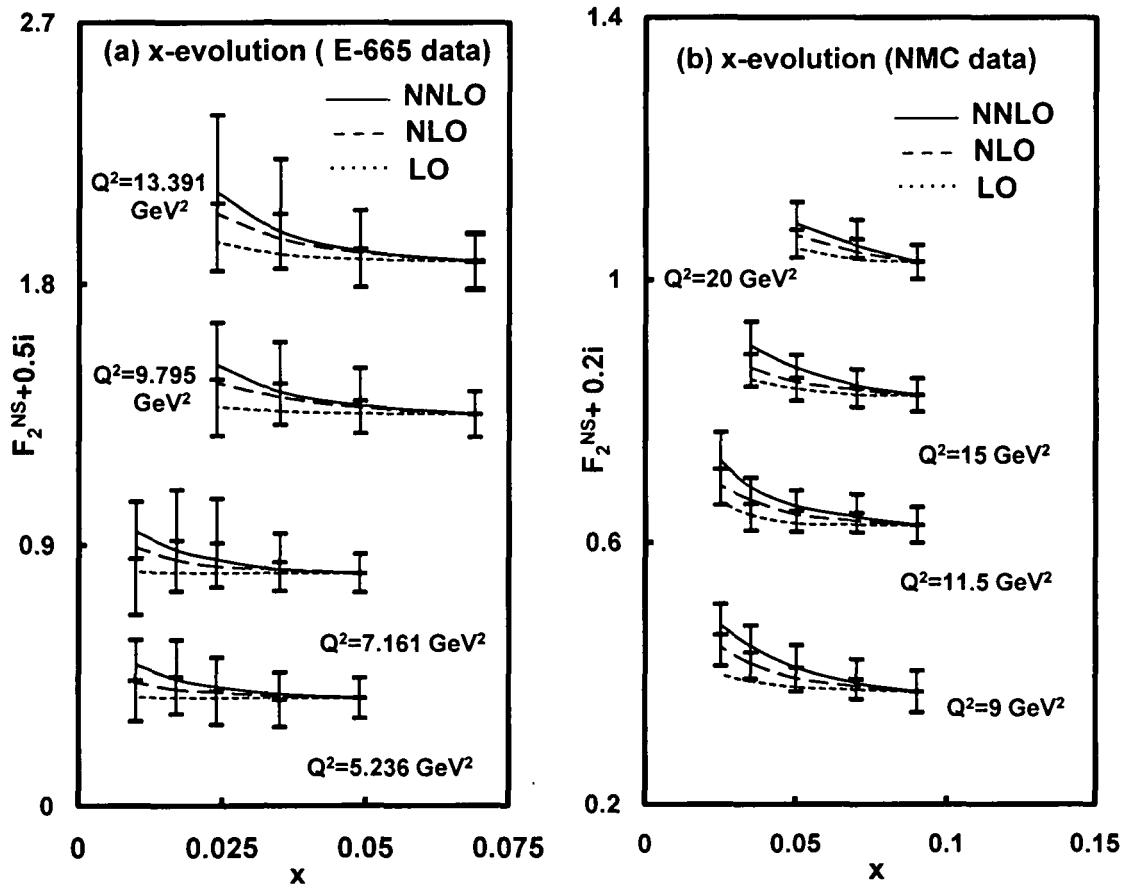


Figure 5.8: x-evolution of non-singlet structure functions in NNLO compared with E665 and NMC data

### 5.3 Conclusion

In this chapter, we have solved the DGLAP evolution equation by method of characteristics and obtain the singlet and non-singlet structure functions. Here we found that the  $t$  and  $x$ -evolution of deuteron structure function as well as non-singlet structure function, which is the combination of proton and deuteron structure functions, are in good consistency with the NMC, E665, CLAS collaboration data sets and NNPDF collaboration parameterization results. If we calculate the errors by considering always the middle sets of experimental data and our corresponding results, then on average, the percentage errors of our results in LO, NLO and NNLO are 4.66%, 2.53% and 1.035% with NMC data, 11.3%, 1.72% and 3.78% with E665 data, 14.8%, 20.7% and 33.8% with CLAS data, and also 4.62%, 2.61% and 0.88% with NNPDF collaboration results respectively. Here except CLAS data, the contribution of NNLO is found to be high at the lower- $x$  and higher- $Q^2$ . CLAS data are available only at lower- $Q^2$  and higher- $x$ , where our methodology is not work good. Here we can claim that in our presentation, we consider very few numbers of parameters comparative to the other methods.  $\square$

## *Part - II*

# Polarized Hadron Structure Functions

*“Science is the belief in the ignorance of experts”*

*– Feynman*

In the spin dependent or polarized deep inelastic scattering program, the spin structure of the nucleon has been studied by using polarized lepton beams scattered by polarized targets. These fixed-target experiments have been used to characterize the spin structure of the proton and neutron and to test additional fundamental QCD and quark-parton model (QPM) sum rules. The first experiments in polarized electron-polarized proton scattering, performed in the 1970s, helped to establish the parton structure of the proton. In the late 1980s, a polarized muon-polarized proton experiment found that a QPM sum rule was violated, which seemed to indicate that the quarks do not account for the spin of the proton. This "proton-spin crisis" gave birth to a new generation of experiments at several high energy physics laboratories around the world. The new and extensive data sample collected from these fixed-target experiments has enabled a careful characterization of the spin-dependent parton substructure of the nucleon. The results have been used to test QCD, to find an independent value for  $\alpha_s(Q^2)$  and to probe with reasonable precision the polarized parton distributions.

Recent interest in the spin structure of the proton, neutron, and deuteron and advances in experimental techniques have led to a number of experiments concerned with DIS of polarized leptons on various polarized targets. Among these are the E143 experiments at SLAC [136] and the Spin Muon Collaboration (SMC) at CERN [137], which used polarized hydrogen and deuterium, the E154 experiment at SLAC [138, 139] and the HERMES collaboration at DESY [140], which used polarized  $^3\text{He}$ , also the HERMES collaboration [141] which used polarized hydrogen [142]. A new material, deuterized lithium  $^6\text{LiD}$ , has recently emerged as a source of polarized deuterium in the E155/E155x experiments at SLAC [143]. Thus the world data of the spin structure functions are obtained from EMC, SMC, SLAC-E143, E154, HERMES and JLAB-CLAS for proton; SMC, SLAC-E143, E155, HERMES and JLAB-CLAS for deuteron; and SLAC-E142, HERMES and JLAB-MIT for neutron.

## Polarized DGLAP Evolution Equations in Leading Order

The polarized structure function  $g_1(x, Q^2)$  for deep-inelastic lepton-nucleon scattering is of fundamental importance in understanding the quark and gluon spin structure of the proton and neutron. According to the polarized DGLAP equations [144, 145],  $g_1(x, Q^2)$  is expected to evolve logarithmically with  $Q^2$ , where  $g_1$  depends both on  $x$ , the fractional momentum carried by the struck parton, and on  $Q^2$ , the squared four momentum of the exchanged virtual photon. There have been a number of theoretical approaches to calculate  $g_1(x, Q^2)$  using phenomenological models of nucleon structure. In this chapter we will solve polarized DGLAP evolution equations in LO by method of characteristics and compared our results with E143 at SLAC experimental data [136] and SMC [137] and COMPASS [146, 147] collaboration data.

### 6.1 Theory

In polarized experiments, when both beam and the target are longitudinally polarized in DIS, the asymmetry is defined as

$$A_{\parallel} = \frac{\sigma^{\uparrow\downarrow} - \sigma^{\uparrow\uparrow}}{\sigma^{\uparrow\downarrow} + \sigma^{\uparrow\uparrow}},$$

where  $\sigma^{\uparrow\downarrow}$  and  $\sigma^{\uparrow\uparrow}$  are the cross section for opposite and same spin direction respectively. Similarly the transverse asymmetry, determined from scattering of a longitudinally polarized beam on a transversely polarized target, is defined as



$$A_{\perp} = \frac{\sigma^{\downarrow\rightarrow} - \sigma^{\uparrow\rightarrow}}{\sigma^{\downarrow\rightarrow} + \sigma^{\uparrow\rightarrow}}.$$

These asymmetries can be expressed in terms of longitudinal ( $A_1$ ) and transverse ( $A_2$ ) virtual photon-nucleon asymmetries as

$$A_{\parallel} = D[A_1 + \eta A_2] \text{ and } A_{\perp} = d \left[ A_2 - \gamma \left( 1 - \frac{y}{2} \right) A_1 \right] \text{ with } D = \frac{2y - y^2}{2(1-y)(1+R) + y^2},$$

$$\eta = \left( \frac{Q}{E} \right) \frac{2(1-y)}{y(2-y)}, \quad d = \frac{\sqrt{1-y}}{1 - \frac{y}{2}} D, \quad \gamma^2 = 4y^2 x^2, \quad y = \frac{M}{Q}, \quad x = \frac{Q^2}{2Mv},$$

where  $D$  is often called the depolarization factor of the virtual photon and  $M$  is the nucleon mass.

For spin  $\frac{1}{2}$  targets (proton and neutron),  $A_1$  and  $A_2$  can be interpreted as virtual photon-nucleon asymmetries,

$$A_1^{p,n} = \frac{\sigma_{1/2} - \sigma_{3/2}}{\sigma_{1/2} + \sigma_{3/2}}, \quad A_2^{p,n} = \frac{2\sigma^{TL}}{\sigma_{1/2} + \sigma_{3/2}},$$

whereas for the deuteron

$$A_1^d = \frac{\sigma_0 - \sigma_2}{\sigma_0 + \sigma_2} \text{ and } A_2^d = \frac{\sigma_0^{TL} - \sigma_1^{TL}}{\sigma_{1/2} + \sigma_{3/2}}.$$

In these expressions, the indices refers to the total spin projections of the photon- hadron system in the direction of the virtual photon, and the  $\sigma^{TL}$  are cross sections arising from the interference of amplitudes for longitudinally and transversely polarized virtual photons [144].

The longitudinal polarized structure function  $g_1(x)$ , obtained from longitudinally polarized leptons scattering off nucleons polarized parallel or anti-parallel to the lepton direction is defined as

$$g_1(x) = \frac{1}{2} \sum_i e_i^2 \Delta q_i(x)$$

where  $\Delta q_i(x) = q_i^+(x) + \bar{q}_i^+(x) - q_i^-(x) - \bar{q}_i^-(x)$ . Here  $q_i^+(x)$  and  $q_i^-(x)$  are the densities of quarks of flavor 'i' with helicity parallel and anti parallel to the

nucleon spin. The polarized structure functions  $g_1(x, Q^2)$  and  $g_2(x, Q^2)$  are related with unpolarized structure function  $F_2(x, Q^2)$  as

$$g_1 = \frac{F_2(x, Q^2) [A_1(x, Q^2) + \gamma A_2(x, Q^2)]}{2x [1 + R_\sigma(x, Q^2)]}, \quad (6.1)$$

$$g_2 = \frac{F_2(x, Q^2) [-A_1(x, Q^2) + A_2(x, Q^2)\gamma]}{2x [1 + R_\sigma(x, Q^2)]} \quad (6.2)$$

where  $t = \ln(Q^2/\Lambda^2)$ ,  $\Lambda$  is the QCD cut-off parameter and  $R_\sigma = \frac{\sigma_L(x, Q^2)}{\sigma_T(x, Q^2)}$  is the ratio of the longitudinal and transverse virtual photon cross section.

The polarized DGLAP evolution equation [145] in the standard form

$$\frac{\partial g_1(x, Q^2)}{\partial \ln Q^2} = P(x, Q^2) \otimes g_1(x, Q^2), \quad (6.3)$$

where  $g_1(x, Q^2)$  is the polarized structure function as the function of  $x$  and  $Q^2$ . Here  $P(x, Q^2)$  is the polarized kernel known perturbatively up to the first few orders in  $\alpha_s(Q^2)$ , the strong coupling constant. Here  $\otimes$  represents the standard Mellin convolution and the notation is given by

$$a(x) \otimes b(x) \equiv \int_0^1 \frac{dy}{y} a(y) b\left(\frac{x}{y}\right). \quad (6.4)$$

Now one can write

$$P(x, Q^2) = \frac{\alpha_s(Q^2)}{2\pi} P^{(0)}(x) + \left(\frac{\alpha_s(Q^2)}{2\pi}\right)^2 P^{(1)}(x), \quad (6.5)$$

where  $P^{(0)}(x)$  and  $P^{(1)}(x)$  are polarized splitting functions in LO and NLO.

Considering polarized splitting functions, the singlet and non-singlet structure functions are obtained from the polarized DGLAP evolution equations in LO as

$$\frac{\partial g_1^S}{\partial t} - \frac{\alpha_s(t)}{2\pi} \left[ \frac{2}{3} \{3 + 4\ln(1-x)\} g_1^S(x, t) + I_1^S(x, t) + I_2^S(x, t) \right] = 0, \quad (6.6a)$$

$$\frac{\partial g_1^{NS}}{\partial t} - \frac{\alpha_s(t)}{2\pi} \left[ \frac{2}{3} \{3 + 4\ln(1-x)\} g_1^{NS}(x, t) + I_1^{NS}(x, t) \right] = 0, \quad (6.6b)$$

where functions  $I_1^S, I_2^S, I_1^{NS}$  are defined in Appendix D.

Also  $\alpha_s(t) = \frac{4\pi}{\beta_0 t}$ , where  $\beta_0 = 11 - \frac{2}{3}N_f$  is the one loop (LO) correction to the QCD  $\beta$ -function and  $N_f$  being the flavors number.

Let us introduce the variable  $u = 1 - \omega$  and note that  $\frac{x}{\omega} = \frac{x}{1-u} = x \sum_{k=0}^{\infty} u^k$ .

Since  $x < \omega < 1$ , so  $0 < u < 1 - x$  and hence the series is convergent for  $|u| < 1$ . So, using Taylor's expansion series

$$g_1^S\left(\frac{x}{\omega}, t\right) = g_1^S\left(x + \frac{xu}{1-u}, t\right) = g_1^S(x, t) + \frac{xu}{1-u} \frac{\partial g_1^S(x, t)}{\partial x} + \frac{1}{2} \left(\frac{xu}{1-u}\right)^2 \frac{\partial^2 g_1^S(x, t)}{\partial x^2} + \dots$$

As  $x$  is small in our region of discussion, so we can rewrite  $g_1^S\left(\frac{x}{\omega}, t\right)$ ,  $g_1^{NS}\left(\frac{x}{\omega}, t\right)$

and  $\Delta G\left(\frac{x}{\omega}, t\right)$  as

$$g_1^S\left(\frac{x}{\omega}, t\right) = g_1^S(x, t) + \frac{xu}{1-u} \frac{\partial g_1^S(x, t)}{\partial x}, \quad (6.7a)$$

$$g_1^{NS}\left(\frac{x}{\omega}, t\right) = g_1^{NS}(x, t) + \frac{xu}{1-u} \frac{\partial g_1^{NS}(x, t)}{\partial x}, \quad (6.7b)$$

$$\Delta G\left(\frac{x}{\omega}, t\right) = \Delta G(x, t) + \frac{xu}{1-u} \frac{\partial \Delta G(x, t)}{\partial x}. \quad (6.7c)$$

In order to solve equation (6.6a) we need to relate the singlet distribution function  $g_1^S(x, t)$  with the gluon distribution function  $\Delta G(x, t)$ . For small- $x$  and high- $Q^2$ , the gluon is expected to be more dominant than the sea quark. Hence, for simplicity, let us assume  $\Delta G(x, t) = k'(x)g_1^S(x, t)$ , where  $k'(x)$  is a suitable function of  $x$  or may be a constant. We may assume  $k'(x) = k, ax^b, ce^{-dx}$  where  $k, a, b, c, d$  are suitable parameters, which can be determined by phenomenological analysis. Such an assumption is used for the unpolarized as well as polarized cases [79, 82, 174]. Using equation (6.7a) and (6.7c) in equation (6.6a) and performing  $u$ -integrations, we get

$$-t \frac{\partial g_1^S(x, t)}{\partial t} + A_f L'_1(x) \frac{\partial g_1^S}{\partial x} + A_f M'_1(x) g_1^S(x, t) = 0, \quad (6.8)$$

where  $A_f = \frac{\alpha_s(t)}{3\pi} t$ ,

$$L'_1(x) = A'_2(x)B(x) + k'(x)A'_4(x), \quad (6.9a)$$

$$M'_1(x) = A'_1(x) + k'(x)A'_3(x) + A'_4(x)\frac{\partial k(x)}{\partial x}. \quad (6.9b)$$

The functions  $A'_1(x)$ ,  $A'_2(x)$ ,  $A'_3(x)$  and  $A'_4(x)$  are

$$A'_1(x) = 2x - x^2 + 4\ln(1-x), \quad (6.10a)$$

$$A'_2(x) = x - x^3 - 2x\ln(x), \quad (6.10b)$$

$$A'_3(x) = \frac{3}{2}N_f(x - x^2), \quad (6.10c)$$

$$A'_4(x) = \frac{3}{2}N_f[-x + x^3 + x\ln(x)]. \quad (6.10d)$$

To introduce method of characteristics, let us consider two new variables  $S$  and  $\tau$  instead of  $x$  and  $t$ , such that

$$\frac{dt}{dS} = -t, \quad (6.11a)$$

$$\frac{dx}{dS} = A_f L'_1(x). \quad (6.11b)$$

These are known as characteristics equations. Now from equation (6.6a),

$$\frac{dg_1^S(S, \tau)}{dS} + M'_1(S, \tau)g_1^S(S, \tau) = 0 \quad (6.12)$$

$$\text{This can be solved as } g_1^S(S, \tau) = g_1^S(0, \tau) \exp \left[ - \int_0^S M'_1(S, \tau) dS \right]. \quad (6.13)$$

For  $t$ -evolution, structure function varies with  $t$  as  $x$  remains constant. Hence equation (6.11a) can be used in equation (6.13), the solution of which is

$$g_1^S(S, \tau) = g_1^S(\tau) \left( \frac{t}{t_0} \right)^{M'_1(S, \tau)}, \quad (6.14)$$

where  $M'_1(S, \tau) = A_f M'_1(x)$  and  $g_1^S(S, \tau) = g_1^S(\tau)$ ;  $S = 0$ ,  $t = t_0$ .

Now we have to replace the co-ordinate system  $(S, \tau)$  to  $(x, t)$  in equation (6.14) with the input function  $g_1^S(\tau) = g_1^S(x, t_0)$  and will get the  $t$ -evolution of singlet structure function in the LO as

$$g_1^S(x, t) = g_1^S(x, t_0) \left( \frac{t}{t_0} \right)^{\frac{3}{2} A_f M_1'(x)} \quad (6.15)$$

Similarly, for x-evolution, structure function varies with x as t remains constant. Hence equation (6.11b) can be used in equation (6.13) and the x-evolution of singlet structure function will be

$$g_1^S(x, t) = g_1^S(x_0, t) \exp \left[ - \int_{x_0}^x \frac{M_1'(x)}{L_1'(x)} dx \right] \quad (6.16)$$

Proceeding in the same way, we get t and x-evolutions of non-singlet (combination of proton and neutron) structure function from equation (6.6b) as

$$g_1^{NS}(x, t) = g_1^{NS}(x, t_0) \left( \frac{t}{t_0} \right)^{\frac{3}{2} A_f A_1'(x)}, \quad (6.17a)$$

$$g_1^{NS}(x, t) = g_1^{NS}(x_0, t) \exp \left( - \int_{x_0}^x \frac{A_1'}{A_2'} dx \right). \quad (6.17b)$$

The deuteron, proton and neutron structure functions measured in DIS can be written in terms of singlet and non-singlet quark distribution functions [80] as

$$g_1^d(x, t) = \frac{5}{9} g_1^S(x, t), \quad (6.18a)$$

$$g_1^p(x, t) = \frac{5}{18} g_1^S(x, t) + \frac{3}{18} g_1^{NS}(x, t), \quad (6.18b)$$

$$g_1^n(x, t) = \frac{5}{18} g_1^S(x, t) - \frac{3}{18} g_1^{NS}(x, t). \quad (6.18c)$$

Thus t and x-evolution of deuteron (singlet) structure functions in LO can be obtained as

$$g_1^d(x, t) = g_1^d(x, t_0) \left( \frac{t}{t_0} \right)^{\frac{3}{2} A_f L_1'(x)} \quad (6.19a)$$

$$g_1^d(x, t) = g_1^d(x_0, t) \exp \left[ - \int_{x_0}^x \frac{M_1'(x)}{L_1'(x)} dx \right]. \quad (6.19b)$$

where  $g_1^d(x, t_0) = \frac{5}{9} g_1^d(x, t_0)$ ,  $g_1^d(x_0, t) = \frac{5}{9} g_1^d(x_0, t)$ ,

$g_1^{NS}(x, t_0) = 3[g_1^p(x, t_0) - g_1^n(x, t_0)]$  and  $g_1^{NS}(x_0, t) = 3[g_1^p(x_0, t) - g_1^n(x_0, t)]$  with  $g_1^d(x, t_0)$ ,  $g_1^p(x, t_0)$ ,  $g_1^n(x, t_0)$  and  $g_1^d(x_0, t)$ ,  $g_1^p(x_0, t)$ ,  $g_1^n(x_0, t)$  are input functions.

For phenomenological analysis we use equations (6.19a) and (6.19b) to study polarized deuteron structure functions, and also equations (6.17a) and (6.17b) to study non-singlet (combination of proton and neutron) structure functions in LO.

## 6.2 Results and Discussions

We compare our results of  $t$ - and  $x$ -evolutions of polarized deuteron  $g_1^d(x, t)$  and non-singlet (a combination of proton and neutron)  $g_1^{NS}(x, t)$  structure functions with data obtained by the SLAC E143 collaboration [136], SM collaboration [137] and COMPASS collaboration [146, 147].

The SLAC E143 gives the measurement of the polarized structure function of deuteron, proton and neutron in deep inelastic scattering by polarized electrons at incident energies of 29.1 GeV<sup>2</sup>, 16.2 GeV<sup>2</sup> and 9.7 GeV<sup>2</sup> on a polarized Ammonia target. Data cover the kinematical ranges of  $x$  from 0.024 to 0.75 and  $Q^2$  from 0.5 to 10 GeV<sup>2</sup>. The SM Collaborations gives the final results of measurements of the virtual photon asymmetry of deuteron (proton) and the polarized deuteron (proton) structure functions in deep inelastic scattering of 100 GeV<sup>2</sup> and 190 GeV<sup>2</sup> polarized muons on polarized deuterons (protons). The data cover the kinematic ranges of  $x$  from 0.0008 to 0.7 and  $Q^2$  from 0.2 to 100 GeV<sup>2</sup>. In COMPASS collaboration, the measurement of the polarized structure function  $g_1^d(x, t)$  at  $Q^2$  values from 1 to 100 GeV<sup>2</sup> and  $x$  values from 0.004 to 0.7 is obtained. The data were taken with a polarized muon beam of mean energy 160 GeV<sup>2</sup> and a polarized Lithium Deuteride target. The data were collected during the period 2002-03 [Ageev et al] and 2002-04 [Alexakhin et al].

In figures 6.1-6.3, we have plotted computed values of polarized deuteron structure function  $g_1^d(x,t)$  against  $Q^2$  values for a fixed- $x$  in LO taking suitable values of  $k'(x) = k$ , a constant,  $k'(x) = ax^b$ , a power function and  $k'(x) = ce^{-dx}$ , an exponential function of  $x$ . In figure 6.4, we have plotted our computed values of polarized non-singlet structure functions  $g_1^{NS}$  against the  $Q^2$  values for LO. Here values of  $g_1^d(x,t)$  and  $g_1^{NS}(x,t)$  at lowest  $Q^2$  have been taken as the input functions. In figures 6.5 - 6.8, the computed values of polarized deuteron structure functions  $g_1^d(x,t)$  have been plotted against  $x$  for fixed  $Q^2$  taking suitable values of  $k'(x) = k$ ,  $ax^b$  and  $ce^{-dx}$ . Here values of  $g_1^d(x,t)$  at highest- $x$  are taken as the input functions. It is seen from the figures that the polarized structure functions are increased with  $Q^2$  at small- $x$ .

In figure 6.1,  $t$ -evolution of polarized deuteron structure functions  $g_1^d(x,t)$  have been plotted against  $Q^2$  for  $x = 0.035, 0.049, 0.063$  and  $0.079$  taking  $k'(x) = k$ , a constant with value  $k = 0.8$  and compared our results with SLAC E143 experimental data.

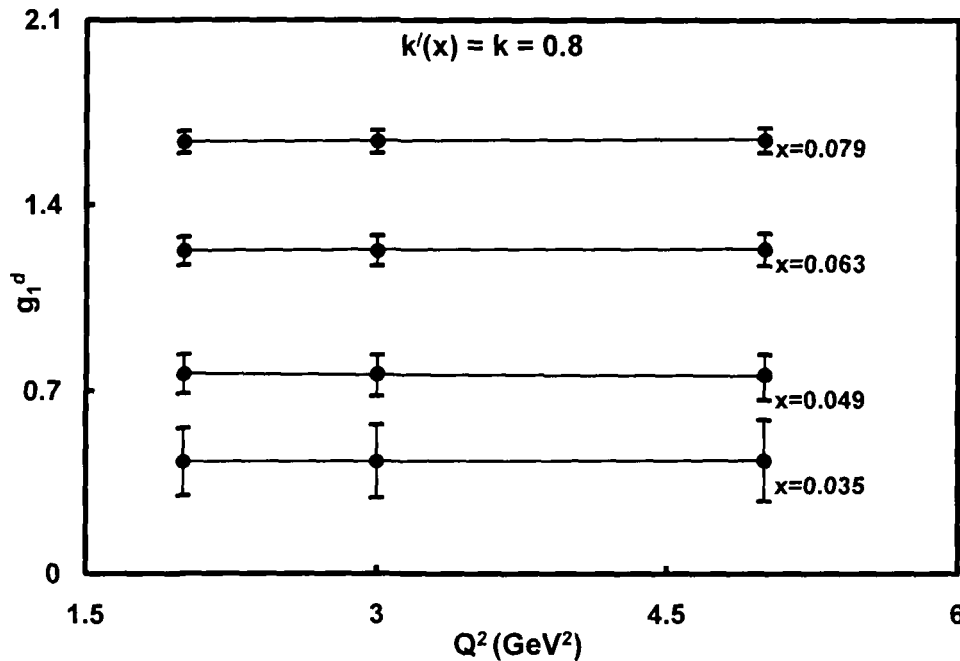


Figure 6.1:  $t$ -evolution of polarized deuteron structure functions in LO at  $k'(x) = k$ , a constant, compared with SLAC E143 data

In figure 6.2,  $t$ -evolution of polarized deuteron structure functions  $g_1^d(x, t)$  have been plotted against  $Q^2$  for  $x = 0.056, 0.071$  and  $0.090$  taking  $k'(x) = ax^b$ , a power function of  $x$  with values  $a = 1.2$  and  $b = 0.8$ . Here our results are compared with SLAC E143 experimental data.

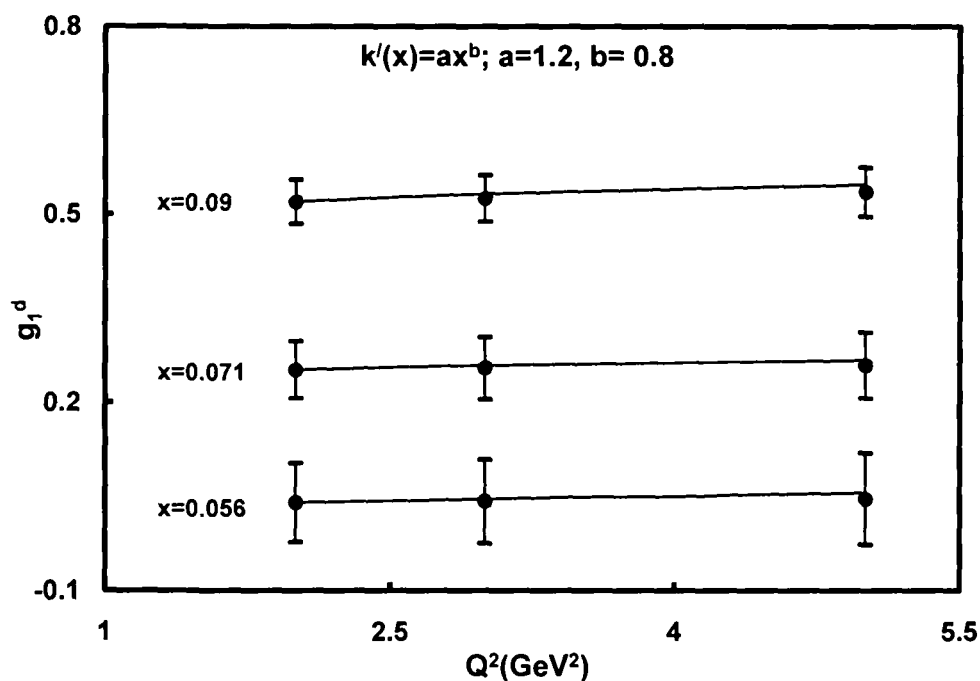


Figure 6.2:  $t$ -evolution of polarized deuteron structure functions in LO at  $k'(x) = ax^b$ , a power function of  $x$ , compared with SLAC E143 data



In figure 6.3, t-evolution of polarized deuteron structure functions  $g_1^d(x,t)$  have been plotted against  $Q^2$  for  $x = 0.035, 0.044, 0.049, 0.056$  and  $0.063$  taking  $k'(x) = ce^{-dx}$ , an exponential function of  $x$  with values  $c = 0.2$  and  $d = 0.06$ . Here also our results are compared with SLAC E143 experimental data.

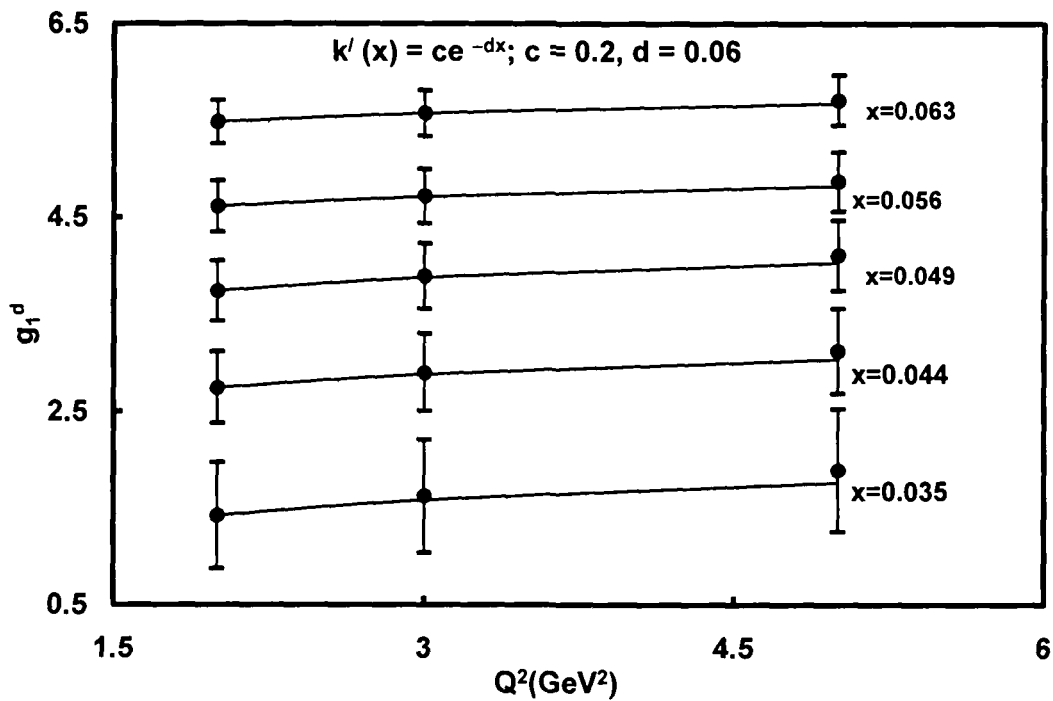


Figure 6.3: t-evolution of polarized deuteron structure functions in LO at  $k'(x) = ce^{-dx}$ , an exponential function of  $x$ , compared with SLAC E143 data

In figure 6.4,  $t$ -evolution of polarized non-singlet structure functions  $g_1^{\text{NS}}(x, t)$  have been plotted against  $Q^2$  for  $x = 0.035, 0.044, 0.049, 0.056$  and  $0.063$ . Our results are compared with SLAC E143 data.

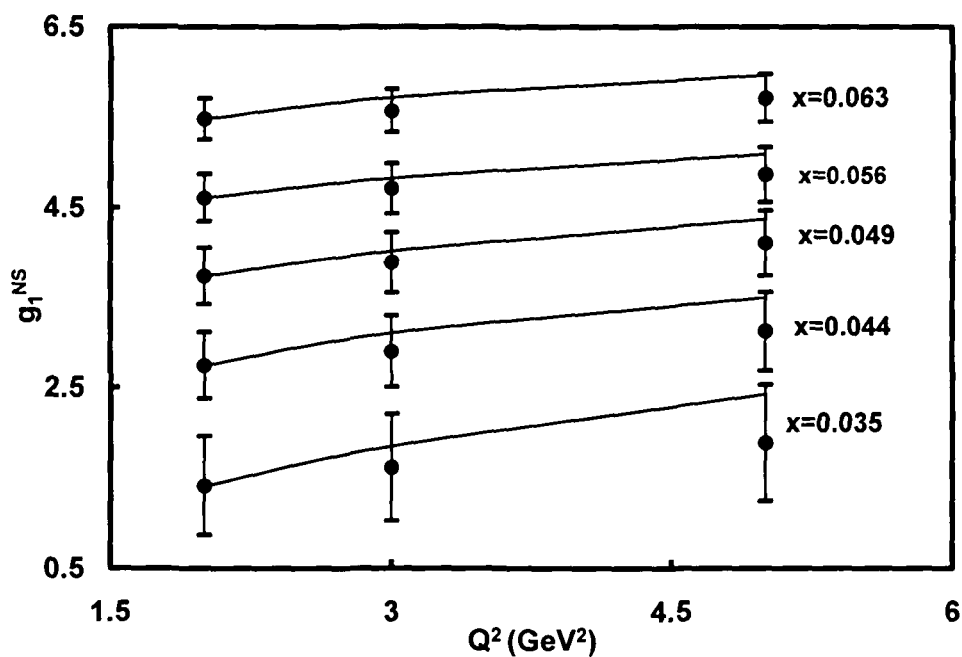


Figure 6.4:  $t$ -evolution of polarized non-singlet structure functions in LO, compared with SLAC E143 data

In figure 6.5,  $x$ -evolution of polarized deuteron structure functions  $g_1^d(x,t)$  have been plotted against  $x$  for  $Q^2 = 5 \text{ GeV}^2$  taking  $k'(x) = k$ , a constant with value  $k = 0.9$ . Our results are compared with SLAC E143 data.

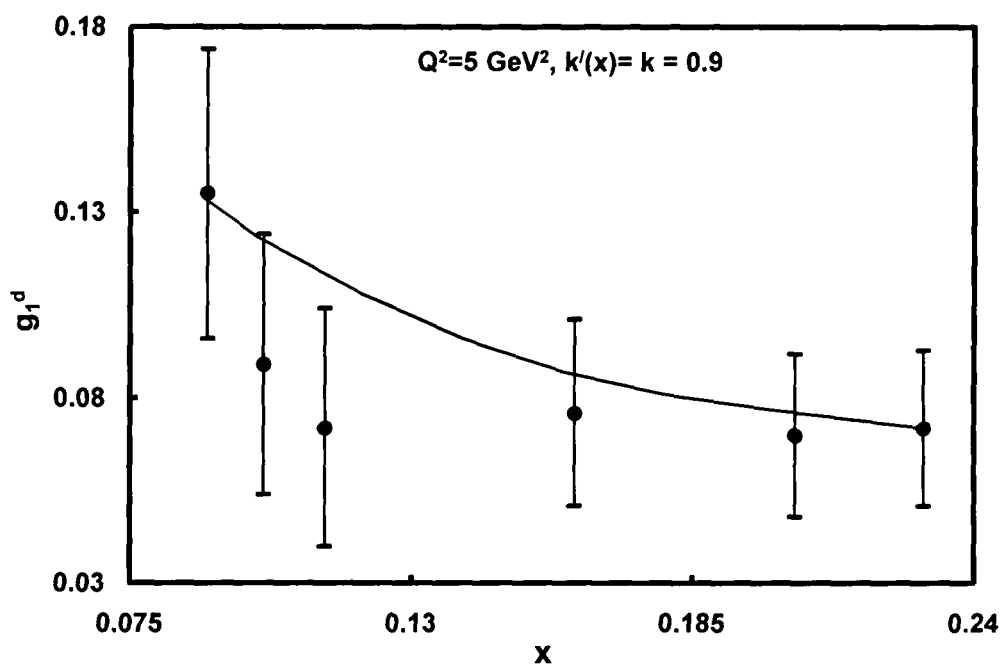
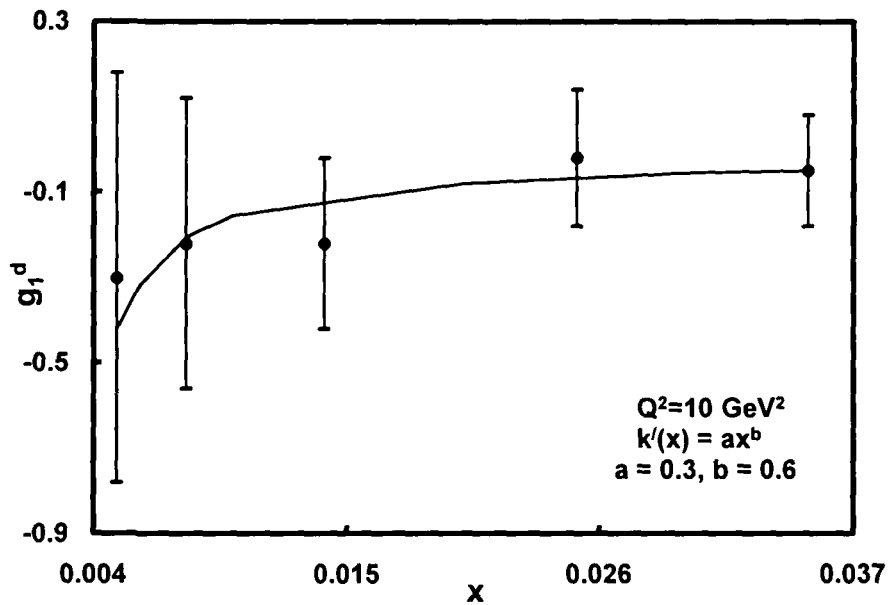


Figure 6.5:  $x$ -evolution of polarized deuteron structure functions in LO at  $k'(x) = k$ , a constant, compared with SLAC E143 data

In figure 6.6, x-evolution of polarized deuteron structure functions  $g_1^d(x,t)$  have been plotted against  $x$  for  $Q^2 = 10 \text{ GeV}^2$  taking  $k'(x) = ax^b$ , a power function of  $x$  with values  $a = 0.3$ ,  $b = 0.6$ . Our results are compared with SM collaboration data.



**Figure 6.6:** x-evolution of polarized deuteron structure functions in LO at  $k'(x) = ax^b$ , a power function of  $x$ , compared with SMC data

In figure 6.7, x-evolution of polarized deuteron structure functions  $g_1^d(x,t)$  have been plotted against  $x$  for  $Q^2 = 10 \text{ GeV}^2$  taking  $k'(x) = ce^{-dx}$ , an exponential function of  $x$ , with values  $c = 0.5$ ,  $d = 0.01$ . Our results are compared with SM collaboration data.

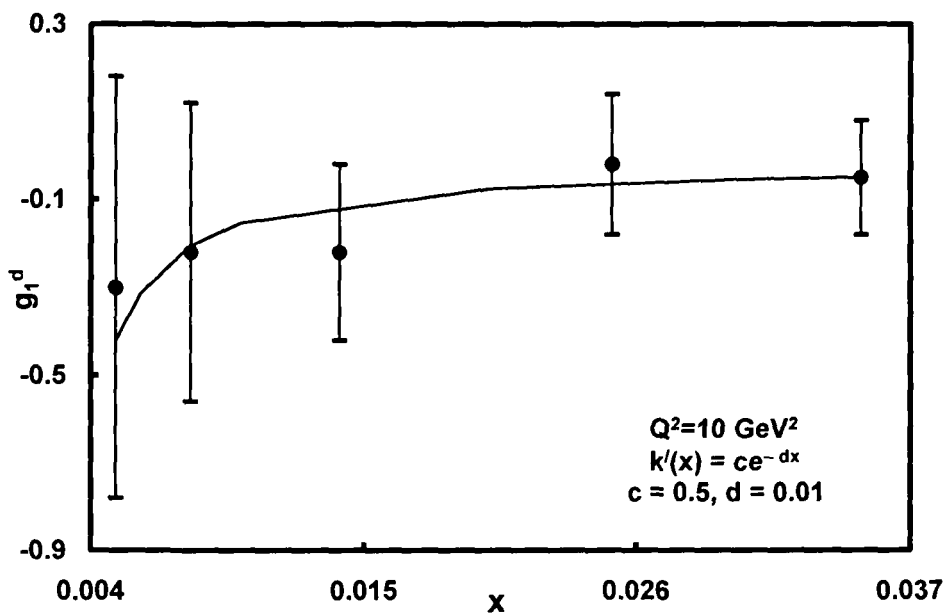


Figure 6.7: x-evolution of polarized deuteron structure functions in LO at  $k'(x) = ce^{-dx}$ , an exponential function of  $x$ , compared with SM collaboration data

In figure 6.8,  $x$ -evolution of polarized deuteron structure functions  $g_1^d(x, t)$  have been plotted against  $x$  for  $Q^2 > 10 \text{ GeV}^2$ , considering  $k'(x) = k$  and  $ax^b$ , compared with COMPASS collaboration data. It observed that the best fit results are obtained with values  $k=1.0$  and  $a = 1.0, b = 0.7$  respectively. Here we have not consider  $k'(x) = ce^{-dx}$ , as it has no significantly different results.

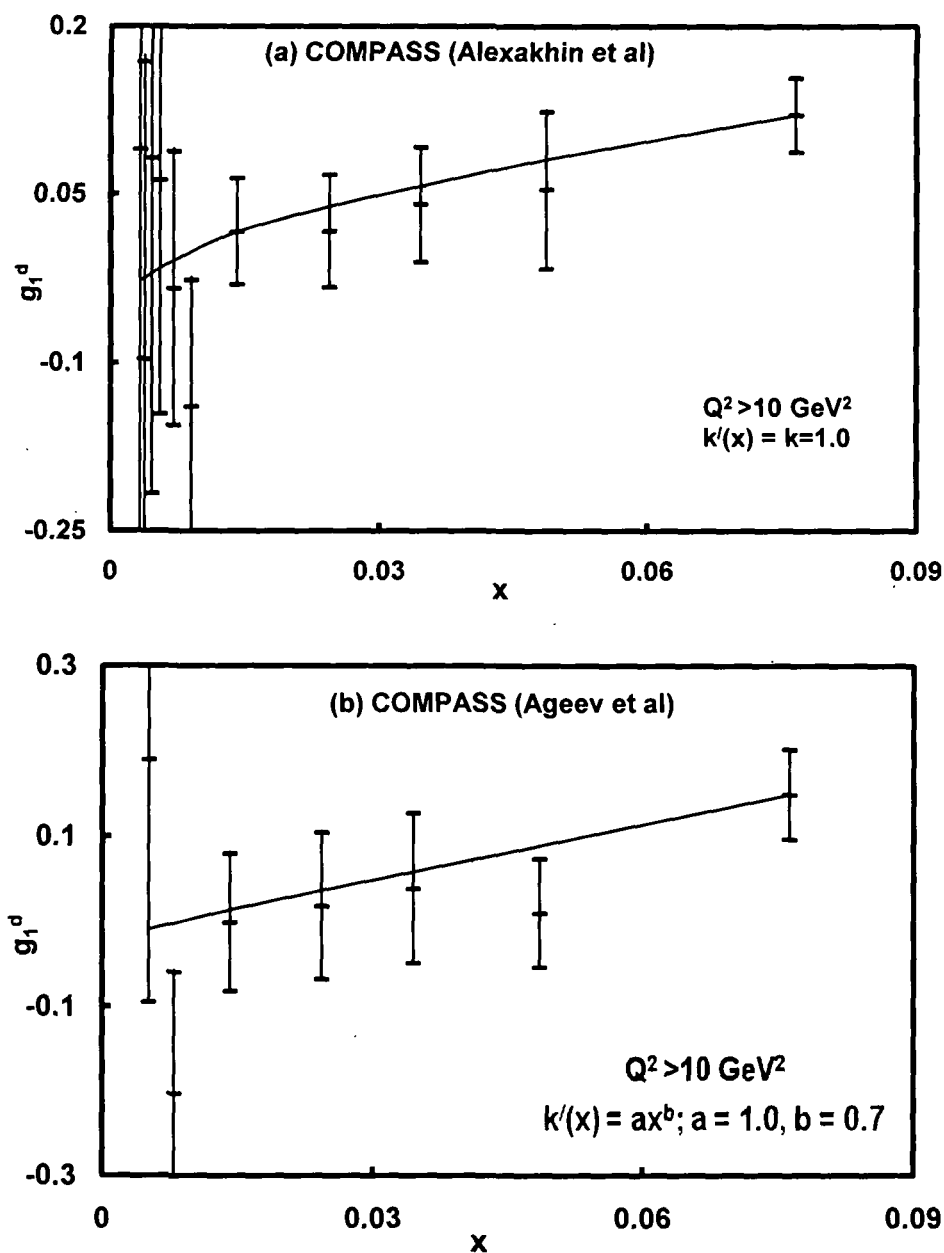


Figure 6.8:  $x$ -evolution of polarized deuteron structure functions in LO, compared with COMPASS collaboration data

### 6.3 Conclusion

In this chapter, we have solved the polarized DGLAP evolution equation in LO by method of characteristics and our results are compared with SLAC E143, SMC and COMPASS collaboration data set. It is observed that polarized structure functions are increased when  $Q^2$  increases or  $x$  decreases. Here our results are significantly compatible with the experimental data. Though some of our results are not accurately matched with experimental data, hope in NLO, which will be discussed in next chapter, we will get more accuracy.  $\square$

## Polarized DGLAP Evolution Equations in Next-to-Leading Order

In this chapter, the polarized structure function  $g_1(x, Q^2)$  for deep-inelastic lepton-nucleon scattering has been obtained by solving DGLAP evolution equations in NLO. We used the Taylor's expansion and then the method of characteristics to solve the evolution equations and then compared our results with SLAC E143 [136] experimental data, SMC [137] and COMPASS [146, 147] collaboration data.

### 7.1 Theory

The general discussion of polarized structure functions has been done in previous chapter. So, this is not done here. The singlet and non-singlet structure functions are obtained from the polarized DGLAP evolution equations in NLO,

$$\frac{\partial g_1^S}{\partial t} - \frac{\alpha_s(t)}{2\pi} \left[ \frac{2}{3} \{3 + 4\ln(1-x)\} g_1^S(x, t) + I_1^S(x, t) + I_2^S(x, t) \right] - \left( \frac{\alpha_s(t)}{2\pi} \right)^2 I_3^S = 0 \quad (7.1)$$

$$\frac{\partial g_1^{NS}}{\partial t} - \frac{\alpha_s(t)}{2\pi} \left[ \frac{2}{3} \{3 + 4\ln(1-x)\} g_1^{NS}(x, t) + I_1^{NS}(x, t) \right] - \left( \frac{\alpha_s(t)}{2\pi} \right)^2 I_2^{NS} = 0 \quad (7.2)$$

Functions  $I_1^S(x, t)$ ,  $I_2^S(x, t)$ ,  $I_3^S(x, t)$ ,  $I_1^{NS}(x, t)$  and  $I_2^{NS}(x, t)$  are discussed in Appendices D and E.

Now using Taylor's expansion series, we get

$$g_1^S\left(\frac{x}{\omega}, t\right) = g_1^S\left(x + \frac{xu}{1-u}, t\right) = g_1^S(x, t) + \frac{xu}{1-u} \frac{\partial g_1^S(x, t)}{\partial x} + \frac{1}{2} \left( \frac{xu}{1-u} \right)^2 \frac{\partial^2 g_1^S(x, t)}{\partial x^2} + \dots$$



As  $x$  is small in our region of discussion, the terms containing higher powers of  $x$  can be neglected and we can rewrite  $g_1^S\left(\frac{x}{\omega}, t\right)$ ,  $g_1^{NS}\left(\frac{x}{\omega}, t\right)$  and  $\Delta G\left(\frac{x}{\omega}, t\right)$  as

$$g_1^S\left(\frac{x}{\omega}, t\right) = g_1^S(x, t) + \frac{xu}{1-u} \frac{\partial g_1^S(x, t)}{\partial x}, \quad (7.3a)$$

$$g_1^{NS}\left(\frac{x}{\omega}, t\right) = g_1^{NS}(x, t) + \frac{xu}{1-u} \frac{\partial g_1^{NS}(x, t)}{\partial x}, \quad (7.3b)$$

$$\Delta G\left(\frac{x}{\omega}, t\right) = \Delta G(x, t) + \frac{xu}{1-u} \frac{\partial \Delta G(x, t)}{\partial x}. \quad (7.3c)$$

In order to solve equation (7.1) we need to relate the singlet structure function  $g_1^S(x, t)$  with the gluon distribution function  $\Delta G(x, t)$  and as discussed in previous chapter, let us assume  $\Delta G(x, t) = k'(x)g_1^S(x, t)$ , where  $k'(x)$  is a suitable function of  $x$  or may be a constant. We may assume  $k'(x) = k, ax^b, ce^{-dx}$  where  $k', a, b, c, d$  are parameters which can be determined by phenomenological analysis.

Using equation (7.3a) and (7.3c) and performing  $u$ -integrations we get from equation (7.1)

$$-t \frac{\partial g_1^S(x, t)}{\partial t} + A_f L'(x) \frac{\partial g_1^S}{\partial x} + A_f M'(x) g_1^S(x, t) = 0. \quad (7.4)$$

Here

$$A_f = \frac{\alpha_s(t)}{3\pi} t,$$

$$L'(x) = L_1'(x) + T_0 L_2'(x), \quad (7.5a)$$

$$M'(x) = M_1'(x) + T_0 M_2'(x), \quad (7.5b)$$

We have considered one numerical parameter  $T_0$ , such that  $T^2(t) = T_0 \cdot T(t)$  with

$T(t) = \frac{\alpha_s(t)}{2\pi}$ . This parameter is not arbitrary, but can be determined by

phenomenological analysis [79, 174]. Also

$$L_1'(x) = A_2'(x) + k'(x)A_4'(x), \quad (7.6a)$$

$$M_1'(x) = A_1'(x) + k'(x)A_3'(x) + A_4'(x) \frac{\partial k'(x)}{\partial x}, \quad (7.6b)$$

$$L'_2(x) = B'_2(x) + k'(x)B'_4(x), \quad (7.6c)$$

$$M'_2(x) = B'_1(x) + k'(x)B'_3(x) + B'_4(x) \frac{\partial k'(x)}{\partial x} \quad (7.6d)$$

where functions  $A'_1(x), A'_2(x), A'_3(x), A'_4(x)$  are discussed in chapter 6 and

$$B'_1(x) = x \int_0^1 f(\omega) d\omega - \int_0^x f(\omega) d\omega + \frac{4}{3} N_f \int_x^1 \Delta P_{qq}(\omega) d\omega,$$

$$B'_2(x) = x \int_x^1 \left[ f(\omega) + \frac{4}{3} N_f \Delta P_{qg}^S(\omega) \right] \frac{1-\omega}{\omega} d\omega,$$

$$B'_3(x) = \int_x^1 \Delta P_{qg}^S(\omega) d\omega \quad \text{and} \quad B'_4(x) = x \int_x^1 \frac{1-\omega}{\omega} \Delta P_{qg}^S(\omega) d\omega.$$

Now let us consider two new variables  $S$  and  $\tau$  instead of  $x$  and  $t$ ,

$$\frac{dt}{dS} = -t, \quad (7.7a)$$

$$\frac{dx}{dS} = A_f L'(x). \quad (7.7b)$$

From equation (7.4),

$$\frac{dg_1^S(S, \tau)}{dS} + M'(S, \tau) g_1^S(S, \tau) = 0. \quad (7.8)$$

This can be solved as

$$g_1^S(S, \tau) = g_1^S(0, \tau) \exp \left[ - \int_0^S M'(S, \tau) dS \right]. \quad (7.9)$$

For  $t$ -evolution, structure function varies with  $t$  remaining  $x$  constant. Hence equation (7.7a) can be used in equation (7.9) and we get

$$g_1^S(S, \tau) = g_1^S(\tau) \left( \frac{t}{t_0} \right)^{M'(S, \tau)}, \quad (7.10)$$

where  $M'(S, \tau) = A_f M'(x)$  and  $g_1^S(S, \tau) = g_1^S(\tau)$ ;  $S = 0, t = t_0$ . Now we have to replace the co-ordinate system  $(S, \tau)$  to  $(x, t)$  in equation (7.10) with the input function  $g_1^S(\tau) = g_1^S(x, t_0)$  and will get the  $t$ -evolution of singlet structure function in the NLO as

$$g_1^S(x, t) = g_1^S(x, t_0) \left( \frac{t}{t_0} \right)^{\frac{3}{2} A_f M'(x)} \quad (7.11)$$

Similarly, for  $x$ -evolution, structure function varies with  $x$  remaining  $t$  constant. Hence equation (7.7b) can be used in equation (7.9) and the  $x$ -evolution of polarized singlet structure function in NLO will be

$$g_1^S(x, t) = g_1^S(x_0, t) \exp \left[ - \int_{x_0}^x \frac{M'(x)}{L'(x)} dx \right]. \quad (7.12)$$

Proceeding in the same way, we get  $t$  and  $x$ -evolutions of non-singlet structure function from equation (7.2) as

$$g_1^{NS}(x, t) = g_1^{NS}(x, t_0) \left( \frac{t}{t_0} \right)^{\frac{3}{2} A_f [A_1'(x) + T_0 B_1'(x)]}, \quad (7.13a)$$

$$g_1^{NS}(x, t) = g_1^{NS}(x_0, t) \exp \left[ - \int_{x_0}^x \frac{A_1'(x) + T_0 B_1'(x)}{A_2'(x) + T_0 B_2'(x)} dx \right]. \quad (7.13b)$$

Similarly,  $t$  and  $x$ -evolutions of deuteron structure functions in NLO are

$$g_1^d(x, t) = g_1^d(x, t_0) \left( \frac{t}{t_0} \right)^{\frac{3}{2} A_f M'(x)}, \quad (7.14a)$$

$$g_1^d(x, t) = g_1^d(x_0, t) \exp \left[ - \int_{x_0}^x \frac{M'(x)}{L'(x)} dx \right]. \quad (7.14b)$$

Here  $g_1^d(x, t_0) = \frac{5}{9} g_1^d(x, t_0)$ ,  $g_1^d(x_0, t) = \frac{5}{9} g_1^d(x_0, t)$ ,

$$g_1^{NS}(x, t_0) = 3[g_1^p(x, t_0) - g_1^n(x, t_0)],$$

$$g_1^{NS}(x_0, t) = 3[g_1^p(x_0, t) - g_1^n(x_0, t)],$$

with  $g_1^d(x, t_0)$ ,  $g_1^p(x, t_0)$ ,  $g_1^n(x, t_0)$  and  $g_1^d(x_0, t)$ ,  $g_1^p(x_0, t)$ ,  $g_1^n(x_0, t)$  are input functions. For phenomenological analysis, we use equations (7.14a) and (7.14b) to study polarized deuteron structure functions and equations (7.13a) and (7.13b) to study polarized non-singlet (combination of proton and neutron) structure functions in NLO.

## 7.2 Results and Discussions

Here we compare our result of  $t$  and  $x$ -evolutions of polarized deuteron  $g_1^d(x,t)$  and non-singlet  $g_1^{NS}(x,t)$  (combination of proton and neutron) structure functions with data measured by the SLAC E143 experiment [136] and SMC [137] and COMPASS collaboration [146, 147]. We compare our results for  $k'(x) = k, ax^b$  and  $ce^{-dx}$  where  $k, a, b, c$  and  $d$  are constants. Each graph is the best fit graph of our work with the corresponding values of the parameters  $k, a, b, c$  and  $d$ . Data points from experimental data sets, at lowest- $Q^2$  values are taken as inputs to test the  $t$ -evolution of our results and data points from experimental data sets at highest- $x$  is taken as inputs to test the  $x$ -evolution of our results. It is seen from the figures that the polarized structure functions are increased with  $Q^2$  at small- $x$ .

In Figure 7.1 we plot  $T^2(t)$  and  $T_0T(t)$ , where  $T(t) = \alpha_s(t)/2\pi$ , against  $Q^2$  in the range  $0 \leq Q^2 \leq 30 \text{ GeV}^2$  as required by our data used for structure functions. Here we observe that the difference between the values of  $T^2(t)$  and  $T_0T(t)$  in this range is negligible for  $T_0 = 0.048$ .

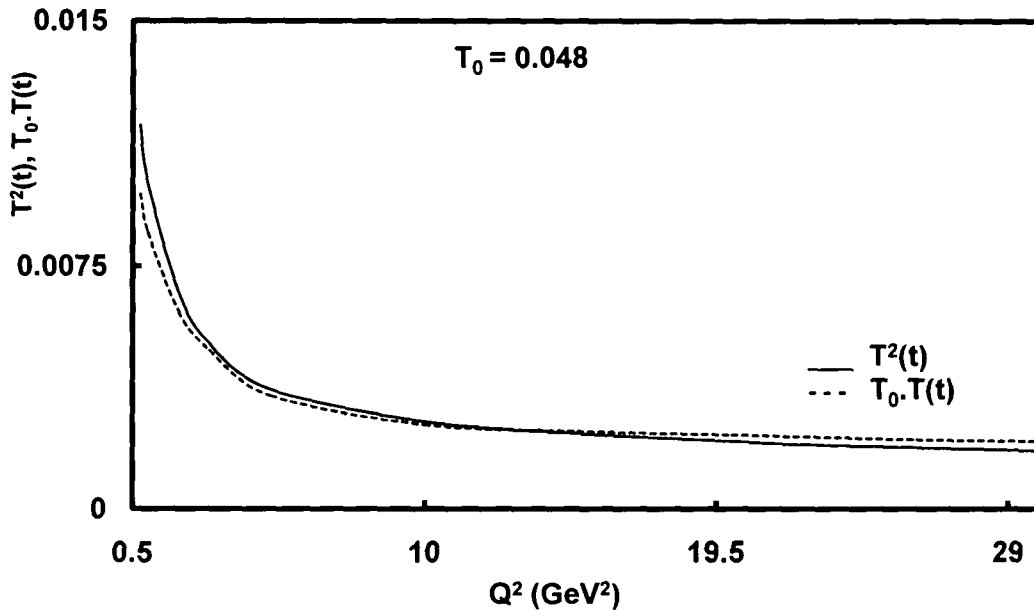


Figure 7.1: Comparison of  $T^2$  and  $T_0T$  values

In figures 7.2, computed values of  $g_1^d(x, t)$  have been plotted against  $Q^2$  for fixed- $x$  in NLO for  $x = 0.056, 0.071$  and  $0.09$  taking suitable values of  $k'(x) = ce^{-dx}$ , an exponential function of  $x$  with values  $c = 0.02$  and  $d = 0.08$ . Here values of  $g_1^d(x, t)$  at lowest  $Q^2$  are taken as the input functions. Our results are compared with SLAC E143 data. All solid dots with vertical error bars represent the experimental data with total systematic and statistical uncertainties. It is observed that  $k'(x)$  is not a strongly influenced function that is, our results do not vary significantly with the form of  $k'(x)$ . Thus  $k'(x) = k$  and  $ax^b$  are not considered here.

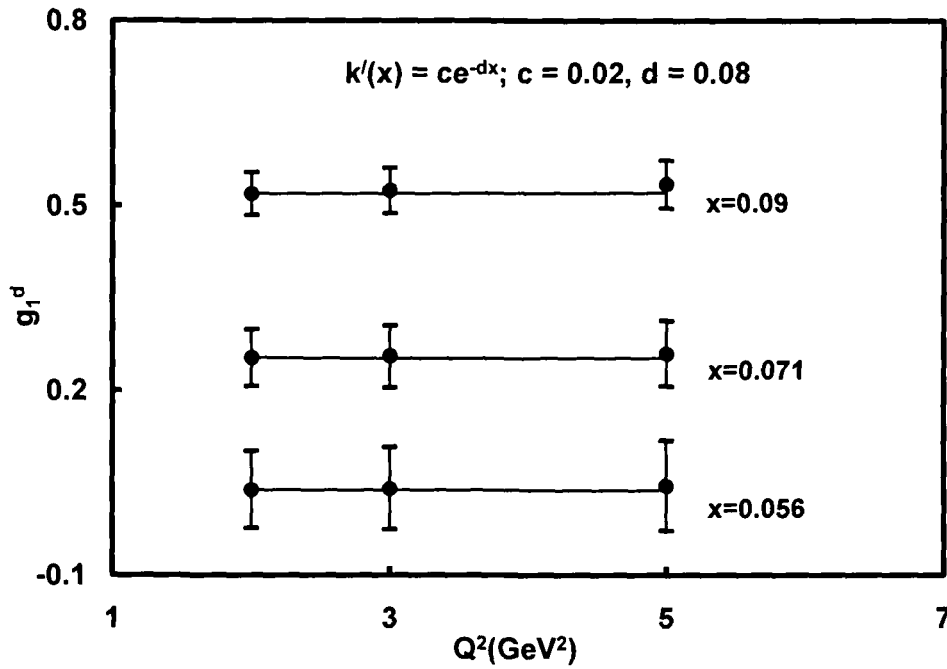


Figure 7.2:  $t$ -evolutions of polarized deuteron structure function in NLO at  $k'(x) = ce^{-dx}$ , an exponential function of  $x$ , compared with SLAC E143 data

In figure 7.3, we have plotted computed values of  $g_1^{NS}(x,t)$  against  $Q^2$  for LO and NLO for  $x = 0.056, 0.071$  and  $0.09$ . Here solid lines represent our NLO results and dotted lines represent LO results. The values of  $g_1^{NS}(x,t)$  at lowest  $Q^2$  are taken as the input functions. Our results are compared with SLAC E143 data. Here also all solid dots with vertical error bars represent the experimental data with total systematic and statistical uncertainties.

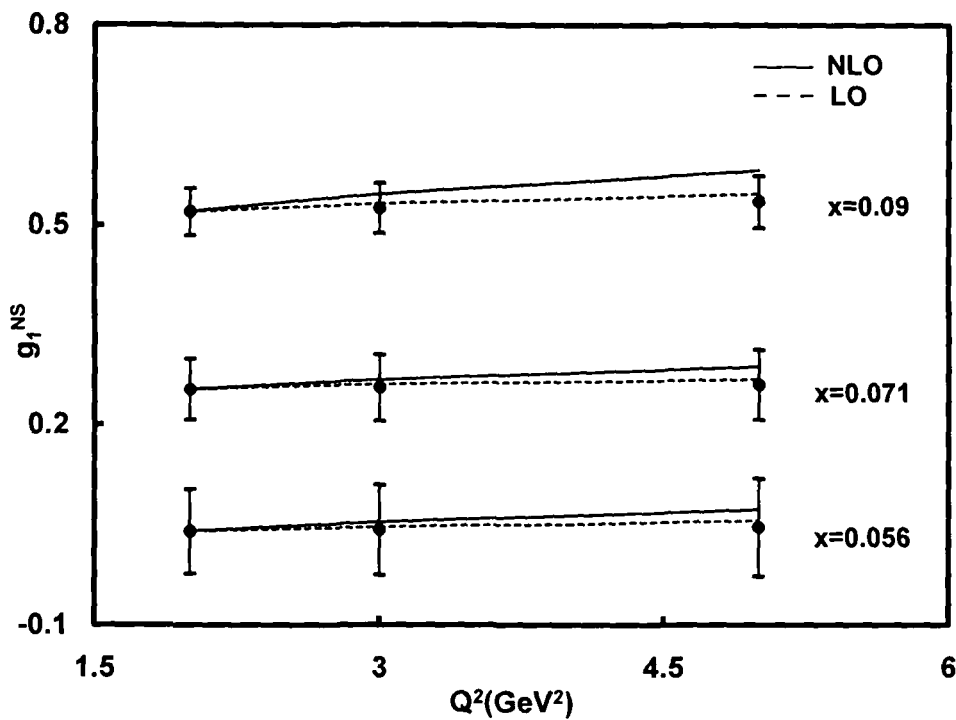


Figure 7.3: t-evolutions of polarized non-singlet structure function in NLO, compared with SLAC E143 data

In Figures 7.4, computed values of  $g_1^d(x,t)$  have plotted against  $x$  for fixed  $Q^2 = 5 \text{ GeV}^2$  in LO and NLO taking suitable value of  $k'(x) = k$ , a constant with value  $k = 0.7$ . Solid line represents our NLO results and dotted line represents LO results. The middle values of vertical lines represent SLAC E143 experimental data with lower and upper values as total systematic and statistical errors. The  $g_1^d(x,t)$  value at highest- $x$  is taken as the input function.

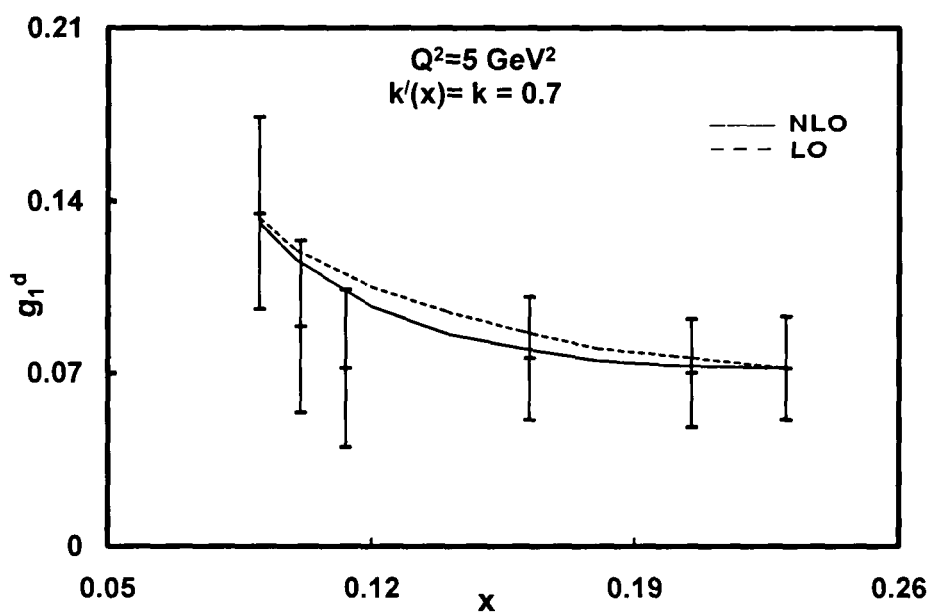


Figure 7.4:  $x$ -evolution of polarized deuteron structure functions in NLO considering  $k'(x) = k$ , a constant, compared with SLAC E143 data

In figure 7.5, computed values of  $g_1^d(x,t)$  have been plotted against  $x$  for fixed- $Q^2$  in LO and NLO for  $Q^2 = 10 \text{ GeV}^2$  taking suitable values of  $k'(x) = ax^b$ , a power function of  $x$  with values  $a = 0.1$  and  $b = 0.03$ . Solid line represents our NLO results and dotted line represents LO result. The middle values of vertical lines represent SMC data with lower and upper values as total statistical and systematic errors. Here the value of  $g_1^d(x,t)$  at highest- $x$  is taken as the input function.

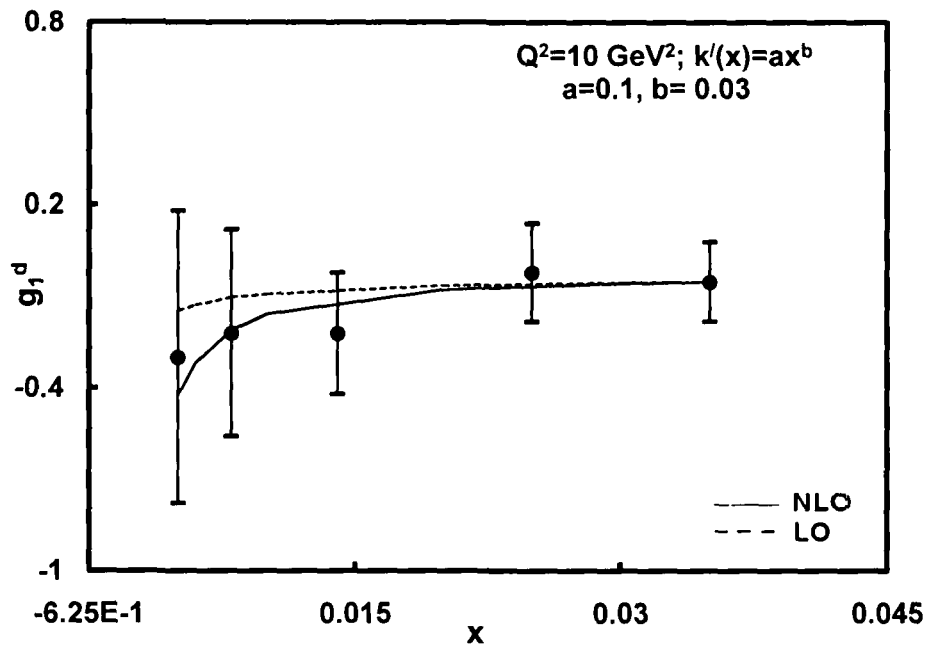


Figure 7.5:  $x$ -evolution of polarized deuteron structure functions in NLO considering  $k'(x) = ce^{-dx}$ , an exponential function of  $x$ , compared with SMC data



In figures 7.6,  $x$ -evolutions of polarized deuteron structure functions  $g_1^d(x,t)$  have been plotted against  $x$  for  $Q^2 > 10 \text{ GeV}^2$ , considering  $k'(x) = k$  and  $ax^b$ . It observed that the best fit results are obtained with values  $k = 1.0$  and  $a = 1.0, b = 0.7$  respectively. Our results are compared with COMPASS collaboration data. Here we have not consider  $k'(x) = ce^{-dx}$ , as it has no significantly different results.

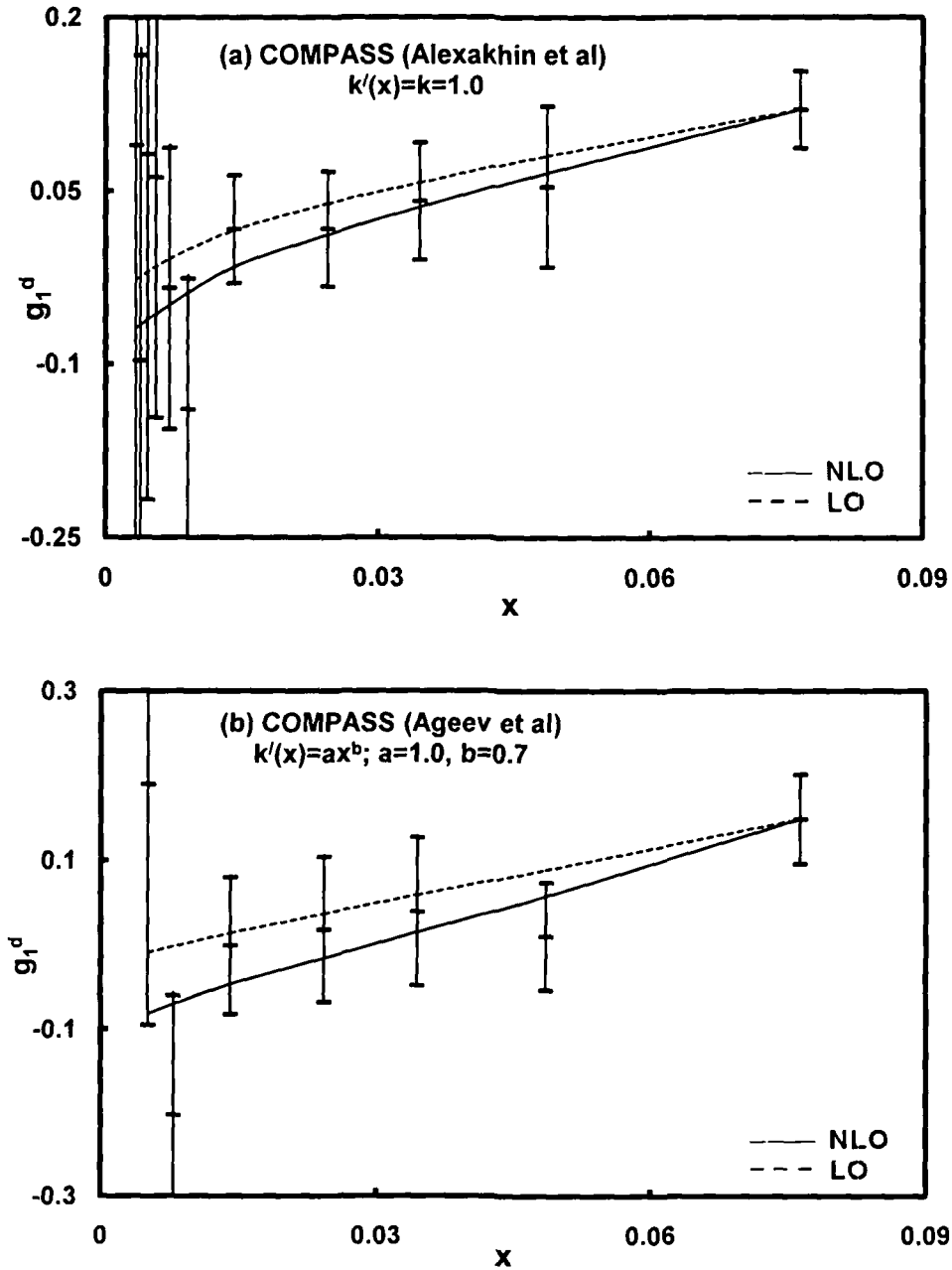


Figure 7.6:  $x$ -evolution of polarized deuteron structure functions in NLO considering  $k'(x) = k$  and  $ax^b$ , compared with COMPASS collaboration data

### 7.3 Conclusion

In this chapter, we have solved the polarized DGLAP evolution equation in NLO by method of characteristics and our results are compared with SLAC E143 experimental results, SMC and COMPASS collaboration data sets. It is observed that our results are significantly compatible with the experimental data. On an average the percentage errors of our results in LO and NLO are 1.03% and 6.39% with SLAC E143 data, 5.94% and 2.91% with SMC data also 6.92% and 2.94% with COMPASS collaboration data. These errors in theoretical results are very less as compared to systematic and statistical uncertainties in the experimental data. It is observed that there is significant contribution of Next-to-Leading order over the Leading order in polarized structure functions. Here  $k'(x)$  is a not strongly influenced function i.e. for different  $k'(x)$  values also we get approximately same results of polarized structure functions.  $\square$

# *Part - III*

## Gluon Distribution Functions

*"If you cannot measure it, then it is not science"*

*– Kelvin*

The gluon distribution function is one of the most important physical observables that govern the physics at high energy (small Bjorken  $x$ ) in the DIS. The basic information about the gluon distribution function of the nucleon can be obtained from a measurement of the DIS structure function  $F_2(x, Q^2)$  and its scaling violation. The measurement of the proton structure function by the H1 [53, 148] and ZEUS [54] group at HERA over a wide kinematics region has enabled us to know about the gluon also in the previously unexplored region in  $x$  and  $Q^2$ . In the small- $x$  region where gluon, being the dominant parton, drives the structure function  $F_2(x, Q^2)$  through the transition  $g \rightarrow q\bar{q}$ . The steep rise of  $F_2(x, Q^2)$  towards small- $x$  observed at HERA, also indicates in perturbative QCD a similar rise of the gluon towards small  $x$ .

Experimental data of polarized structure functions are available from results of experiments performing on SLAC [149-156], CERN [157-164] and DESY [140, 141]. The results were analysed by many groups worldwide and polarization quark structure functions as well as gluon distribution functions were presented [165-174]. The spin of the nucleon is known to be  $1/2$ . However, the EMC experiment has found that the spin of the quarks contributes only a small fraction to the proton spin. Ever since it has been a longstanding problem how the nucleon spins are divided among the quarks and gluons. The spin density contribution of the quarks to the nucleon spin  $\Delta\Sigma$  can be probed in deep inelastic scattering. The result obtained by the HERMES collaboration [175] is  $\Delta\Sigma = 0.30 \pm 0.04 \pm 0.09$ , clearly showing that the gluon contributions to the nucleon spin are needed. The gluon spin density  $\Delta G$  can be probed in the photon-gluon fusion process as planned in the COMPASS experiment. The first direct exploration of the gluon polarization has been performed by the HERMES collaboration [176] and found a value of  $\Delta G/G = 0.41 \pm 0.18$  (stat)  $\pm 0.03$  (syst) at an average fraction of the nucleon momentum carried by the struck gluon of  $\langle xG \rangle = 0.17$ . Due to limitations in large angle tracking it is planned to start with the measurement of  $g_1$  at small- $x$  values, which is important for the study of possible scaling violations.

## Unpolarized Gluon Distribution Functions in Leading Order and Next-to-Leading Order

In this chapter, the unpolarized gluon distribution functions have been obtained by solving Dokshitzer-Gribove-Lipatov-Altarelli-Parisi (DGLAP) evolution equations in LO and NLO at the small- $x$  limit. Here we have used a Taylor series expansion and then the method of characteristics to solve the evolution equations. We have also calculated  $t$  and  $x$ -evolutions of gluon distribution functions and the results are compared with GRV1998 [177] and MRST2004 [178] gluon parameterizations.

### 8.1 Theory

The DGLAP evolution equations in standard forms for unpolarized gluon distribution functions in LO and NLO [91, 179, 180, 181] are

$$\frac{\partial G(x, t)}{\partial t} - \frac{\alpha_S}{2\pi} \frac{2}{3} \left\{ \left( \frac{11}{12} - \frac{N_f}{18} + \ln(1-x) \right) G(x, t) + I_g^1 \right\} = 0, \quad (8.1)$$

$$\frac{\partial G(x, t)}{\partial t} - \frac{\alpha_S}{2\pi} \frac{2}{3} \left\{ \left( \frac{11}{12} - \frac{N_f}{18} + \ln(1-x) \right) G(x, t) + I_g^1 \right\} - \left( \frac{\alpha_S}{2\pi} \right)^2 I_g^2 = 0, \quad (8.2)$$

where functions  $I_g^1(x, t)$  and  $I_g^2(x, t)$  are defined in Appendix F.

Let us introduce the variable  $u = 1 - \omega$  and using Taylor's expansion series we can rewrite

$$G\left(\frac{x}{\omega}, t\right) = G(x, t) + \frac{xu}{1-u} \frac{\partial G(x, t)}{\partial x} + \frac{1}{2} \left(\frac{xu}{1-u}\right)^2 \frac{\partial^2 G(x, t)}{\partial x^2} + \dots$$

$$\approx G(x, t) + \frac{xu}{1-u} \frac{\partial G(x, t)}{\partial x}, \quad (8.3a)$$

$$F_2^S\left(\frac{x}{\omega}, t\right) = F_2^S(x, t) + \frac{xu}{1-u} \frac{\partial F_2^S(x, t)}{\partial x}. \quad (8.3b)$$

Since  $x$  is small in our region of discussion, the terms containing  $x^2$  and higher powers of  $x$  are neglected. Using equations (8.3a) and (8.3b) and performing  $u$ -integrations we get equation (8.1) of the form

$$\frac{\partial G(x, t)}{\partial t} - \frac{A_f}{t} \left[ A_1^g(x)G(x, t) + A_2^g(x) \frac{\partial G(x, t)}{\partial x} + A_3^g(x)F_2^S(x, t) + A_4^g(x) \frac{\partial F_2^S(x, t)}{\partial x} \right] = 0, \quad (8.4)$$

where  $A_f = \frac{\alpha_s(t)}{3\pi} t = \frac{4}{3\beta_0} = \frac{4}{33-2N_f}$ , as defined in chapter 3, and also

$$A_1^g(x) = -\frac{11}{6} + 2x - \frac{1}{2}x^2 + \frac{1}{3}x^3 - \ln(x), \quad A_2^g(x) = 1 + \frac{4}{3}x - 3x^2 + x^3 - \frac{1}{4}x^4 + 2x \ln(x),$$

$$A_3^g(x) = \frac{2}{9} \left\{ -\frac{3}{2} + 2x - \frac{1}{2}x^2 - 2\ln(x) \right\}, \quad A_4^g(x) = \frac{2}{9} \left\{ 2 + \frac{1}{2}x - 3x^2 + \frac{1}{2}x^3 + 4x \ln(x) \right\}.$$

Now let us assume,  $F_2^S(x, t) = R(x)G(x, t)$ , where  $R(x)$  is a suitable function of  $x$  or may be a constant. Now equation (8.4) gives

$$-t \frac{\partial G(x, t)}{\partial t} + A_f L_1^g(x) \frac{\partial G(x, t)}{\partial x} + A_f M_1^g(x) G(x, t) = 0, \quad (8.5)$$

where

$$L_1^g(x) = A_2^g(x) + R(x)A_4^g(x) \quad \text{and} \quad M_1^g(x) = A_1^g(x) + R(x)A_3^g(x) + A_4^g(x) \frac{\partial R(x)}{\partial x}$$

Now let us consider two new variables  $S$  and  $\tau$  instead of  $x$  and  $t$ , such that

$$\frac{dt}{dS} = -t, \quad (8.6a)$$

$$\frac{dx}{dS} = A_f L_1^g(x). \quad (8.6b)$$

Putting these in equation (8.5), we get

$$\frac{dG(S, \tau)}{dS} + M_1^g(S, \tau)G(S, \tau) = 0, \quad (8.7)$$

where  $M_1^g(S, \tau) = A_f M_1^g(x)$ . Equations (8.7) can be solved as,

$$G(S, \tau) = G(0, \tau) \exp \left[ - \int_0^S M_1^g(S, \tau) dS \right] \quad (8.8)$$

For t-evolution, gluon distribution function varies with t remaining x constant. Hence equation (8.6a) can be used to solve the equation (8.7). Now we have to replace the co-ordinate system (S,  $\tau$ ) to (x, t), considering when S = 0, t = t<sub>0</sub> and the input function as G( $\tau$ ) = G(x, t<sub>0</sub>). So the t-evolution of gluon distribution function in LO is given by

$$G(x, t) = G(x, t_0) \left( \frac{t}{t_0} \right)^{A_f M_1^g(x)}, \quad (8.9)$$

Using equation (8.6b) and replacing the co-ordinate system (S,  $\tau$ ) to (x, t), with consideration when  $\tau = 0$ , x = x<sub>0</sub> and the input function as G(S) = G(x<sub>0</sub>, t), the x-evolution of gluon distribution function in LO is given by

$$G(x, t) = G(x_0, t) \exp \left( - \int_{x_0}^x \frac{M_1^g(x)}{L_1^g(x)} dx \right) \quad (8.10)$$

Similarly the t and x-evolution of gluon distribution functions in NLO are given by

$$G(x, t) = G(x_0, t) \left( \frac{t}{t_0} \right)^{A_f \{M_1^g(x) + T_0 M_2^g(x)\}}, \quad (8.11)$$

$$G(x, t) = G(x_0, t) \exp \left( - \int_{x_0}^x \frac{M_1^g(x) + T_0 M_2^g(x)}{L_1^g(x) + T_0 L_2^g(x)} dx \right), \quad (8.12)$$

where

$$L_2^g(x) = B_2^g(x) + R(x)B_4^g(x) \text{ and } M_2^g(x) = B_1^g(x) + R(x)B_3^g(x) + B_4^g(x) \frac{\partial R(x)}{\partial x}.$$

We also consider  $\left(\frac{\alpha_s(t)}{2\pi}\right)^2 = T_0 \left(\frac{\alpha_s(t)}{2\pi}\right)$ , where  $T_0$  is a numerical parameter, not

arbitrary choose but determined by phenomenological analysis [79, 174]. The

other functions are  $B_1^g(x) = -\frac{52}{3} \ln x$ ,  $B_2^g(x) = -\frac{52}{3} (1-x + x \ln x)$ ,

$B_3^g(x) = \int_x^1 A(\omega) d\omega$  and  $B_4^g(x) = x \int_x^1 \frac{1-\omega}{\omega} A(\omega) d\omega$ .

## 8.2 Results and Discussions

Here we have compared our result of t-evolution for gluon distribution function  $G(x, t)$  in LO and NLO with GRV1998 global parameterizations [177] and x-evolution with GRV1998 and MRST2004 [178] parameterizations. We consider GRV1998 parameterization for  $10^{-2} \leq x \leq 10^{-5}$  and  $20 \leq Q^2 \leq 40 \text{ GeV}^2$ , where they used H1 [182] and ZEUS [183] high precision data on  $G(x, Q^2)$ . They have chosen  $\alpha_s(M_Z^2) = 0.114$  and  $\Lambda_{\overline{MS}}(N_f = 4) = 246 \text{ MeV}$ . The input densities have been fixed using the data sets HERA [182], SLAC[184], BCDMS [185], NMC [113] and E665 [114]. The resulting input distribution at  $Q^2 = 0.04 \text{ GeV}^2$  is given by  $xg = 20.80 x^{1.6} (1-x)^{4.1}$ .

We have taken the MRST2004 fit to the H1 [53] and ZEUS [54] data with  $x < 0.01$  and  $2 \leq Q^2 \leq 500 \text{ GeV}^2$  for  $Q^2 = 100 \text{ GeV}^2$ , in which they have taken parametric form for the starting distribution at  $Q_0^2 = 1 \text{ GeV}^2$  given by

$$xg = A_g x^{-\lambda_g} (1-x)^{3.7} \left(1 + \varepsilon_g \sqrt{x} + \gamma_g x\right) - A x^{-\delta} (1-x)^{10},$$

where power of the  $(1-x)$  factors are taken from MRST2001 fit [56]. Here

$A_g, \lambda_g, \gamma_g, \varepsilon_g, A$  and  $\delta$  are taken as free parameters. The optimum fit corresponds to  $\alpha_s(M_Z^2) = 0.119$  and  $\Lambda_{\overline{MS}} = 323 \text{ MeV}$  with  $N_f = 4$ .

Our results represent the best fit graphs of our work with different parameterization curves. Results of parameterization at lowest- $Q^2$  values are taken as input to test the t-evolution equations and those at highest-x is taken as input to test the x-evolution equations. We have compared our results for  $R(x)$



as a constant  $R$ , a power function  $ax^b$  and an exponential function  $ce^{-dx}$ . In our work for gluon distribution function, we have found the values of the gluon distribution function remains almost same for  $b < 0.0001$  and for  $d < 0.001$ . So, we have chosen  $b = 0.0001$  and  $d = 0.001$  and the best fit graphs are observed by changing the values of  $R$ ,  $a$  and  $c$ . If we plot  $T^2(t)$  and  $T_0T(t)$  against  $Q^2$ , then we can see that for  $T_0 = 0.048$ , the values of  $T^2$  and  $T.T_0$  are nearly same in our region of discussion, as we have seen in figure 4.1 of chapter 4. Thus we consider  $T_0 = 0.048$  in calculation of  $G(x, t)$  at NLO and the consideration of parameter  $T_0$  does not give any abrupt change in our results.

In figures 8.1, we have plotted our results of  $t$ -evolution of gluon distribution function in LO from equation (8.9) and compared with GRV1998 parameterization for  $R(x) = R$ , a constant. Here we have plotted our results of gluon distribution function against  $Q^2$  for  $x = 10^{-5}$  and  $x = 10^{-4}$  and we get the best fit with  $R = 0.5$  and  $R = 0.8$  respectively.

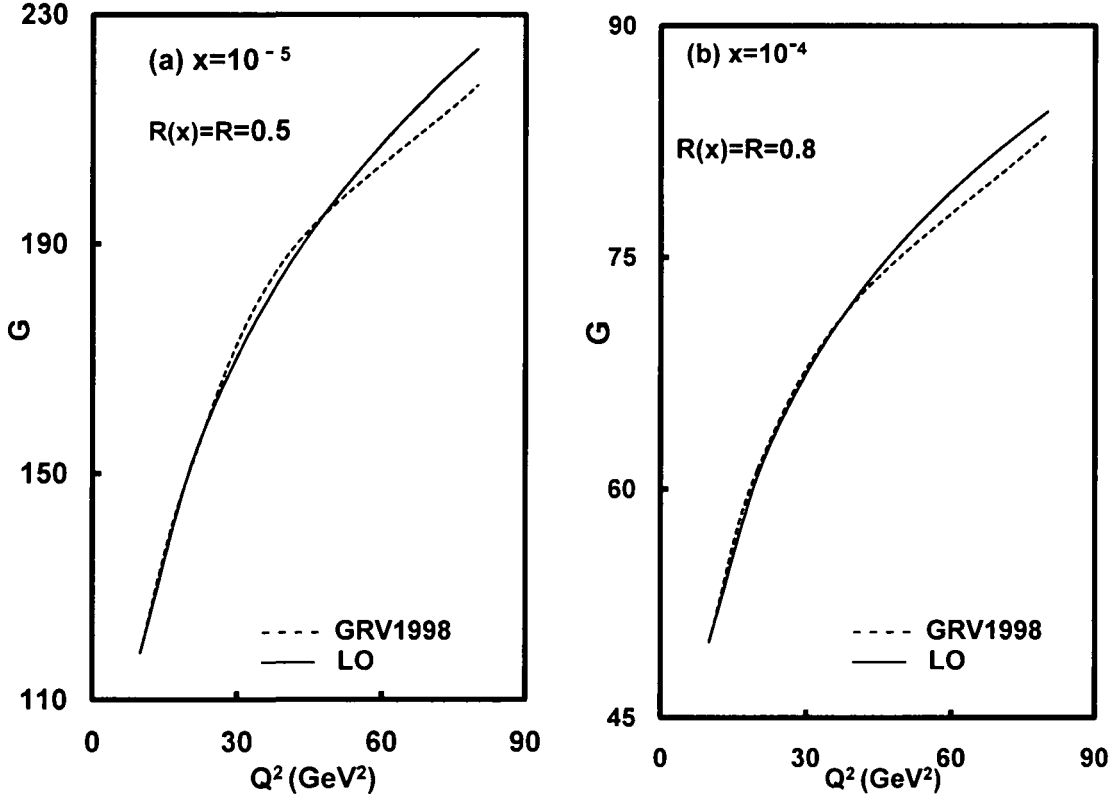


**Figure 8.1:**  $t$ -evolution of gluon distribution functions in LO for  $R(x) = R$ , a constant, compared with GRV1998 parameterization graphs

In figures 8.2, we have plotted our results of t-evolution of gluon distribution function in LO from equation (8.9) and compared with GRV1998 parameterization at  $x=10^{-5}$  for  $R(x) = ax^b$  and  $ce^{-dx}$  respectively. Here we have plotted our results against  $Q^2$  for  $R(x) = ax^b$  as well as  $R(x) = ce^{-dx}$  and we get the best fit with  $a = 0.9$ ,  $b = 0.0001$  and  $c = 0.8$ ,  $d = 0.001$ .

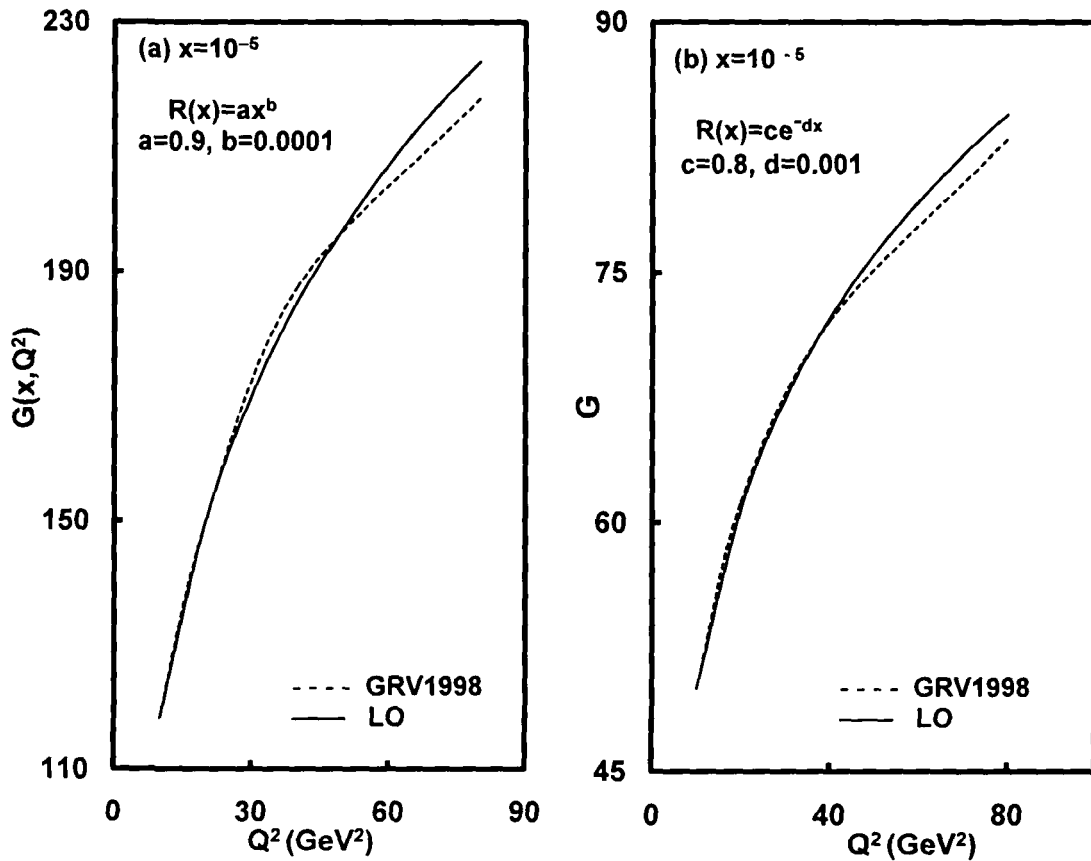
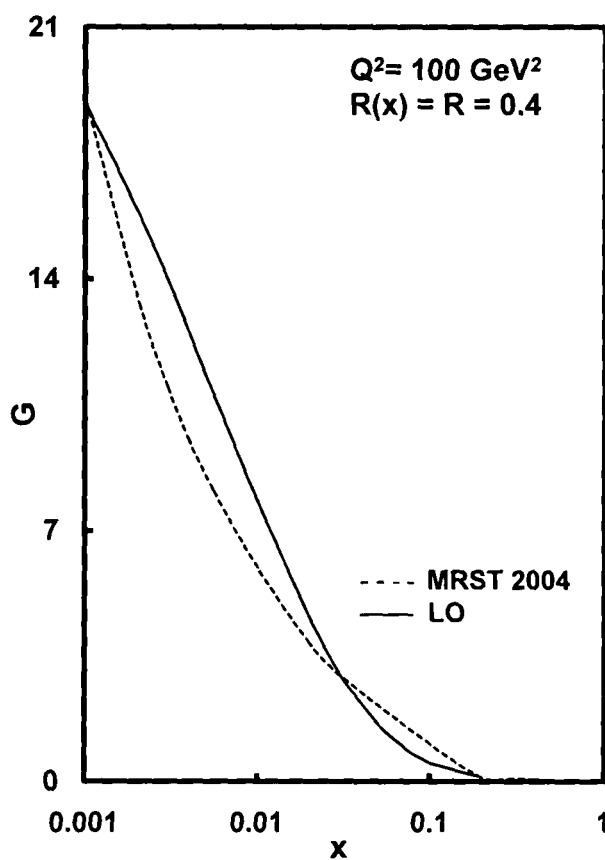


Figure 8.2: t-evolution of gluon distribution functions in LO for  $R(x) = ax^b$  and  $ce^{-dx}$  compared with GRV1998 parameterization graphs

In figure 8.3 we have plotted our results of gluon distribution function against  $x$  for  $Q^2= 100 \text{ GeV}^2$  with  $R(x) = R$  and compared with MRST2004 and best fit has been found for  $R= 0.4$ .



**Figure 8.3:**  $x$ -evolution of gluon distribution functions in LO for  $R(x) = R$ , compared with MRST2004 parameterization

In figures 8.4 and 8.5, we have plotted our results of t-evolutions of gluon distribution function in NLO from equation (8.11) and compared with GRV1998 gluon parameterization for  $R(x) = R$  and  $ax^b$ . These results are also compared with our LO results obtained from equation (8.9). In figure 8.4, we have plotted our results of gluon distribution function against  $Q^2$  for  $x = 10^{-5}$  and we get the best fit with  $R = 0.8$  in NLO and  $R = 0.9$  in LO.

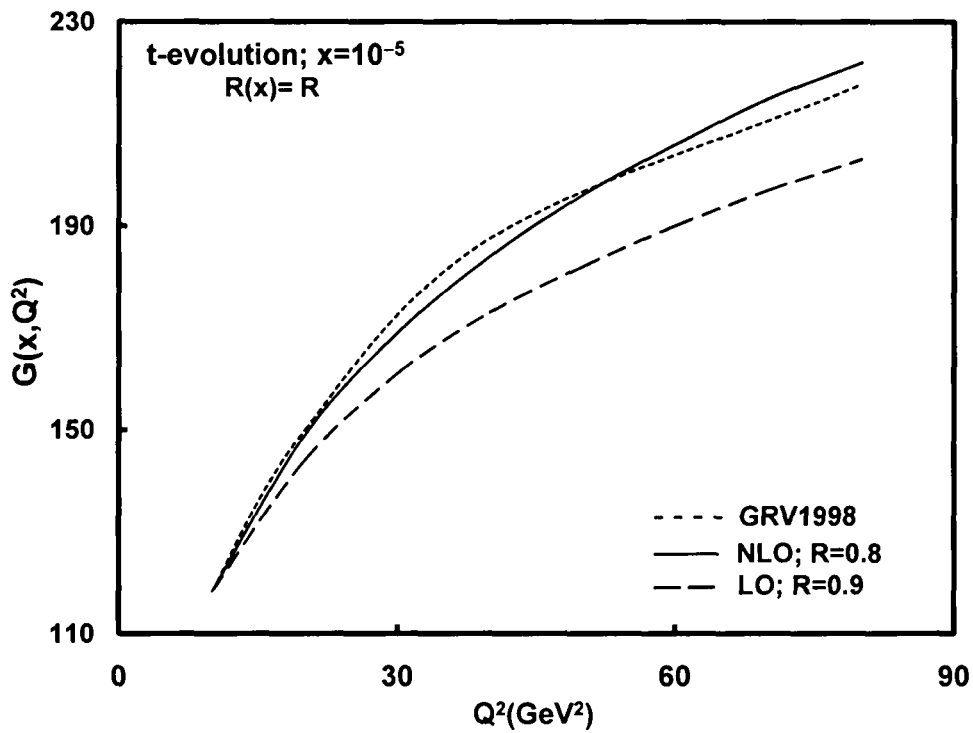


Figure 8.4: t-evolution of gluon distribution functions in NLO for  $R(x) = R$ , compared with GRV1998 parameterization

In figures 8.5 our results of gluon distribution function in NLO have been plotted against  $Q^2$  for  $x = 10^{-4}$  with  $R(x) = ax^b$  and we get the best fit with  $a = 0.8$  and  $b = 0.001$  in NLO and  $a = 0.9$  and  $b = 0.0001$  in LO.

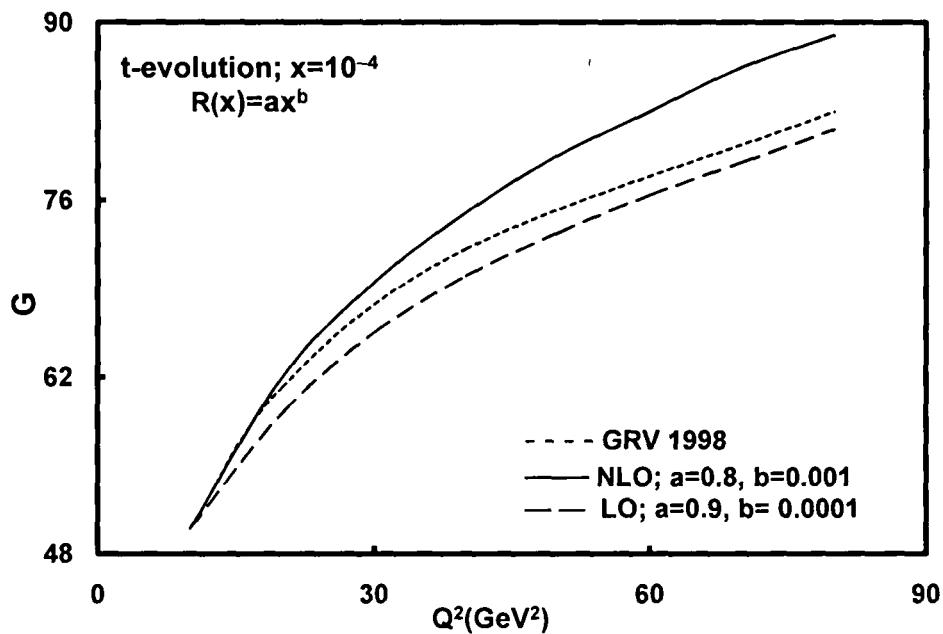
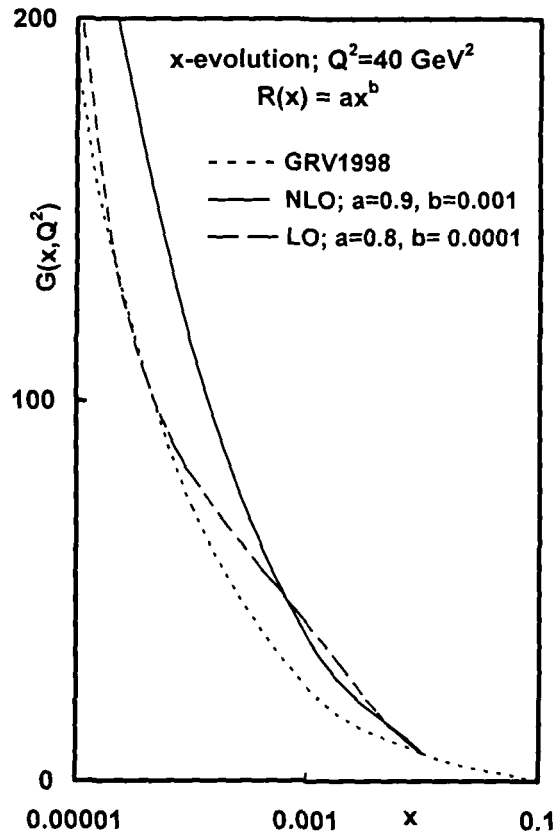


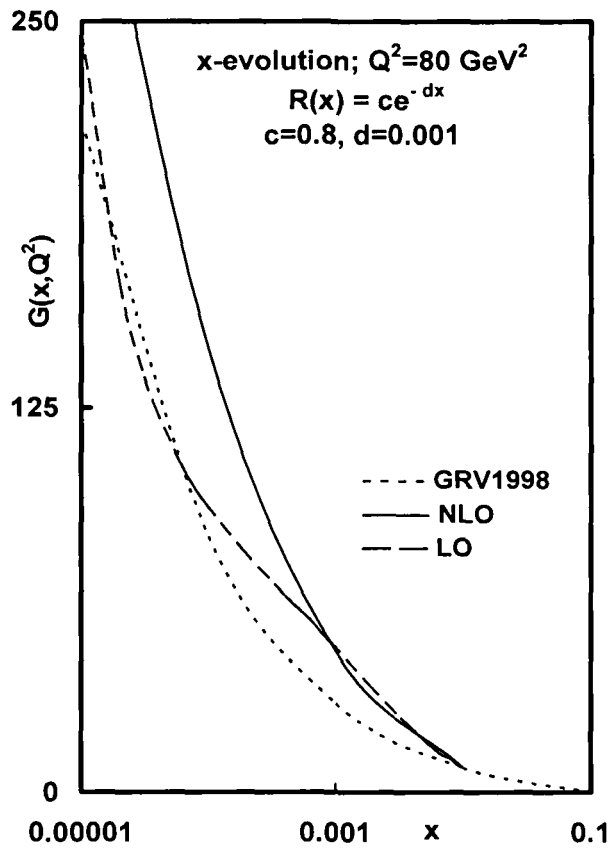
Figure 8.5: t-evolution of gluon distribution functions in NLO for  $R(x) = ax^b$ , compared with GRV1998 parameterization

In figure 8.6, we have plotted our results of  $x$ -evolution of gluon distribution function in NLO from equation (8.12) and compared with GRV1998 gluon parameterization for  $R(x) = ax^b$ . These results are also compared with our LO results. We have plotted our results for  $Q^2 = 40 \text{ GeV}^2$  and the best fit has found for  $a = 0.9$  and  $b = 0.001$  in NLO and for  $a = 0.8$  and  $b = 0.0001$  in LO.



**Figures 8.6:**  $x$ -evolution of gluon distribution functions in NLO for  $R(x) = ax^b$ , compared with GRV1998 parameterization

In figure 8.7, we have plotted our results of x-evolution of gluon distribution function in NLO from equation (8.12) and compared with GRV1998 gluon parameterization for  $R(x) = ce^{-dx}$ . These results are also compared with our LO results. We have plotted our results for  $Q^2= 80 \text{ GeV}^2$  and the best fit has found with  $c = 0.8$  and  $d = 0.001$  in both NLO and LO.



Figures 8.7: x-evolution of gluon distribution functions in NLO for  $R(x)= ce^{-dx}$ , compared with GRV1998 parameterization

In figure 8.8 we have plotted our results of gluon distribution function against  $x$  for  $Q^2=100 \text{ GeV}^2$  with  $R(x) = R$ , a constant and  $R(x) = ax^b$ , a power function of  $x$ . Our results are compared with MRST2004 as well as our LO results. The best fit has been found with  $R= 0.4$  in both NLO and LO and also with  $a = 0.5, b = 0.0001$  in NLO and  $a = 0.5, b = 0.001$  in LO respectively.

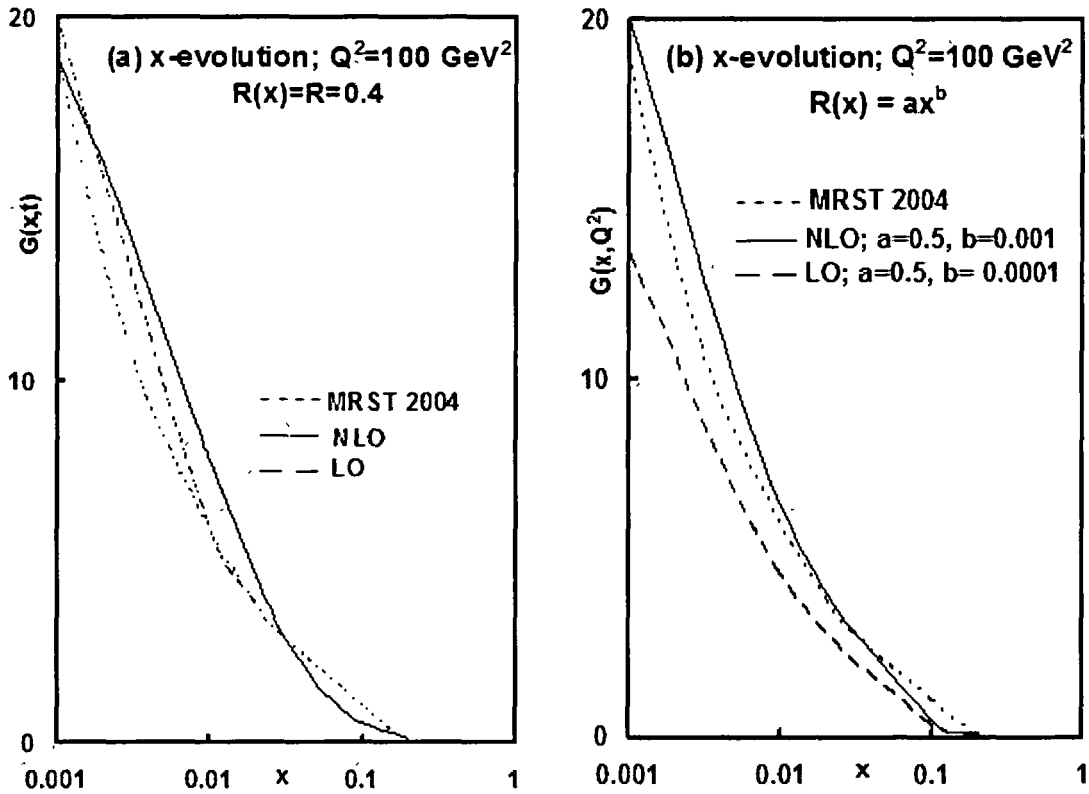


**Figure 8.8:** x-evolution of gluon distribution functions in NLO for  $R(x) = R$ , a constant and  $ax^b$ , compared with MRST2004 parameterization



### 8.3 Conclusion

In this chapter, we have solved the DGLAP evolution equation by using method of characteristics and get gluon distribution function in LO and NLO. We have calculated here the  $t$  and  $x$ -evolutions of gluon distribution functions. It is shown that our results are in good agreement with GRV1998 and MRST2004 global parameterizations especially at small- $x$  and high- $Q^2$  region. Here from global parameterizations and our results we have seen that the gluon distribution functions increase when  $x$  decreases and  $Q^2$  increases for fixed values of  $Q^2$  and  $x$  respectively. On an average, the mean percentage errors of our LO and NLO results are 7.73% and 1.86% with GRV1998 and also 11.45% and 3.63% with MRST2004 global parameterizations respectively. These errors of our results are very less as compared to systematic and statistical uncertainties in the experimental data. Thus there is significant contribution of Next-to-Leading order over the Leading order in unpolarized gluon distribution functions.  $\square$

## Polarized Gluon Distribution Functions in Leading Order and Next-to-Leading Order

Quark and gluon contributions to the nucleon spin are described by polarized parton distribution functions (polarized PDF) and their first moments. It became clear that only a small fraction of nucleon spin is carried by quarks and antiquarks. Therefore, a large gluon polarization or effect of orbital angular momenta should be possible sources for explaining the origin of the nucleon spin. Polarized PDFs have been investigated by global analyses of data on polarized lepton - nucleon DIS and proton - proton collisions [65, 165, 166, 168, 179, 187 -194]. Polarized quark distributions are determined relatively well, however the polarized gluon distribution is not accurately determined. The gluon distribution contributes to the structure function  $g_1$  as a higher order effect in the expansion by the running coupling constant  $\alpha_s$  of QCD.

In this chapter, the polarized gluon distribution functions have been obtained by solving DGLAP evolution equations in LO and NLO at the small- $x$  limit. Here we have used a Taylor's series expansion and then the method of characteristics to solve the evolution equations. We have also calculated  $t$  and  $x$ -evolutions of gluon distribution function and the results are compared with the graph obtained by B Ziaja with the help of numerical method [195]. Here the detailed phenomenological study is not possible due to shortage of experimental data of polarized gluon distribution function.

## 9.1 Theory

The DGLAP evolution equations in standard forms for polarized gluon distribution functions  $\Delta G(x, t)$ , in LO and NLO [134, 173, 180, 181] are

$$\frac{\partial \Delta G(x, t)}{\partial t} - \frac{\alpha_s}{2\pi} J_1^G(x, t) = 0, \quad (9.1)$$

$$\frac{\partial \Delta G(x, t)}{\partial t} - \frac{\alpha_s}{2\pi} J_1^G(x, t) - \left(\frac{\alpha_s}{2\pi}\right)^2 J_2^G(x, t) = 0, \quad (9.2)$$

where integrals  $J_1^G(x, t)$ ,  $J_2^G(x, t)$  are defined in Appendix G.

Let us introduce the variable  $u = 1 - \omega$  and using Taylor's expansion series we can rewrite

$$\Delta G\left(\frac{x}{\omega}, t\right) \approx \Delta G(x, t) + \frac{xu}{1-u} \frac{\partial \Delta G(x, t)}{\partial x}, \quad (9.3a)$$

$$g_1^S\left(\frac{x}{\omega}, t\right) = g_1^S(x, t) + \frac{xu}{1-u} \frac{\partial g_1^S(x, t)}{\partial x}. \quad (9.3b)$$

Using equations (9.3a) and (9.3b) and performing  $u$ -integrations we get equation (9.1) as

$$\frac{\partial \Delta G(x, t)}{\partial t} - \frac{A_f}{t} \left[ A_1'^g(x) \Delta G(x, t) + A_2'^g(x) \frac{\partial \Delta G(x, t)}{\partial x} + A_3'^g(x) g_1^S(x, t) + A_4'^g(x) \frac{\partial g_1^S(x, t)}{\partial x} \right] = 0. \quad (9.4)$$

Equation (9.4) is a partial differential equation of two variables and two functions. To convert it to one function, we have to establish a relation between them. At high- $Q^2$  and small- $x$ , we can assume that sea quarks and gluons have no clear cut distinction. Thus we can assume that  $g_1^S(x, t) = R'(x) \Delta G(x, t)$ , where  $R'(x)$  is a suitable function of  $x$  or may be a constant. Now equation (9.4) gives

$$-t \frac{\partial \Delta G(x, t)}{\partial t} + A_f L_1^g(x) \frac{\partial \Delta G(x, t)}{\partial x} + A_f M_1^g(x) \Delta G(x, t) = 0, \quad (9.5)$$

where

$$L_1^g(x) = A_2'^g(x) + R'(x) A_4'^g(x). \quad (9.6a)$$

$$M_1^{\prime g}(x) = A_1^{\prime g}(x) + R'(x)A_3^{\prime g}(x) + A_4^{\prime g}(x) \frac{\partial R'(x)}{\partial x}, \quad (9.6b)$$

To introduce the method of characteristics, let us consider two new variables  $S$  and  $\tau$  instead of  $x$  and  $t$ , such that

$$\frac{dt}{dS} = -\tau, \quad (9.7a)$$

$$\frac{dx}{dS} = A_r L_1^{\prime g}(x). \quad (9.7b)$$

Putting these in equation (9.4), we get

$$\frac{d\Delta G(x, t)}{dt} + M_1^{\prime g}(S, \tau)\Delta G(S, \tau) = 0, \quad (9.8)$$

where  $M_1^{\prime g}(S, \tau) = A_r M_1^{\prime g}(x)$ .

Equation (9.8) can be solved as

$$\Delta G(S, \tau) = \Delta G(0, \tau) \exp \left[ - \int_0^S M_1^{\prime g}(S, \tau) dS \right] \quad (9.9)$$

For  $t$ -evolution, polarized gluon distribution functions vary with  $t$ , remaining  $x$  constant. Hence equation (9.7a) can be used to solve the equation (9.8). Now we have to replace the co-ordinate system  $(S, \tau)$  to  $(x, t)$ , considering when  $S = 0$ ,  $t = t_0$  and the input function as  $\Delta G(\tau) = \Delta G(x, t_0)$ . So the  $t$ -evolution of polarized gluon distribution function in LO is given by

$$\Delta G(x, t) = \Delta G(x, t_0) \left( \frac{t}{t_0} \right)^{A_r M_1^{\prime g}(x)}. \quad (9.10)$$

Using equation (9.7b) and replacing the co-ordinate system  $(S, \tau)$  to  $(x, t)$ , with consideration when  $\tau = 0$ ,  $x = x_0$  the input function is  $\Delta G(S) = \Delta G(x_0, t)$ , we get the  $x$ -evolution of polarized gluon distribution function in LO as

$$\Delta G(x, t) = \Delta G(x_0, t) \exp \left( - \int_{x_0}^x \frac{M_1^{\prime g}(x)}{L_1^{\prime g}(x)} dx \right). \quad (9.11)$$

Considering the same procedure as in unpolarized cases, the  $t$  and  $x$ -evolution of polarized gluon distribution functions in NLO are given by

$$\Delta G(x, t) = \Delta G(x_0, t) \left( \frac{t}{t_0} \right)^{A_f \{M_1^g(x) + T_0 M_2^g(x)\}}, \quad (9.12)$$

$$\Delta G(x, t) = \Delta G(x_0, t) \exp \left( - \int_{x_0}^x \frac{M_1^g(x) + T_0 M_2^g(x)}{L_1^g(x) + T_0 L_2^g(x)} dx \right), \quad (9.13)$$

where

$$L_2^g(x) = B_2^g(x) + R'(x)B_4^g(x), \quad M_2^g(x) = B_1^g(x) + R'(x)B_3^g(x) + B_4^g(x) \frac{\partial R'(x)}{\partial x}$$

and  $\left( \frac{\alpha_s(t)}{2\pi} \right)^2 = T_0 \left( \frac{\alpha_s(t)}{2\pi} \right)$ . Here  $T_0$  is a numerical parameter, which is not

arbitrary chosen but obtained by phenomenological analysis [79, 174].

Here  $\Delta G(x_0, t)$  and  $\Delta G(x, t_0)$  are input functions. For phenomenological analysis we use equations (9.10) and (9.11) to study polarized gluon distribution functions in LO and equations (9.12) and (9.13) to study polarized gluon distribution functions in NLO.

## 9.2 Results and Discussions

In this chapter, we compare our result of  $x$  evolution of polarized gluon distribution function  $\Delta G(x, t)$  in LO and NLO with the graphs obtained by numerical method of B Ziaja [195]. Each graph of our result is the best fit graph of our works with the numerical method. Here values at  $x = 0.001$  is taken as input to test the  $x$ -evolution equations of our results. We compared our results for  $R'(x) = R', ax^b$  and  $ce^{-\square dx}$ , where  $R', a, b, c$  and  $d$  are constants. In all figures, we have plotted computed values of polarized gluon distribution function  $\Delta G(x, t)$  against the  $x$  values for a fixed  $Q^2$  qualitatively. Here we have plotted the graphs for  $Q^2 = 10 \text{ GeV}^2$  in the range of  $0.001 \leq x \leq 0.00001$ . In all graphs, solid lines represent our NLO results, dash lines represent our LO results of best fitted graphs and numerical methods are represented by the dotted lines. Since experimental data as well as parameterization results on  $t$ -evolution of

polarized gluon distribution function is not found elsewhere, so we could not compare our t-evolution results here.

As value of  $T_0$  has obtained in chapter 4 and chapter 7, here it is not shown. But same value,  $T_0 = 0.048$ , is considered here. In figure 9.1, we have plotted our results for LO and NLO considering  $R'(x) = R'$ , a constant. It is found that best fit results are for  $R' = 0.8$  in both LO and NLO.

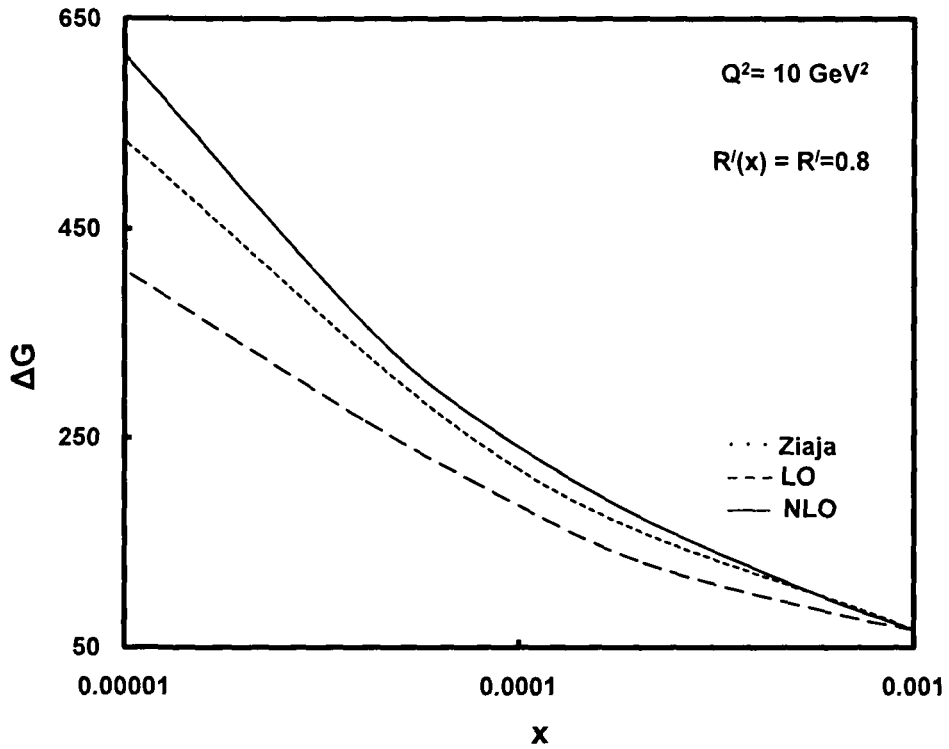


**Figure 9.1:**  $x$ -evolution of polarized gluon distribution functions in LO and NLO with  $R'(x) = R'$ , compared with the graph obtained by numerical method

In figure 9.2, we have plotted our results for  $R'(x) = ax^b$ , a power function of  $x$ . It is found that best fit results are for  $a = 0.01$  and  $b = 0.002$  in both LO and NLO.

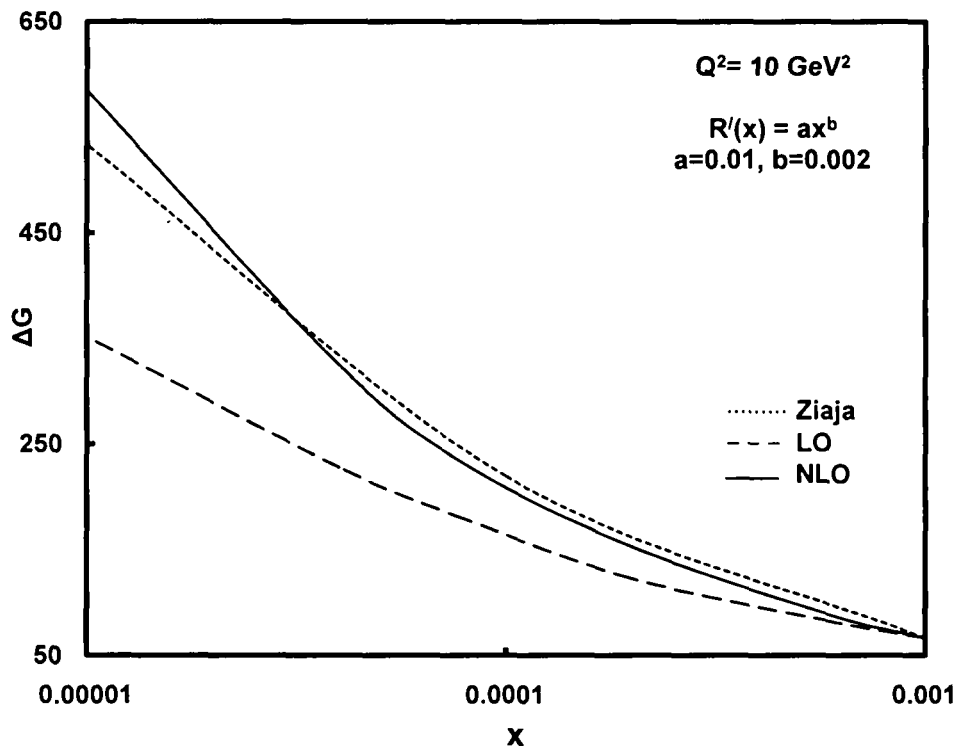


**Figure 9.2:**  $x$ -evolution of polarized gluon distribution functions in LO and NLO with  $R'(x) = ax^b$ , compared with the graph obtained by numerical method

In figure 9.3, we have plotted our results for  $R'(x) = ce^{-dx}$ , an exponential function of  $x$ . It is found that our best fit results are for  $c = 0.2$  and  $d = 0.03$  in both LO and NLO.

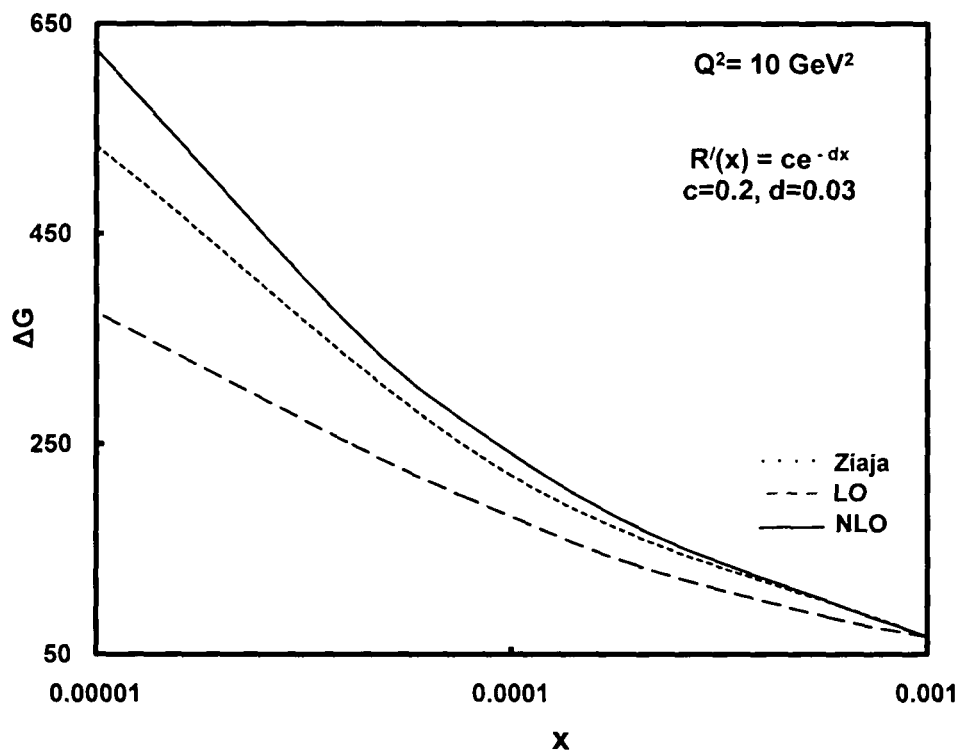


**Figure 9.3:**  $x$ -evolution of polarized gluon distribution functions in LO and NLO with  $R'(x) = ce^{-dx}$ , compared with the graph obtained by numerical method



### 9.3 Conclusion

In this chapter, we have solved DGLAP evolution equations for polarized gluon distribution function in LO and NLO using method of characteristics. Experimental data on t-evolution of polarized gluon distribution function is not found elsewhere. Thus we could not compare our t-evolution results of polarized gluon distribution function. Our x-evolution graphs for polarized gluon distribution functions in both LO and NLO are compared are in good consistency with the results obtained by solving unified evolution equation by numerical method especially at small-x and high- $Q^2$  region. The mean percentage error of our LO and NLO results are 11.47% and 5.81% with data obtained from numerical method. Thus the NLO shows significantly better fitting to the data sets obtained by numerical method than that of in LO and hence the NLO corrections have significant effect and we cannot ignore the contribution of NLO terms in high- $Q^2$  and small-x region. The polarized gluon contribution, which is largely responsible for scaling violations, appears to be positive, although quite poorly determined at this time. A major motivation for future high-energy polarized scattering experiments is to obtain more information on the polarized gluon contributions to the nucleon spin.  $\square$

# Conclusion

*"Errors are not in the art but in the artificers"*

– *Newton*

---

## Conclusion

In this thesis, we solved unpolarized DGLAP evolution equations up to NNLO and polarized DGLAP evolution equations up to NLO by applying first Taylor's expansion and then Method of Characteristics, and obtained unique solutions for both unpolarized and polarized singlet, non-singlet structure functions and gluon distribution functions in the small- $x$  and high- $Q^2$  region. We derived  $t$  and  $x$ -evolutions of singlet (deuteron), non-singlet (combination of proton and neutron or proton and deuteron) and gluon distribution functions and compared them with experimental data sets, parameterizations and result from numerical method with satisfactory phenomenological success. In all the results, from experiments, global fits or numerical method, it is seen that all the mentioned structure functions increase when  $x$  decreases for fixed values of  $Q^2$  and when  $Q^2$  increases for fixed values of  $x$ .

We have seen that our results of unpolarized deuteron and non-singlet structure functions are in good agreement with NMC, E665, CLAS collaboration and NNPDF collaborations data sets and the results of unpolarized gluon distribution function are in good agreement with MRST2004 and GRV1998 global parameterizations. Results of polarized structure functions are also in good agreement with SLAC E143, SMC and COMPASS collaboration data sets and with the graph obtained by solving unified evolution equation by numerical method especially at small- $x$  and high- $Q^2$  region. Again from our results of the best fitted graphs, it is clear that the singlet and non-singlet structure functions as well as gluon distribution functions in NLO show significantly better fitting to the experimental and parameterization data than that of in LO. So, the higher order term in NLO has appreciable contribution in the small- $x$  region to the parton distribution functions. In Chapter 5, we have

seen that  $T_1$  is much smaller than  $T_0$ , so, we expect NNLO contributions to the DGLAP evolution equations should be small. But from the comparison of  $t$  and  $x$ -evolution graphs of our results for LO, NLO and NNLO, it is seen that NNLO corrections have significant effect. This indicates that we should not ignore the contribution of NNLO terms in our region of small- $x$  and high- $Q^2$ . We speculate that contributions from higher and higher orders to the DGLAP evolution equations will be smaller and smaller and ultimately leading to insignificant effect to the structure functions. Though we have considered some parameters like  $k(x)$ ,  $T_0$  and  $T_1$  etc., but since the numbers of assumed parameters are less. For simplified solutions of DGLAP evolution equations we have considered numerical variables  $T_0$  and  $T_1$ , not arbitrarily. The values are chosen such that differences between  $T^2(t)$  and  $T_0 T(t)$ , and also  $T^3(t)$  and  $T_1 T(t)$  are negligible.

Thus we can conclude that though there are various methods to solve DGLAP evolution equation to calculate quark structure functions and gluon distribution functions, the Method of characteristics is also a viable alternative. Though mathematically vigorous, it changes the integro-differential equations into ordinary differential equations and then makes it possible to obtain unique solutions.

As the future directives, to obtain completely unique solutions, we can try to solve coupled evolution equations both for singlet structure functions and gluon distribution functions. We can also try to solve the equations in higher and higher orders to have more precise results if and when relevant kernels are available. Non-perturbative low- $Q^2$  sector is also an area of future study, though some work has been going on at present also [196]. At higher energy,  $x$  values are still smaller and number of partons increases more. So, hadrons can be considered as some statistical systems. Studies on structure functions considering this model are going on [197, 198, 199] and we can give more importance on them. Lastly at small- $x$ , recombination among partons may be considered a dominating factor. Study on evolution equations and structure functions considering this effect is also an important subject at present and future.  $\square$

## Bibliography

- [1]. Hakim, J. *The Story of Science : Aristotle Leads the Way* (Smithsonian Books, 2004)
- [2]. Griffiths, D. *Introduction to Elementary Particles* (John Wiley & Sons, New York, 1987)
- [3]. Levin, V. E. *Nuclear Physics and Nuclear Reactors* (MIR Publishers, Moscow, 1981)
- [4]. Kopylov, G. I. *Elementary Kinematics of Elementary Particles* (Mir Publishers, Moscow, 1983)
- [5]. Collins, P. D. B., Martin, A. D. and Dalitz, R. H. *Hadron Interactions* (Adam Hilger Ltd., Bristol, 1984)
- [6]. Sutton, C. *Elementary Particles* (Encyclopedia Britannica, 2001)
- [7]. *Elementary Particles* (Encyclopedia, Microsoft Encarta 1993- 2001, 2001)
- [8]. Watson, A. *The Quantum Quark* (Cambridge University Press, 2004)
- [9]. Amsler, C. *et al* (Particle Data Group) Review of Particle Physics Quarks, *Physics Letters B* **667** (1), 1-1340 (2008).
- [10]. Weise, W. and Green, A. M. *Quarks and Nuclei* (World Scientific, 1984)
- [11]. Franzini, P. *Elementary Particle Physics* (Lecture Notes, University of Rome, Spring 2002)
- [12]. Englert, F. and Brout, R. *Phys Rev Lett* **13**, 321 (1964)
- [13]. P Higgs, P. *Phys Rev Lett* **13**, 508 (1964)
- [14]. Guralnik, G., Hagen, C. R. and Kibble, T. W. B. *Phys Rev Lett* **13**, 585 (1964)
- [15]. Guralnik, G. *Inter J of Modern Phys A* **24**, 2601 (2009)
- [16]. <http://prl.aps.org/50years/milestones#1964>

- 
- [17]. Greiner, W., Schramm, S. and Stein, E. *Quantum Chromodynamics* (Springer-Verlag New York, 1994)
- [18]. Taylor, R. E. *Proceedings of International Symposium on electron and Photon Interactions at High Energies* (SLAC, Stanford, 1967)
- [19]. Halzen, F and Martin, A. D. *Quarks and Lepton, An Introductory Course in Modern Particle Physics* (John Wiley and Sons, New York, 1990)
- [20]. Griffiths, D. *Introduction to Elementary Particles* (John Wiley & Sons, New York, 1987)
- [21]. Collins, P. D. B., Martin, A. D. and Dalitz, R. H. *Hadron Interactions* (Adam Hilger Ltd, Bristol, 1984)
- [22]. Leader, E. *Spin in Particle Physics* (Cambridge University Press, 2001)
- [23]. E-155 Collab, Anthony, P. L. *et al*, *SLAC - PUB 8813*, (2002)
- [24]. Igo, G. *Phys Rev D* **63**, 057501 (2001)
- [25]. Gribov, V. N. and Lipatov, L. N. *Soviet J Nucl Phys* **15**, 438 (1972)
- [26]. Lipatov, L. N. *Soviet J Nucl Phys* **20**, 95 (1975)
- [27]. Dokshitzer, Y. *Soviet Phys JETP* **46**, 641 (1977)
- [28]. Altarelli, G. and Parisi, G. *Nucl Phys B* **126**, 298 (1977)
- [29]. Kuraev, E. A., Lipatov, L. N. and Fadin, V. S. *Sov Phys JETP* **44**, 443 (1976)
- [30]. Kuraev, E. A., Lipatov, L. N. and Fadin, V. S. *Sov Phys JETP* **45**, 199 (1977)
- [31]. Balitski, Y. Y. and Lipatov, L. N. *Soviet J Nucl Phys* **28**, 822 (1978)
- [32]. Gribov, L. V., Levin, E. M. and Ryskin, M. G. *Nucl Phys B* **188**, 555 (1981)
- [33]. Gribov, L. V., Levin, E. M. and Ryskin, M. G. *Zh Eksp Theo Fiz* **80**, 2132 (1981); *Soviet Phys JETP* **53**, 1113 (1981)
- [34]. Gribov, L. V., Levin, E. M. and Ryskin, M. G. *Phys Rep* **1009**, 1 (1983)
- [35]. Ciafaloni, M. *Nucl Phys B* **296**, 49 (1988)
- [36]. Catani, S., Fiorani F. and Marchesini, G. *Phys Lett B* **234**, 339 (1990)
- [37]. Catani, S., Fiorani F. and Marchesini, G. *Nucl Phys B* **336**, 18 (1990)
- [38]. Marchesini, G. *Nucl Phys B* **445**, 49 (1995)
-

- 
- [39]. Mueller, A. H. and Qiu, J. *Nucl Phys B* **268**, 427 (1986)
- [40]. Qiu, J. *Nucl Phys B* **291**, 746 (1987)
- [41]. Miyama, M. and Kumano, S. *Comput Phys Commun* **94**, 185 (1996)
- [42]. Zhu, W. *Nucl Phys B* **551**, 245 (1999)
- [43]. Zhu W. and Ruan, J. *Nucl Phys B* **559**, 378 (1999)
- [44]. Balitsky, I. I. *Phys Rev Lett* **81**, 2024 (1998); *Phys Rev D* **60**, 014020 (1999)
- [45]. Kovchegov, Yu V. *Phys Rev D* **60**, 034008 (1999)
- [46]. Marian, J. J., Kovner, A. and Weigert, H. *Phys Rev D* **59**, 014015 (1999)
- [47]. Weigert, H. *Nucl Phys A* **703**, 823 (2002)
- [48]. Balitsky, I. I. *Nucl Phys B* **463**, 99 (1996)
- [49]. Ruan, J., Shen, Z., Yang J. and Zhu, W. *Nuclear Physics B* **760**, 128 (2007)
- [50]. Gell-Mann, M. *Phys Lett* **8**, 214 (1964)
- [51]. Weinberg, S. *Phys Rev Lett* **31**, 494 (1973)
- [52]. Gross, D. J. and Wilczek, F. *Phys Rev D* **8**, 3633 (1973)
- [53]. H1 Collab, Adloff, C. *et al.* *Eur Phys J C* **21**, 33 (2001)
- [54]. ZEUS Collab, Chekanov, S. *et al.* *Eur Phys J C* **21**, 443 (2001)
- [55]. Bjorken, J.D. and Paschos, E. A. *Phys Rev* **185**, 1975 (1969)
- [56]. Martin, A. D., Roberts, M. G., Stirling, W. J. and Throne, R. S. *Eur Phys J C* **23**, 73 (2002)
- [57]. Vogt, A. *Comput Phys Commun* **170**, 65 (2005)
- [58]. Botje, M. *Eur Phys J C* **14**, 285 (2000)
- [59]. Cafarella, A., Coriano, C. and Guzzi, M. *Comput Phys Commun* **179**, 665 (2008)
- [60]. Salam, G. P. and Rojo, J. *Comput Phys Commun* **180**, 120 (2009)
- [61]. Cabibbo, N. and Petronzio, R. *Nucl Phys B* **137**, 395 (1978)
- [62]. Toldra, R. *Comput Phys Commun* **143**, 287 (2002)
- [63]. Kobayashi, R., Konuma, M. and Kumano, S. *Comput Phys Commun* **86**, 264 (1995)
- [64]. Gluck, M., Reya, E. and Vogt, A. *Z Phys C* **48**, 471 (1990)
- [65]. Gluck, M., Reya, E., Stratmann, M. and Vogelsang, W. *Phys Rev D* **63**, 094005 (2001)
-

- [66]. Blumlein, J. and Bottcher, H. *Nucl Phys B* **636**, 225 (2002)
- [67]. Santorelli, P. and Scrimieri, E. *Phys Lett B* **459**, 599 (1999)
- [68]. Ratcliffe, P. G. *Phys Rev D* **63**, 116004 (2001)
- [69]. Narayan, S. *A Course of Mathematical Analysis* (S Chand & Company Pvt. Ltd., New Delhi, 1987)
- [70]. Sharma J. N. and Vasishtha, A. R. *Mathematical Analysis-II* (Krishna Prakashan Mandir, Meerut, 1990)
- [71]. Spiegel, M. R. *Advanced Calculus* (Schaum's Outline Series, McGraw-Hill, 1962)
- [72]. Raisnghania, M. D. *Advanced Differential Equations* (S Chand & Company Ltd., New Delhi, 1991)
- [73]. Ayres, F. Jr *Differential Equations* (Schaum's Outline Series, McGraw-Hill, 1988)
- [74]. Miller, F. H. *Partial Differential Equation* (John and Willey, 1960)
- [75]. Sneddon, I. *Elements of Partial Differential Equations* (Mc Graw Hill, New York, 1957).
- [76]. Collins, P. D. B. *An introduction to Regge Theory and High Energy Physics* (Cambridge University Press, 1977)
- [77]. Farlow, S. J. *Partial Differential Equation for Scientist and Engineers* (John Willey, 1982)
- [78]. Choudhury, D. K. and Saharia, P. K. *Pramana J Phys* **58**, 599 (2002)
- [79]. Baishya, R. and Sarma, J. K. *Phys Rev D* **74**, 107702 (2006)
- [80]. Abbott, L. F., Atwood, W. B. and Barnett, R. M. *Phys Rev D* **22**, 582 (1980)
- [81]. Altarelli, G. *Phys Rep* **18**, 1 (1981)
- [82]. Choudhury, D. K., Sarma, J. K. and Medhi, G. K. *Phys Lett B* **403**, 139 (1997)
- [83]. Choudhury, D. K. and Sarma, J. K. *Pramana J Phys* **38**, 481 (1997)
- [84]. Rajkhowa, R. and Sarma, J. K. *Indian J Phys* **78**, 9 979 (2004); *Indian J Phys* **79**, 1 55 (2005)



- 
- [85]. Choudhury, D. K., Sarma, J. K. and Medhi, G. K. Gauhati University Journal of Science, Golden Jubilee volume, 39 (1998); Sarma, J. K. and Das, B. *Phys Lett B* **304**, 323 (1993)
- [86]. Soyez, G. *Phys Rev D* **69**, 096005 (2004); *hep-ph/0401177* (2004)
- [87]. Donnachie, A. and Landshoff, P. V. *Phys Lett B* **533**, 277 (2002); *Phys Lett B* **550**, 160 (2002)
- [88]. Fadin, V. S., Fiore, R., Kozlov, M. G. and Reznichenko, A. V. *Phys Lett B* **639**, 74 (2006) [*arXiv:hep-ph/0602006* (2006)] ; Fadin, V. S., Fiore, R. *Phys Rev D* **64**, 114012 (2001)
- [89]. Sarma, J. K. And Medhi, G. K. *Eur Phys J C* **16**, 481 (2000)
- [90]. Jamil, U. and Sarma, J. K. *IJAMES* **2**, 69 (2008)
- [91]. Jamil, U. and Sarma, J. K. *Pramana, J Phys* **69**, 167 (2007)
- [92]. Saikia, A. *Pramana, J Phys* **48**, 1 (1997)
- [93]. Kotikov, V. and Parente, G. *Phys Lett B* **379**, 195 (1996)
- [94]. Donnachie, A. and Landshoff, P. V. *Phys Lett B* **437**, 408 (1998)
- [95]. Gayler, J. *arXiv:hep-ph/0206062* (2002)
- [96]. Badelek, B. *Acta Phys Pol B* **34**, 2943 (2003)
- [97]. Soffer, J. and Teryaev, O. V. *Phys Rev D* **56**, 1549 (1997)
- [98]. Desgrolard, P., Lengyel, A. and Martynov, E. *arXiv:hep-ph/0110149* (2001)
- [99]. Kentzer, C. P. *Reformulation of the method of characteristics for multidimensional flows* ( Springer Berlin, Heidelberg, 2006)
- [100]. Ball, R. D. and Forte, S. *Phys Lett B*, **335**, 77 (1994); *Phys Lett B* **336**, 77 (1994)
- [101]. Kotikov, A. V. and Parente, G. *Nucl Phys B* **549**, 242 (1999)
- [102]. Gehrmann, T. and Stirling, W. J. *Phys Lett B* **365**, 267 (1996)
- [103]. Forte, S. and Ball, R. D. *Acta Phys. Pol. B* **26**, 2087 (1995)
- [104]. Mankiewick, L., Saalfeld, A. and Weigl, T. *Phys Lett B* **393**, 175 (1997)
- [105]. Deka, R. and Choudhury, D. K. *Z Phys C* **75**, 679 (1997)
- [106]. Toldra, R. *Comput Phys Commun* **143**, 287 (2002)
- [107]. Stecker, F. W. *J Phys G* **29**, R47 (2003)

- 
- [108]. Sarkar, S. and Toldra, R. *Nucl Phys B* **621**, 495 (2002)
- [109]. Neerven, W. L. van and Vogt, A. *Nucl Phys B* **588**, 345 (2000); *Nucl Phys B* **568**, 263 (2000); *Phys Lett B* **490**, 111 (2000)
- [110]. Moch, S., Vermaseren, J. A. M. and Vogt, A. *Nucl Phys Proc Suppl* **116**, 100 (2003); *Nucl Phys B* **688**, 101 (2004)
- [111]. Moch, S. Vermaseren, J. A. M. *Nucl Phys B* **573**, 853 (2000)
- [112]. Cafarella, A., Coriano, C. and Guzzi, M. *Nucl Phys B* **748**, 253 (2006); *JHEP* **08**, 030 (2007)
- [113]. Arneodo, M. *et al.* CERN-NA-037, NMC, *Nucl Phys B* **483**, 3 (1997)
- [114]. E-665 Collab, Adams, M. R. *et al*, *Phys Rev D* **54**, 3006 (1996)
- [115]. CLAS Collaboration, Osipenka, *et al.* *Phys Rev C* **73**, 045205 (2006)
- [116]. <http://durpdg.dur.ac.uk/hepdata/online/f2/structindex.html>
- [117]. <http://www.sofia.ecm.ub.es/f2neural>
- [118]. Forte, S., Garrido, L., Latorre, J. I. and Piccione, A. *JHEP* **05**, 065 (2002)
- [119]. NNPDF Collaboration; Debbio, L. D. *et al.* *JHEP* **03**, 080 (2005)
- [120]. BCDMS Collaboration; *Phys. Lett. B* **237**, 592 (1990)
- [121]. Furmanski, W. and Petronzio, R. *Phys Lett B* **97**, 437 (1980)
- [122]. Furmanski, W. and Petronzio, R. *Nucl Phys B* **195**, 237 (1982)
- [123]. Furmanski, W. and Petronzio, R. *Z Phys C* **11**, 293 (1982)
- [124]. Baishya, R. and Sarma, J. K. *Indian J Phys* **83**, 1333 (2009)
- [125]. Baishya, R. and Sarma, J. K. *Eur J Phys C* **60**, 4 (2009)
- [126]. Neerven, W. L. van and Vogt, A. *Nucl Phys B* **588**, 345 (2000)
- [127]. Neerven, W. L. van and Vogt, A. *Nucl Phys B* **568**, 263 (2000)
- [128]. Neerven, W. L. van and Vogt, A. *Phys Lett B* **490**, 111 (2000)
- [129]. Moch, S., Vermaseren, J. A. M. and Vogt, A. *Nucl Phys Proc Suppl* **116**, 100 (2003)
- [130]. Moch, S. and Vermaseren, J. A. M. *Nucl Phys B* **573**, 853 (2000)
- [131]. Moch, S. and Vogt, A. *Nucl Phys Proc Sup* **116**, 100 (2003)
- [132]. Moch, S., Vermaseren, J. A. M. and Vogt, A. *Nucl Phys B* **688**, 101 (2004)
- [133]. Vogt, A, Moch, S. and Vermaseren, J. A. M. *Nucl Phys B* **691**, 1129 (2004)
- [134]. Glück, M., Reya, E. and Schuck, C. *Nucl Phys B* **754**, 178 (2006)
-

- [135]. Cafarella, A., Corianò, C. and Guzi, M. *Nucl Phys B* **748**, 253 (2006)
- [136]. E143 Collab, Abe, K. *et al. Phys Rev D* **58**, 112003 (1998)
- [137]. SM Collab, Adeva, B. *et al. Phys Rev D* **58**, 112001 (1998)
- [138]. E154 Collab, Abe, K. *et al. Phys Lett B* **405**, 180 (1997)
- [139]. E154 Collab, Abe, K. *et al. Phys Rev Lett* **79**, 26 (1997)
- [140]. HERMES Collab, Ackersta, K. *et al. Phys Lett B* **404**, 383 (1997)
- [141]. HERMES Collab, Airapetian, A. *et al. Phys Lett B* **442**, 484 (1998)
- [142]. Bultmann, S. *et al. Report SLAC-PUB-7904* (August 1998)
- [143]. E155 Collaboration, Anthony, P. L. *et al. Phys Lett B* **463**, 339 (1999)
- [144]. Hoodbhoy, P. *et al. Nucl Phys B* **312**, 571 (1989); Jaffe, R.L. *Comments Nucl Part Phys* **19**, 239 (1990)
- [145]. Hirai, M., Kumano, S. and Myiama, *Comput Phys Comm* **108**, 38 (1998); Altarelli, G., Ball, R. D. and Forte, S. *Nucl Phys B* **575**, 313 (2000)
- [146]. COMPASS Collaboration; Ageev, E. S. *et al. Phys Lett B* **612**, 154 (2005)
- [147]. COMPASS Collaboration; Alexakhin, V. Yu. *et al. Phys Lett B* **647**, 8 (2007)
- [148]. H1 Collab, Adloff, C. *et al. Nucl Phys B* **497**, 3 (1997)
- [149]. Alguard, M. J. *et al. Phys Rev Lett* **37**, 1261 (1976)
- [150]. Alguard, M. J. *et al. Phys Rev Lett* **41**, 70 (1978)
- [151]. Baum, G. *et al. Phys Rev Lett* **45**, 2000 (1980)
- [152]. E142 Collab, Anthony, P. L. *et al. Phys Rev Lett* **71**, 959 (1993)
- [153]. E143 Collab, Abe, K. *et al. Phys Rev Lett* **74**, 346 (1995)
- [154]. E143 Collab, Abe, K. *et al. Phys Rev Lett* **75**, 25 (1995)
- [155]. E143 Collab, Abe, K. *et al. Phys Lett B* **364**, 61 (1995)
- [156]. E155 Collab, Anthony, P. L. *et al. Phys Lett B* **493**, 19 (2000)
- [157]. EM Collab, Ashman, J. *et al. Phys Lett B* **206**, 364 (1988)
- [158]. EM Collab, Ashman, J. *et al. Nucl Phys B* **328**, 1 (1989)
- [159]. SM Collab, Adeva, B. *et al. Phys Lett B* **302**, 533 (1993)
- [160]. SM Collab, Adams, D. *et al. Phys Lett B* **329**, 399 (1994)
- [161]. SM Collab, Adams, D. *et al. Phys Lett B* **357**, 248 (1995)
- [162]. SM Collab, Adeva, B. *et al. Phys Lett B* **412**, 414 (1997)

- [163]. SM Collab, Adams, D. *et al.* *Phys Rev D* **56**, 5330 (1997)
- [164]. SM Collab, Adams, D. *et al.* *Phys Lett B* **396**, 338 (1997)
- [165]. Gehrman, T. and Stirling, W. J. *Phys Rev D* **53**, 6100 (1996)
- [166]. Altarelli, G., Ball, R. D., Forte, S. and Ridolfi, G. *Nucl Phys B* **496**, 337 (1997)
- [167]. Altarelli, G., Ball, R. D., Forte, S. and Ridolfi, G. *Acta Phys Pol B* **29**, 1145 (1998)
- [168]. SM Collab, Adeva, B. *et al.* *Phys Rev D* **58**, 112002 (1998)
- [169]. Ghosh, D. K., Gupta, S. and Indumath, D. *Phys Rev D* **62**, 094012 (2000)
- [170]. Tatur, S., Bartelski, J. and Kurzela, M. *Acta Phys Pol B* **31**, 647 (2000)
- [171]. Tatur, S. and Bartelski, J. *Acta Phys Pol B* **32**, 2101 (2001)
- [172]. Bartelski, J. and Tatur, S. *Phys Rev D* **65**, 034002 (2002)
- [173]. Shah, N. H. and Sarma, J. K. *Phys Rev D* **77**, 074023 (2008)
- [174]. Baishya, R., Jamil, U. and Sarma, J. K. *Phys Rev D* **79**, 034030 (2009)
- [175]. HERMES Collab, Ackerstaff, K. *et al.* *Phys Lett B* **464**, 123 (1999)
- [176]. HERMES Collab, Airapetian, A. *et al.* *Phys Rev Lett* **84**, 2584 (2000)
- [177]. Gluck, M., Reya, E. and Vogt, A. *Z Phys C* **67**, 433 (1995); *Eur Phys J C* **5**, 461 (1998)
- [178]. Martin, A. D., Ryskin, M. G. and Watt, G. *Phys Rev D* **70**, 091502 (2004)
- [179]. Hirai, M., Kumano, I. S. and Saito, N. *Phys Rev D* **74**, 014015 (2006)
- [180]. Choudhury, D. K. and Saharia, P. K. *Pramana J Phys* **60**, 563 (2003)
- [181]. Choudhury, D. K. and Saharia, P. K. *Pramana J Phys* **65**, 193 (2005)
- [182]. H1 Collab, Aid, S. *et al.* *Nucl Phys B* **470**, 3 (1996)
- [183]. ZEUS Collab, Derrick, M. *et al.* *Z Phys C* **69**, 607 (1996)
- [184]. Whitlow, L. W. *et al.* *Phys Lett B* **282**, 475 (1992)
- [185]. BCDMS Collab, Benvenuti, A. C. *et al.* *Phys Lett B* **223**, 485 (1989)
- [186]. CDF Collab, Affolder, T. *et al.* *Phys Rev D* **64**, 032001 (2001)
- [187]. Gordon, L. E., Goshtasbpour, M. and Ramsey, G. P. *Phys Rev D* **58**, 094017 (1998)
- [188]. Florian, D. de, Navarro, G. A. and Sassot, R. *Phys Rev D* **71**, 094018 (2005)

- [189]. Bourrely, C., Soffer, J. and Buccella, F. *Eur J Phys C* **41**, 327 (2005)
- [190]. Blumlein, J. and Bottcher, H. *Nucl Phys B* **636**, 225 (2002)
- [191]. Leader, E., Sidorov, A. V. and Stamenov, D. B. *Phys Rev D* **73**, 034023 (2006); *Phys Rev D* **75**, 074027 (2007)
- [192]. AA Collab, Goto, Y. *et al.* *Phys Rev D* **62**, 034017 (2000)
- [193]. AA Collab, Hirai, M., Kumano, S. and Saito, N. *Phys Rev D* **69**, 054021 (2004)
- [194]. Florian, D. de, Sassot, R. Stratmann, M. and Vogelsang, W. *Phys Rev Lett* **101**, 072001 (2008)
- [195]. Ziaja, B. *Eur J Phys C* **28**, 475 (2003); *Acta Phys Polon B* **34**, 3013 (2003)
- [196]. Dasgupta, M., Magnea, L. and Salam, G. *JHEP* **0802**, 055 (2008); *arXiv:hep-ph/0805.2267* (2008)
- [197]. Trevisan, L. A., Frederico, T. and Tomio, L. *Eur Phys J C* **11**, 351 (1999)
- [198]. Trevisan, L. A., Mirez, C., Frederico, T. and Tomio, L. *Eur Phys J C* **56**, 221 (2008)
- [199]. Bhalerao, R. S. *Phys Lett. B* **380**, 1 (1996)

# *Appendices*

*“One must divide one’s time between politics and equations. But our equations are much more important to me”*

*– Einstein*

## I. Appendix A

Functions for unpolarized DGLAP evolution equation in LO are

$$I_1^S(x, t) = 2 \int_x^1 \frac{d\omega}{1-\omega} \left[ (1+\omega^2) F_2^S\left(\frac{x}{\omega}, t\right) - 2F_2^S(x, t) \right]$$

$$I_2^S(x, t) = 2N_f \int_x^1 \left\{ \omega^2 + (1-\omega)^2 \right\} G\left(\frac{x}{\omega}, t\right) d\omega$$

$$I_1^{NS}(x, t) = 2 \int_x^1 \frac{d\omega}{1-\omega} \left[ (1+\omega^2) F_2^{NS}\left(\frac{x}{\omega}, t\right) - 2F_2^{NS}(x, t) \right]$$

## II. Appendix B

Functions for unpolarized DGLAP evolution equation in NLO are

$$I_3^S = \left[ (x-1)F_2^S(x, t) \int_0^1 f(\omega) d\omega + \int_x^1 f(\omega) F_2^S\left(\frac{x}{\omega}, t\right) d\omega + \int_x^1 F_{qq}^S(\omega) F_2^S\left(\frac{x}{\omega}, t\right) d\omega + \int_x^1 F_{qg}^S(\omega) G\left(\frac{x}{\omega}, t\right) d\omega \right]$$

$$I_2^{NS} = \left[ (x-1)F_2^{NS}(x, t) \int_0^1 f(\omega) d\omega + \int_x^1 f(\omega) F_2^{NS}\left(\frac{x}{\omega}, t\right) d\omega \right]$$

$$\text{with } f(\omega) = C_F^2 [P_F(\omega) - P_A(\omega)] + \frac{1}{2} C_F C_A [P_G + P_A(\omega)] + C_F T_R N_f P_{N_f}(\omega),$$

$$F_{qq}^S(\omega) = 2C_F T_R N_f F_{qq}(\omega),$$

$$F_{qg}^S(\omega) = C_F T_R N_f F_{qg}^I(\omega) + C_G T_R N_f F_{qg}^2(\omega),$$

$$P_F(\omega) = -\frac{2(1+\omega^2)}{(1-\omega)} \ln(\omega) \ln(1-\omega) - \left( \frac{3}{1-\omega} + 2\omega \right) \ln \omega - \frac{1}{2} (1+\omega) \ln \omega + 5(1-\omega),$$

$$P_G(\omega) = \frac{(1+\omega^2)}{(1-\omega)} \left( \ln^2(\omega) + \frac{11}{3} \ln(\omega) + \frac{67}{9} - \frac{\pi^2}{3} \right) + 2(1+\omega) \ln \omega + \frac{40}{3} (1-\omega),$$

$$P_{N_f}(\omega) = \frac{2}{3} \left[ \frac{1+\omega^2}{1-\omega} \left( -\ln \omega - \frac{5}{3} \right) - 2(1-\omega) \right],$$

$$P_A(\omega) = \frac{2(1+\omega^2)}{(1+\omega)} \int_{\frac{\omega}{1+\omega}}^{\frac{1}{1+\omega}} \frac{dk}{k} \ln\left(\frac{1-k}{k}\right) + 2(1+\omega) \ln(\omega) + 4(1-\omega),$$

$$F_{\text{qg}}^1(\omega) = 4 - 9\omega - (1 - 4\omega)\ln\omega - (1 - 2\omega)\ln^2(\omega) + 4\ln(1 - \omega) \\ + \left[ 2\ln^2\left(\frac{1-\omega}{\omega}\right) - 4\ln\left(\frac{1-\omega}{\omega}\right) - \frac{2}{3}\pi^2 + 10 \right] P_{\text{qg}}(\omega),$$

$$F_{\text{qg}}^2(\omega) = \frac{182}{9} + \frac{14}{9}\omega + \frac{40}{9\omega} + \left(\frac{136}{3}\omega - \frac{38}{3}\right)\ln\omega - 4\ln(1 - \omega) - (2 + 8\omega)\ln^2\omega$$

$$+ \left[ -\ln^2\omega + \frac{44}{3}\ln\omega - 2\ln^2(1 - \omega) + 4\ln(1 - \omega) + \frac{\pi^2}{3} - \frac{218}{3} \right] P_{\text{qg}}(\omega) + 2P_{\text{qg}}(-\omega) \int_{\left(\frac{\omega}{1+\omega}\right)}^{\left(\frac{1}{1+\omega}\right)} \frac{dz}{z} \ln \frac{1-z}{z}$$

### III. Appendix C

Functions for unpolarized DGLAP evolution equation in NNLO are

$$I_4^S(x, t) = \int_x^1 \frac{d\omega}{\omega} \left[ P_{\text{qq}}^{(2)}(x) F_2^{\text{NS}}\left(\frac{x}{\omega}, t\right) + P_{\text{qg}}(x) G\left(\frac{x}{\omega}, t\right) \right]$$

$$I_3^{\text{NS}}(x, t) = \int_x^1 \frac{d\omega}{\omega} \left[ P_{\text{NS}}^{(2)}(x) F_2^{\text{NS}}\left(\frac{x}{\omega}, t\right) \right]$$

where

$$P_{\text{NS}}^{(2)}(x, t) = n_f \left\{ \left[ L_1(-163.9x^{-1} - 7.208x) + 151.49 + 44.51x - 43.12x^2 + 4.82x^3 \right] (1-x) \right. \\ \left. + L_0 L_1(-173.1 + 46.18L_0) + 178.04L_0 + 6.892L_0^2 + \frac{40}{27}(L_0^4 - 2L_0^3) \right\},$$

$$P_{\text{PS}}^{(2)}(x) \cong \left\{ \begin{array}{l} \left[ \begin{array}{l} -5.926L_1^3 - 9.751L_1^2 - 72.11L_1 + 177.4 + 392.9x - 101.4x^2 \\ -57.04L_0L_1 - 661.6L_0 + 131.4L_0^2 - \frac{400}{9}L_0^3 + \frac{160}{27}L_0^4 \\ -506.0x^{-1} - \frac{3584}{27}x^{-1}L_0 \end{array} \right] (1-x), \\ + n_f^2 \left[ \begin{array}{l} 1.778L_1^2 + 5.944L_1 + 100.1 - 125.2x + 49.26x^2 - 12.59x^3 \\ -1.889L_0L_1 + 61.75L_0 + 17.89L_0^2 + \frac{32}{27}L_0^3 + \frac{256}{81}x^{-1} \end{array} \right] \end{array} \right.$$



$$P_{qg}(x) \cong n_f \left[ \begin{aligned} & \left( \frac{100}{27} L_1^4 - \frac{70}{9} L_1^3 - 120.5 L_1^2 + 104.42 L_1 + 2522 - 3316x + 2126x^2 \right) \\ & + L_0 L_1 (1823 - 25.22 L_0) - 252.5 x L_0^3 + 424.9 L_0 + 881.5 L_0^2 \\ & - \frac{44}{3} L_0^3 + \frac{536}{27} L_0^4 - 1268.3 x^{-1} - \frac{896}{3} x^{-1} L_0 \end{aligned} \right] \\ + n_f^2 \left[ \begin{aligned} & \left( \frac{20}{27} L_1^3 + \frac{200}{27} L_1^2 - 5.496 L_1 - 252.0 + 158.0x + 145.4x^2 - 139.28x^3 \right) \\ & - 98.07 x L_0^2 + 11.70 x L_0^3 - L_0 L_1 (53.09 + 80.616 L_0) \\ & - 254.0 L_0 - 90.80 L_0^2 - \frac{376}{27} L_0^3 - \frac{16}{9} L_0^4 + \frac{1112}{243} x^{-1} \end{aligned} \right]$$

with  $L_0 = \ln(x)$ ,  $L_1 = \ln(1-x)$ .

Also

$$C_1(x) = n_f \int_0^{1-x} \frac{d\omega}{1-\omega} \left[ \begin{aligned} & \left\{ \ln(\omega) \ln(1-\omega) [-173.1 + 46.18 \ln(1-\omega)] + 178.04 \ln(1-\omega) \right\} \\ & \left\{ + 6.892 \ln^2(1-\omega) + \frac{40}{27} (\ln^4(1-\omega) - 2 \ln^3(1-\omega)) \right\} \\ & + \omega \left\{ \ln(\omega) (-163.9(1-\omega)^{-1} - 7.208(1-\omega)) + 151.49 \right\} \\ & \left\{ + 44.51(1-\omega) - 43.12(1-\omega)^2 + 4.82(1-\omega)^3 \right\} \\ & \left\{ - 5.926 \ln^3(\omega) - 9.751 \ln^2(\omega) - 72.11 \ln(\omega) + 177.4 \right. \\ & \left. + 392.9(1-\omega) - 101.4(1-\omega)^2 - 57.04 \ln(1-\omega) \ln(\omega) \right\} \\ & + \omega \left\{ - 661.6 \ln(1-\omega) + 131.4 \ln^2(1-\omega) - \frac{400}{9} \ln^3(1-\omega) \right. \\ & \left. + \frac{160}{27} \ln^4(1-\omega) - 506.0(1-\omega)^{-1} - \frac{3584}{27} (1-\omega)^{-1} \ln(1-\omega) \right\} \\ & + n_f \omega \left\{ \begin{aligned} & 1.778 \ln^2(\omega) + 5.944 \ln(\omega) + 100.1 - 125.2(1-\omega) \\ & + 49.26(1-\omega)^2 - 12.59(1-\omega)^3 - 1.889 \ln(1-\omega) \ln(\omega) \\ & + 61.75 \ln(1-\omega) + 17.89 \ln^2(1-\omega) + \frac{32}{27} \ln^3(1-\omega) \end{aligned} \right\} \\ & \left. + \frac{256}{81} (1-\omega)^{-1} \right\} \end{aligned} \right]$$

$$C_2(x) = n_f \int_0^{1-x} \frac{x d\omega}{(1-\omega)^2} \left[ \begin{array}{l} \left\{ \ln(\omega)\ln(1-\omega)[-173.1 + 46.18\ln(1-\omega)] + 178.04\ln(1-\omega) \right\} \\ \left\{ + 6.892\ln^2(1-\omega) + \frac{40}{27}(\ln^4(1-\omega) - 2\ln^3(1-\omega)) \right\} \\ + \omega \left\{ \ln(\omega)(-163.9(1-\omega)^{-1} - 7.208(1-\omega)) + 151.49 \right\} \\ \left\{ + 44.51(1-\omega) - 43.12(1-\omega)^2 + 4.82(1-\omega)^3 \right\} \\ \left\{ - 5.926\ln^3(\omega) - 9.751\ln^2(\omega) - 72.11\ln(\omega) + 177.4 \right. \\ \left. + 392.9(1-\omega) - 101.4(1-\omega)^2 - 57.04\ln(1-\omega)\ln(\omega) \right. \\ \left. - 661.6\ln(1-\omega) + 131.4\ln^2(1-\omega) - \frac{400}{9}\ln^3(1-\omega) \right\} \\ \left\{ + \frac{160}{27}\ln^4(1-\omega) - 506.0(1-\omega)^{-1} - \frac{3584}{27}(1-\omega)^{-1}\ln(1-\omega) \right\} \\ + n_f \omega \left\{ \begin{array}{l} 1.778\ln^2(\omega) + 5.944\ln(\omega) + 100.1 - 125.2(1-\omega) \\ + 49.26(1-\omega)^2 - 12.59(1-\omega)^3 - 1.889\ln(1-\omega)\ln(\omega) \\ + 61.75\ln(1-\omega) + 17.89\ln^2(1-\omega) + \frac{32}{27}\ln^3(1-\omega) \\ + \frac{256}{81}(1-\omega)^{-1} \end{array} \right\} \end{array} \right] \omega$$

$$C_3(x) = n_f \int_0^{1-x} \frac{d\omega}{1-\omega} \left[ \begin{array}{l} \left\{ \frac{100}{27}\ln^4\ln(\omega) - \frac{70}{9}\ln^3(\omega) - 120.5\ln^2(\omega) + 104.42\ln(\omega) \right\} \\ \left\{ + 2522 - 3316(1-\omega) + 2126(1-\omega)^2 - 252.5(1-\omega)\ln^3(1-\omega) \right\} \\ \left\{ + \ln(\omega)\ln(1-\omega)(1823 - 25.22\ln(1-\omega)) + 424.9\ln(1-\omega) \right\} \\ \left\{ + 881.5\ln^2(1-\omega) - \frac{44}{3}\ln^3(1-\omega) + \frac{536}{27}\ln^4(1-\omega) \right\} \\ \left\{ - 1268.3(1-\omega)^{-1} - \frac{896}{3}(1-\omega)^{-1}\ln(1-\omega) \right\} \\ + n_f \left\{ \begin{array}{l} \frac{20}{27}\ln^3(\omega) + \frac{200}{27}\ln^2(\omega) - 5.496\ln(\omega) - 252.0 \\ + 158.0(1-\omega) + 145.4(1-\omega)^2 - 139.28(1-\omega)^3 \\ - 98.07(1-\omega)\ln^2(1-\omega) + 11.70(1-\omega)\ln^3(1-\omega) \\ - \ln(\omega)\ln(1-\omega)(53.09 + 80.616\ln(1-\omega)) \\ - 254.0\ln(1-\omega) - 90.80\ln^2(1-\omega) - \frac{376}{27}\ln^3(1-\omega) \\ - \frac{16}{9}\ln^4(1-\omega) + \frac{1112}{243}(1-\omega)^{-1} \end{array} \right\} \end{array} \right]$$

$$C_4(x) = n_f \int_0^{1-x} \frac{x d\omega}{(1-\omega)^2} \left[ \begin{array}{l} \left. \begin{array}{l} \frac{100}{27} \ln^4 \ln(\omega) - \frac{70}{9} \ln^3(\omega) - 120.5 \ln^2(\omega) + 104.42 \ln(\omega) \\ + 2522 - 3316(1-\omega) + 2126(1-\omega)^2 - 252.5(1-\omega) \ln^3(1-\omega) \\ + \ln(\omega) \ln(1-\omega) (1823 - 25.22 \ln(1-\omega)) + 424.9 \ln(1-\omega) \\ + 881.5 \ln^2(1-\omega) - \frac{44}{3} \ln^3(1-\omega) + \frac{536}{27} \ln^4(1-\omega) \\ - 1268.3(1-\omega)^{-1} - \frac{896}{3} (1-\omega)^{-1} \ln(1-\omega) \end{array} \right\} \omega \\ + n_f \left\{ \begin{array}{l} \frac{20}{27} \ln^3(\omega) + \frac{200}{27} \ln^2(\omega) - 5.496 \ln(\omega) - 252.0 \\ + 158.0(1-\omega) + 145.4(1-\omega)^2 - 139.28(1-\omega)^3 \\ - 98.07(1-\omega) \ln^2(1-\omega) + 11.70(1-\omega) \ln^3(1-\omega) \\ - \ln(\omega) \ln(1-\omega) (53.09 + 80.616 \ln(1-\omega)) \\ - 254.0 \ln(1-\omega) - 90.80 \ln^2(1-\omega) - \frac{376}{27} \ln^3(1-\omega) \\ - \frac{16}{9} \ln^4(1-\omega) + \frac{1112}{243} (1-\omega)^{-1} \end{array} \right\} \end{array} \right]$$

#### IV. Appendix D

Functions for polarized DGLAP evolution equation in LO are

$$I_1^S(x, t) = \frac{4}{3} \int_x^1 \frac{d\omega}{1-\omega} \left[ (1+\omega^2) g_1^S\left(\frac{x}{\omega}, t\right) - 2g_1^S(x, t) \right]$$

$$I_2^S(x, t) = N_f \int_x^1 \left\{ \omega^2 - (1-\omega)^2 \right\} \Delta G\left(\frac{x}{\omega}, t\right) d\omega$$

$$I_1^{NS}(x, t) = \frac{4}{3} \int_x^1 \frac{d\omega}{1-\omega} \left[ (1+\omega^2) g_1^{NS}\left(\frac{x}{\omega}, t\right) - 2g_1^{NS}(x, t) \right]$$

#### V. Appendix E

Functions for polarized DGLAP evolution equation in NLO are

$$I_3^S(x, t) = (x-1) g_1^S(x, t) \int_0^1 f(\omega) d\omega + \int_x^1 f(\omega) g_1^S\left(\frac{x}{\omega}, t\right) d\omega \\ + \int_x^1 \Delta P_{qq}^S(\omega) g_1^S\left(\frac{x}{\omega}, t\right) d\omega + \int_x^1 \Delta P_{qg}^S(\omega) \Delta G\left(\frac{x}{\omega}, t\right) d\omega$$

$$I_2'^{NS}(x, t) = \left[ (x-1)g_1^{NS}(x, t) \int_0^1 f(\omega) d\omega + \int_x^1 f(\omega) g_1^{NS}\left(\frac{x}{\omega}, t\right) d\omega + \int_x^1 \Delta P_{qq}^S(\omega) g_1^{NS}\left(\frac{x}{\omega}, t\right) d\omega \right]$$

with

$$f(\omega) = C_F^2 [P_F(\omega) - P_A(\omega)] + \frac{1}{2} C_F C_A [P_G + P_A(\omega)] + C_F T_R N_f P_{N_f}(\omega),$$

$$P_F(\omega) = -\frac{2(1+\omega^2)}{(1-\omega)} \ln(\omega) \ln(1-\omega) - \left( \frac{3}{1-\omega} + 2\omega \right) \ln \omega - \frac{1}{2} (1+\omega) \ln \omega + \frac{40}{3} (1-\omega)$$

$$P_A(\omega) = \frac{2(1+\omega^2)}{(1+\omega)} \int_{\frac{\omega}{1+\omega}}^{\frac{1}{1+\omega}} \frac{dk}{k} \ln\left(\frac{1-k}{k}\right) + 2(1+\omega) \ln(\omega) + 4(1-\omega)$$

$$P_G(\omega) = \frac{(1+\omega^2)}{(1-\omega)} \left( \ln^2(\omega) + \frac{11}{3} \ln(\omega) + \frac{67}{9} - \frac{\pi^2}{3} \right) + 2(1+\omega) \ln \omega + \frac{40}{3} (1-\omega)$$

$$P_{N_f}(\omega) = \frac{2}{3} \left[ \frac{1+\omega^2}{1-\omega} \left( -\ln \omega - \frac{5}{3} \right) - 2(1-\omega) \right], \quad \Delta P_{qq}^S(\omega) = 2C_F T_R N_f \Delta P_{qq}(\omega),$$

$$\Delta P_{qq}(\omega) = (1-\omega) - (1-3\omega) \ln \omega - (1+\omega) \ln^2 \omega,$$

$$\Delta P_{qg}^S(\omega) = C_F T_R N_f \Delta P_{qg}^1(\omega) + C_G T_R N_f \Delta P_{qg}^2(\omega),$$

$$\Delta P_{qg}^1(\omega) = -22 + 27\omega - 9 \ln \omega + 8(1-\omega) \ln(1-\omega)$$

$$+ (2\omega - 1) \left[ 2 \ln^2(1-\omega) - 4 \ln(1-\omega) \ln \omega + \ln^2 \omega - \frac{2}{3} \pi^2 \right]$$

$$\Delta P_{qg}^2(\omega) = 2(12 - 11\omega) + 2(1 + 8\omega) \ln \omega - 8(1-\omega) \ln(1-\omega)$$

$$- 2 \left[ \ln^2(1-\omega) - \frac{\pi^2}{6} \right] (2\omega - 1) - \left[ 2 \int_{\frac{1}{1+\omega}}^{\frac{1}{1+\omega}} \frac{dz}{z} \ln \frac{1-z}{z} - 3 \ln^2 \omega \right] (-2\omega - 1)$$

## VI. Appendix F

Functions for unpolarized gluon distribution functions are

$$I_g^1(x, t) = \int_x^1 d\omega \left[ \frac{\omega G\left(\frac{x}{\omega}, t\right) - G(x, t)}{1-\omega} + \left\{ \omega(1-\omega) + \frac{1-\omega}{\omega} \right\} G\left(\frac{x}{\omega}, t\right) + \frac{2}{9} \left( \frac{1+(1-\omega)^2}{\omega} \right) F_2^S\left(\frac{x}{\omega}, t\right) \right],$$

$$I_g^2(x, t) = \int_x^1 d\omega \left[ P_{gg}^2(\omega) G\left(\frac{x}{\omega}, t\right) + A(\omega) F_2^S\left(\frac{x}{\omega}, t\right) \right], \text{ where } P_{gg}^2(\omega) \cong \frac{52}{3\omega}.$$

Also

$$A(\omega) = C_F^2 \cdot A_1(\omega) + C_F \cdot C_G \cdot A_2(\omega) + C_F \cdot T_R \cdot N_F \cdot A_3(\omega),$$

$$A_1(\omega) = -\frac{5}{2} - \frac{7}{2}\omega + \left(2 + \frac{7}{2}\omega\right) + \left(-1 + \frac{\omega}{2}\right) \ln^2 \omega - 2\omega \cdot \ln(1-\omega) \\ + \left\{ -3\ln(1-\omega) - \ln^2(1-\omega) \right\} \frac{1+(1-\omega)^2}{\omega},$$

$$A_2(\omega) = \frac{28}{9} + \frac{65}{18}\omega + \frac{44}{9}\omega^2 + \left(-12 - 5\omega - \frac{8}{3}\omega^2\right) \ln \omega + (4+\omega) \ln^2 \omega + 2\omega \cdot \ln(1-\omega) \\ + \left\{ -2\ln\omega \ln(1-\omega) + \frac{1}{2} \ln^2 \omega + \frac{11}{3} \ln(1-\omega) + \ln^2(1-\omega) - \frac{1}{6} \pi^2 + \frac{1}{2} \right\} \frac{1+(1-\omega)^2}{\omega} \\ - \frac{1+(1+\omega)^2}{\omega} \int_{\omega/1+\omega}^{1+\omega} \frac{dz}{z} \ln \frac{1-z}{z},$$

$$A_3(\omega) = -\frac{4}{3}\omega \cdot \left\{ \frac{20}{9} + \frac{4}{3} \ln(1-\omega) \right\} \left\{ \frac{1+(1-\omega)^2}{\omega} \right\}.$$

## VII. Appendix G

Functions for polarized gluon distribution functions are

$$J_1^G(x, t) = \left\{ 6 \left( \frac{11}{12} - \frac{N_f}{18} + \ln(1-x) \right) \Delta G(x, t) + 6I_G \right\} \\ J_2^G(x, t) = (x-1) \Delta G(x, t) \int_0^1 \Delta P_{gg}^S(\omega) d\omega + \int_x^1 \Delta P_{gg}^S(\omega) \Delta G\left(\frac{x}{\omega}, t\right) d\omega \\ + \int_0^1 \Delta P_{gq}^S(\omega) g_1^S\left(\frac{x}{\omega}, t\right) d\omega$$

with

$$I_G = \int_x^1 d\omega \left[ \frac{1}{2} \left\{ \frac{(1 + \omega^4) \Delta G(\frac{x}{\omega}, t) - 2 \Delta G(x, t)}{1 - \omega} + \left( \frac{1}{\omega} + \omega^3 - \frac{(1 - \omega)^3}{\omega} \right) \Delta G(\frac{x}{\omega}, t) \right\} \right. \\ \left. + \int_x^1 \frac{2}{9} \left\{ \frac{1 - (1 - \omega)^2}{\omega} g_1^S(\frac{x}{\omega}, t) \right\} d\omega, \right]$$

$$\Delta P_{gg}^S(\omega) = -C_G T_R N_f \Delta P_{gg}^1(\omega) - C_F T_R N_f \Delta P_{gg}^2(\omega) + C_G^2 \Delta P_{gg}^3(\omega),$$

$$\Delta P_{gg}^1(\omega) = 4(1 - \omega) + \frac{4}{3}(1 + \omega) \ln \omega + \frac{20}{9} \left( \frac{1}{1 - \omega} - 2\omega + 1 \right),$$

$$\Delta P_{gg}^2(\omega) = 10(1 - \omega) + 2(5 - \omega) \ln \omega + 2(1 + \omega) \ln^2 \omega,$$

$$\Delta P_{gg}^3(\omega) = \frac{1}{3}(29 - 67\omega) \ln \omega - \frac{19}{2}(1 - \omega) + 4(1 + \omega) \ln^2 \omega \\ - \int_{\omega/1+\omega}^{1/1+\omega} \frac{dz}{z} \ln \frac{1-z}{z} \left( \frac{1}{1+\omega} + 2\omega + 1 \right) \\ + \left\{ \frac{67}{9} - 4 \ln(1 - \omega) \ln \omega + \ln^2 \omega - \frac{\pi^2}{3} \right\} \left( \frac{1}{1 - \omega} - 2\omega + 1 \right),$$

$$\Delta P_{gp}^S(\omega) = C_F T_R N_f \Delta P_{gq}^1(\omega) + C_F^2 \Delta P_{gq}^2(\omega) + C_F C_G \Delta P_{gq}^3(\omega),$$

$$\Delta P_{gq}^1(\omega) = -\frac{4}{9}(4 + \omega) - \frac{4}{3}(2 - \omega) \ln(1 - \omega),$$

$$\Delta P_{gq}^2(\omega) = -\frac{1}{2} - \frac{1}{2}(4 - \omega) \ln \omega - (2 + \omega) \ln(1 - \omega) + \left\{ -4 - \ln^2(1 - \omega) + \frac{1}{2} \ln^2 \omega \right\} (2 - \omega),$$

$$\Delta P_{gq}^3(\omega) = (4 - 13\omega) \ln \omega + \frac{1}{3}(10 + \omega) \ln(1 - \omega) + \frac{1}{9}(41 + 35\omega) \\ + \frac{1}{2} \left\{ -2 \int_{\omega/1+\omega}^{1/1+\omega} \frac{dz}{z} \ln \frac{1-z}{z} + 3 \ln^2 \omega \right\} (2 + \omega) \\ + \left\{ \ln^2(1 - \omega) - 2 \ln(1 - \omega) \ln \omega - \frac{\pi^2}{6} \right\} (2 - \omega). \square$$

## List of Publications

### (a) Papers published/ accepted for publication in referred journals:

1. "Evolution of spin-dependent structure functions from DGLAP equations in leading order and next-to-leading order"  
R. Baishya, U. Jamil and J. K. Sarma  
Physical Review D 79, 034030 (2009)
2. "Semi numerical solution of non-singlet Dokshitzer-Gribov-Lipatov-Altarelli-Parisi evolution equation up to next-next-to-leading order at small-x"  
R. Baishya and J. K. Sarma  
European Physical Journal C 60 (2009) 585 - 591
3. "Solutions of non-singlet DGLAP evolution equation in leading order and next to leading order at small-x"  
R. Baishya and J. K. Sarma  
Indian Journal of Physics 83 (9) 1333-1341 (2009)
4. "Method of Characteristics and solution of DGLAP evolution equation in leading and next to leading order at small-x"  
R. Baishya and J. K. Sarma  
Physical Review D 74, 107702 (2006)
5. "Method of Characteristics and solution of DGLAP evolution equation in leading order at small-x"  
R. Baishya, R. Rajkhowa and J. K. Sarma  
Journal of Assam Science Society, Vol. 46, No. 1 (2005) 44

**(b) Papers published/ accepted for publication in Proceedings:**

1. "Solution of non singlet DGLAP evolution equation in next - next to leading order at small  $x$ " - R. Baishya and J. K. Sarma; Accepted for publication in Indian Journal of Physics as proceedings of 'Quark-Matter 2008, 20th International Conference on Ultra-Relativistic Nucleus Nucleus Collisions', Jaipur, India, February 4-10, 2008.
2. "Solution of DGLAP evolution equation in next - next to leading order (NNLO) at small  $x$ " - R. Baishya and J. K. Sarma; HEP workshop in IIT, Guwahati, February 21-23, 2008
3. "Recent Development in High Energy Physics" - R. Baishya and J. K. Sarma; 'National Seminar on Physics of 20<sup>th</sup> century', D. K. College, Mirza; 18<sup>th</sup> December 2006
4. "Method of Characteristics and solution of DGLAP evolution equation in leading order (LO) and next to leading order (NLO) at small  $x$ " - R. Baishya and J. K. Sarma; 'The 17<sup>th</sup> DAE-BRNS High Energy Physics Symposium', IIT, Kharagpur, December 11-15, 2006.
5. " $t$  and  $x$  evolutions of gluon structure functions in leading order at small  $x$  by method of characteristics" - R. Baishya and J. K. Sarma; 'Seminar on Quantum Revolution and Afterwards', Birjhora Mahavidyalaya, Bongaigaon, 21<sup>st</sup> January, 2006.
6. "Method of characteristics and solution of DGLAP evolution equation in leading order at small  $x$ " - R. Baishya and J. K. Sarma; '50<sup>th</sup> Annual Technical Session of Assam Science Society and National Conference on Current Trends of Research in Science and Technology' Gauhati University, 28 & 29 January 2005



# *Addenda*

*"All science is either physics or stamp collecting"*

*– Rutherford*

# Evolution of spin-dependent structure functions from DGLAP equations in leading order and next to leading order

R. Baishya\*

*Physics Department, J. N. College, Boko-781123, Assam, India*

U. Jamil and J. K. Sarma

*Physics Department, Tezpur University, Napaam-784028, Assam, India*

(Received 15 December 2008; published 25 February 2009)

In this paper the spin-dependent singlet and nonsinglet structure functions have been obtained by solving Dokshitzer, Gribov, Lipatov, Altarelli, Parisi evolution equations in leading order and next to leading order in the small  $x$  limit. Here we have used Taylor series expansion and then the method of characteristics to solve the evolution equations. We have also calculated  $t$  and  $x$  evolutions of deuteron structure functions, and the results are compared with the SLAC E-143 Collaboration data.

DOI: 10.1103/PhysRevD.79.034030

PACS numbers: 12.38.-t, 12.39.-x, 13.60.Hb, 13.88.+e

## I. INTRODUCTION

High-energy lepton-nucleon scattering has served as a sensitive probe for the substructure of the proton and the neutron. Experiments with high-energy electrons, muons, and neutrinos have been used to characterize the parton substructure of the nucleon and to establish the current theory of strong interactions, quantum chromodynamics (QCD), etc. Here the observations are scaling violations for the unpolarized nucleon structure functions, the measurement of the strong coupling constant  $\alpha_S(Q^2)$ , the confirmation of numerous QCD sum rules, and the extraction of the parton distributions inside the nucleon. The solutions of the unpolarized DGLAP equation [1] for the QCD evolution of parton distribution functions have been discussed considerably over the past years [2–8]. There exist two main classes of approaches: those that solve the equation directly in  $x$  space, and those that solve it for Mellin transforms of the parton densities and subsequently invert the transform back to  $x$  space. Some available programs that deal with DGLAP evolution are PEGASUS [5], which is based on the use of Mellin moments, and QCDNUM [6], CANDIA [7], and HOPPET [8], which are all based on  $x$  space.

In the polarized deep-inelastic scattering (DIS) program, the spin structure of the nucleon has been studied by using polarized lepton beams scattered by polarized targets. These fixed-target experiments have been used to characterize the spin structure of the proton and neutron and to test additional fundamental QCD and quark-parton model (QPM) sum rules. The first experiments in polarized electron-polarized proton scattering, performed in the 1970s, helped establish the parton structure of the proton. In the late 1980s, a polarized muon-polarized proton experiment found that a QPM sum rule was violated, which

seemed to indicate that the quarks do not account for the spin of the proton. This “proton-spin crisis” gave birth to a new generation of experiments at several high-energy physics laboratories around the world. The new and extensive data sample collected from these fixed-target experiments has enabled a careful characterization of the spin-dependent parton substructure of the nucleon. The results have been used to test QCD, to find an independent value for  $\alpha_S(Q^2)$ , and to probe with reasonable precision the polarized parton distributions.

Recent interest in the spin structure of the proton, neutron, and deuteron and advances in experimental techniques have led to a number of experiments concerned with DIS of polarized leptons on various polarized targets. Among these are the E143 experiments at SLAC [9] and those of the SMC Collaboration at CERN [10], which used polarized hydrogen and deuterium; the E154 experiment at SLAC [11] and the HERMES Collaboration experiments at DESY [12], which used polarized  $^3\text{He}$ ; and the HERMES experiment [13], which used polarized hydrogen [14]. A new material, deuterized lithium  $^6\text{LiD}$ , has recently emerged as a source of polarized deuterium in the E155/E155x experiments at SLAC [15]. The spin-dependent structure function  $g_1(x, Q^2)$  for deep-inelastic lepton-nucleon scattering is of fundamental importance in understanding the quark and gluon spin structure of the proton and neutron. According to the DGLAP equations [16],  $g_1(x, Q^2)$  is expected to evolve logarithmically with  $Q^2$ , where  $g_1$  depends both on  $x$ , the fractional momentum carried by the struck parton, and on  $Q^2$ , the squared four-momentum of the exchanged virtual photon. There have been a number of theoretical approaches [8, 17] to calculate  $g_1(x, Q^2)$  using phenomenological models of nucleon structure. In this paper we will try to solve polarized DGLAP evolution equations up to next to leading order (NLO) by the method of characteristics [6, 18] and compare our results with experimental data [9]. Since the method of

\*rjitboko@yahoo.co.in

characteristics gives a unique solution of the partial differential equation, this phenomenological work signifies an important role in the evolution of structure functions.

## II. THEORY

When both the beam and the target are longitudinally polarized in DIS, the asymmetry is defined as

$$A_{\parallel} = \frac{\sigma^{\parallel\rightarrow} - \sigma^{\parallel\leftarrow}}{\sigma^{\parallel\rightarrow} + \sigma^{\parallel\leftarrow}},$$

where  $\sigma^{\parallel\rightarrow}$  and  $\sigma^{\parallel\leftarrow}$  are the cross sections for the opposite and same spin directions, respectively. Similarly, the transverse asymmetry, determined from scattering of a longitudinally polarized beam on a transversely polarized target, is defined as

$$A_{\perp} = \frac{\sigma^{\leftarrow\rightarrow} - \sigma^{\rightarrow\leftarrow}}{\sigma^{\leftarrow\rightarrow} + \sigma^{\rightarrow\leftarrow}}.$$

These asymmetries can be express in terms of longitudinal ( $A_1$ ) and transverse ( $A_2$ ) virtual photon-nucleon asymmetries as

$$A_{\parallel} = D[A_1 + \eta A_2] \quad \text{and} \quad A_{\perp} = d\left[A_2 - \gamma\left(1 - \frac{y}{2}\right)A_1\right],$$

where  $D = \frac{2y-y^2}{2(1-y)(1+R)+y^2}$ ,  $\eta = \left(\frac{Q}{E}\right) \frac{2(1-y)}{y(2-y)}$ ,  $d = \frac{\sqrt{1-y}}{1-y} D$ ,  $\gamma^2 = 4y^2x^2$ , and  $y = \frac{M}{Q}$ . The virtual photon-nucleon asymmetries for the proton, neutron, and deuteron are defined as

$$A_1^{p,n} = \frac{\sigma_{1/2} - \sigma_{3/2}}{\sigma_{1/2} + \sigma_{3/2}}, \quad A_2^{p,n} = \frac{2\sigma^{TL}}{\sigma_{1/2} + \sigma_{3/2}},$$

$$A_1^d = \frac{\sigma_0 - \sigma_2}{\sigma_0 + \sigma_2}, \quad \text{and} \quad A_2^d = \frac{\sigma_0^{TL} - \sigma_1^{TL}}{\sigma_{1/2} + \sigma_{3/2}}.$$

The longitudinal spin-dependent structure function  $g_1(x)$  is defined as

$$g_1(x) = \frac{1}{2} \sum_i e_i^2 \Delta q_i(x)$$

where  $q_i(x) = q_i^+(x) + \bar{q}_i^+(x) - q_i^-(x) - \bar{q}_i^-(x)$ . Here  $q_i^+(x)$  and  $q_i^-(x)$  are the densities of quarks of flavor “ $i$ ” with helicity parallel and antiparallel to the nucleon spin.

The spin-dependent structure functions  $g_1(x, Q^2)$  and  $g_2(x, Q^2)$  are related to the spin-independent structure function  $F_2(x, Q^2)$  as

$$g_1 = \frac{F_2(x, Q^2)[A_1(x, Q^2) + \gamma A_2(x, Q^2)]}{2x[1 + R_{\sigma}(x, Q^2)]}, \quad (1a)$$

$$g_2 = \frac{F_2(x, Q^2)[-A_1(x, Q^2) + A_2(x, Q^2)/\gamma]}{2x[1 + R_{\sigma}(x, Q^2)]}, \quad (1b)$$

where  $R_{\sigma} = \frac{\sigma_L(x, Q^2)}{\sigma_T(x, Q^2)}$  is the ratio of the longitudinal and transverse virtual photon cross sections. The deuteron, proton, and neutron structure functions measured in DIS

can be written in terms of singlet and nonsinglet quark distribution functions as

$$g_1^d(x, t) = \frac{5}{2} g_1^S(x, t), \quad (2a)$$

$$g_1^p(x, t) = \frac{5}{18} g_1^S(x, t) + \frac{3}{18} g_1^{NS}(x, t), \quad (2b)$$

$$g_1^n(x, t) = \frac{5}{18} g_1^S(x, t) - \frac{3}{18} g_1^{NS}(x, t), \quad (2c)$$

where  $t = \ln(Q^2/\Lambda^2)$ ;  $\Lambda$  is the QCD cutoff parameter.

The polarized DGLAP evolution equation [16] in the standard form is given by

$$\frac{\partial g_1(x, Q^2)}{\partial \ln Q^2} = P(x, Q^2) \otimes g_1(x, Q^2), \quad (3)$$

where  $g_1(x, Q^2)$  is the spin-dependent structure function as a function of  $x$  and  $Q^2$ , where  $x$  is the Bjorken variable and  $Q^2$  is the four-momentum transfer in a DIS process. Here  $P(x, Q^2)$  is the spin-dependent kernel known perturbatively up to the first few orders in  $\alpha_S(Q^2)$ , the strong coupling constant. Here  $\otimes$  represents the standard Mellin convolution, and the notation is given by

$$a(x) \otimes b(x) \equiv \int_0^1 \frac{dy}{y} a(y) b\left(\frac{x}{y}\right). \quad (4)$$

One can write

$$P(x, Q^2) = \frac{\alpha_S(Q^2)}{2\pi} P^{(0)}(x) + \left(\frac{\alpha_S(Q^2)}{2\pi}\right)^2 P^{(1)}(x), \quad (5)$$

where  $P^{(0)}(x)$  and  $P^{(1)}(x)$  are spin-dependent splitting functions in LO and NLO.

The singlet and nonsinglet structure functions are obtained from the polarized DGLAP evolution equations as

$$\frac{\partial g_1^S}{\partial t} - \frac{\alpha_S(t)}{2\pi} \left[ \frac{2}{3} \{3 + 4 \ln(1-x)\} g_1^S(x, t) + I_1^S(x, t) + I_2^S(x, t) \right] = 0, \quad (6a)$$

$$\frac{\partial g_1^{NS}}{\partial t} - \frac{\alpha_S(t)}{2\pi} \left[ \frac{2}{3} \{3 + 4 \ln(1-x)\} g_1^{NS}(x, t) + I_1^{NS}(x, t) \right] = 0, \quad (6b)$$

in LO and

$$\frac{\partial g_1^S}{\partial t} - \frac{\alpha_S(t)}{2\pi} \left[ \frac{2}{3} \{3 + 4 \ln(1-x)\} g_1^S(x, t) + I_1^S(x, t) + I_2^S(x, t) \right] - \left(\frac{\alpha_S(t)}{2\pi}\right)^2 I_3^S = 0, \quad (7a)$$

$$\frac{\partial g_1^{NS}}{\partial t} - \frac{A_f}{t} \left[ \{3 + 4 \ln(1-x)\} g_1^{NS}(x, t) + I_1^{NS}(x, t) \right] - \left(\frac{\alpha_S(t)}{2\pi}\right)^2 I_2^{NS} = 0 \quad (7b)$$

in NLO, where

$$I_1^S(x, t) = \frac{4}{3} \int_x^1 \frac{d\omega}{1-\omega} \left[ (1+\omega^2) g_1^S\left(\frac{x}{\omega}, t\right) - 2g_1^S(x, t) \right], \quad (8a)$$

$$I_2^S(x, t) = N_f \int_x^1 \{\omega^2 - (1-\omega)^2\} \Delta G\left(\frac{x}{\omega}, t\right) d\omega, \quad (8b)$$

$$I_3^S = \left[ (x-1) g_1^S(x, t) \int_0^1 f(\omega) d\omega + \int_x^1 f(\omega) g_1^S\left(\frac{x}{\omega}, t\right) d\omega + \int_x^1 \Delta P_{qq}^S(\omega) g_1^S\left(\frac{x}{\omega}, t\right) d\omega \right. \\ \left. + \int_x^1 \Delta P_{qg}^S(\omega) \Delta G\left(\frac{x}{\omega}, t\right) d\omega \right], \quad (8c)$$

$$I_1^{NS}(x, t) = \frac{4}{3} \int_x^1 \frac{d\omega}{1-\omega} \left[ (1+\omega^2) g_1^{NS}\left(\frac{x}{\omega}, t\right) - 2g_1^{NS}(x, t) \right], \quad (8d)$$

$$I_2^{NS} = \left[ (x-1) g_1^{NS}(x, t) \int_0^1 f(\omega) d\omega + \int_x^1 f(\omega) g_1^{NS}\left(\frac{x}{\omega}, t\right) d\omega + \int_x^1 \Delta P_{qq}^S(\omega) g_1^{NS}\left(\frac{x}{\omega}, t\right) d\omega \right] \quad (8e)$$

with

$$f(\omega) = C_F^2 [P_F(\omega) - P_A(\omega)] + \frac{1}{2} C_F C_A [P_G + P_A(\omega)] + C_F T_R N_f P_{N_f}(\omega),$$

$$P_F(\omega) = -\frac{2(1+\omega^2)}{(1-\omega)} \ln(\omega) \ln(1-\omega) - \left( \frac{3}{1-\omega} + 2\omega \right) \ln \omega - \frac{1}{2} (1+\omega) \ln \omega + \frac{40}{3} (1-\omega),$$

$$P_A(\omega) = \frac{2(1+\omega^2)}{(1+\omega)} \int_{\omega/(1+\omega)}^{(1/(1+\omega))} \frac{dk}{k} \ln\left(\frac{1-k}{k}\right) + 2(1+\omega) \ln(\omega) + 4(1-\omega),$$

$$P_G(\omega) = \frac{(1+\omega^2)}{(1-\omega)} \left( \ln^2(\omega) + \frac{11}{3} \ln(\omega) + \frac{67}{9} - \frac{\pi^2}{3} \right) + 2(1+\omega) \ln \omega + \frac{40}{3} (1-\omega),$$

$$P_{N_f}(\omega) = \frac{2}{3} \left[ \frac{1+\omega^2}{1-\omega} \left( -\ln \omega - \frac{5}{3} \right) - 2(1-\omega) \right],$$

$$\Delta P_{qq}^S(\omega) = 2C_F T_R N_f \Delta P_{qq}(\omega),$$

$$\Delta P_{qq}(\omega) = (1-\omega) - (1-3\omega) \ln \omega - (1+\omega) \ln^2 \omega,$$

$$\Delta P_{qg}^S(\omega) = C_F T_R N_f \Delta P_{qg}^1(\omega) + C_G T_R N_f \Delta P_{qg}^2(\omega),$$

$$\Delta P_{qg}^1(\omega) = -22 + 27\omega - 9 \ln \omega + 8(1-\omega) \ln(1-\omega) + (2\omega-1) [2 \ln^2(1-\omega) - 4 \ln(1-\omega) \ln \omega + \ln^2 \omega - \frac{2}{3} \pi^2],$$

$$\Delta P_{qg}^2(\omega) = 2(12-11\omega) + 2(1+8\omega) \ln \omega - 8(1-\omega) \ln(1-\omega)$$

$$- 2 \left[ \ln^2(1-\omega) - \frac{\pi^2}{6} \right] (2\omega-1) - \left[ 2 \int_{\omega/(1-\omega)}^{1/(1-\omega)} \frac{dz}{z} \ln \frac{1-z}{z} - 3 \ln^2 \omega \right] (-2\omega-1)$$

The strong coupling constant  $\alpha_S(Q^2)$  is related to the  $\beta$  function as [4]

$$\beta(\alpha_S) = \frac{\partial \alpha_S(Q^2)}{\partial \log Q^2} \\ = -\frac{\beta_0}{4\pi} \alpha_S^2 - \frac{\beta_1}{16\pi^2} \alpha_S^3 - \frac{\beta_2}{64\pi^3} \alpha_S^4 + \dots,$$

where

$$\beta_0 = \frac{11}{3} N_C - \frac{4}{3} T_f = 11 - \frac{2}{3} N_f,$$

$$\beta_1 = \frac{34}{3} N_C^2 - \frac{10}{3} N_C N_f - 2C_F N_f = 102 - \frac{38}{3} N_f,$$

$$\beta_2 = \frac{2857}{54} N_C^3 + 2C_F^2 T_f - \frac{205}{9} C_F N_C T_f + \frac{44}{9} C_F T_f^2 \\ + \frac{158}{27} N_C T_f^2 \\ = \frac{2857}{6} - \frac{6673}{18} N_f + \frac{325}{54} N_f^2$$

are the one-loop, two-loop, and three-loop corrections to the QCD  $\beta$  function,  $N_f$  being the flavor number. We have

set  $N_C = 3$ ,  $C_F(\omega) = \frac{N_C^2 - 1}{2N_C} = \frac{4}{3}$ , and  $T_f = \frac{1}{2}N_f$ . Let us introduce the variable  $u = 1 - \omega$  and note that  $\frac{x}{\omega} = \frac{x}{1-u} = x \sum_{k=0}^{\infty} u^k$ .

Since  $x < \omega < 1$ ,  $0 < u < 1 - x$ , and hence the series is convergent for  $|u| < 1$ . Now using Taylor's expansion series,

$$\begin{aligned} g_1^S\left(\frac{x}{\omega}, t\right) &= g_1^S\left(x + \frac{xu}{1-u}, t\right) \\ &= g_1^S(x, t) + \frac{xu}{1-u} \frac{\partial g_1^S(x, t)}{\partial x} + \frac{1}{2} \left(\frac{xu}{1-u}\right)^2 \\ &\quad \times \frac{\partial^2 g_1^S(x, t)}{\partial x^2} + \dots \end{aligned}$$

Here, if we introduce the higher order terms in the Taylor expansion, then there is also no modification of the solution. When we solve the second-order partial differential equation using the Monges method, which will be produced by introducing the second-order terms in the Taylor expansion, then it ultimately becomes first order, as before, due to the form of the DGLAP equation. Similarly, by introducing more terms in the Taylor expansion, we hope that for these cases the terms can also be neglected due to still smaller values of  $x$  [19]. Thus  $x$  is small in our region of discussion, the terms containing  $x^2$  and higher powers of  $x$  can be neglected, and we can rewrite  $g_1^S\left(\frac{x}{\omega}, t\right)$ ,  $g_1^{NS}\left(\frac{x}{\omega}, t\right)$ , and  $\Delta G\left(\frac{x}{\omega}, t\right)$  as

$$g_1^S\left(\frac{x}{\omega}, t\right) = g_1^S(x, t) + \frac{xu}{1-u} \frac{\partial g_1^S(x, t)}{\partial x}, \quad (9a)$$

$$g_1^{NS}\left(\frac{x}{\omega}, t\right) = g_1^{NS}(x, t) + \frac{xu}{1-u} \frac{\partial g_1^{NS}(x, t)}{\partial x}, \quad (9b)$$

$$\Delta G\left(\frac{x}{\omega}, t\right) = \Delta G(x, t) + \frac{xu}{1-u} \frac{\partial \Delta G(x, t)}{\partial x}. \quad (9c)$$

In order to solve Eqs. (6a) and (7a), we need to relate the singlet distribution  $g_1^S(x, t)$  with the gluon distribution  $\Delta G(x, t)$ . For small  $x$  and high  $Q^2$ , the gluon is expected to be more dominant than the sea quark. But for lower  $Q^2$ , there is no such clear-cut distinction between the two. Hence, for simplicity, let us assume  $\Delta G(x, t) = k(x)g_1^S(x, t)$ , where  $k(x)$  is a suitable function of  $x$  or may be a constant [20].

Using Eqs. (9a) and (9c) in Eqs. (8a) and (8b) and performing  $u$  integrations, Eq. (6a) takes the form

$$-t \frac{\partial g_1^S(x, t)}{\partial t} + A_f L(x) g_1^S(x, t) + A_f M(x) \frac{\partial g_1^S}{\partial x} = 0 \quad (10)$$

where

$$A_f = \frac{\alpha_s(t)}{3\pi} t,$$

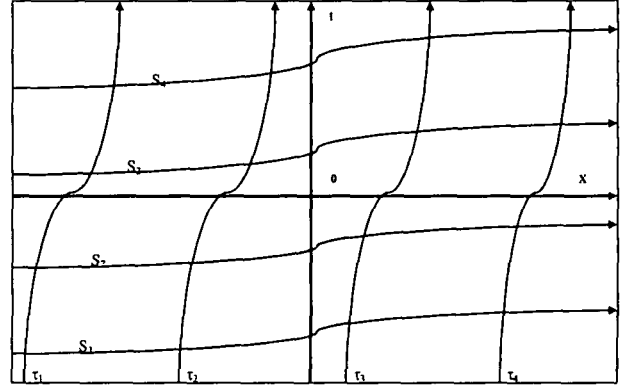


FIG. 1. Characteristic curves.

$$L(x) = A(x) + k(x)C(x) + D(x) \frac{\partial k(x)}{\partial x}, \quad (11a)$$

$$M(x) = B(x) + k(x)D(x), \quad (11b)$$

$$A(x) = 2x - x^2 + 4 \ln(1 - x), \quad (11c)$$

$$B(x) = x - x^3 - 2x \ln(x), \quad (11d)$$

$$C(x) = \frac{3}{2}N_f(x - x^2), \quad (11e)$$

$$D(x) = \frac{3}{2}N_f[-x + x^3 + x \ln(x)]. \quad (11f)$$

To introduce the method of characteristics [18], let us consider two new variables,  $S$  and  $\tau$ , instead of  $x$  and  $t$ , such that

$$\frac{dt}{dS} = -t, \quad (12a)$$

$$\frac{dx}{dS} = A_f M(x), \quad (12b)$$

which are known as characteristic equations. Figure 1 indicates the characteristic curves in the  $x$ - $t$  plane. Here the vertical curvy lines represent the  $t$ -evolution curves. In a particular vertical curvy line  $\tau$  is constant and  $S$  varies from 0 to  $\alpha$ . Putting these equations in Eq. (10), we get

$$\frac{dg_1^S(S, \tau)}{dS} + L(S, \tau)g_1^S(S, \tau) = 0 \quad (13)$$

which can be solved as

$$g_1^S(S, \tau) = g_1^S(0, \tau) \exp\left[-\int_0^S L(S, \tau) dS\right].$$

For the evolution of  $t$ , the structure function varies with  $t$ , while  $x$  remains a constant. Hence Eq. (12a) can be used in Eq. (13), the solution of which is

$$g_1^S(S, \tau) = g_1^S(\tau) \left(\frac{t}{t_0}\right)^{L(S, \tau)}, \quad (14)$$

where  $L(S, \tau) = 3/2A_f L(x)$  and  $g_1^S(S, \tau) = g_1^S(\tau)$  for  $S = 0$ ,  $t = t_0$ .

Replacing the coordinate system  $(S, \tau)$  to the original coordinate system  $(x, t)$  in Eq. (14) with the input function

$g_1^S(\tau) = g_1^S(x, t_0)$ , we get the  $t$  evolution of the singlet structure function in the LO as

$$g_1^S(x, t) = g_1^S(x, t_0) \left( \frac{t}{t_0} \right)^{(3/2)A_f L(x)}. \quad (15)$$

Proceeding in the same way, we get the  $t$  evolution of the nonsinglet structure function from Eq. (7b) as

$$g_1^{NS}(x, t) = g_1^{NS}(x, t_0) \left( \frac{t}{t_0} \right)^{(3/2)A_f A(x)}. \quad (16)$$

The  $t$  and  $x$  evolution of the deuteron, proton, and neutron structure functions in LO can be obtained as

$$g_1^d(x, t) = g_1^d(x, t_0) \left( \frac{t}{t_0} \right)^{(3/2)A_f L(x)}, \quad (17a)$$

$$\begin{aligned} g_1^{NS}(x, t) &= 3[g_1^p(x, t_0) - g_1^n(x, t_0)] \left( \frac{t}{t_0} \right)^{(3/2)A_f A(x)} \\ &= g_1^{NS}(x, t_0) \left( \frac{t}{t_0} \right)^{(3/2)A_f A(x)} \end{aligned} \quad (17b)$$

and

$$g_1^d(x, t) = g_1^d(x_0, t) \exp \left[ - \int_{x_0}^x \frac{L(x)}{M(x)} dx \right], \quad (18a)$$

$$\begin{aligned} g_1^{NS}(x, t) &= 3[g_1^p(x_0, t) - g_1^n(x_0, t)] \exp \left[ - \int_{x_0}^x \frac{A(x)}{B(x)} dx \right] \\ &= g_1^{NS}(x_0, t) \exp \left[ - \int_{x_0}^x \frac{A(x)}{B(x)} dx \right], \end{aligned} \quad (18b)$$

where  $g_1^d(x, t_0)$ ,  $g_1^p(x, t_0)$ ,  $g_1^n(x, t_0)$  and  $g_1^d(x_0, t)$ ,  $g_1^p(x_0, t)$ ,  $g_1^n(x_0, t)$  are input functions.

Similarly, in the NLO the  $t$  and  $x$  evolution of the deuteron, proton, and neutron structure functions will be obtain as

$$g_1^d(x, t) = g_1^d(x, t_0) \left( \frac{t}{t_0} \right)^{(3/2)A_f [L(x) + T_0 L_1(x)]}, \quad (19a)$$

$$\begin{aligned} g_1^{NS}(x, t) &= 3[g_1^p(x, t_0) - g_1^n(x, t_0)] \left( \frac{t}{t_0} \right)^{(3/2)A_f [A(x) + T_0 B_1(x)]} \\ &= g_1^{NS}(x, t_0) \left( \frac{t}{t_0} \right)^{(3/2)A_f [A(x) + T_0 B_1(x)]} \end{aligned} \quad (19b)$$

and

$$g_1^d(x, t) = g_1^d(x_0, t) \exp \left[ - \int_{x_0}^x \frac{L(x) + T_0 L_1(x)}{M(x) + T_0 M_1(x)} dx \right], \quad (20a)$$

$$\begin{aligned} g_1^{NS}(x, t) &= 3[g_1^p(x, t) - g_1^n(x, t)] \\ &= g_1^{NS}(x_0, t) \exp \left[ - \int_{x_0}^x \frac{A(x) + T_0 B_1(x)}{B(x) + T_0 B_3(x)} dx \right], \end{aligned} \quad (20b)$$

where

$$L_1(x) = B_1(x) + k(x)B_2(x) + B_4(x)\partial k(x)/\partial x, \quad (21a)$$

$$M_1(x) = B_3(x) + k(x)B_4(x), \quad (21b)$$

$$\begin{aligned} B_1(x) &= x \int_0^1 f(\omega) d\omega - \int_0^x f(\omega) d\omega \\ &\quad + \frac{4}{3} N_f \int_x^1 \Delta P_{qq}(\omega) d\omega, \end{aligned} \quad (21c)$$

$$B_2(x) = \int_x^1 \Delta P_{qg}^S(\omega) d\omega, \quad (21d)$$

$$B_3(x) = x \int_x^1 \left[ f(\omega) + \frac{4}{3} N_f \Delta P_{qg}^S(\omega) \right] \frac{1-\omega}{\omega} d\omega, \quad (21e)$$

$$B_4(x) = x \int_x^1 \frac{1-\omega}{\omega} \Delta P_{qg}^S(\omega) d\omega. \quad (21f)$$

Here we consider one numerical parameter,  $T_0$ , such that  $T^2(t) = T_0 T(t)$ , where  $T(t) = \frac{\alpha_s(t)}{2\pi}$  and  $T_0 = \frac{\alpha_s}{2\pi}$  with  $\alpha_s = 0.1240 \pm 0.0008(\text{stat}) \pm 0.0010(\text{exp}) \pm 0.0011(\text{had})$  [21].

### III. RESULTS AND DISCUSSION

In this paper, we compare our result for the  $t$  evolution of the polarized singlet (deuteron)  $g_1^d(x, t)$  and nonsinglet (combination of the proton and the neutron)  $g_1^{NS}(x, t)$

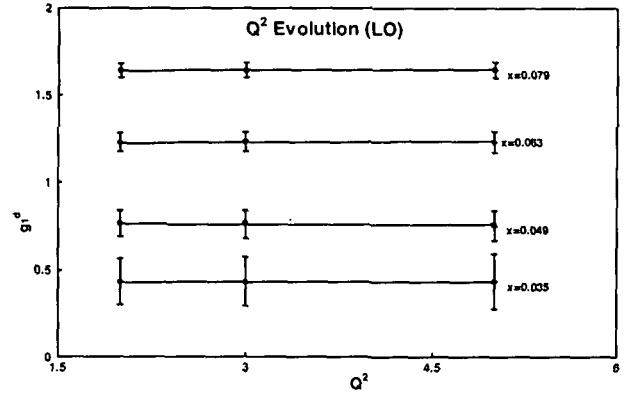


FIG. 2. Deuteron structure function in LO.

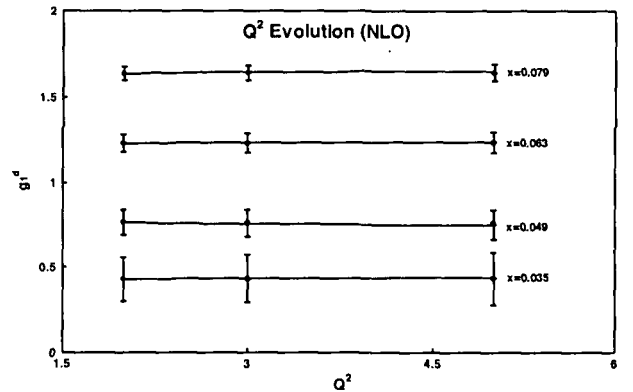


FIG. 3. Deuteron structure function in NLO.

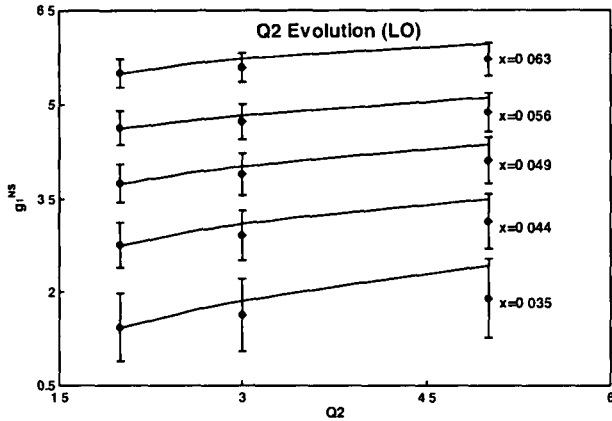


FIG 4 Nonsinglet structure function in LO

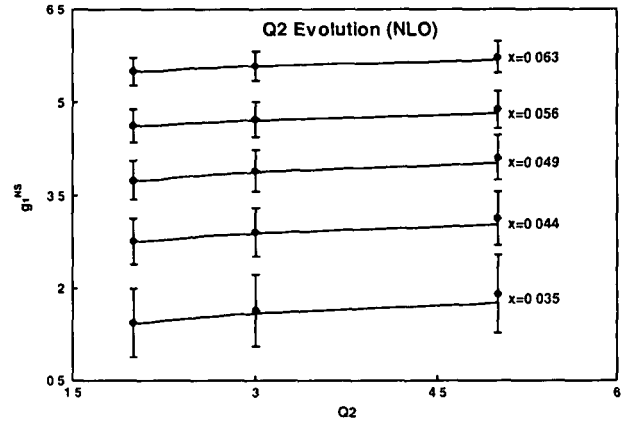


FIG 5 Nonsinglet structure function in NLO

structure functions measured by the SLAC E-143 Collaboration at beam energies of 291, 162, and 97 GeV. In Figs 2 and 3, we have plotted the computed values of  $g_1^d$  against  $Q^2$  values for a fixed  $x$  in LO and NLO, respectively. In Figs 4 and 5 we have plotted the computed values of  $g_1^{NS}$  against the  $Q^2$  values for LO and NLO. Here the vertical lines represent the data ranges from experiment, and horizontal lines represent our computed values.

Though there are various methods to solve the DGLAP evolution equations to calculate polarized quark and gluon

structure functions, our method of characteristics to solve these equations is also a viable alternative. Though mathematically vigorous, it changes the integro-differential equations into ordinary differential equations and then makes it possible to obtain unique solutions.

#### ACKNOWLEDGMENTS

One of us (R. B.) is grateful to DAE-BRNS for financial assistance in the form of a major research project.

- 
- [1] G. Altarelli and G. Parisi, *Nucl. Phys.* **B126**, 298 (1977), G. Altarelli, *Phys. Rep.* **81**, 1 (1982).
  - [2] R. Baishya and J. K. Sarma, *Phys. Rev. D* **74**, 107702 (2006).
  - [3] W. L. van Neerven and A. Vogt, *Nucl. Phys.* **B588**, 345 (2000), **B568**, 263 (2000), *Phys. Lett. B* **490**, 111 (2000), S. Moch, J. A. M. Vermaseren, and A. Vogt, *Nucl. Phys. B, Proc. Suppl.* **116**, 100 (2003), *Nucl. Phys.* **B688**, 101 (2004), S. Moch and J. A. M. Vermaseren, *Nucl. Phys.* **B573**, 853 (2000).
  - [4] A. Cafarella, C. Coriano, and M. Guzzi, *Nucl. Phys.* **B748**, 253 (2006), *J. High Energy Phys.* **08** (2007) 030.
  - [5] A. Vogt, *Comput. Phys. Commun.* **170**, 65 (2005).
  - [6] M. Botje, *Eur. Phys. J. C* **14**, 285 (2000).
  - [7] A. Cafarella, C. Coriano, and M. Guzzi, *Comput. Phys. Commun.* **179**, 665 (2008).
  - [8] G. P. Salam and J. Rojo, *Comput. Phys. Commun.* **180**, 120 (2009).
  - [9] K. Abe *et al.* (E-143 Collaboration), *Phys. Rev. D* **58**, 112003 (1998).
  - [10] B. Adeva *et al.* (SMC Collaboration), *Phys. Rev. D* **58**, 112001 (1998).
  - [11] K. Abe *et al.* (E-154 Collaboration), *Phys. Lett. B* **405**, 180 (1997), *Phys. Rev. Lett.* **79**, 26 (1997).
  - [12] K. Ackersta *et al.* (HERMES Collaboration), *Phys. Lett. B* **404**, 383 (1997).
  - [13] A. Airapetian *et al.* (HERMES Collaboration), *Phys. Lett. B* **442**, 484 (1998).
  - [14] S. Bultmann *et al.*, Report No. SLAC-PUB-7904, 1998.
  - [15] P. L. Anthony *et al.* (E155 Collaboration), *Phys. Lett. B* **463**, 339 (1999).
  - [16] G. Altarelli, R. D. Ball, and S. Forte, *Nucl. Phys.* **B575**, 313 (2000), M. Hirai, S. Kumano, and Myiama, *Comput. Phys. Commun.* **108**, 38 (1998).
  - [17] A. Cafarella and C. Coriano, *Comput. Phys. Commun.* **160**, 213 (2004), *J. High Energy Phys.* **11** (2003) 059.
  - [18] S. J. Farlow, *Partial Differential Equations for Scientists and Engineers* (John Wiley, New York, 1982), I. Sneddon, *Elements of Partial Differential Equations* (McGraw-Hill, New York, 1957).
  - [19] D. K. Choudhury, J. K. Sarma, and G. K. Medhi, *Phys. Lett. B* **403**, 139 (1997), *Gauhati University Journal of Science*, Golden Jubilee volume, 39 (1998), D. K. Choudhury and J. K. Sarma, *Pramana J. Phys.* **38**, 481 (1992).
  - [20] J. K. Sarma and B. Das, *Phys. Lett. B* **304**, 323 (1993).
  - [21] G. Dissertori *et al.*, *J. High Energy Phys.* **02** (2008) 040.

# Semi numerical solution of non-singlet Dokshitzer–Gribov–Lipatov–Altarelli–Parisi evolution equation up to next-to-next-to-leading order at small $x$

R. Baishya<sup>1,a</sup>, J.K. Sarma<sup>2,b</sup>

<sup>1</sup>Physics Department, J. N. College, Boko 781123, Assam, India

<sup>2</sup>Physics Department, Tezpur University, Napam 784028, Assam, India

Received: 1 December 2007 / Revised: 11 December 2008  
© Springer-Verlag / Società Italiana di Fisica 2009

**Abstract** The non-singlet structure functions have been obtained by solving Dokshitzer–Gribov–Lipatov–Altarelli–Parisi (DGLAP) evolution equations in next-next-to-leading order (NNLO) in the small- $x$  limit. Here a Taylor series expansion has been used to solve the evolution equations and we obtain the semi numerical solution. Results are compared with the Fermi Lab experiment E665 data and New Muon Collaboration (NMC) data.

**PACS** 12.38-t · 12.39-x · 13.60.Hb

## 1 Introduction

The one- and two-loop splitting functions have been known for a long time [1–4]. The computation of the three-loop contributions to the anomalous dimensions is needed to complete the NNLO calculations for deep inelastic scattering (DIS). The NNLO corrections should be included in order to arrive at quantitatively reliable predictions for hard processes at present and future high energy colliders. Recently the three-loop splitting functions are introduced with good phenomenological success [5–11]. Though various methods like Laguerre polynomials, brute-force methods, Mellin transformation etc. [12–18] are available in order to obtain a numerical solution of DGLAP evolution equations, exact analytical solutions are not known [11, 19]. Here we solve the DGLAP evolution equation in NNLO analytically to get a semi numerical solution with good agreement with experimental data. Hence it is significant as an important phenomenological work for studying structure functions.

<sup>a</sup> e-mail: rjtboko@yahoo.co.in

<sup>b</sup> e-mail: jks@tezu.ernet.in

## 2 Theory

The DGLAP evolution equation in the non-singlet sector in the standard form is given by

$$\frac{\partial F_2^{\text{NS}}(x, Q^2)}{\partial \ln Q^2} = P_{\text{NS}}(x, Q^2) \otimes F_2^{\text{NS}}(x, Q^2), \quad (2.1)$$

where  $F_2^{\text{NS}}(x, Q^2)$  is the non-singlet structure function as the function of  $x$  and  $Q^2$ , where  $x$  is the Bjorken variable and  $Q^2$  is the four momentum transfer in a DIS process. Here  $P_{\text{NS}}(x, Q^2)$  is the non-singlet kernel known perturbatively up to the first few orders in  $\alpha_S(Q^2)$ , the strong coupling constant. Here  $\otimes$  represents the standard Mellin convolution and the notation is

$$a(x) \otimes b(x) \equiv \int_0^1 \frac{dy}{y} a(y) b\left(\frac{x}{y}\right). \quad (2.2)$$

One can write

$$P_{\text{NS}}(x, Q^2) = \frac{\alpha_S(Q^2)}{2\pi} P_{\text{NS}}^{(0)}(x) + \left(\frac{\alpha_S(Q^2)}{2\pi}\right)^2 P_{\text{NS}}^{(1)}(x) + \left(\frac{\alpha_S(Q^2)}{2\pi}\right)^3 P_{\text{NS}}^{(2)}(x), \quad (2.3)$$

where  $P_{\text{NS}}^{(0)}(x)$ ,  $P_{\text{NS}}^{(1)}(x)$  and  $P_{\text{NS}}^{(2)}(x)$  are non-singlet splitting functions in LO, NLO and NNLO respectively.  $P_{\text{NS}}^{(0)}(x)$  and  $P_{\text{NS}}^{(1)}(x)$  are defined in Ref. [2–4], and using these, the DGLAP equation have been solved up to NLO [1]. By adding  $P_{\text{NS}}^{(2)}(x)$  with previous terms we will get the NNLO evolution equation. The splitting functions  $P_{\text{NS}}^{(2)}(x)$  can be obtained from the N-space results of the Mellin space by an inverse Mellin transformation.

Applying all these and simplifying, the DGLAP evolution equations for the non-singlet structure function in LO,



NLO and NNLO can be written as

$$\frac{\partial F_2^{\text{NS}}}{\partial t} - \frac{\alpha_S(t)}{2\pi} \left[ \frac{2}{3} \{3 + 4 \ln(1-x)\} F_2^{\text{NS}}(x, t) + I_1^{\text{NS}}(x, t) \right] = 0, \tag{2.4}$$

$$\frac{\partial F_2^{\text{NS}}}{\partial t} - \frac{A_f}{t} [\{3 + 4 \ln(1-x)\} F_2^{\text{NS}}(x, t) + I_1^{\text{NS}}(x, t)] - \left( \frac{\alpha_S(t)}{2\pi} \right)^2 I_2^{\text{NS}} = 0 \tag{2.5}$$

and

$$\frac{\partial F_2^{\text{NS}}}{\partial t} - \frac{\alpha_S(t)}{2\pi} \left[ \frac{2}{3} \{3 + 4 \ln(1-x)\} F_2^{\text{NS}}(x, t) + I_1^{\text{NS}}(x, t) \right] - \left( \frac{\alpha_S(t)}{2\pi} \right)^2 I_2^{\text{NS}}(x, t) - \left( \frac{\alpha_S(t)}{2\pi} \right)^3 I_3^{\text{NS}}(x, t) = 0, \tag{2.6}$$

where

$$I_1^{\text{NS}}(x, t) = \frac{4}{3} \int_x^1 \frac{d\omega}{1-\omega} \left[ (1+\omega^2) F_2^{\text{NS}}\left(\frac{x}{\omega}, t\right) - 2 F_2^{\text{NS}}(x, t) \right], \tag{2.7a}$$

$$I_2^{\text{NS}}(x, t) = (x-1) F_2^{\text{NS}}(x, t) \int_0^1 f(\omega) d\omega + \int_x^1 f(\omega) F_2^{\text{NS}}\left(\frac{x}{\omega}, t\right) d\omega \tag{2.7b}$$

and

$$I_3^{\text{NS}}(x, t) = \int_x^1 \frac{d\omega}{\omega} \left[ P_{\text{NS}}^{(2)}(x) F_2^{\text{NS}}\left(\frac{x}{\omega}, t\right) \right]. \tag{2.7c}$$

Here  $t = \ln \frac{Q^2}{\Lambda^2}$ ,  $\Lambda$  is the QCD cut off parameter. Also

$$f(\omega) = C_F^2 [P_F(\omega) - P_A(\omega)] + \frac{1}{2} C_F C_A [P_G + P_A(\omega)] + C_F T_R N_f P_{N_f}(\omega),$$

$$P_F(\omega) = -\frac{2(1+\omega^2)}{(1-\omega)} \ln(\omega) \ln(1-\omega) - \left( \frac{3}{1-\omega} + 2\omega \right) \ln \omega - \frac{1}{2} (1+\omega) \ln \omega + \frac{40}{3} (1-\omega),$$

$$P_G(\omega) = \frac{(1+\omega^2)}{(1-\omega)} \left( \ln^2(\omega) + \frac{11}{3} \ln(\omega) + \frac{67}{9} - \frac{\pi^2}{3} \right) + 2(1+\omega) \ln \omega + \frac{40}{3} (1-\omega),$$

$$P_{N_f}(\omega) = \frac{2}{3} \left[ \frac{1+\omega^2}{1-\omega} \left( -\ln \omega - \frac{5}{3} \right) - 2(1-\omega) \right],$$

$$P_A(\omega) = \frac{2(1+\omega^2)}{(1+\omega)} \int_{\frac{\omega}{1+\omega}}^{\frac{1}{1+\omega}} \frac{dk}{k} \ln\left(\frac{1-k}{k}\right) + 2(1+\omega) \ln(\omega) + 4(1-\omega)$$

and

$$P_{\text{NS}}^{(2)}(x, t) = n_f \left[ \{L_1(-163.9x^{-1} - 7.208x) + 151.49 + 44.51x - 43.12x^2 + 4.82x^3\} (1-x) + L_0 L_1 [-173.1 + 46.18L_0] + 178.04L_0 + 6.892L_0^2 + \frac{40}{27} (L_0^4 - 2L_0^3) \right]$$

with  $C_A = C_G = 3$ ,  $L_0 = \ln(x)$ ,  $L_1 = \ln(1-x)$ . Here results are from direct  $x$ -space evolution [8, 9, 20].

The strong coupling constant,  $\alpha_S(Q^2)$ , is related with the  $\beta$ -function by

$$\beta(\alpha_S) = \frac{\partial \alpha_S(Q^2)}{\partial \log Q^2} = -\frac{\beta_0}{4\pi} \alpha_S^2 - \frac{\beta_1}{16\pi^2} \alpha_S^3 - \frac{\beta_2}{64\pi^3} \alpha_S^4 + \dots,$$

where

$$\beta_0 = \frac{11}{3} N_C - \frac{4}{3} T_f,$$

$$\beta_1 = \frac{34}{3} N_C^2 - \frac{10}{3} N_C N_f - 2 C_F N_f$$

and  $\beta_2 = \frac{2857}{54} N_C^3 + 2 C_F^2 T_f - \frac{205}{9} C_F N_C T_f + \frac{44}{9} C_F T_f^2 + \frac{158}{27} N_C T_f^2$  are the one-loop, two-loop and three-loop corrections to the QCD  $\beta$ -function and  $N_f$  being the flavor number.

We have set  $N_C = 3$ ,  $C_F = \frac{N_C^2-1}{2N_C} = \frac{4}{3}$  and  $T_f = \frac{1}{2} N_f$ , with

$$\frac{\alpha(Q^2)}{2\pi} = \frac{2}{\beta_0 t} \left[ 1 - \frac{\beta_1 \log t}{\beta_0^2 t} + \frac{1}{\beta_0^3 t} \left\{ \frac{\beta_1^2}{\beta_0} (\log^2 t - \log t - 1) + \beta_2 \right\} + O\left(\frac{1}{t^3}\right) \right].$$

Now let us introduce the variable  $u = 1 - \omega$ , and since  $x < \omega < 1$ , we have  $0 < u < 1 - x$ ; hence the series is convergent for  $|u| < 1$  and we can use Taylor's expansion series

$$F_2^{\text{NS}}\left(\frac{x}{\omega}, t\right) = F_2^{\text{NS}}\left(x + \frac{xu}{1-u}, t\right) = F_2^{\text{NS}}(x, t) + \frac{xu}{1-u} \frac{\partial F_2^{\text{NS}}(x, t)}{\partial x} + \frac{1}{2} \left( \frac{xu}{1-u} \right)^2 \frac{\partial^2 F_2^{\text{NS}}(x, t)}{\partial x^2} + \dots$$

It has been observed that if we introduce the higher order terms in a Taylor expansion, then also there is no modification of the solution. Because when we solve the second order partial differential equation by the Monges method, which will be produced by introducing the second order terms in Taylor expansion, ultimately it becomes of the first order as before, due to the form of the DGLAP equation. Similarly by introducing more terms in a Taylor expansion, we hope for these cases also the terms can be neglected due to the still smaller values of  $x$  [21, 22]. Hence we can rewrite

$$F_2^{NS}\left(\frac{x}{\omega}, t\right) \approx F_2^{NS}(x, t) + \frac{xu}{1-u} \frac{\partial F_2^{NS}(x, t)}{\partial x}. \tag{2.8}$$

Using (2.8) in (2.7a), (2.7b) and (2.7c), and performing the  $u$ -integrations, (2.4), (2.5) and (2.6) become of the form

$$\frac{\partial F_2^{NS}(x, t)}{\partial t} - \frac{\alpha_S}{2\pi} \left[ A_1(x) F_2^{NS}(x, t) + A_2(x) \frac{\partial F_2^{NS}(x, t)}{\partial x} \right] = 0, \tag{2.9a}$$

$$\frac{\partial F_2^{NS}(x, t)}{\partial t} - \frac{\alpha_S}{2\pi} \left[ A_1(x) F_2^{NS}(x, t) + A_2(x) \frac{\partial F_2^{NS}(x, t)}{\partial x} \right] - \left(\frac{\alpha_S}{2\pi}\right)^2 \left[ B_1(x) F_2^{NS}(x, t) + B_2(x) \frac{\partial F_2^{NS}(x, t)}{\partial x} \right] = 0 \tag{2.9b}$$

and

$$\frac{\partial F_2^{NS}(x, t)}{\partial t} - \frac{\alpha_S}{2\pi} \left[ A_1(x) F_2^{NS}(x, t) + A_2(x) \frac{\partial F_2^{NS}(x, t)}{\partial x} \right] - \left(\frac{\alpha_S}{2\pi}\right)^2 \left[ B_1(x) F_2^{NS}(x, t) + B_2(x) \frac{\partial F_2^{NS}(x, t)}{\partial x} \right] - \left(\frac{\alpha_S}{2\pi}\right)^3 \left[ C_1(x) F_2^{NS}(x, t) + C_2(x) \frac{\partial F_2^{NS}(x, t)}{\partial x} \right] = 0, \tag{2.9c}$$

where

$$\begin{aligned} A_1(x) &= 2x + x^2 + 4 \ln(1 - x), \\ A_2(x) &= x - x^3 - 2x \ln(x), \\ B_1(x) &= x \int_0^1 f(\omega) d\omega - \int_0^x f(\omega) d\omega \\ &\quad + \frac{4}{3} N_f \int_x^1 F_{qq}(\omega) d\omega, \end{aligned}$$

$$B_2(x) = x \int_x^1 \left[ f(\omega) + \frac{4}{3} N_f F_{qg}^S(\omega) \right] \frac{1-\omega}{\omega} d\omega,$$

$C_1(x)$

$$\begin{aligned} &= n_f \int_0^{1-x} \frac{d\omega}{1-\omega} \\ &\quad \times \left[ \ln(\omega) (-163.9(1-\omega)^{-1} - 7.208(1-\omega)) + 151.49 \right. \\ &\quad \left. + 44.51(1-\omega) - 43.12(1-\omega)^2 + 4.82(1-\omega)^3 \right] \omega \\ &\quad + \left\{ \ln(\omega) \ln(1-\omega) [-173.1 + 46.18 \ln(1-\omega)] \right. \\ &\quad \left. + 178.04 \ln(1-\omega) + 6.892 \ln^2(1-\omega) \right. \\ &\quad \left. + \frac{40}{27} (\ln^4(1-\omega) - 2 \ln^3(1-\omega)) \right\}, \end{aligned}$$

and

$C_2(x)$

$$\begin{aligned} &= n_f \int_0^{1-x} \frac{x d\omega}{(1-\omega)^2} \\ &\quad \times \left[ \ln(\omega) (-163.9(1-\omega)^{-1} - 7.208(1-\omega)) + 151.49 \right. \\ &\quad \left. + 44.51(1-\omega) - 43.12(1-\omega)^2 + 4.82(1-\omega)^3 \right] \omega \\ &\quad + \left\{ \ln(\omega) \ln(1-\omega) [-173.1 + 46.18 \ln(1-\omega)] \right. \\ &\quad \left. + 178.04 \ln(1-\omega) + 6.892 \ln^2(1-\omega) \right. \\ &\quad \left. + \frac{40}{27} (\ln^4(1-\omega) - 2 \ln^3(1-\omega)) \right\}. \end{aligned}$$

Hence (2.9a), (2.9b) and (2.9c) take the forms

$$-t \frac{\partial F_2^{NS}(x, t)}{\partial t} + L_1(x) \frac{\partial F_2^{NS}(x, t)}{\partial x} + M_1(x) F_2^{NS}(x, t) = 0, \tag{2.10a}$$

$$-t \frac{\partial F_2^{NS}(x, t)}{\partial t} + L_2(x) \frac{\partial F_2^{NS}(x, t)}{\partial x} + M_2(x) F_2^{NS}(x, t) = 0 \tag{2.10b}$$

and

$$\begin{aligned}
 & -t \frac{\partial F_2^{NS}(x, t)}{\partial t} + L_3(x) \frac{\partial F_2^{NS}(x, t)}{\partial x} \\
 & + M_3(x) F_2^{NS}(x, t) = 0
 \end{aligned}
 \tag{2.10c}$$

where  $L_1(x) = \frac{2}{\beta_0}(A_2)$ ,  $M_1(x) = \frac{2}{\beta_0}(A_1)$ ,

$$L_2(x) = \frac{2}{\beta_0} \left[ 1 - \frac{\beta_1 \log t}{\beta_0^2 t} \right] (A_2 + T_0 B_2),$$

$$M_2(x) = \frac{2}{\beta_0} \left[ 1 - \frac{\beta_1 \log t}{\beta_0^2 t} \right] (A_1 + T_0 B_1),$$

$$\begin{aligned}
 L_3(x) &= \frac{2}{\beta_0} \left[ 1 - \frac{\beta_1 \log t}{\beta_0^2 t} + \frac{1}{\beta_0^3 t} \right. \\
 &\quad \times \left. \left\{ \frac{\beta_1^2}{\beta_0} (\log^2 t - \log t - 1) + \beta_2 \right\} \right] \\
 &\quad \times (A_2 + T_0 B_2 + T_1 C_2)
 \end{aligned}$$

and

$$\begin{aligned}
 M_3(x) &= \frac{2}{\beta_0} \left[ 1 - \frac{\beta_1 \log t}{\beta_0^2 t} + \frac{1}{\beta_0^3 t} \right. \\
 &\quad \times \left. \left\{ \frac{\beta_1^2}{\beta_0} (\log^2 t - \log t - 1) + \beta_2 \right\} \right] \\
 &\quad \times (A_1 + T_0 B_1 + T_1 C_1).
 \end{aligned}$$

Here we consider the two numerical parameters  $T_0$  and  $T_1$ , such that  $T^2(t) = T_0 \cdot T(t)$  and  $T^3(t) = T_1 \cdot T(t)$  with  $T(t) = \frac{\alpha_S(t)}{2\pi}$ , where  $T_0$  and  $T_1$  are two suitable numerical parameters. It is observed from Fig. 2.1 that the values of  $T^2(t)$  and  $T_0 \cdot T(t)$  as well as  $T^3(t)$  and  $T_1 \cdot T(t)$  are comparatively same. Due to the introduction of these two para-

eters the numerical error is very much less as compared to the other errors.

The general solution [23–26] of (2.10a) is  $F(U, V) = 0$ , where  $F(U, V)$  is an arbitrary function. Here  $U(x, t, F_2^{NS}) = K_1$  and  $V(x, t, F_2^{NS}) = K_2$  are two independent solutions of the equation

$$\frac{dx}{L_1(x, t)} = \frac{dt}{-t} = \frac{dF_2^{NS}(x, t)}{-M_1(x, t) F_2^{NS}(x, t)}. \tag{2.11}$$

Solving equation (2.11) we obtain

$$U(x, t, F_2^{NS}) = t \cdot \exp \left[ \int \frac{1}{L_1(x)} dx \right] \text{ and}$$

$$V(x, t, F_2^{NS}) = F_2^{NS}(x, t) \exp \left[ \int \frac{M_1(x)}{L_1(x)} dx \right].$$

It thus has no unique solution. The simplest possibility is that a linear combination of  $U$  and  $V$  is to satisfy  $F(U, V) = 0$  so that  $\alpha \cdot U + \beta \cdot V = 0$ , where  $\alpha$  and  $\beta$  are arbitrary constants [21, 22]. Putting the values of  $U$  and  $V$  in this equation we get

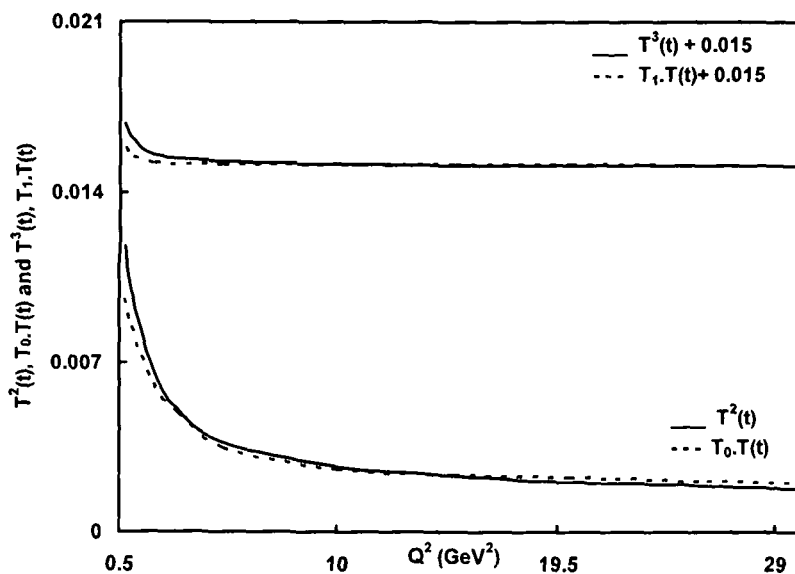
$$\begin{aligned}
 & \alpha t \cdot \exp \left[ \int \frac{1}{L_1(x)} dx \right] + \beta \cdot F_2^{NS}(x, t) \\
 & \quad \times \exp \left[ \int \frac{M_1(x)}{L_1(x)} dx \right] = 0,
 \end{aligned}
 \tag{2.12}$$

which implies that

$$\begin{aligned}
 F_2^{NS}(x, t) &= -\gamma \cdot t \cdot \\
 & \quad \times \exp \left[ \int \left( \frac{1}{L_1(x)} - \frac{M_1(x)}{L_1(x)} \right) dx \right],
 \end{aligned}
 \tag{2.13}$$

where  $\gamma = \frac{\alpha}{\beta}$  is another constant.

**Fig. 2.1**  $T^2(t)$ ,  $T_0 \cdot T(t)$  and  $T^3(t)$ ,  $T_1 \cdot T(t)$  versus  $Q^2$  ( $\text{GeV}^2$ )



Now, defining

$$F_2^{NS}(x, t_0) = -\gamma \cdot t_0 \exp \left[ \int \left( \frac{1}{L_1(x)} - \frac{M_1(x)}{L_1(x)} \right) dx \right],$$

at  $t = t_0$ , where,  $t_0 = \ln(Q_0^2/\Lambda^2)$  at any lower value  $Q = Q_0$ , we get from (2.13)

$$F_2^{NS}(x, t) = F_2^{NS}(x, t_0) \left( \frac{t}{t_0} \right). \tag{2.14a}$$

Again defining

$$F_2^{NS}(x_0, t) = -\gamma t \cdot \exp \left[ \int \left( \frac{1}{L_1(x)} - \frac{M_1(x)}{L_1(x)} \right) dx \right]_{x=x_0},$$

we obtain

$$F_2^{NS}(x, t) = F_2^{NS}(x_0, t) \times \exp \left[ \int_{x_0}^x \left( \frac{1}{L_1(x)} - \frac{M_1(x)}{L_1(x)} \right) dx \right]. \tag{2.14b}$$

Equations (2.14a) and (2.14b) give the  $t$ - and  $x$ -evolution of the non-singlet structure function  $F_2^{NS}(x, t)$  in LO, respectively.

To get the solution of (2.10b) and (2.10c), let us introduce functions  $\bar{L}_i(x)$  such that  $L_i(x, t) = \frac{\beta_0 t}{2} T(t) \bar{L}_i(x)$ . Then (2.10b) and (2.10c) become

$$F_2^{NS}(x, t) = -\gamma t^{(1+\frac{b}{\beta_1})} e^{\frac{b}{t}} \times \exp \left[ \int \left( \frac{1}{\bar{L}_2(x)} - \frac{M_2(x)}{\bar{L}_2(x)} \right) dx \right] \tag{2.15}$$

and

$$F_2^{NS}(x, t) = -\gamma t^{1+(\frac{b-b^2}{\beta_1})} e^{(\frac{b-c-b^2 \ln^2 t}{t})} \times \exp \left[ \int dx \left( \frac{1}{\bar{L}_3(x)} - \frac{M_3(x)}{\bar{L}_3(x)} \right) \right]. \tag{2.16}$$

Now, defining

$$F_2^{NS}(x, t_0) = -\gamma t_0^{(1+\frac{b}{\beta_0})} e^{\frac{b}{t_0}} \exp \left[ \int \left( \frac{1}{\bar{L}_2(x)} - \frac{M_2(x)}{\bar{L}_2(x)} \right) dx \right]$$

at  $t = t_0$ , where  $t_0 = \ln(Q_0^2/\Lambda^2)$  at any lower value  $Q = Q_0$ , (2.15) gives

$$F_2^{NS}(x, t) = F_2^{NS}(x, t_0) \left( \frac{t^{(1+b/t)}}{t_0^{(1+b/t_0)}} \right) e^{(\frac{b}{t} - \frac{b}{t_0})}. \tag{2.17a}$$

Again defining

$$F_2^{NS}(x_0, t) = -\gamma t^{(1+\frac{b}{\beta_1})} e^{\frac{b}{t}} \times \exp \left[ \int \left( \frac{1}{\bar{L}_2(x)} - \frac{M_2(x)}{\bar{L}_2(x)} \right) dx \right]_{x=x_0}, \tag{2.17b}$$

$$F_2^{NS}(x, t) = F_2^{NS}(x_0, t) \exp \left[ \int_{x_0}^x \left( \frac{1}{\bar{L}_2(x)} - \frac{M_2(x)}{\bar{L}_2(x)} \right) dx \right].$$

Equations (2.17a) and (2.17b) give the  $t$ - and  $x$ -evolution of the non-singlet structure function  $F_2^{NS}(x, t)$  in NLO, respectively.

Proceeding in the same way, the  $t$ - and  $x$ -evolutions of the non-singlet structure function  $F_2^{NS}(x, t)$  in NNLO can be obtained from (2.16) as

$$F_2^{NS}(x, t) = F_2^{NS}(x, t_0) \times \left( \frac{t^{(b-b^2)/t}}{t_0^{(b-b^2)/t_0}} \right) e^{(-b^2 \frac{\ln^2 t}{t} + b^2 \frac{\ln^2 t_0}{t_0})} \tag{2.18a}$$

and

$$F_2^{NS}(x, t) = F_2^{NS}(x_0, t) \times \exp \left[ \int_{x_0}^x \left( \frac{1}{\bar{L}_3(x)} - \frac{M_3(x)}{\bar{L}_3(x)} \right) dx \right] \tag{2.18b}$$

with  $b = \frac{\beta_1}{\beta_0^2}$  and  $c = \frac{\beta_2}{\beta_0^3}$ .

To compare our result with experimental data, we have to consider the relation between proton and deuteron structure functions measured in DIS with the non-singlet quark distribution function:  $F_2^{NS}(x, t) = 3[2F_2^p(x, t) - F_2^d(x, t)]$ .

### 3 Results and discussion

In this report, we have compared our results of  $t$ - and  $x$ -evolutions of the non-singlet structure function  $F_2^{NS}(x, t)$  with E665 experiment data [27] (taken at Fermi Lab in inelastic muon scattering with an average beam energy of 470 GeV<sup>2</sup>) and NMC data [28] (in muon-deuteron DIS with incident momentum 90, 120, 200, 280 GeV<sup>2</sup>). Figures 3.1a and 3.2a represent the  $t$ -evolution of a non-singlet structure function where our computed values from (2.14a), (2.17a) and (2.18a) are plotted against  $Q^2$  for different values of  $x$ . In the  $x$ -evolutions at Figs. 3.1b and 3.2b, our computed values from (2.14b), (2.17b) and (2.18b) are plotted against  $x$  for different values of  $Q^2$ . Here vertical error bars are statistical and systematic uncertainties. In all graphs, lowest- $t$  and highest- $x$  points are taken as inputs for  $F_2^{NS}(x, t_0)$  and  $F_2^{NS}(x_0, t)$  respectively. It is observed from the figures that

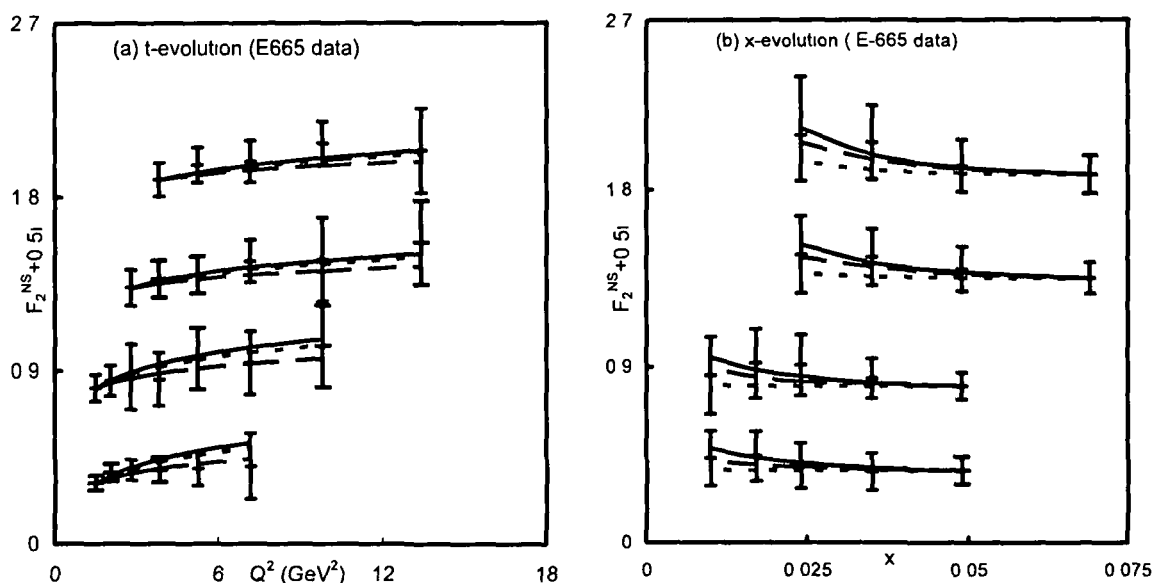


**Fig. 3.1** a, b E665 data *Dotted lines* are our LO, *dashed lines* are NLO and *solid lines* are NNLO results For clarity, data are scaled up by  $+0.5i$  ( $i = 0, 1, 2, 3$ ) starting from the bottom of all graphs in each figure

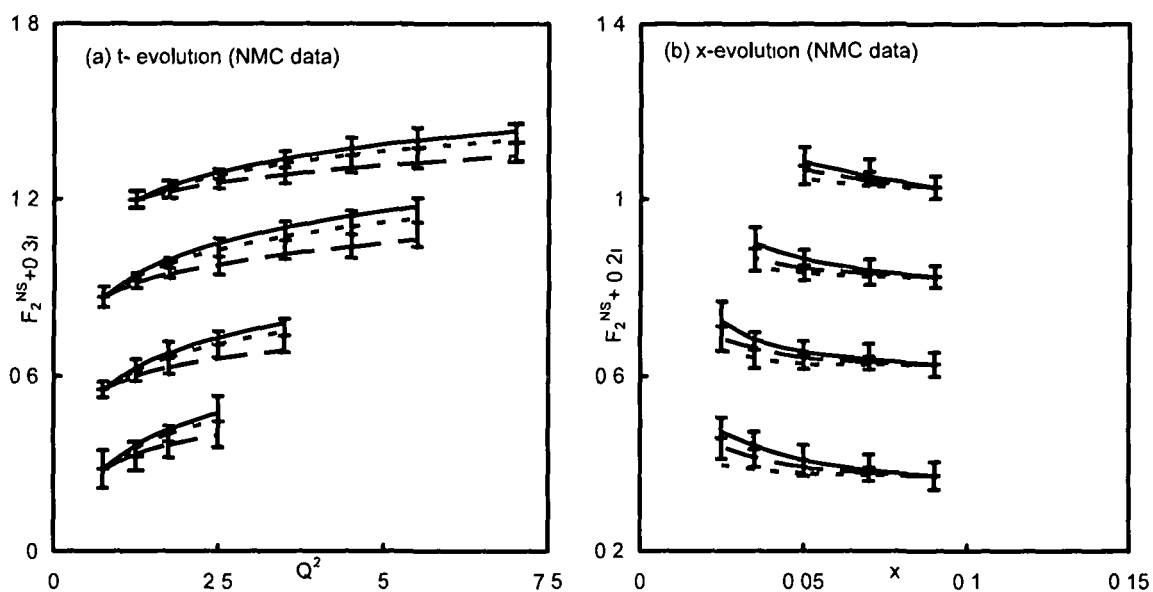


**Fig. 3.2** a, b NMC data *Dotted lines* are LO results, *dashed lines* are NLO and *solid lines* are our NNLO results For clarity, data are scaled up by  $+0.3i$  (in Fig 3.1a) and  $+0.2i$  (in Fig 3.1b) (with  $i = 0, 1, 2, 3$ ) starting from the bottom of all graphs in each figure

for LO, NLO and NNLO the total contributions are better in the higher- $Q^2$  and smaller- $x$  region This is so because the DGLAP equations hold well in the higher- $Q^2$  and smaller- $x$  region

## References

- 1 R Baishya, J K Sarma, Phys Rev D **74**, 107702 (2006) arXiv hep-ph/07070412
- 2 W Furmanski, R Petronzio, Phys Lett B **97**, 437 (1980)
- 3 W Furmanski, R Petronzio, Z Phys C **11**, 293 (1982)
- 4 W Furmanski, R Petronzio, Nucl Phys B **195**, 237 (1982)
- 5 W L van Neerven, A Vogt, Nucl Phys B **588**, 345 (2000) arXiv hep-ph/0006154
- 6 W L van Neerven, A Vogt, Nucl Phys B **568**, 263 (2000) arXiv hep-ph/9907472
- 7 W L van Neerven, A Vogt, Phys Lett B **490**, 111 (2000) arXiv hep-ph/0007362
- 8 S Moch, J A M Vermaseren, A Vogt, Nucl Phys Proc Suppl **116**, 100 (2003) arXiv hep-ph/0211296

- 9 S Moch, J A M Vermaseren, A Vogt, Nucl Phys B **688**, 101 (2004) arXiv hep-ph/0403192
- 10 S Moch, J A M Vermaseren, Nucl Phys B **573**, 853 (2000) arXiv hep-ph/9912355
- 11 M Hirai, S Kumano, X Myiama, Comput Phys Commun **108**, 38 (1998)
- 12 R Toldra, Comput Phys Commun **143**, 287 (2002)
- 13 N Cabibbo, R Petronzio, Nucl Phys B **137**, 395 (1978)
- 14 M Gluck, E Reya, A Vogt, Z Phys C **48**, 471 (1990)
- 15 M Stramann, W Vogelsang, Phys Rev D **64**, 114007 (2001)
- 16 A Vogt, Comput Phys Commun **170**, 65 (2005) arXiv hep-ph/0408244
- 17 M Dasgupta, G P Salam, Eur Phys J C **24**, 213 (2002) arXiv hep-ph/0110213
- 18 S Weinzierl, Comput Phys Commun **148**, 314 (2002) arXiv hep-ph/0203112
- 19 A Cafarella, C Coriand, M Guzi, Nucl Phys B **748**, 253 (2006) arXiv hep-ph/0512358
- 20 T Gehrman, E Remiddi, Comput Phys Commun **141**, 296 (2001) arXiv hep-ph/0107173
- 21 J K Sarma, D K Choudhury, G K Medhi, Phys Lett B **403**, 139 (1997)
- 22 J K Sarma, B Das, Phys Lett B **304**, 323 (1993)
- 23 F Ayres Jr, *Differential Equations* Schaum's Outline Series (McGraw-Hill, New York, 1988)
- 24 F H Miller, *Partial Differential Equation* (Wiley, New York, 1960)
- 25 I Sneddon, *Elements of Partial Differential Equations* (McGraw-Hill, New York, 1957)
- 26 S J Farlow, *Partial Differential Equation for Scientist and Engineers* (Wiley, New York, 1982)
- 27 M R Adams et al (E665), Phys Rev D **54**, 3006 (1996)
- 28 M Arneodo et al (CERN-NA-037, NMC), Nucl Phys B **483**, 3 (1997)



## Solution of non-singlet DGLAP evolution equation in leading order and next to leading order at small-x

R Baishya<sup>1\*</sup> and J K Sarma<sup>2</sup>

<sup>1</sup>Department of Physics J N College Boko-781 123 Assam India

<sup>2</sup>Department of Physics Tezpur University Napaam 784 028 Assam India

Email rjtboko@yahoo.co.in

Received 15 July 2008 accepted 12 February 2009

---

**Abstract** The non singlet structure functions have been obtained by solving Dokshitzer Gribove Lipatov Alterelli Parisi (DGLAP) evolution equations in leading order (LO) and next to leading order (NLO) at the small x limit. Here a Taylor Series expansion has been used and then the method of characteristics has been used to solve the evolution equations. We have also calculated t and x evolutions of deuteron structure function and the results are compared with the New Muon Collaboration (NMC) and E665 data.

**Keywords** DIS DGLAP equation small x method of characteristics structure function

**PACS Nos** 12.35.Eq 12.38.t 12.39.x 13.60.Hb

---

### 1. Introduction

Structure functions in deep-inelastic lepton-hadron scattering (DIS) remain among the most important probes of perturbative Quantum Chromodynamics (PQCD) and of the partonic structure of hadrons. Indeed, experiments have proceeded towards very high accuracy and a greatly extended kinematic coverage during the past two decades. An accurate knowledge of the parton densities will be indispensable for interpreting many results at the future for hadrons structure. The non-perturbative Bjorken-x dependence of the structure functions at one scale, the scaling violations can be calculated in the QCD-improved parton model in terms of a power series expansion in the strong coupling constant  $\alpha_s$ . The next-to-leading order (NLO) ingredients for such analyses are available since 1980 for unpolarized structure functions in mass less perturbative QCD [1]. The corresponding

---

\*Corresponding Author

results for the next-to-next-to leading order (NNLO) are complete at present, though there is enormous complexity in the required loop calculations [2-6]. One of the most useful and famous evolution equation is the Dokshitzer, Gribov, Lipatov, Alterelli, Parisi (DGLAP) equation [7-14] to give  $t \left[ = \ln \left( Q^2 / \Lambda^2 \right) \right]$ ,  $\Lambda$ , is the QCD cut off parameter] and  $x$  evolutions of structure functions. Hence the solutions of DGLAP evolution equations give quark and gluon structure functions that produce ultimately proton, neutron and deuteron structure functions.

Though various methods are available in order to obtain a numerical solution of DGLAP evolution equations, exact analytical solutions of these equations are not known [5-6]. Various analytical methods have been reported to solve DGLAP evolution equations and one of the limitations of these solutions is that, as they are partial differential equations (PDE), their ordinary solutions are not unique one. On the other hand, this limitation can be overcome by using method of characteristics [15-18]. The singlet structure functions at small- $x$  in LO and NLO have been obtained from DGLAP equation by using the method of characteristics in the Ref. [18]. In this paper, we obtain a solution of DGLAP equations for non-singlet structure functions at small- $x$  in LO and NLO by using the method of characteristics. The results are compared with E665 and NMC data [19, 20].

## 2. Theory

The non singlet combinations of quark and anti quark densities,  $q_i$  and  $q_i^-$ , are given by

$$q_{NS}^{\pm} = q_i \pm q_i^- - (q_u \pm q_u^-), \quad q_{NS}^V = \sum_{r=1}^{N_f} (q_r - q_r^-) \quad (1)$$

$N_f$  stands for the number of effectively massless flavours. The corresponding splitting functions are denoted by  $P_{NS}^{\pm}$  and  $P_{NS}^V = P_{NS}^- + P_{NS}^S$ . For an integro-differential equation of DGLAP type, which is in a perturbative fashion, the kernel  $P(x)$  is known perturbatively up to the first few orders in  $\alpha_s$ , approximations which are commonly known as LO, NLO, NNLO. The evolution equation in the non singlet sector [21-23] is

$$\frac{\partial F_2^{NS}(x, Q^2)}{\partial \ln Q^2} = P_{NS}(x, Q^2) \otimes F_2^{NS}(x, Q^2) \quad (2)$$

Here  $\otimes$  stand for the Mellin convolution in the momentum variable [4, 6] and define as

$$a(x) \otimes b(x) \equiv \int_0^1 \frac{dy}{y} a(y) b\left(\frac{x}{y}\right) \quad (3)$$



Also

$$P(x, Q^2) = \frac{\alpha_s(Q^2)}{2\pi} \rho^{(0)}(x) + \left( \frac{\alpha_s(Q^2)}{2\pi} \right)^2 \rho^{(1)}(x) + \dots \quad (4)$$

Here  $\rho^{(0)}(x)$ ,  $\rho^{(1)}(x)$  are splitting functions [24] in LO, NLO respectively. The DGLAP evolution equations for non-singlet structure functions in LO and NLO [1, 21, 22] can be written as

$$\frac{\partial F_2^{NS}}{\partial t} - \frac{\alpha_s(t)}{2\pi} \left[ \frac{2}{3} \{3 + 4 \ln(1-x)\} F_2^{NS}(x,t) + I_1^{NS}(x,t) \right] = 0 \quad (5)$$

$$\frac{\partial F_2^{NS}}{\partial t} - \frac{A_V}{t} \left[ \{3 + 4 \ln(1-x)\} F_2^{NS}(x,t) + I_1^{NS}(x,t) \right] - \left( \frac{\alpha_s(t)}{2\pi} \right)^2 I_2^{NS} = 0 \quad (6)$$

where

$$I_1^{NS}(x,t) = \frac{4}{3} \int_x^1 \frac{d\omega}{1-\omega} \left[ (1+\omega^2) F_2^{NS}\left(\frac{x}{\omega}, t\right) - 2F_2^{NS}(x,t) \right], \quad (7a)$$

$$I_2^{NS} = \left[ (x-1) F_2^{NS}(x,t) \int_0^1 f(\omega) d\omega + \int_x^1 f(\omega) F_2^{NS}\left(\frac{x}{\omega}, t\right) d\omega \right]. \quad (7b)$$

$$f(\omega) = C_F^2 [P_F(\omega) - P_A(\omega)] + \frac{1}{2} C_F C_A [P_G + P_A(\omega)] + C_F T_R N_f P_{N_f}(\omega),$$

$$P_F(\omega) = -\frac{2(1+\omega^2)}{(1-\omega)} \ln(\omega) \ln(1-\omega) - \left( \frac{3}{1-\omega} + 2\omega \right) \ln\omega - \frac{1}{2}(1+\omega) \ln\omega + \frac{40}{3}(1-\omega),$$

$$P_G(\omega) = \frac{(1+\omega^2)}{(1-\omega)} \left[ \ln^2(\omega) + \frac{11}{3} \ln(\omega) + \frac{67}{9} - \frac{\pi^2}{3} \right] + 2(1+\omega) \ln\omega + \frac{40}{3}(1-\omega),$$

$$P_{N_f}(\omega) = \frac{2}{3} \left[ \frac{1+\omega^2}{1-\omega} \left( -\ln\omega - \frac{5}{3} \right) - 2(1-\omega) \right],$$

$$P_A(\omega) = \frac{2(1+\omega^2)}{(1+\omega)} \int_{\left(\frac{\omega}{1+\omega}\right)}^{\left(\frac{1}{1+\omega}\right)} \frac{dk}{k} \ln\left(\frac{1-k}{k}\right) + 2(1+\omega) \ln(\omega) + 4(1-\omega),$$

with  $C_A=C_G=3$ ,  $C_F = \frac{(N_f^2 - 1)}{2N_f}$ ,  $T_f = \frac{1}{2}$ ,  $\alpha_s(t) = \frac{4\pi}{\beta_0 t} \left[ 1 - \frac{\beta_1 \ln t}{\beta_0^2 t} \right]$ .

$\beta_0 = 11 - \frac{2}{3}N_f$  and  $\beta_1 = 102 - \frac{38}{3}N_f$  are the one loop (LO) and two loop (NLO) correction to the QCD  $\beta$ -function and  $N_f$  being the flavors number. We can neglect  $\beta_1$  for LO.

Let us introduce the variable  $u = 1 - \omega$  and since  $x < \omega < 1$ , so  $0 < u < 1 - x$ , hence the series is convergent for  $|u| < 1$ .

Now  $\frac{x}{\omega} = \frac{x}{1-u} = \left( x + \frac{xu}{1-u} \right)$ .

So, using Taylor's expansion series we can rewrite

$$\begin{aligned} F_2^{NS} \left( \frac{x}{\omega}, t \right) &= F_2^{NS} \left( x + \frac{xu}{1-u}, t \right) \\ &= F_2^{NS} (x, t) + \frac{xu}{1-u} \frac{\partial F_2^{NS} (x, t)}{\partial x} + \frac{1}{2} \left( \frac{xu}{1-u} \right)^2 \frac{\partial^2 F_2^{NS} (x, t)}{\partial x^2} + \dots \\ F_2^{NS} \left( \frac{x}{\omega}, t \right) &= F_2^{NS} (x, t) + \frac{xu}{1-u} \frac{\partial F_2^{NS} (x, t)}{\partial x} \end{aligned} \quad (8)$$

Since  $x$  is small in our region of discussion, the terms containing  $x^2$  and higher powers of  $x$  can be neglected. Using eq. (8) in eq. (7a) and (7b) and performing  $u$ -integrations, eq. (5) becomes the form

$$-t \frac{\partial F_2^{NS} (x, t)}{\partial t} + A_V A(x) F_2^{NS} (x, t) + A_V B(x) \frac{\partial F_2^{NS}}{\partial x} = 0 \quad (9)$$

where

$$A_V = \frac{\alpha_s(t)}{3\pi} t = \frac{4}{3\beta_0} = \frac{4}{33 - 2N_f}$$

$$A(x) = 2x + x^2 + 4 \ln(1-x), \quad (10a)$$

$$B(x) = x - x^3 - 2x \ln(x), \quad (10b)$$

To introduce method of characteristics, let us consider two new variables  $S$  and  $\tau$  instead of  $x$  and  $t$ , such that

$$\frac{dt}{dS} = -t, \tag{11a}$$

$$\frac{dx}{dS} = A_\gamma B(x) \tag{11b}$$

which are known as characteristics eqs. [15-18]. Putting these equations in (9), we get

$$\frac{dF_2^{NS}(S, \tau)}{dS} + L(S, \tau)F_2^{NS}(S, \tau) = 0, \tag{12}$$

which can be solved as-

$$F_2^{NS}(S, \tau) = F_2^{NS}(\tau) \left( \frac{t}{t_0} \right)^{L(S, \tau)}, \tag{13}$$

where  $L(S, \tau) = 3/2 A_\gamma A(x)$  and  $F_2^{NS}(S, \tau) = F_2^{NS}(\tau)$  for initial condition  $S = 0, t = t_0$ .

Now we have to replace the co-ordinate system  $(S, \tau)$  to  $(x, t)$  with the input function  $F_2^{NS}(\tau) = F_2^{NS}(x, t_0)$  and will get the  $t$ - evolution of non singlet structure function in the LO as

$$F_2^{NS}(x, t) = F_2^{NS}(x, t_0) \left( \frac{t}{t_0} \right)^{\frac{3}{2} A_\gamma A(x)} \tag{14a}$$

Similarly the  $x$ - evolution of non singlet structure function will be

$$F_2^{NS}(x, t) = F_2^{NS}(x_0, t) \exp \left[ - \int_{x_0}^x \frac{A(x)}{B(x)} dx \right]. \tag{14b}$$

In the NLO, the  $t$  and  $x$  evolution of non singlet structure functions will be obtain as

$$F_2^{NS}(x, t) = F_2^{NS}(x, t_0) \left( \frac{t}{t_0} \right)^{\frac{3}{2} A_\gamma [A(x) + T_{\sigma A}(x)]}, \tag{15a}$$

$$F_2^{NS}(x,t) = F_2^{NS}(x_0,t) \exp \left[ - \int_{x_0}^x \frac{A(x) + T_0 A_1(x)}{B(x) + T_0 B_1(x)} dx \right], \tag{15b}$$

with

$$A_1(x) = x \int_0^1 f(\omega) d\omega - \int_0^x f(\omega) d\omega + \frac{4}{3} N_f \int_x^1 F_{qq}(\omega) d\omega, \tag{16a}$$

$$B_1(x) = x \int_x^1 \left[ f(\omega) + \frac{4}{3} N_f F_{qq}^S(\omega) \right] \frac{1-\omega}{\omega} d\omega. \tag{16b}$$

Here we introduce an extra assumption  $\left( \frac{\alpha_s(t)}{2\pi} \right)^2 = T_0 \left( \frac{\alpha_s(t)}{2\pi} \right)$  [18], where  $T_0$  is a numerical parameter. By a suitable choice of  $T_0$  we can reduce the error to a minimum.

To compare our results with experimental data, we have to consider the relations between deuteron and proton structure functions measured in DIS with non-singlet quark distribution functions as

$$F_2^{NS}(x,t) = 3 \{ 2F_2^p(x,t) - F_2^d(x,t) \}. \tag{17}$$

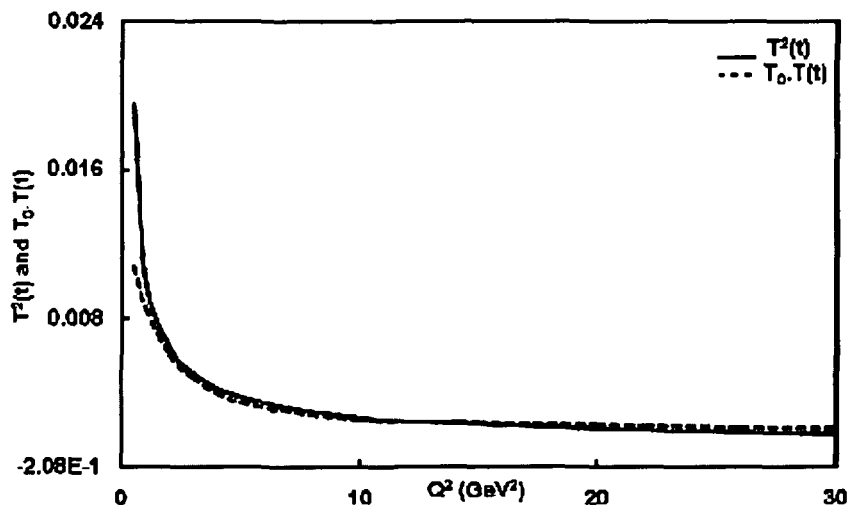


Figure 1.  $T^2$  and  $T_0 T$  curves.

3. Results and discussion

Here, we compare our result of  $t$  and  $x$  evolution of non-singlet structure function  $F_2^{NS}$  measured by E665 [19] (The data were taken at Fermilab experiment E665 in inelastic muon scattering with an average beam energy of 470 GeV) and NMC [20] (NMC in muon

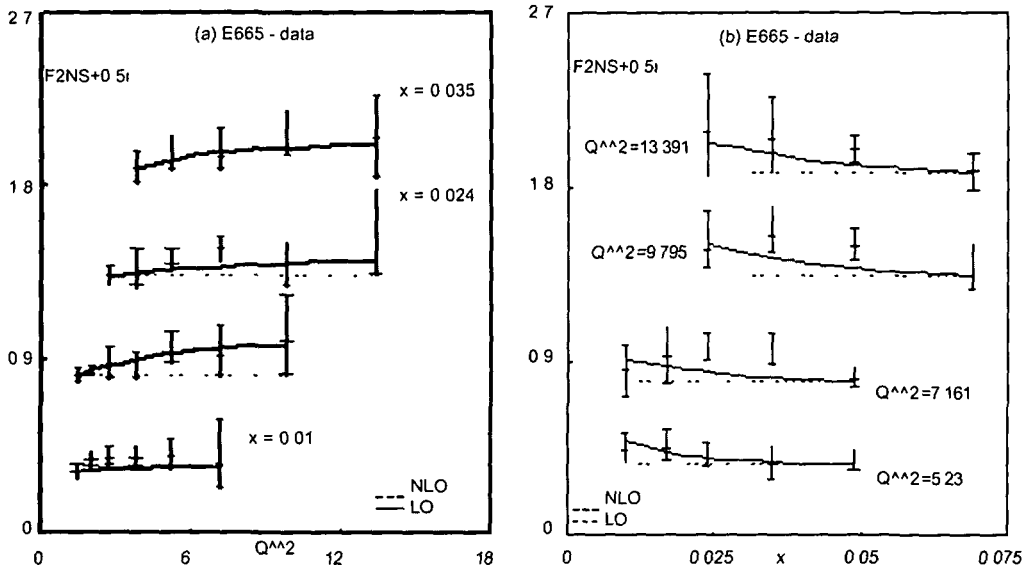


Figure 2 (a & b) Evolution of non-singlet structure function compared to E665 data

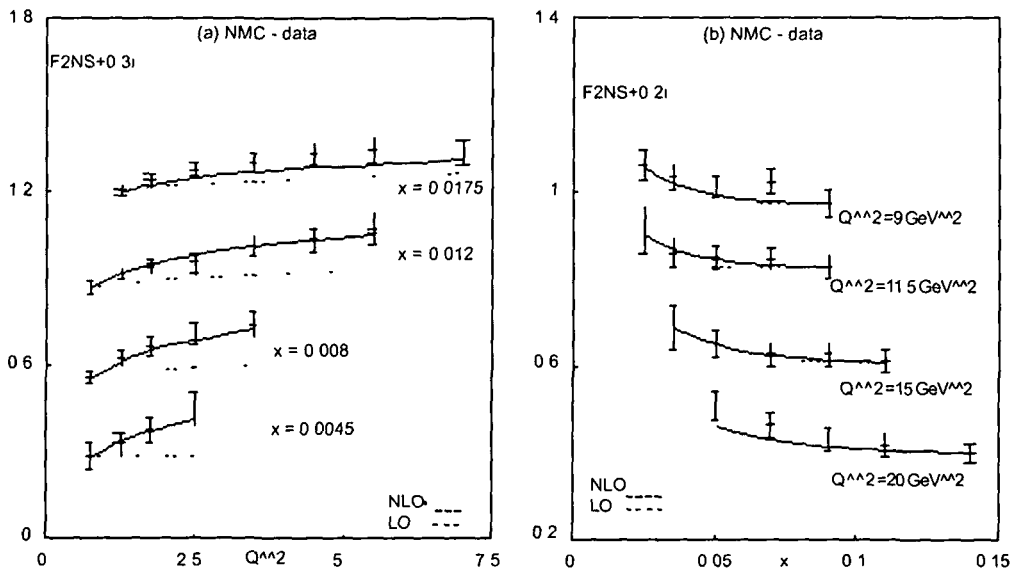


Figure 3 (a & b) Evolution of non-singlet structure function compared to NMC data

deuteron DIS with incident momentum 90, 120, 200, 280 GeV) We consider the range of  $0.01 \leq x \leq 0.0489$  and  $1.496 \leq Q^2 \leq 13.391$  for E665,  $0.0045 \leq x \leq 0.14$  and  $0.75 \leq Q^2 \leq 20$  for NMC data It is observed that within these range  $T_0$  is satisfied for  $0.08 \leq T_0 \leq 0.25$  (Figure 1) Figure 2(a) and Figure 3(a) represent the  $t$  evolution and Figure 2(b) and Figure 3(b) represent the  $x$  evolution of non-singlet structure function For convenience, value of each data point is increased by adding 0.5 $_i$  or 0.3 $_i$  or 0.2 $_i$ , where  $i = 0, 1, 2, 3$ , are the numberings of curves counting from the bottom of the lowermost curve as the 0<sup>th</sup> order Here errors bars represent total combined statistical and systematic uncertainty Our results are compatible with experimental values and fitness is better in NLO than the LO case

#### 4. Conclusion

Though there are various methods to solve DGLAP evolution equation to calculate quark and gluon structure functions, our method of characteristics to solve these equations is also a viable alternative Though mathematically vigorous, it changes the integro-differential equations into ODE and then makes it possible to obtain unique solutions

#### Acknowledgment

One of the authors (RB) is grateful to DAE- BRNS for financial support to fulfil this work as major research project

#### References

- [1] W Furmanski and R Petronzio *Z Phys* **C11** 293 (1982)
- [2] W L van Neerven and A Vogt *Nucl Phys* **B603** 42 (2001)
- [3] S Moch, J A M Vermaseren and A Vogt *Nucl Phys* **B588** 345 (2000)
- [4] A Vogt S Moch and J A M Vermaseren *Nucl Phys* **B691** 129 (2004)
- [5] M Hirai, S Kumano and Myiama *Comput Phys Commun* **108** 38 (1998)
- [6] A Cafarella C Coriano and M Guzi *Nucl Phys* **B748** 253 (2006)
- [7] G Altarelli and G Parisi *Nucl Phys* **B126** 298 (1977)
- [8] G Altarelli *Phys Rep* **18** 1 (1981)
- [9] V N Gribov and L N Lipatov *Sov J Nucl Phys* **15** 438 (1972)
- [10] Y L Dokshitzer *Sov Phys JEPT* **46** 641 (1977)
- [11] D K Choudhury and J K Sarma *Pramana J Phys* **38** 481 (1997)
- [12] D K Choudhury, J K Sarma and G K Medhi *Phys Lett* **B403** 139 (1997)
- [13] J K Sarma and B Das *Phys Lett* **B304** 323 (1993)
- [14] R Rajkhowa and J K Sarma *Indian J Phys* **78** A(3) 367 (2004)
- [15] S J Farlow *Partial Diff Eq for Scientist and Engineers* (New York John Willey) (1982)
- [16] I Sneddon *Elements of Partial Differential Equations* (New York McGraw Hill) (1957)
- [17] D K Choudhury and P K Saharia *Pramana J Phys* **58** 599 (1997)

- [18] R Baishya and J K Sarma *Phys Rev* **D74** 107702 (2006)
- [19] M R Adams *et al* E665 *Phys Rev* **D54** 3006 (1996)
- [20] M Arneodo *et al* CERN- NA-037, NMC *Nucl Phys* **B483** 3 (1997)
- [21] A Retey and J A M Vermaseren, arXiv hep-ph/0007294 v2 (2001)
- [22] [http://www arXiv hep-ph/0512358](http://www.arXiv.org/abs/hep-ph/0512358) v5 (2006)
- [23] [http://www arXiv hep-ph/0712 0327v2](http://www.arXiv.org/abs/hep-ph/0712032) (2008)
- [24] W Furmanski and R Petronzio *Phys Lett* **B97** 437 (1980)

# Method of characteristics and solution of DGLAP evolution equation in leading and next to leading order at small $x$

R Baishya\*

Physics Department, J N College, Boko-781123, Assam, India

J K Sarma

Physics Department, Tezpur University, Napaam-784028, Assam, India

(Received 17 October 2006, published 20 November 2006)

In this paper the singlet and nonsinglet structure functions have been obtained by solving Dokshitzer, Gribov, Lipatov, Altarelli, Parisi (DGLAP) evolution equations in leading order and next to leading order at the small  $x$  limit. Here we have used Taylor series expansion and then the method of characteristics to solve the evolution equations. We have also calculated  $t$  and  $x$  evolutions of the deuteron structure function and the results are compared with the New Muon Collaboration data.

DOI 10.1103/PhysRevD.74.107702

PACS numbers 12.38.-t, 12.39.-x, 13.60.Hb

## I. INTRODUCTION

The solutions of DGLAP evolution equations give quark and gluon structure functions that ultimately produce proton, neutron, and deuteron structure functions [1–9]. Though various methods like brute force approaches, the Mellin moments method, etc. are available in order to obtain a numerical solution of DGLAP evolution equations, exact analytical solutions of singlet equations are not known [10, 11]. Because the evolution equations are partial differential equations (PDE), their ordinary solutions are not unique solutions, but rather a range of solutions. On the other hand, this limitation can be overcome by using the method of characteristics. The method of characteristics is an important technique for solving initial value problems of first order PDE. It turns out that if we change coordinates from  $(x, t)$  to suitable new coordinates  $(S, \tau)$  then the PDE becomes an ordinary differential equation (ODE). Then we can solve the ODE by the standard method.

## II. THEORY

The DGLAP evolution equations for singlet and nonsinglet structure functions in leading order (LO) and next to leading order (NLO) in standard form [5–7] are

$$\frac{\partial F_2^S}{\partial t} - \frac{\alpha_S(t)}{2\pi} \left[ \frac{2}{3} \{3 + 4 \ln(1-x)\} F_2^S(x, t) + I_1^S(x, t) + I_2^S(x, t) \right] = 0, \quad (1)$$

$$\frac{\partial F_2^{NS}}{\partial t} - \frac{\alpha_S(t)}{2\pi} \left[ \frac{2}{3} \{3 + 4 \ln(1-x)\} F_2^{NS}(x, t) + I_1^{NS}(x, t) \right] = 0, \quad (2)$$

$$\frac{\partial F_2^S}{\partial t} - \frac{\alpha_S(t)}{2\pi} \left[ \frac{2}{3} \{3 + 4 \ln(1-x)\} F_2^S(x, t) + I_1^S(x, t) + I_2^S(x, t) \right] - \left( \frac{\alpha_S(t)}{2\pi} \right)^2 I_3^S = 0, \quad (3)$$

$$\frac{\partial F_2^{NS}}{\partial t} - \frac{A_f}{t} \left[ \{3 + 4 \ln(1-x)\} F_2^{NS}(x, t) + I_1^{NS}(x, t) \right] - \left( \frac{\alpha_S(t)}{2\pi} \right)^2 I_2^{NS} = 0, \quad (4)$$

where  $I_1^S, I_2^S, I_3^S, I_1^{NS}, I_2^{NS}$  are integral functions

Using Taylor's expansion series we can rewrite  $F_2^S(\frac{x}{\omega}, t)$  and  $G(\frac{x}{\omega}, t)$  as [7,8]

$$F_2^S\left(\frac{x}{\omega}, t\right) = F_2^S(x, t) + \frac{xu}{1-u} \frac{\partial F_2^S(x, t)}{\partial x}$$

$$\text{and } G\left(\frac{x}{\omega}, t\right) = G(x, t) + \frac{xu}{1-u} \frac{\partial G(x, t)}{\partial x}$$

Since  $x$  is small in our region of discussion, the terms containing  $x^2$  and higher powers of  $x$  are neglected.

In order to solve Eq. (1), we need to relate the singlet distribution  $F_2^S(x, t)$  with the gluon distribution  $G(x, t)$ . For small  $x$  and high  $Q^2$ , the gluon is expected to be more dominant than the sea quark. But for lower  $Q^2$ , there is no such clear cut distinction between the two. Hence, for simplicity, let us assume  $G(x, t) = k(x)F_2^S(x, t)$ , where  $k(x)$  is a suitable function of  $x$  or may be a constant. We may assume  $k(x) = k, ax^b, ce^{dx}$  where  $k, a, b, c, d$  are suitable parameters which can be determined by phenomenological analysis. But the possibility of the breakdown of the relation cannot be ruled out either [8,9].

Performing  $u$  integrations, Eq. (1) becomes

$$-t \frac{\partial F_2^S(x, t)}{\partial t} + A_f L(x) F_2^S(x, t) + A_f M(x) \frac{\partial F_2^S}{\partial x} = 0 \quad (5)$$

To introduce the method of characteristics, let us consider two new variables  $(S, \tau)$  instead of  $(x, t)$ , such that  $\frac{dt}{dS} = -t$

\*Email address rjtboko@yahoo.co.in



and  $\frac{dL}{dS} = A_f M(x)$ . Putting these equations in (5), we get  $\frac{dF_2^S(S, \tau)}{dS} + L(S, \tau)F_2^S(S, \tau) = 0$ , which can be solved as  $F_2^S(S, \tau) = F_2^S(\tau) \left(\frac{L}{L_0}\right)^{L(S, \tau)}$ .

Now we have to replace the coordinate system  $(S, \tau)$  to  $(x, t)$  with the input function  $F_2^S(\tau) = F_2^S(x, t_0)$  and we will get the  $t$  evolution of the singlet structure function in the LO as  $F_2^S(x, t) = F_2^S(x, t_0) \left(\frac{L}{L_0}\right)^{A_f L(x)}$ . Similarly the  $x$  evolution of the singlet structure function will be

$$F_2^S(x, t) = F_2^S(x_0, t) \exp\left[-\int_{x_0}^x \frac{L(x)}{M(x)} dx\right].$$

Hence the  $t$  and  $x$  evolution of deuteron structure functions in LO can be obtained as

$$F_2^d(x, t) = F_2^d(x, t_0) \left(\frac{t}{t_0}\right)^{A_f L(x)}$$

$$\text{and } F_2^d(x, t) = F_2^d(x_0, t) \exp\left[-\int_{x_0}^x \frac{L(x)}{M(x)} dx\right],$$

where  $F_2^d(x, t_0) = \frac{5}{2} F_2^S(x, t_0)$  and  $F_2^d(x_0, t) = \frac{5}{2} F_2^S(x_0, t)$  are input functions.

In the NLO, the  $t$  and  $x$  evolution of deuteron structure functions will be obtain as

$$F_2^d(x, t) = F_2^d(x, t_0) \left(\frac{t}{t_0}\right)^{(3/2)A_f[L(x)+T_0L_1(x)]},$$

$$F_2^d(x, t) = F_2^d(x_0, t) \exp\left[-\int_{x_0}^x \frac{L(x) + T_0L_1(x)}{M(x) + T_0M_1(x)} dx\right],$$

where

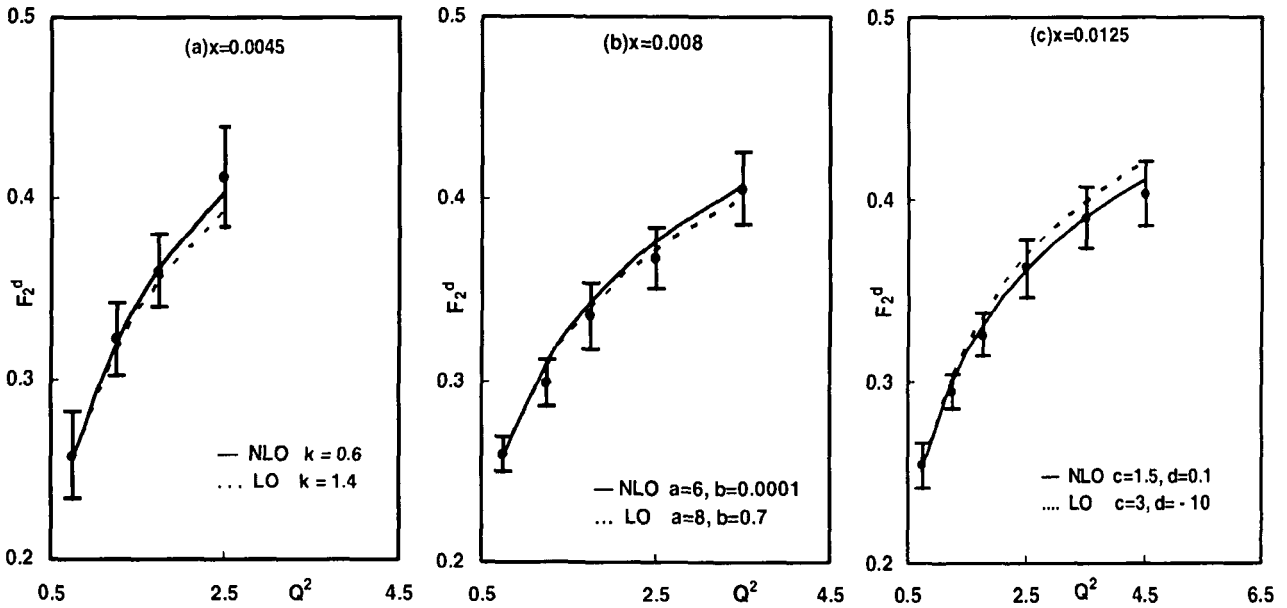


FIG. 1.  $t$  evolution of the deuteron structure function in LO and NLO.

$$L_1(x) = B_1(x) + k(x)B_2(x) + B_4(x)\partial k(x)/\partial x;$$

$$M_1(x) = B_3(x) + k(x)B_4(x);$$

$$B_1(x) = x \int_0^1 f(\omega) d\omega - \int_0^x f(\omega) d\omega + \frac{4}{3} N_f \int_x^1 F_{qg}^S(\omega) d\omega;$$

$$B_2(x) = \int_x^1 F_{qg}^S(\omega) d\omega;$$

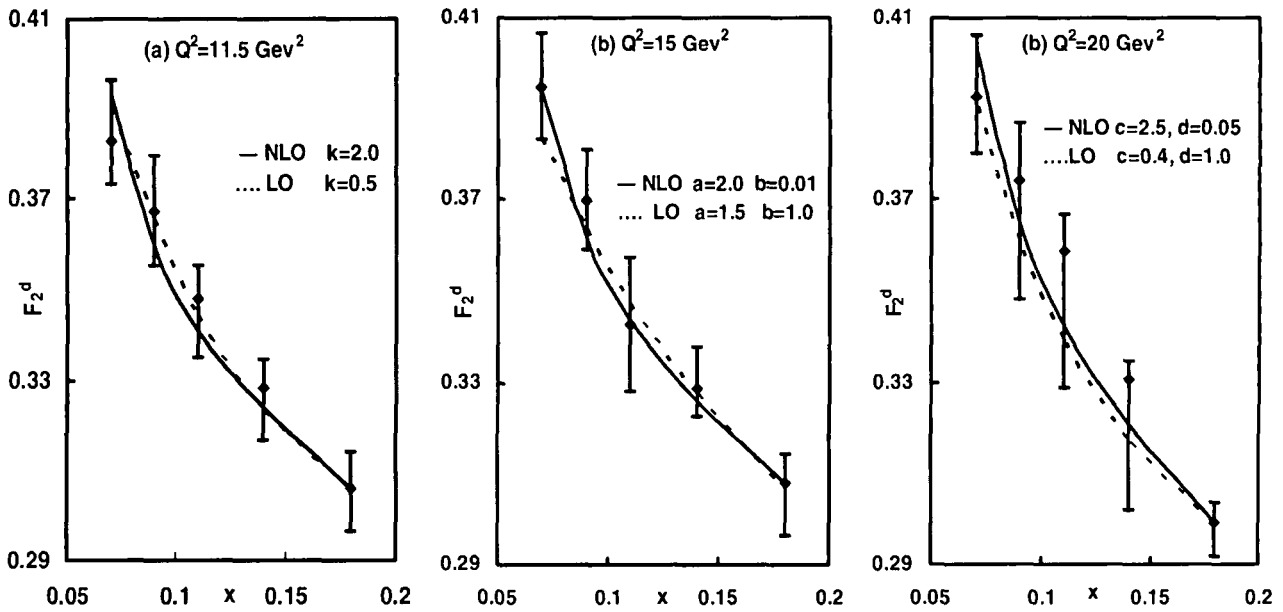
$$B_3(x) = x \int_x^1 \left[ f(\omega) + \frac{4}{3} N_f F_{qg}^S(\omega) \right] \frac{1-\omega}{\omega} d\omega;$$

$$B_4(x) = x \int_x^1 \frac{1-\omega}{\omega} F_{qg}^S(\omega) d\omega.$$

Here we consider an extra assumption  $\left(\frac{\alpha_S(t)}{2\pi}\right)^2 = T_0 \left(\frac{\alpha_S(t_0)}{2\pi}\right)$ , where  $T_0$  is a numerical parameter. By a suitable choice of  $T_0$  we can reduce the error to a minimum.

### III. RESULTS AND DISCUSSION

In this paper, we compare our result of  $t$  and  $x$  evolution of the deuteron structure function  $F_2^d$  measured by the New Muon Collaboration in muon deuteron deep inelastic scattering with incident momentum 90, 120, 200, 280 GeV [12]. For quantitative analysis, we consider the QCD cutoff parameter  $\Lambda_{\overline{MS}} = 0.323$  GeV for  $\alpha_S(M_Z^2) = 0.119 \pm 0.002$  and  $N_f = 4$ . It is observed that our result is very sensitive to arbitrary parameters  $k, a, b, c$ , and  $d$ . In Fig. 1, for  $t$  evolution, we have plotted computed values of  $F_2^d$

FIG. 2.  $x$  evolution of the deuteron structure function in LO and NLO.

against  $Q^2$  values for a fixed  $x$  in LO and NLO. Here the solid lines represent the best fitting curves in NLO and the dotted lines represent those for LO evolutions. In Fig. 2, for  $x$  evolution, we have plotted computed values of  $F_2^d$  against the  $x$  values for a fixed  $Q^2$ . Here also the solid lines represent the best-fit curves for NLO and the dotted lines represent for LO evolutions.

Though there are various numerical methods to solve DGLAP evolution equations to obtain quark and gluon structure functions, the method of characteristics to solve these equations analytically is also a viable alternative. Though mathematically vigorous, it changes the integro-differential equations into ODE and then makes it possible to obtain unique solutions.

- [1] V. N. Gribov and L. N. Lipatov, *Sov. J. Nucl. Phys.* **15**, 438 (1972).  
 [2] Y. L. Dokshitzer, *Sov. Phys. JETP* **46**, 641 (1977).  
 [3] G. Altarelli and G. Parisi, *Nucl. Phys.* **B126**, 298 (1977).  
 [4] G. Altarelli, *Phys. Rep.* **18**, 1 (1981).  
 [5] L. F. Abbott, W. B. Atwood, and R. M. Barnett, *Phys. Rev. D* **22**, 582 (1980).  
 [6] W. Furmanski and R. Petronzio, *Phys. Lett.* **97B**, 437 (1980); *Nucl. Phys.* **B195**, 237 (1982).  
 [7] W. Furmanski and R. Petronzio, *Z. Phys. C* **11**, 293

- (1982).  
 [8] D. K. Choudhury, J. K. Sarma, and G. K. Medhi, *Phys. Lett. B* **403**, 139 (1997).  
 [9] J. K. Sarma and B. Das, *Phys. Lett. B* **304**, 323 (1993).  
 [10] M. Hirai, S. Kumano, and Myiama, *Comput. Phys. Commun.* **108** 38 (1998).  
 [11] A. Cafarella *et al.*, *Nucl. Phys.* **B748**, 253 (2006).  
 [12] M. Arneodo *et al.*, CERN-NMC, Report No. CERN-NA-037; *Nucl. Phys.* **B483**, 3 (1997).